2016

TOWARDS AN UNDERSTANDING OF PHARMACOLOGICALLY INDUCED INTRACELLULAR CHANGES IN NICOTINIC ACETYLCHOLINE RECEPTORS: A FLUORESCENCE MICROSCOPY APPROACH

Ashley M. Loe
University of Kentucky, amfo228@g.uky.edu
Author ORCID Identifier:
http://orcid.org/0000-0003-0656-3755
Digital Object Identifier: https://doi.org/10.13023/ETD.2016.461

STUDENT AGREEMENT:

I represent that my thesis or dissertation and abstract are my original work. Proper attribution has been given to all outside sources. I understand that I am solely responsible for obtaining any needed copyright permissions. I have obtained needed written permission statement(s) from the owner(s) of each third-party copyrighted matter to be included in my work, allowing electronic distribution (if such use is not permitted by the fair use doctrine) which will be submitted to UKnowledge as Additional File.

I hereby grant to The University of Kentucky and its agents the irrevocable, non-exclusive, and royalty-free license to archive and make accessible my work in whole or in part in all forms of media, now or hereafter known. I agree that the document mentioned above may be made available immediately for worldwide access unless an embargo applies.

I retain all other ownership rights to the copyright of my work. I also retain the right to use in future works (such as articles or books) all or part of my work. I understand that I am free to register the copyright to my work.

REVIEW, APPROVAL AND ACCEPTANCE

The document mentioned above has been reviewed and accepted by the student's advisor, on behalf of the advisory committee, and by the Director of Graduate Studies (DGS), on behalf of the program; we verify that this is the final, approved version of the student's thesis including all changes required by the advisory committee. The undersigned agree to abide by the statements above.

Ashley M. Loe, Student

Dr. Christopher I. Richards, Major Professor

Dr. Mark Lovell, Director of Graduate Studies

TOWARDS AN UNDERSTANDING OF PHARMACOLOGICALLY INDUCED INTRACELLULAR CHANGES IN NICOTINIC ACETYLCHOLINE RECEPTORS: A FLUORESCENCE MICROSCOPY APPROACH

DISSERTATION

A dissertation submitted in partial fulfillment of the
requirements for the degree of Doctor of Philosophy in the
College of Arts and Sciences
at the University of Kentucky

By
Ashley Mae Loe

Lexington, Kentucky

Director: Dr. Christopher I. Richards, Assistant Professor of Chemistry

Lexington, Kentucky

2016

ABSTRACT OF DISSERTATION

TOWARDS AN UNDERSTANDING OF PHARMACOLOGICALLY INDUCED INTRACELLULAR CHANGES IN NICOTINIC ACETYLCHOLINE RECEPTORS: A FLUORESCENCE MICROSCOPY APPROACH

Upregulation of nicotinic acetylcholine receptors (nAChRs) is a well-documented response to chronic nicotine exposure. Nicotinic acetylcholine receptors are pentameric ligand-gated ion channels consisting of alpha (α2-10) and beta (β2-4) subunits. Nicotine, an agonist of nAChRs, alters trafficking and assembly of some subtypes of nAChRs, leading to an increase in expression of high sensitivity receptors on the plasma membrane. These physiological changes in nAChRs are believed to contribute to nicotine addiction, although the mechanism of these processes has not been resolved. Recently, many studies have converged on the idea that nicotine induces upregulation by an intracellular mechanism. In this dissertation, expression levels of nAChRs were quantified upon exposure to nicotine and its primary metabolite, cotinine. A pH sensitive variant of GFP, super ecliptic pHluorin (SEP), was integrated with a nAChR subunit to study expression and trafficking of nAChRs by differentiating intracellular and plasma membrane inserted receptors. In this work, cotinine is shown to increase the number of α4β2 nAChRs within a cell. Cotinine also affects trafficking of α4β2, evident by a redistribution of intracellular receptors and an increase in single vesicle insertion events on the plasma membrane. This work shows both nicotine and cotinine alter the overall assembly of α4β2 to favor the high sensitivity $(\alpha4)_2(\beta2)_3$ version. Since cotinine and nicotine induce similar physiological changes in nAChRs, the metabolite potentially plays a role in the mechanism of nicotine addiction.

Although an intracellular mechanism for upregulation has been supported, a shift in assembly to the high sensitivity $(\alpha4)_2(\beta2)_3$ version exclusively in the endoplasmic reticulum has not previously been detected. In order to study organelle specific changes in stoichiometry, a novel method was developed to isolate single nAChRs in nanovesicles derived from native cell membranes. Separation of nanovesicles originating from the

endoplasmic reticulum and plasma membrane, encompassing isolated nAChRs, allows precise changes in stoichiometry to be monitored in subcellular regions. In this work, single molecule bleaching steps of green fluorescent protein (GFP) encoded in each alpha subunit of the pentamer are detected. The number of bleaching steps, or transitions to a nonfluorescent state upon continuous excitation, corresponds to the number of GFP-labeled alpha subunits present. Therefore, the stoichiometry can be deduced by detection of two bleaching steps, as in $(\alpha4)_2(\beta2)_3$, or three bleaching steps, seen in $(\alpha4)_3(\beta2)_2$. Using this method on isolated nAChRs, a shift to assembly of high sensitivity $(\alpha4)_2(\beta2)_3$ receptors is detected definitively within the endoplasmic reticulum. In addition, an increase in $(\alpha4)_2(\beta2)_3$ receptors located on the plasma membrane is shown when nicotine is present. This work provides convincing evidence that nicotine acts intracellularly, within the endoplasmic reticulum, to alter stoichiometry of nAChRs.

KEYWORDS: nicotinic acetylcholine receptors, nicotine, cotinine, fluorescence microscopy, total internal reflection fluorescence microscopy, single molecule photobleaching

Ashley M. Loe

November 7, 2016
Date

TOWARDS AN UNDERSTANDING OF PHARMACOLOGICALLY INDUCED INTRACELLULAR CHANGES IN NICOTINIC ACETYLCHOLINE RECEPTORS: A FLUORESCENCE MICROSCOPY APPROACH

By

Ashley Mae Loe

Dr. Christopher I. Richards
Director of Dissertation

Dr. Mark A. Lovell
Director of Graduate Studies

November 7, 2016
Date

To my family,

for your support, encouragement and

unconditional love

ACKNOWLEDGMENTS

First and foremost, I would like to thank my advisor, Dr. Chris Richards, for giving me the opportunity to work in his lab. Without his guidance, mentorship, and unfaltering patience, I would not be the scientist I am today. He always encouraged me to try, and had unwavering confidence in me. I am honored to be one of his first students.

I would also like to extend a sincere thank you to my doctoral committee members, Dr. Mark Lovell, Dr. Stephen Testa, and Dr. Jim Pauly. Your time, guidance and support throughout this process is greatly appreciated. I also wish to thank all of the faculty and staff who have influenced me over the years, both here at University of Kentucky as well as Muskingum University where I obtained by bachelor's degree. I would never have attended graduate school without the encouragement of Dr. Raymond Rataiczak, Drs. Paul and Shelley Szalay, and Bill Pattison. I also want to thank the members of the Richards' lab, as well as many friends along the way, for their scientific advice, help, friendship, and sometimes counseling.

To my Mom, Dad and Zach, I cannot thank you enough for the endless support and involvement over the years. Starting at a young age, you always stressed the importance of education. You instilled in me a desire to learn and understand, and that has empowered my desire to achieve my goals. From the encouraging phone calls to relaxing visits, you always find a way to keep me focused. Thank you for all you have done.

Finally, I want to thank my husband, Ryan, for being my pillar of strength through this entire process. You have been there to support me through all of the ups and downs since day one. I cannot imagine where I would be without you. I look forward to what the future holds for us.

TABLE OF CONTENTS

LIST OF TABLES

LIST OF FIGURES

CHAPTER 1: INTRODUCTION AND BACKGROUND

1.1 Nicotine History and Usage

1.1.1 Tobacco Consumption

Smoking harms almost every organ in the body, making tobacco consumption the leading preventable cause of death [1, 2]. The use of tobacco products began as early as 5000-3000 BC [3], and, despite health warnings, still affects an estimated 1 billion people world-wide today [2]. In the United States alone, more than 480,000 deaths are due to cigarette smoking. This is approximately one in five total deaths annually, or 1300 deaths every day [4]. On average, smokers die approximately 10 years earlier than non-smokers, with up to half of tobacco users dying as a result of prolonged tobacco consumption [1, 2]. Tobacco use results in an increased risk for developing lung diseases, cardiovascular disease, chronic obstructive pulmonary disease (COPD), diabetes and several types of cancer [1, 4, 5]. Many smokers are aware of these risks, with 68.9% of adult smokers in the United States claiming they would like to stop smoking. However, the additive component in tobacco, nicotine, is one of the primary barriers in successful smoking cessation [6-9]. Nicotine acts as an agonist of nicotinic acetylcholine receptors (nAChRs). These receptors are also activated by the endogenous neurotransmitter acetylcholine [10]. It is well documented that chronic nicotine exposure induces a variety of physiological changes in nicotinic acetylcholine receptors (nAChRs), leading to an undefined link between nAChRs and nicotine addiction.

1.1.2 Nicotine

Nicotine has a long history of being cultivated and used by humans due to its vast pharmacological effects. (S)-Nicotine is the most abundant alkaloid isolated from the tobacco plant, *Niotiana tabacum*, and has been manufactured into a variety of tobacco products. The concentration of nicotine varies greatly between types of products and species of tobacco used, but typically accounts for 1-2% of the dry tobacco weight and around 3-8% of a tobacco product [11, 12]. The most typical form of use is smoking, in which nicotine is vaporized and inhaled along with other toxic substances such as carbon monoxide, carbon dioxide, hydrogen cyanide, other carcinogenic components, and numerous aldehydes and ketones. Also, since nearly 75% of the volatiles emitted from a cigarette enters the environment [13], nonsmokers exposed to second hand smoke in their environment are also at risk for developing lung cancer and other smoke exposure related diseases [14]. Nicotine is rapidly absorbed throughout the body, reaching the brain within 8 seconds of inhalation [15]. This allows a smoker to titrate their dose, or vary the rate and intensity of puffs on a cigarette, to achieve a desired effect. Nicotine is reported by users to enhance cognitive and psychomotor behaviors [16-19], but is also inherently toxic and increases blood pressure and heart rate. Tobacco is also thought to be addictive, causing moderate changes in nicotine-rewarded learning processes within the brain [20]. Model systems have shown that low concentrations of nicotine have measurable physiological effects. In smokers, these effects are primarily mediated by the nicotinic acetylcholine receptors (nAChRs), where nicotine binds as a full agonist.

1.1.3 Cotinine, the Primary Metabolite of Nicotine

Once consumed, approximately 80% of nicotine is metabolized to cotinine by the enzyme cytochrome P450 2A6 [21-24]. Nicotine and cotinine are very similar in structure, varying by only an acetyl group [25], as shown in Figure 1.1. Tobacco exposure leads to the accumulation of cotinine in the body due to cotinine's long pharmacological half-life of approximately 20-24 hours, which is about ten times that of nicotine [3, 26]. This accumulation is highly dependent on the rate of cotinine formation in combination with the rate of cotinine removal, both of which are mediated by the cytochrome P450 2A6 enzyme. Variations in the gene coding for this enzyme, CYP2A6, have been linked to differences in rate of cotinine accumulation between individuals [3, 25]. Lower levels of cotinine are seen in individuals expressing a shorter form of CYP2A6, such as CYP2A6*4 [27], while cotinine accumulates in individuals with slower CYP2A6 activity [28]. Also, rates of cotinine clearance from the body vary between ethnic groups, with African Americans showing less cotinine clearance than Caucasians [29-31], possibly due to the frequency of reduced function variants of the CYP2A6 gene. Individuals that prefer menthol cigarettes also have higher levels of cotinine in their bloodstream compared to other smokers, regardless of genetic background [32]. One possible reason for this is that menthol soothes airway irritation, which may allow smokers to inhale more nicotine. Menthol may also slow the metabolism of nicotine, causing higher concentrations of nicotine and metabolites to accumulate [33, 34]. Recent studies suggest menthol increases expression of some nAChR subtypes [35, 36]. Taken together, these variations lead to differences in cotinine levels between individuals with the same tobacco exposure.

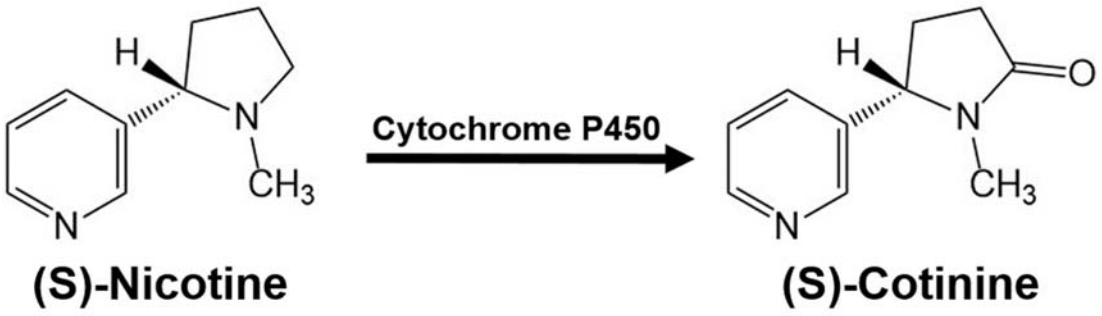

Figure 1.1 Structures of nicotine and cotinine. Nicotine and its primary metabolite, cotinine, differ in structure by only an acetyl group. Nicotine is metabolized to cotinine by the enzyme cytochrome P450 2A6.

Traditionally, cotinine has been used as a biomarker for nicotine exposure [14]. The effective concentration of nicotine and other compounds that are absorbed from a cigarette is not directly related to the number of cigarettes consumed. Cotinine is used to assess the amount of nicotine ingested by smokers as well as secondhand exposure in nonsmokers. On average, manufactured cigarettes contain between 6 and 12 mg of nicotine, although the amount of nicotine entering the bloodstream of a smoker varies greatly [13]. Cotinine as a biomarker enables the assessment of a correlation between tobacco consumption and risk of disease compared to unexposed controls. It meets criteria for a good biomarker, such its specificity for nicotine exposure and easy detectability. Cotinine is more ideal as a biomarker than nicotine due to its longer pharmacological half-life, meaning detected concentrations are less reliant on the time of sampling than in measuring nicotine [14]. For these reasons, cotinine has long been thought of as nothing more than a convenient biomarker to link tobacco exposure to risk of disease.

Recently, cotinine has generated some interest as a pharmacologically active compound. Cotinine has been shown to reduce effects of chronic stress such as synaptic loss, anxiety, and depression [37]. It has also been shown to facilitate increases in cognition and executive function [23], and improvements in memory, learning, and attention [25, 38]. Although nicotine is addictive, increases blood pressure and heart rate, and is inherently toxic [39], exposure to cotinine does not lead to these effects and is not considered addictive [14]. Cotinine is also able to cross the blood-brain barrier [40] and acts as a partial agonist to nicotinic acetylcholine receptors [41-44], and therefore may be at least partially responsible for physiological effects previously attributed to nicotine exposure.

1.2 Nicotinic Acetylcholine Receptor Structure and Assembly

1.2.1 Neuronal Nicotinic Acetylcholine Receptor Overview

Nicotinic acetylcholine receptors (nAChRs) are ligand-gated transmembrane ion channels, activated by the endogenous neurotransmitter acetylcholine. nAChRs are cation-selective, ionotropic members of the cys-loop superfamily of receptors, expressing throughout the central and peripheral nervous systems [45, 46]. nAChRs primarily mediate fast synaptic transmission in the periphery and modulate neurotransmitter function in the central nervous system [47, 48]. The cys-loop superfamily includes other receptors that function as cationic or anionic ion channels [49]. Cationic members are 5-HT_3 (5-hydroxytryptamine) receptors, in addition to nAChRs. Anionic channels include $GABA_A$ (γ-aminobutryic acid), $GABA_c$, and glycine receptors. The cys-loop superfamily is characterized by a large N-terminal extracellular domain containing a stable cys-loop of two cysteine residues linked in a disulfide bridge around 13 hydrophobic amino acids [46, 50-52]. As ligand-gated ion channels, nAChRs are functional upon activation by an agonist, such as acetylcholine or nicotine, which induces a conformational change in the extracellular region of the receptor to open the channel, allowing the flux of cations such as Na^+, K^+, or Ca^{2+} on the timescale of microseconds to milliseconds [45, 46]. Another functional characteristic of nAChRs is that they desensitize, or decrease in response to agonist, after repeated activation, much faster than any other ion channel. Upon desensitization, nAChRs adopt a high affinity, non-conducting conformation, in spite of agonist binding [53, 54] This desensitization is more prevalent for the cation channels, such as nAChR, than typical anion channels [55]. For α4β2 nAChRs, this desensitization happens within seconds to a few minutes of agonist exposure. [56]. It is also noteworthy

that many nAChRs are thought to be desensitized when exposed to typical levels of nicotine seen in smokers [57, 58]. Upon nAChR activation, these membrane receptors are involved in the rapid, phasic effects of acetylcholine in the brain, leading to the release of essential neurotransmitters, including dopamine, serotonin, glutamate, and γ-aminobutyric acid (GABA) [45]. For this reason, there has been significant interest in targeting nAChRs to treat numerous neurological disorders such as Alzheimer's disease, Parkinson's disease, epilepsy, ADHD, schizophrenia, and tobacco addiction [59-65].

1.2.2 nAChR Subunits and Assembly

A substantial challenge in using nAChRs as drug targets rises from the complex diversity of nAChR subtypes. Mature nAChRs are pentameric, formed by the assembly of five individual subunits around a central hydrophilic pore, as illustrated in Figure 1.2. Neuronal subunits are categorized as alpha (α2-α10) and beta (β2-β4) subunits [45, 46, 52, 66], with each pentameric combination differing in expression, distribution, physiological and pharmacological properties throughout the nervous system. Each subunit weighs 40-70 kDa, contributing to an assembled pentamer with a mass of 270-300 kDa [67]. There are nine alpha (α2, α3, α4, α5, α6, α7, α9, α10) and three beta (β2, β3, β4) subunits expressed in the human brain, each encoded by a distinct gene. After translation, free subunits are assembled into pentameric receptors in the endoplasmic reticulum, and trafficked to the plasma membrane to function as an ion channel.

Since functional nAChRs are a combination of five individual subunits, multiple subtypes can be assembled. Subtypes are broadly classified as homopentamers or

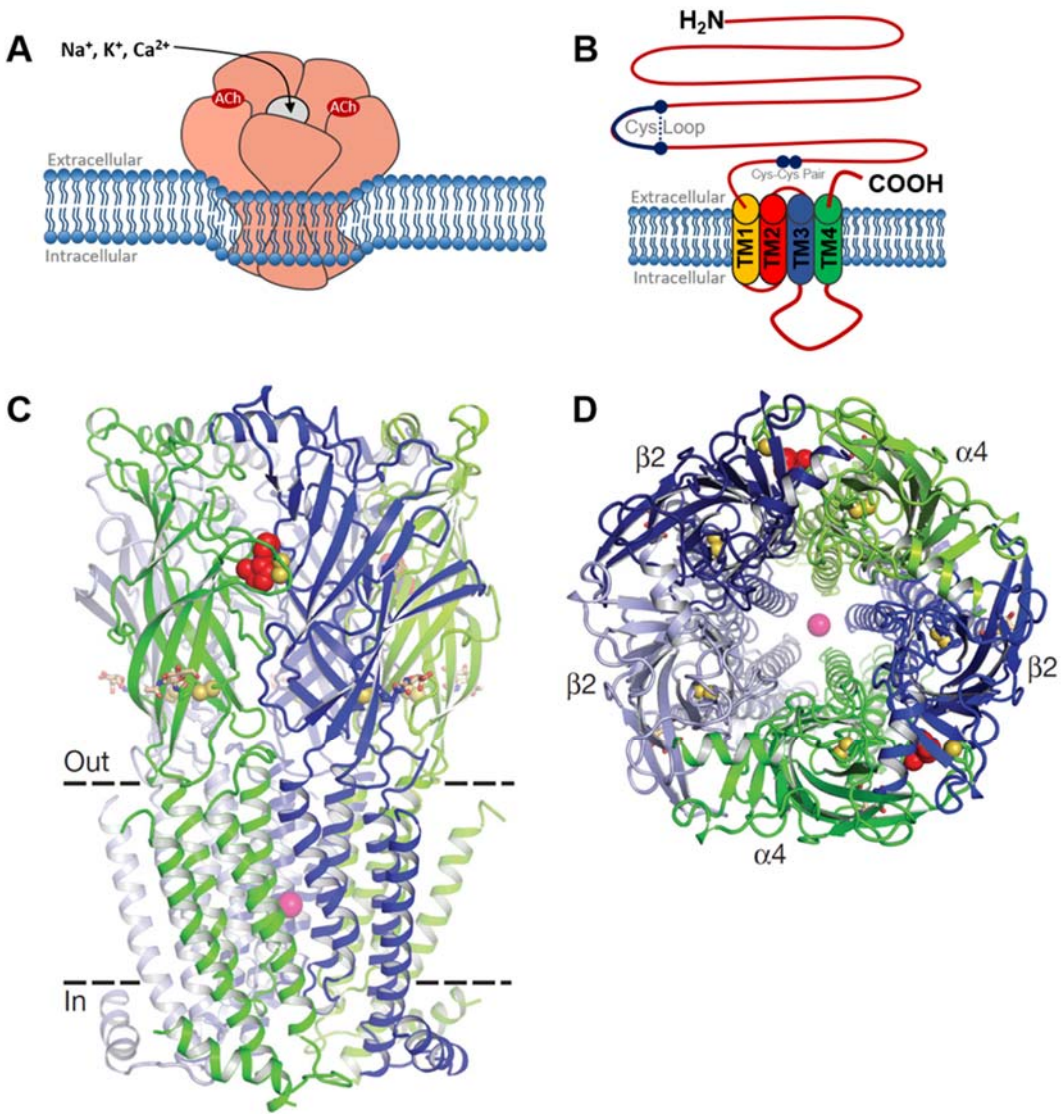

Figure 1.2 Structure of nAChRs. (A) Cartoon of a pentameric nAChR. Functional nAChRs are cation channels with ligand binding between adjacent subunits. (B) Each subunit has a large N-terminal, a cys-loop, four TMDs, a variable loop between TM3 and TM4, and a short C-terminal. Alpha subunits have a cys-cys pair involved in binding. (C) Crystal structure of $(\alpha4)_2(\beta2)_3$ with α4 subunits shown in green and β2 subunits shown in blue. Spheres represent nicotine (red), sodium (pink), and disulfide bonds (yellow). (D) Perpendicular view of the $(\alpha4)_2(\beta2)_3$ crystal structure from the extracellular region.

heteropentamers. Homopentamers consist of five identical subunits, with a binding domain between each subunit, as seen in α7 or α9 subtypes. Heteropentamers are a combination of five alternating alpha and beta subunits. These subtypes require at least two essential alpha and two essential beta subunits, with two orthosteric agonist binding sites between adjacent alpha and beta subunits [68-71]. A recent crystal structure of $(\alpha4)_2(\beta2)_3$ shows that this heteropentamer has a peudo-symmetrical cylindrical shape around the axis of the channel, as shown in Figure 1.2C. These alternating subunits are in a specific α4-β2-α4-β2-β2 order around the hydrophilic pore (Figure 1.2D) [54].

Although slight differences between subunits give rise to distinct pharmacological properties, all subunits show substantial sequence homology. Overall, the genes that encode neuronal nAChRs are 40-55% homologous [67]. As a result, all subunits have a similar linear amino acid sequence, with an approximately 200 amino acid extracellular N-terminal, four alpha helical transmembrane (TM) domains packed around the hydrophilic pore, a variable loop between TM3 and TM4, and a short extracellular COOH-terminal domain, as shown in Figure 1.2B. Homology is highest throughout the transmembrane domains, as well as certain portions of the extracellular region involved in binding. TM2 of each subunit lines the hydrophilic pore, along with a portion of TM1 [72]. This transmembrane region is involved in gating cations passing through the pore, by action of a series of electronegative glutamic acid residues [73]. The residues in TM2 allow ion flux, selectivity, and channel conductivity. Opposite of this lies TM4, which interacts with the hydrophobic lipid bilayer. TM1 and TM3 are perpendicular to these, completing the helix bundle [46]. The largest intracellular domain, a variable region between TM3 and TM4, is highly diverse between subunits [74]. The structure, suspected to be a mix of α-helices

and β-strands, is involved in regulation, desensitization, and specific cellular functions of each unique subunit. Recently, a crystal structure of $(\alpha4)_2(\beta2)_3$ confirmed an amphipathic MX helix in this intracellular region [54]. Within this TM3-TM4 region, trafficking motifs specific to a particular subunit are present. These trafficking motifs control trafficking of assembled pentameric receptors out of the endoplasmic reticulum [75, 76]. To date, it is known that export LXM motifs (where X is any amino acid), located in the TM3-TM4 loop of α4, α3, and β4 subunits, govern trafficking out of the endoplasmic reticulum (ER). Also, a retention RXRR motif in the β2 subunit is associated with retention in the ER [76]. The large extracellular NH_2 domain has an overall β-barrel configuration. A recent crystal structure of $(\alpha4)_2(\beta2)_3$ shows this extracellular N-terminal is composed of α-helices and ten β-strands [54]. This extracellular region contains the cys-loop, a cys-cys pair, and critical amino acid residues involved in binding [45, 46, 52]. Although the cys-loop is highly conserved, slight variations in residues within each subtype are partially responsible for differences in ligand binding response, signal transduction, and kinetics.

Since nAChRs are ligand-gated ion channels, ions pass through the pore as a result of an agonist binding in a binding site. This is traditionally within the orthosteric binding pockets located at the interface of essential alpha and beta subunits for a heteromeric receptor, or between alpha subunits in a homomeric receptor. This binding within the β-barrel of the large extracellular domain results in a conformation change, rotating TM2 of each subunit towards an open conformation to allow ion flux. The alpha subunit is required at the front, or "positive" side of the binding site, where the cys-cys pair is located alongside hydrophobic residues to determine ligand affinity. The back, or "negative" side of the binding site then is in the adjacent subunit, often a beta subunit, where key residues

determine ligand selectivity [46]. Loops A, B, and C from the alpha subunit, and loops D, E, and F from the beta subunit, come together to complete the orthosteric binding site at the interface of these subunits [54].

All alpha subunits are traditionally distinguished by the presence of two vicinal cysteines at positions 191 and 192, known as the cys-cys pair, within the extracellular domain near TM1. This cys-cys pair is necessary for agonist binding, in addition to key hydrophobic residues within the alpha subunit. These are primarily aromatic amino acids, known as an "aromatic box", and include Tyr 93, Trp 149, Tyr 190, and Tyr 198 [45, 46]. These aromatic residues are thought to stabilize the positively charged endogenous agonist, acetylcholine, in a cation-π interaction. This cation-π interaction is a noncovalent interaction between the electron rich π system of the aromatic residues and positively charged ligands that bind within this binding pocket, including acetylcholine and nicotine [77-79]. The positively charged ligand is also stabilized by electronegativity in the binding site from the disulfide bridge and cys-cys pair. The $(\alpha 4)_2(\beta 2)_3$ nAChR was recently co-crystalized with nicotine binding in the orthosteric agonist site. In this position, nicotine is oriented to form the cation-π, with addition stability from aromatic and hydrophobic interactions with side chains in the binding pocket [54].

In heteropentameric subtypes, the first four positions are alternating alpha and beta subunits, with ligand binding occurring at the interface of adjacent subunits. If the heteropentamers consist of just two types of subunits, the fifth position can be occupied by either an alpha or beta subunit. This gives rise to the possibility for different stoichiometries to exist for the same subtype of nAChR. A heteropentamer can assemble as either a three alpha, two beta version, $(\alpha)_3(\beta)_2$, or a three beta, two alpha version $(\alpha)_2(\beta)_3$

depending on an α or β being incorporated into the fifth position. These two stoichiometries, although they belong to the same subtype, differ slightly in terms of sensitivity to agonists, expression, or rates of desensitization. For example, the differences in EC_{50} of the α4β2 subtype as a result of stoichiometry indicate that $(\alpha4)_2(\beta2)_3$ is of higher sensitivity to agonists than the alternative low sensitivity $(\alpha4)_3(\beta2)_2$ stoichiometry [80], while $(\alpha4)_3(\beta2)_2$ stoichiometry shows higher permeability to calcium [81]. Also, an additional agonist binding site was recently discovered at the α4(+)/α4(-) interface of $(\alpha4)_3(\beta2)_2$ [82-84]. A recent crystal structure of $(\alpha4)_2(\beta2)_3$ shows differences in the negative side of the subunit interface when an alpha versus beta subunit occupies the fifth position. When β2 is present, three hydrophobic groups are located in the potentially negative side of this binding pocket. However, when the fifth position is filled with an α4, the hydrophobic groups are replaced with polar side chains. The presence of polar groups in the α4(-) could account for differences in agonist binding to the α4(+)/α4(-) interface in $(\alpha4)_3(\beta2)_2$ [54]. It is suggested that occupation of this binding site by an agonist contributes to nAChR activation and agonist sensitivity [82, 84]. Different stoichiometries also vary in their specificity to pharmacological agents, which plays an important role in utilizing these subtypes as drug targets. In addition, pharmacological agents can preferentially induce the expression of one stoichiometry over another. This is the case after exposure to nicotine, for nicotine has been shown to alter the expression of α4β2 stoichiometry to favor $(\alpha4)_2(\beta2)_3$ [85].

Although the first four positions are alternating alpha and beta subunits, the fifth position can be occupied with an additional alpha or beta subunit, or an accessory subunit such as α5 or β3 [86-88]. Accessory subunits can only be incorporated into the fifth

position of a pentamer, as they cannot bind ligands or form functional receptors on their own. The α5 subunit possesses the necessary cys-cys pair to be characterized as an alpha subunit, but lacks one of the key aromatic residues to enable agonist binding. In this case, the tyrosine in position 198 is substituted for an aspartic acid residue, unable to participate in the cation-π interaction required to stabilize an agonist. In the case of the β3 subunit, a tryptophan residue in loop D is absent, preventing ligand binding on the complementary face [89]. Incorporation of an accessory subunit can further alter receptor trafficking or function. For example, it has been shown that the α4β2α5 and α4β2β3 subtypes have higher calcium permeability than $(\alpha4)_2(\beta2)_3$, comparable to $(\alpha4)_3(\beta2)_2$ [81]. The β3 subunit also mediates striatal dopamine release in α6* containing nAChRs [88].

1.3 Major nAChR Subtypes and Distribution

In the central nervous system, the most abundant subtypes of nAChRs are composed to α4, β2 and α7 subunits, as shown in Figure 1.3. Other subunits are localized to more specific regions of the brain, such as α6, or can also be found throughout the peripheral nervous system, such as α3 and β4. The majority of nAChR capable of binding nicotine with high affinity are thought to be α4β2* [90]. Due to a possibility of the inclusion of other types of subunits, IUPHAR nomenclature includes an asterisk (*) to signify other subunits may be present in the pentamer. In general, neuronal nAChR are primarily located on the presynaptic terminus. Here, nAChRs are the target of tonically released acetylcholine, and are believed to modulate neurotransmitter release [91].

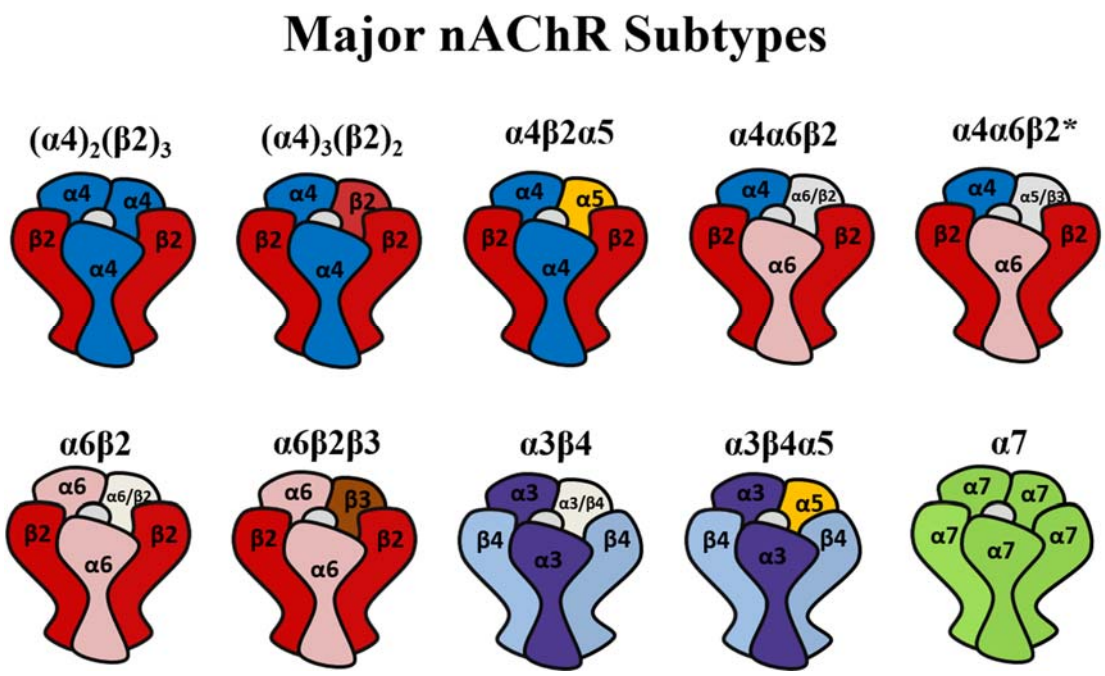

Figure 1.3 Major nAChR subtypes in the brain. The most common subtypes in the brain contain β2* subunits. Subtypes containing α6, α3 or β4 are localized to more specific regions.

1.3.1 α4β2 Subtype*

The α4β2* subtype accounts for more than 90% of high affinity binding sites within the brain [92, 93]. In β2 knock-out models, all high affinity nicotine binding sites are eliminated [94]. Knocking out α4 decreases high affinity binding sites, but compensation from other α subtypes is possible in these models [95]. This suggests the majority of nAChRs are, at least partially, composed of α4 and β2 subunits. The α4β2 subtype has a 100-fold higher affinity to nicotine than any other subtype, with K_i equal to 1-3 nM [96]. The α4β2* is also the subtype with the highest functional sensitivity to nicotine, inducing a response at a concentration of 116 nM in the high sensitivity $(\alpha4)_2(\beta2)_3$ stoichiometry and 2700 nM in the low sensitivity $(\alpha4)_3(\beta2)_2$ stoichiometry in clonal cell lines [80, 97-99]. The low sensitivity $(\alpha4)_3(\beta2)_2$ stoichiometry also shows higher permeability to calcium [81]. Overall, the α4β2* subtype is recognized by high affinity for nicotine.

The highest levels of this subtype are typically found within the midbrain regions and cortex, making them important mediators of memory, cognition, and sensory processing [45, 51]. Nicotine induced activation of subtypes containing α4* are required for nicotine reward, tolerance and sensitization [100]. The α4β2* subtype, particularly the β2 subunit, is required for systemic nicotine reinforcement [101-104]. Specifically, β2 present in the ventral tegmental area (VTA) is crucial for nicotine self-administration and tolerance [18, 105, 106]. Beta 2 knock-out models also show a decrease in cognitive function, while α4 knock-out models lose neuroprotective effects and conditioned place preference for nicotine [100, 107]. These data suggest α4β2 plays a role in rewarding properties of nicotine.

1.3.2 α6β2 and β3 Subtypes*

α6* subtypes are characterized by selective antagonism to α-conotoxin MII [108]. As another subtype containing the β2 subunit, α6β2* is also required to establish systemic nicotine reinforcement and self-administration. The α6 subunit is often coexpressed with α4, as seen in the dopaminergic neurons of the VTA, although each cannot functionally compensate for the absence of the other in knock-out models [18]. Alpha 6 subunits are typically localized to dopaminergic neurons, such as within the VTA, substantia nigra, and locus coeruleus [109, 110]. The α6 subunit has also been shown to contribute to the locomotor stimulating effects of nicotine, potentially due to enhanced transmission in these regions [111, 112]. An accessory subunit, β3, often assembles with the α6β2 subtype. The gene coding for this subunit is part of the CHRNB3/CHRNA6 gene cluster on chromosome 8, along with α6 [113]. Addition of β3 is shown to impact striatal dopamine release and related behaviors [88]. Incorporation of the β3 subunit also increases expression of α6β2 and alters the response to nicotine [114, 115]. Together, α6β2* subtypes may be involved in nicotine reward and withdrawal [116].

1.3.3 α7 Subtype*

The α7 subtype typically exists as a homopentamer, but recent evidence suggests β2 can also be incorporated into the functional pentamer [117-119]. The α7 subtype is the second most common subtype in the brain. Unlike α4β2, α7 has a very low affinity for nicotine, but is able to bind the muscle-type antagonist, α-bungarotoxin, with high specificity [10, 120]. This subtype is characterized by fast activation, fast rates of desensitization, and high calcium permeability [64, 121], giving it a role in slower calcium

dependent intracellular signaling [122]. It is involved in recent learning and neuronal plasticity [123], in addition to rapid signaling and neurotransmitter release. The α7 subtype is distributed throughout the brain, and is most prominent in the hippocampus, hypothalamus, and cortex regions [45]. Data from α7 knock-out mice suggest this subtype may mediate long term effects of nicotine, but is not involved in the acute rewarding effects of nicotine [18].

1.3.4 α3β4 and α5 Subtypes*

The ganglionic nAChR subtype, α3β4, are localized to very specific regions of the brain, such as the thalamus, medial habenula, and interpenduncular nucleus, but express abundantly throughout the peripheral nervous system [124, 125]. They have a lower affinity for nicotine than α4β2*, and are therefore less likely to be desensitized at the concentrations of nicotine often seen in smokers [126]. Although α3 knockout mice suffer from high perinatal mortality, β4 knockouts have provided insight into the role of α3β4 on nicotine-mediated behaviors. The β4 subunit has been connected to the aversive properties of nicotine, including effects of withdrawal [127], seizures [128], and anxiety [126]. In addition, overexpression of β4 increased nicotine self-administration [126].

The α3 and β4 subunits are often co-expressed with an accessory subunit, α5. The α5 is therefore often incorporated into the fifth position of the α3β4 pentamer. The genes coding for these three subunits are part of the CHRNA5/CHRNA3/CHRNB4 gene cluster on chromosome 15q25 [129-131]. Incorporation of the α5 subunit alters desensitization and calcium permeability in α3* nAChRs [132]. Knock out models of α5 self-administer greater amounts of nicotine, and have higher rates of desensitization on dopaminergic

neurons [133]. The accessory α5 can also be assembled with α4β2*, where it increases receptor function [134]. Single nucleotide polymorphisms within the CHRNA5/CHRNA3/CHRNB4 gene cluster have also been connected to an increased risk of nicotine dependence and small-cell lung cancer causally related to cigarette smoking [135-138]. One such variant is a single nucleotide polymorphism in the α5 sequence that translates to an amino acid change from aspartic acid to asparagine at position 398 (α5-D398N) [139, 140]. This D398N variant increases the risk of tobacco dependence by about 30% in individuals with just one allele with the polymorphism, and is also associated with the "pleasurable buzz" from tobacco use [141]. Although α5 does not appear to influence the development of nicotine dependence, this subunit might affect self-administration of nicotine. Together, α3β4α5 may play a modulatory role in nicotine reward pathways.

1.4 Nicotine Induced Upregulation of nAChRs

1.4.1 Upregulation of α4β2 in the Brain*

In vivo fMRI and PET measurements have shown that smokers have 25-330% more nAChRs compared to non-smoker [142-144]. Chronic nicotine exposure is known to alter reward systems within the brain. It is suspected that nicotine alters dopamine reward circuits to increase their sensitivity to successive nicotine exposure. Some studies suggest nicotine dependence is initiated by activation of the ventral tegmental area, ultimately resulting in dopamine release into the nucleus accumbens [145, 146]. Regardless, nicotine exposure increases dopamine release in midbrain regions [57, 147-149]. In an attempt to resolve a mechanism for these changes, upregulation of nAChRs as a result of nicotine exposure has been given significant interest. Countless articles have implicated

upregulation in the addictive nature of nicotine [6, 45, 46, 55, 64, 66, 76, 150, 151]. Since its discovery in 1983, the definition of upregulation has evolved to fit current evidence, although a mechanism of this upregulation is yet to be resolved. At this time, nAChR upregulation is considered an increase in receptor number, as well as changes in trafficking and stoichiometric assembly [55, 97, 152-155]. Due to complex cellular processes that affect upregulation, the mechanism and functional consequences are yet to be understood. However, it is now accepted that this upregulation is post-translational, evident by a lack of change in receptor subunit mRNA levels [150, 156]. It is therefore believed that post-transcriptional mechanisms are responsible for increases in nAChR abundance.

The upregulation of nAChRs is brain region and cell type specific. Upregulation is robustly measured in the brainstem, cerebellum, prefrontal cortex, and hippocampus [156-159]. Other regions, such as the thalamus and medial habenula, appear to be less affected, if at all [160, 161]. In some regions, such as the VTA and substantia nigra, a cell-specific effect has been reported. In the midbrain, α4* nAChRs upregulate in GABAergic neurons of the VTA, substantia nigra pars reticulata (SNr), and substantia nigra pars compacta (SNc) [158, 162]. In contrast, no upregulation has been detected on dopaminergic neurons of these regions. Differences in α4* containing subtypes and stoichiometries between these regions has been proposed as a possible explanation. It is suggested that GABAergic neurons in these regions contain α4β2α5 nAChRs, in addition to α4β2 [163]. Nicotine might alter the incorporation of α5, leading to an upregulation of receptors. However, dopaminergic neurons in these regions express many variations of β2* containing nAChRs, including α4β2*, α4α6β2*, and α6β2* [164, 165]. The lack of upregulation seen in dopaminergic neurons may suggest that α4β2* are assembled with

other subunits, such as α6. The upregulation of α4β2* is accompanied by an increase in sensitivity to nicotine [166]. This is thought to be the result of an increase in the number of high sensitivity $(\alpha4)_2(\beta2)_3$ stoichiometry receptors in relation to $(\alpha4)_3(\beta2)_2$ stoichiometry [81, 97, 154, 167]. As a result of chronic nicotine exposure, nAChRs respond to lower concentrations of acetylcholine and other agonists as the sensitivity to stimulation is increased.

The pharmacological consequences of these changes in α4* expression are not well defined. Some studies suggest the increase in α4* of the GABAergic neurons of the VTA increases the baseline firing rate and excitatory effect of nicotine in these neurons, while the baseline firing rate and excitatory effects are decreased in dopaminergic neurons. This would mean it is possible that upregulation on GABAergic neurons increases inhibition of dopaminergic neurons in the VTA [162, 168, 169]. Other studies have shown nicotine increases firing frequency of dopaminergic neurons of the VTA [145, 146]. These measurements could be subtype dependent. The α6 subunit is robustly expressed in dopaminergic neurons of the VTA, and therefore is likely to co-assemble with α4 and β2 subunits in this region. However, the functional role of α6* within this region is not fully resolved [18, 112]. Based on current studies, it is likely that α4* and α6* subunits affect the function of dopaminergic neurons in the VTA.

1.4.2 Effects of Other nAChR Ligands

Most smoking cessation agents on the market today have targeted the α4β2* subtype. One such drug, cytisine, is an alkaloid isolated from the seeds of *Cytisus laborinum*. This drug has been available for more than 40 years. It is currently available

in Europe [151, 170-172], and has a similar efficacy to FDA-approved drugs available in the United States [173, 174]. Cytisine acts as a partial agonist at α4β2, and a full agonist of α7 and α3β4 [151]. Cytisine has been shown to upregulate α4β2, as well as alter the stoichiometry. While nicotine increases the assembly of the high sensitivity, $(\alpha4)_2(\beta2)_3$ isoform, previous studies suggest cytisine exposure results in a preference for the low sensitivity, $(\alpha4)_3(\beta2)_2$, receptor at the plasma membrane [85, 151, 154]. A potential explanation for this difference lies in recent evidence that an additional binding site for cytisine exists at the α/α interface within $(\alpha4)_3(\beta2)_2$ [82, 175]. Another α4β2 partial agonist, varenicline, is available as a smoking cessation agent in the United States [176]. This drug, a derivative of cytisine, also acts as a full agonist at α7 nAChRs, and exhibits weak actions at α3β2 and α6β2 [177]. Varenicline has also been shown to increase expression of α4β2 [176, 178], and may decrease α6β2 nAChRs. Mecamylamine, a nonselective nAChR antagonist, also facilitates smoking cessation [179]. However, it is not commonly used in smoking cessation today due to its widespread ganglionic side effects. This drug is a noncompetitive open channel blocker that also upregulates α4β2 nAChRs [150]. Bupropion, originally marketed as an antidepressant in 1989, has also been approved as a smoking cessation agent [180, 181]. Recently, bupropion was determined to act as a noncompetitive antagonist of nAChRs. Photoaffinity labeling studies show bupropion has two distinct binding sites on the *Torpedo* nAChR. One high affinity site is found in the middle of the ion channel, within TM2. A second site is near the extracellular end of TM1 within α subunits [181]. Another interesting nAChR ligand, sazetidine A, shows stoichiometry dependent binding properties. This nicotine analog acts as a partial agonist at the $(\alpha4)_2(\beta2)_3$ isoform but as an antagonist at the $(\alpha4)_3(\beta2)_2$ isoform [182, 183]. Overall,

a variety of pharmacological agents with various binding properties interact with specific nAChR stoichiometries or induce upregulation of these receptors, summarized in Table 1.1. This is a key factor when targeting specific subtypes for development of more effective smoking cessation agents.

1.4.3 Upregulation Theories

Upregulation of nAChRs has been measured in a variety of samples, including humans, mice, cultured neurons, and clonal cell lines [68, 184, 185]. In both humans and rodents, nicotine induced upregulation is detected throughout the midbrain, prefrontal cortex, brainstem, and cerebellum [115, 156, 159, 168]. The robustness of upregulation suggests a common mechanism is responsible between samples. However, the exact mechanism of upregulation has not been resolved although many suggestions have been put forward. Long standing theories include upregulation as a result of activation or desensitization [186]. The assumption was that nAChR activation initiates Na^+ and Ca^{2+} flux to alter downstream events. These theories are being phased out, at least for most subtypes, in response to findings that upregulation occurs at concentrations lower than required for activation. Upregulation has been measured at 100 nM nicotine, when less than 4% high sensitivity $(\alpha4)_2(\beta2)_3$ are activated, while no low sensitivity $(\alpha4)_3(\beta2)_2$ are activated [55]. In addition, antagonists have been shown to upregulate, suggesting ion flow is not required for an increase in receptor number [150, 187, 188]. However, the binding of ligands to nAChRs is likely necessary for upregulation to occur [187], even if this is independent of receptor activation or desensitization. Although nAChR activation or

Table 1.1: nAChR Ligand Properties

Ligand	Type	Cessation Efficacy (12 Months)	nAChR Upregulation?
Nicotine	Agonist	18%	Yes
Cytisine	Partial Agonist: α4β2 Full Agonist: α7, α3β4	14%	Yes
Varenicline	Partial Agonist: α4β2 Full Agonist: α7	20.5%	Yes
Mecamylamine	Noncompetitive Antagonist Nonselective Open Channel Blocker	40%	Yes
Bupropion	Noncompetitive Antagonist αTM1 or TM2	15.2%	N/A
Sazetidine A	Partial Agonist: $(\alpha4)_2(\beta2)_3$ Antagonist: $(\alpha4)_3(\beta2)_2$		

desensitization might not be required for upregulation, both are likely to contribute to behaviors related to nicotine addiction [189].

Another mechanism suggests surface binding is able to increase without an increase in receptor number, as receptors change conformation to a high affinity binding state [190, 191]. This conformational change interpretation suggests upregulation is independent of increases in trafficking through the secretory pathway or a net increase in receptors on the plasma membrane. Instead, the mechanism suggests nAChRs transition into an "upregulated" high affinity state on the plasma membrane, allowing the same number of receptors to bind a higher concentration of ligand [190, 191]. Since other detection methods, independent of binding detection, show an increase in nAChR number, this event is unlikely to be responsible for robustly measured increases in nAChRs, but is perhaps complementary to the primary mechanism of upregulation.

An increase in nAChR stability on the plasma membrane has also been suggested, although contradictory results have been reported for this mechanism. This includes a decreased turnover on the plasma membrane, and slower internalization and degradation to result in a net increase in number of nAChRs on the plasma membrane [97, 188]. Early studies using high nicotine concentrations found a four-fold increase in the time receptors remain on the plasma membrane surface after inhibition of protein synthesis [188]. Surface biotinylation in conjunction with more physiologically relevant nicotine concentration also show a large increase in half-life of nAChRs on the plasma membrane [97]. Increased half-life of nAChRs as a result of decreased ER degradation, and consequently increased subunit assembly [191] has also been proposed. Other studies, at varying concentrations of nicotine, fail to detect any differences in nAChR turnover upon

nicotine treatment [152, 153, 190], and contribute changes to trafficking. At this point, it is unclear if nicotine increases stability of nAChRs, and perhaps works synergistically with other mechanisms to increase membrane expression of nAChRs.

Recently, evidence has strongly supported the theory that nicotine acts intracellularly to induce upregulation, known as "inside-out" neuropharmacology [160]. Indications for an intracellular mechanism include increased maturation enhancement of subunits and pharmacological chaperoning effects in the presence of nicotine [55, 97, 115, 123, 153]. A pharmacological chaperone binds the target protein and stabilizes this protein in its most stable state [160]. These effects are measured at low concentrations of nicotine, 100-200 nM, that remain in the brain of smokers at a steady state [192, 193]. This hypothesis began in the mid 90's, following evidence that nicotine exposure increased an intracellular storage of nAChRs that was undetectable from surface binding mechanisms [194]. Further evidence suggests 85% of high affinity [^{3}H]-epibatidine binding sites are located intracellularly [195]. Nicotine and other ligands are able to permeate cell membranes, interact with intracellular receptors, and alter the expression of nAChRs. Intracellular actions of nicotine influence pharmacological chaperoning, matchmaking, and intracellular trafficking [152, 160]. In early stages of subunit maturation, glycosylation sites are occupied to facilitate movement towards the plasma membrane. This maturation is a slow, inefficient process that dramatically increases in the presence of nicotine [153]. As a pharmacological matchmaker, nicotine stabilizes subunit-subunit interactions. FRET, Förster resonance energy transfer, measurements have provided evidence that nicotine increases these inter-subunit interactions by showing α4 and β2 subunits are in close proximity within the whole-cell region measured, which includes the endoplasmic

reticulum [115, 196, 197]. As a pharmacological chaperone, nicotine would act as a stabilizing agent for the lowest energy conformation of nAChRs. This requires binding at a pharmacologically relevant site on the substrate. Nicotine then facilitates movement of nAChRs through the secretory pathway, ultimately resulting in an increase of nAChRs located on the plasma membrane. It has been shown that intracellular cycling is a necessary component for upregulation. Brefeldin A, an inhibitor of anterograde transport, blocks nicotine-induced upregulation [152]. The number of ER exit sites and density of nAChRs at these sites is increased, indicating anterograde transport, mediated by COPII, is increased [198]. Retrograde transport, mediated by COPI, is also required to achieve upregulation. Mutations of COPI binding motifs prevent upregulation in the presence of nicotine without altering the increase in ER exit sites and density [115].

Regardless of the mechanism, upregulation involves changes in receptor trafficking, subunit assembly including changes in stoichiometry, changes in ER export and vesicle transport, and increases in number of receptors on the plasma membrane. New evidence continues to suggest an intracellular mechanism for these processes, but definitive evidence of changes within the endoplasmic reticulum are yet to be resolved. Future efforts in the development of therapeutics may target similar substrates as nicotine, and modulate pharmacological chaperoning and intracellular trafficking as well. Therefore, understanding the mechanism of nicotine induced upregulation is vital to understanding the process of nicotine addiction.

1.5 Novel Methods to Study nAChRs

1.5.1 Fluorescence Microscopy

Advances in the understanding of nAChR expression and upregulation are, in part, due to improvements in measurement techniques. In the last two decades, the use of fluorescence microscopy has expanded rapidly in biological imaging. Fluorescence microscopy has allowed investigators to monitor protein dynamics, study protein interactions and expression, resolve structures, and determine cellular pathways. Fluorescence measurements are enabled by labeling proteins and subcellular components with fluorescent probes. Such labels are often fluorophore conjugated antibodies, stains, organic dyes [199, 200], quantum dots [201], or fluorescent proteins. The ability to selectively label biomolecules of interest, coupled with high sensitivity detection, makes fluorescence microscopy an exceptionally powerful technique.

Fluorescent probes, or fluorophores, are able to specifically identify target cells, proteins, or subcellular components amongst nonfluorescent background. This is possible because fluorophores are excited by specific wavelengths of excitation and subsequently emit light of longer wavelength. The most basic principle of fluorescence microscopy is to excite the fluorescent component of the sample with the desired wavelength, and collect exclusively the emitted fluorescence from the sample, demonstrated in Figure 1.4. Separation of excitation and emission wavelengths is accomplished using appropriate filters. The wavelength of excitation, typically from a laser or lamp, passes through an excitation filter to allow passage of only the specific, desired wavelength. The filtered wavelength then reflects off a dichroic mirror before passing through the objective towards the sample. Once the excitation wavelength reaches the sample, fluorophores emit a longer

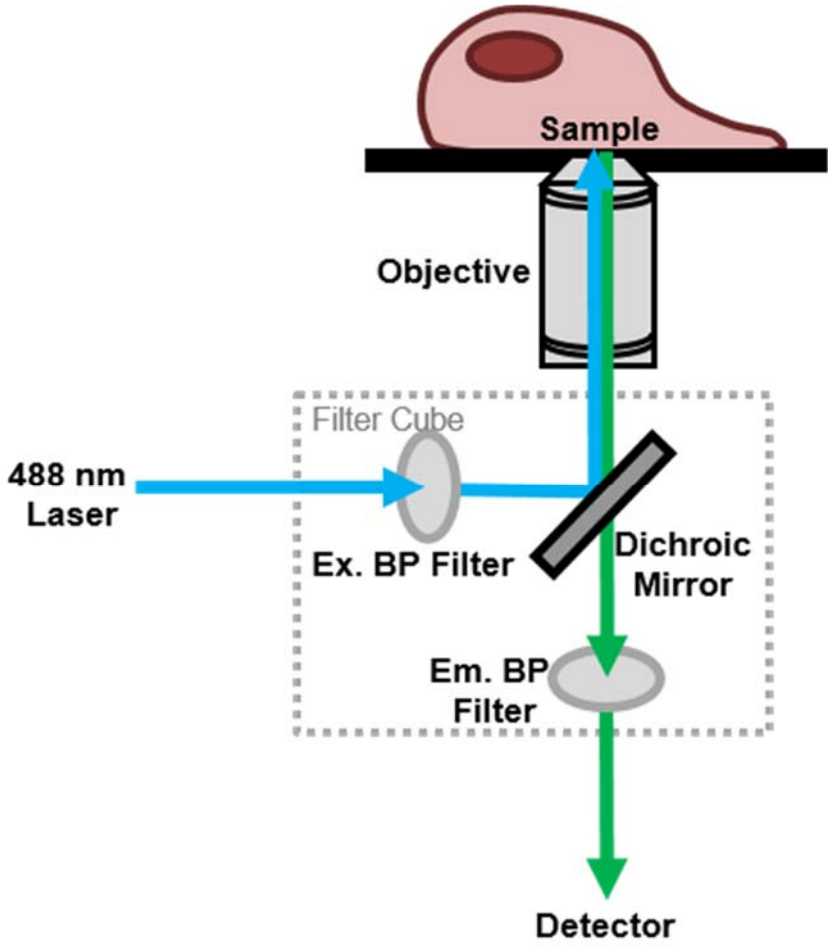

Figure 1.4 Basic setup of a fluorescence microscope. The excitation beam passes through a bandpass (BP) filter, reflects off a dichroic mirror, and passes through the objective lens before reaching the sample. Upon excitation, fluorophores in the sample emit a longer wavelength of radiation that is able to pass through the dichroic mirror and a bandpass filter to be collected by a detector.

wavelength of light. This emission is collected by the objective before subsequently passing through a barrier filter blocking the stronger, shorter excitation wavelength. Also, since the emission wavelength is longer than that of excitation, it is able to pass through the dichroic mirror towards the detector. The intensity of emission is quantifiable, as it is a relative measure of concentration of fluorophore present.

1.5.2 Green Fluorescent Protein and Derivatives

A key milestone in the advancement of fluorescence microscopy was the discovery of green fluorescent protein (GFP) [202, 203]. GFP, like all fluorescent proteins, are genetically encoded reporter molecules. The primary amino acid sequence for GFP is directly incorporated into the amino acid sequence of the protein of interest. Since expression of the fluorophore is genetically linked to expression of the protein of interest, sensitivity is increased and nonspecific binding issues are eliminated [203]. Since its isolation from the *Aequorea victoria* jellyfish in 1991, GFP has been crystallized [204] and cloned [205]. Since these early studies, GFP has been engineered to produce a wide class of fluorescent proteins, varying in wavelengths of excitation or emission across the visible spectrum [203].

The 27 kDa structure of GFP consists of 11 beta-sheets folded into a beta-barrel, with an alpha-helix located along the central axis, as shown in Figure 1.5 [206]. This structure is essential to stabilize the tripeptide that acts as the fluorophore component of the structure. This tripeptide contains residues of Ser65, Tyr66, and Gly67. The wild-type GFP from the *Aequorea victoria* jellyfish has a major excitation peak at 395 nm, with emission at 508 nm, and a minor excitation peak at 475 nm with corresponding emission

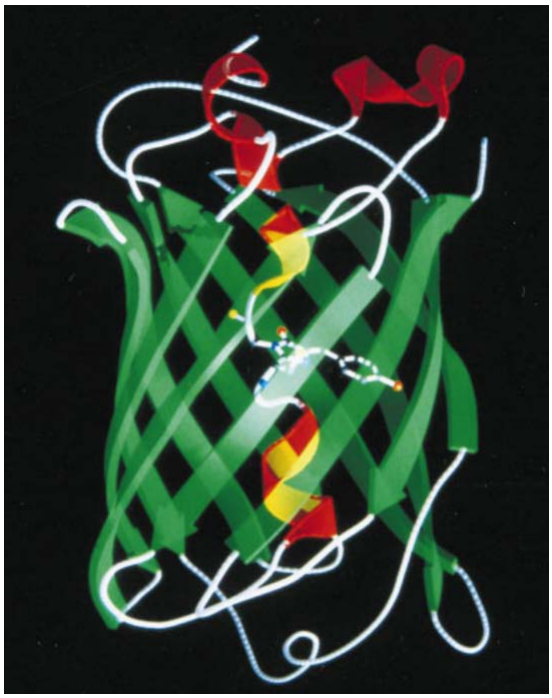

Figure 1.5 Structure of GFP. A three-dimensional ribbon diagram of wild type GFP isolated from *Aequorea victoria* jellyfish. The structure contains 11 beta sheets, shown in green, alpha helices shown in red, and the three amino acid chromophore.

at 503 nm [207]. In order to fold more efficiently at 37ºC, the most commonly used variant is enhanced green fluorescent protein, or eGFP. This contains key mutations of F64L and S65T to increase stability at physiological temperature and shift the maximum excitation wavelength to 488 nm, and emission to around 508 nm [202, 208]. Other variants, derived from the mutagenesis of GFP, range in photostability, photoactivability, or pH sensitivity, allowing the choice of fluorophore to be tailored to a particular application [202]. GFP based techniques have been used to study countless biological systems, including the nAChRs. Fluorescent proteins have been successfully expressed in a diverse set of systems, including cultured cells, neurons, and even mice [35, 168, 209] GFP and variants have been used to measure nAChR trafficking, subcellular distribution, and expression levels throughout the cell and on the plasma membrane [85, 115, 168, 198, 210].

1.5.3 Total Internal Reflection Fluorescence Microscopy

Superior spatial and temporal resolution can be achieved with specialized fluorescence microscopy techniques. One such technique is total internal reflection fluorescence, or TIRF. This technique utilizes totally internally reflected excitation light to selectively excite fluorophores near a sample-glass interface, such as adherent cells on a glass coverslip. By focusing on just one optical plane at this interface, TIRF minimizes out-of-focus fluorescence and increase the signal-to-noise ratio, particularly at the plasma membrane. Specifically focusing on the plasma membrane is particularly useful when evaluating nAChRs, since the majority of nAChR are thought to be internal [195]. Total internal reflection of the excitation beam occurs at the interface of two materials with

different refractive indices [211, 212]. In objective-style TIRF, illustrated in Figure 1.6, the laser beam is transitioned laterally across the back aperture of the objective lens using a stepper motor. The beam penetrates through the coverslip, and reflects off the lower refractive index sample. If the angle of incidence is greater than the critical angle, the beam is totally internally reflected, forming an evanescent wave. The critical angle, in relation to the normal, is given by Snell's law:

$$\Theta_c = \sin^{-1}(\eta_1 / \eta_2) \qquad \text{(Eq. 1.1)}$$

where η_1 is the lower refractive index of the sample while η_2 is the higher refractive index of the coverslip. For cell based studies, the numerical aperture of the objective must be higher than the 1.38 refractive index of the cell sample to reach TIR.

If the angle of incidence is less than the critical angle, excitation light is able to propagate through the entire sample. This is seen in traditional wide field imaging, or epifluorescence mode. If the beam of excitation is parallel to the normal, or at some angle less than the critical angle, fluorophores throughout the entire cell are excited (Figure 1.6A). Once the beam passes the critical angle, only fluorophores located within the evanescent field are excited (Figure 1.6B). The evanescent wave decays exponentially with distance from this sample-coverslip interface, and is responsible for excitation of fluorophores when TIRF is achieved. Typically, this evanescent wave penetrates approximately 150 nm into the sample, meaning only fluorophores within this region are excited. In a cellular sample, this corresponds to fluorophores, or fluorescent proteins integrated with a nAChR near the plasma membrane to be detected. This increases the signal to noise ratio since background fluorescence from the intracellular region is reduced or eliminated [211, 212].

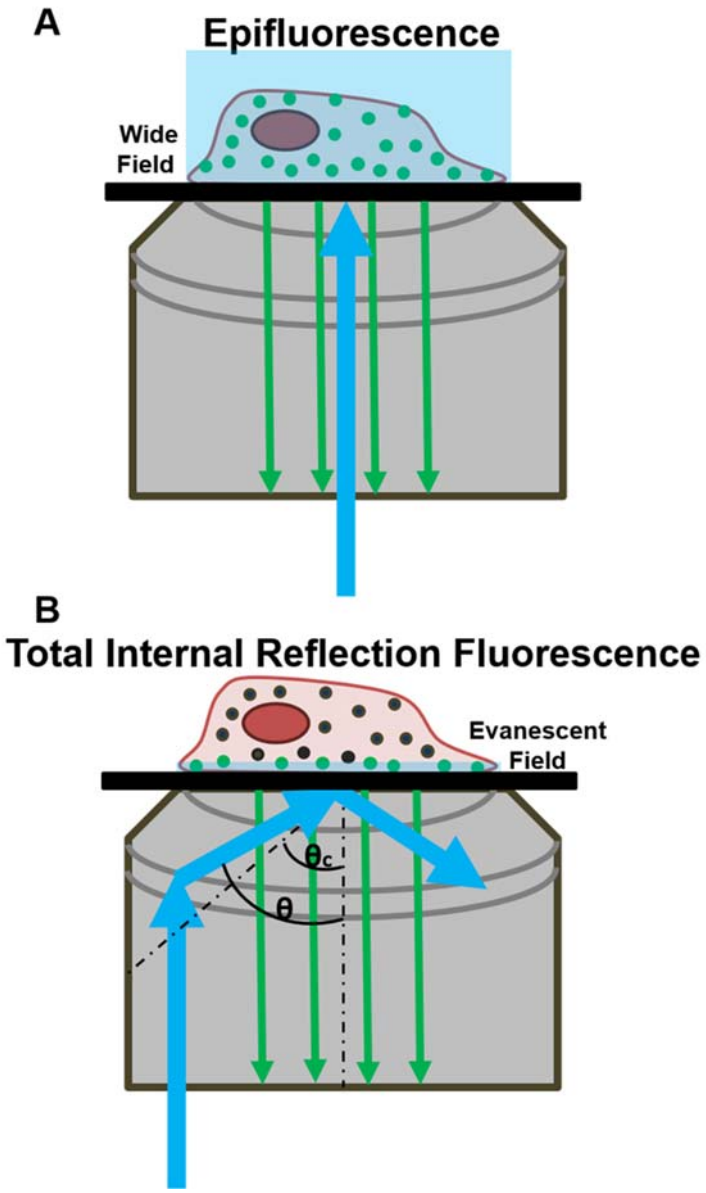

Figure 1.6: Schematic of epifluorescence and total internal reflection fluorescence. (A) In epifluorescence, a wide field of excitation passes through the entire depth of a sample, exciting fluorophores throughout the sample. (B) In total internal reflection fluorescence (TIRF), the beam of excitation approaches the sample at an angle higher than a critical angle (Θ_c), causing total internal reflection of the incoming beam. The resulting evanescent wave is responsible for exciting fluorophores within approximately 150 nm from the sample-coverslip interface.

Photodamage to a living specimen is also reduced since the majority of the cell is not exposed to radiation, allowing live cell imaging over the course of time.

Due to increased resolution at the plasma membrane, TIRF is ideally suited to measure cellular events in this region. TIRF has been successfully used to monitor endocytosis [213, 214], exocytosis [215], and intracellular signaling events [216]. TIRF has also been used to image nAChRs coupled to a pH sensitive derivative of GFP, superecliptic pHluorin (SEP) [198] to determine subcellular localization and trafficking. Due to the high resolution and sensitivity achievable with TIRF, subcellular localization and trafficking dynamics of membrane receptors can be resolved with SEP [217, 218].

1.5.4 Single Molecule Fluorescence Microscopy

Ensemble techniques, simultaneously detecting multiple fluorophores, have been quintessential in most recent advancements in the understanding of subcellular components [219]. These bulk studies have been used to elucidate structure and cellular dynamics for many biological systems. Recent advances in fluorescence microscopy have led to the development of complementary single molecule techniques. These single molecule techniques measure fluorescence from a single fluorophore to provide a more detailed understanding of biological processes measured with ensemble techniques. Ensemble techniques, due to detection of multiple fluorophores, measure an average intensity across an entire sample. Due to the averaging of multiple signals, individual dynamics are lost. Single molecule techniques, on the other hand, are able to detect specific structural and kinetic events by resolving measurements from a individual fluorophore. Such techniques

have been used to help resolve dynamics of many complex biological systems to date, including ion channels [220-224].

One commonly used single molecule technique is single molecule photobleaching. In biological samples, there is rising interest in detecting photobleaching of a GFP genetically encoded into a protein of interest. An inherent property of fluorophores is that, eventually, they transition into a dark state upon continuous excitation, known as bleaching. The photobleaching of a single GFP molecule is a discrete process, meaning fluorescence intensity will decrease as a stepwise decay. This is ideal to measure structural properties of complex biological proteins, such as the nAChRs. Since a single GFP molecule corresponds to a single stepwise decrease in intensity, the number to steps reveal the number of GFP molecules, or GFP-labeled subunits, that are present in the complex. Limitations of single molecule techniques are mostly based on signal sensitivity. Labeled membrane proteins, including nAChRs, diffuse along the plasma membrane and accumulate in high densities [225]. Autofluorescence from the bulk of the cell makes it difficult to isolate a single GFP or nAChR. Also, higher excitation intensities are required to produce emission that is intense enough for detection. In order to reduce these complications, new techniques are being developed to isolate single receptors.

CHAPTER 2: OVERVIEW AND STATEMENT OF PROJECTS

2.1 Project Motivation and General Overview

One of the most well-documented effects of chronic nicotine exposure is the upregulation of its target, nAChRs. This upregulation of nAChRs is believed to contribute to the addictive nature of nicotine, although functional consequences are not completely understood [6, 45, 55, 64, 66, 76]. Upregulation of nAChRs is defined as an increase in receptor number, changes in receptor trafficking, or altered assembly of stoichiometry. The upregulation of α4β2* is accompanied by an increase in sensitivity to nicotine. This is the result of an increase in the number of high sensitivity $(\alpha4)_2(\beta2)_3$ stoichiometry receptors compared to $(\alpha4)_3(\beta2)_2$ stoichiometry [81, 97, 154]. As a result of chronic nicotine exposure, nAChRs respond to lower concentrations of acetylcholine and other agonists as the sensitivity to stimulation is increased. Despite significant research interest, a full mechanism for upregulation has not been resolved. New evidence continues to converge on the idea an intracellular mechanism is responsible for these processes, but definitive evidence of changes within the endoplasmic reticulum need to be detected. Nicotine and other ligands are thought to permeate cell membranes, interact with intracellular receptors, and alter the expression of nAChRs. Evidence for an intracellular mechanism for nicotine induced effects include pharmacological chaperoning, matchmaking, and intracellular trafficking [160]. Upregulation has been robustly measured in a variety of systems, yet seems to be cell type and brain region dependent *in vivo.* Also, upregulation has been documented as a result of exposure to both agonists and antagonists. Understanding these changes on a mechanistic level is important to the development of nAChRs as drug targets. For this reason, cutting edge methodologies are being developed and employed to pinpoint

distinct changes in localization, assembly, export, vesicle trafficking and stoichiometry in order to further understand the physiology of these receptors. In an effort to develop more effective therapeutics, nicotine's role in modulating upregulation needs to be better defined. This dissertation utilizes novel techniques to elucidate the mechanism of nicotine induced upregulation to identify target nAChR structures for the development of smoking cessation therapeutics.

2.2 Cotinine Alters Expression, Trafficking, and Assembly of a Subset of nAChRs

Traditionally, the importance of nicotine's primary metabolite, cotinine, has been limited to a biomarker of nicotine exposure [14]. More recently, cotinine has been shown to also be a pharmacologically active compound, reducing effects of chronic stress and increasing cognitive and executive function [23, 37]. Cotinine has been shown to cross the blood-brain barrier [40] and acts as a partial agonist to nicotinic acetylcholine receptors [41-44]. Also, tobacco exposure leads to the accumulation of cotinine throughout the body due to cotinine's long pharmacological half-life [3, 26]. However, nAChR expression studies have focused almost exclusively on nicotine's effects, with few studies considering the effect of cotinine or other nicotine metabolites on nAChR assembly or trafficking [38]. Since nicotine and cotinine are structurally similar, differing by only an acetyl group (Figure 1.1), we hypothesized that cotinine could induce similar changes as nicotine in trafficking and expression of nAChRs, and therefore may be at least partially responsible for physiological effects previously attributed to nicotine exposure. To test this hypothesis, transiently transfected Neuroblastoma (N2a) cells were exposed to cotinine treatment for 48 hours. The alpha subunits of an assembled nAChR pentamer were genetically labeled

with a pH sensitive version of GFP, known as superecliptic pHluorin (SEP). Total internal reflection fluorescence was used to measure expression and distribution of SEP-labeled nAChRs. We further hypothesized that cotinine may alter the assembly of α4β2, as seen with nicotine exposure. To test this hypothesis, transiently transfected human embryonic kidney (HEK-293T) cells underwent nitrogen cavitation after exposure to cotinine to encapsulate single nAChRs in nanoscale containers derived from the endogenous cell membrane. The alpha subunits of the assembled nAChR pentamer were genetically labeled with a GFP. Isolated nanovesicles underwent single molecule photobleaching upon continuous 488 nm excitation. The number of bleaching steps corresponds to the number of alpha subunits present, and thus the stoichiometry.

2.2.1 Total Internal Reflection Fluorescence (TIRF)

Due to their endogenous role as acetylcholine receptors in the central nervous system, functional nAChRs are located on the plasma membrane. Although the functional consequences of nicotine induced upregulation of nAChRs is not fully understood, receptors in this region are likely to contribute to upregulation induced effects. In order to increase resolution of fluorophore-labeled nAChRs at the plasma membrane, TIRF microscopy is used. Specifically focusing on the plasma membrane is particularly useful when evaluating nAChRs, since the majority of nAChR are thought to be internal [195]. TIRF limits detection to the plasma membrane and nearby peripheral endoplasmic reticulum to selectively quantify nAChRs within the trafficking pathway. TIRF excitation focuses on a single optical plane, limiting excitation to a narrow region extending approximately 150 nm from the interface between an adherent cell and glass. In live cells

expressing nAChRs, this excitation volume corresponds to the cell plasma membrane or nearby peripheral endoplasmic reticulum, limiting detection to nAChRs within this region.

A basic TIRF microscopy setup is illustrated in Figure 2.1. Since the nAChRs are genetically linked to an SEP fluorophore, a 488 nm diode-pumped solid state (DPSS) laser is used for excitation. The excitation beam is fiber coupled to a stepper motor, allowing the beam to be translated laterally across the back aperture of a high numerical aperature objective. In order to surpass the critical angle required to achieve TIRF, an objective with a numerical aperture higher than the refractive index of the sample (> 1.38 for cells) is required. Total internal reflection of the incident radiation forms an evanescent wave responsible for SEP excitation. Emission is collected on an electron multiplying charge coupled device (EMCCD). Since the bulk of the sample is not excited, background fluorescence is decreased and an increased signal to noise ratio at the plasma membrane is observed [211, 212].

2.2.2 Super-Ecliptic pHluorin (SEP) to Measure Expression

Super-ecliptic pHluorin (SEP), a pH sensitive variant of GFP, takes advantage of pH differences between subcellular regions within a cell. This fluorophore has been successfully incorporated into numerous receptor subunits, including AMPA, GABA, and nAChRs [198, 217, 226]. The pH sensitivity corresponds to a change in fluorescence emission based on the pH of the local environment of the fluorophore. Below a pH of 6, SEP remains in an off state, but fluoresces at higher pHs when excited with 488 nm excitation. This pH sensitive property makes SEP particularly useful to study subcellular localization and vesicle dynamics [198, 217, 226]. The alpha subunits of an assembled

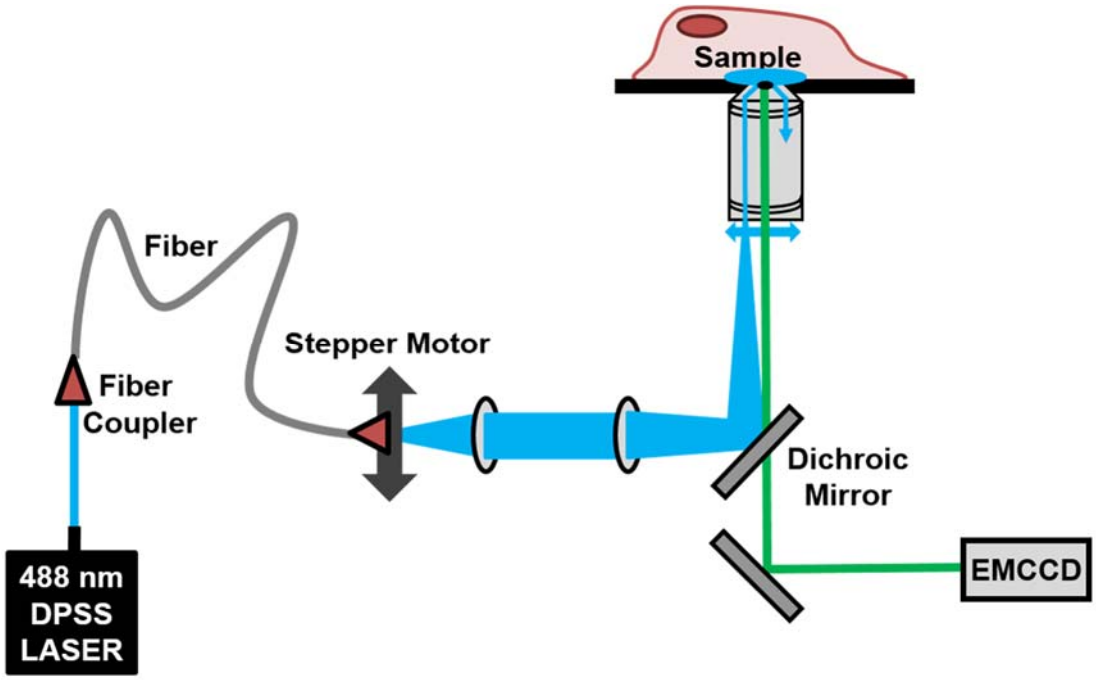

Figure 2.1 Schematic of a TIRF microscope. To excite SEP, a 488 nm DPSS laser is fiber coupled to a stepper motor. The critical angle is reached by moving the position of the incident beam laterally across the back aperture of the objective. SEP emission is detected by an electron-multiplying charge coupled device (EMCCD).

nAChR pentamer were genetically labeled with an SEP on the C-terminus of the nAChR subunit. The C-terminus of the nAChR, including the SEP, is exposed to the luminal pH in the endoplasmic reticulum and trafficking vesicles, but the extracellular pH upon insertion into the plasma membrane. Therefore, existing pH gradients within a cell, or manipulation of extracellular pH, modulates the fluorescence of SEP, enabling direct monitoring of nAChR-SEP location. Using this pH sensitive fluorophore in conjunction with TIRF microscopy allows subcellular localization and single vesicle insertion events to be resolved within the evanescent wave excitation volume. Differences in expression, distribution and trafficking of nAChRs within this field of view upon exposure to cotinine are measured.

2.2.2.1 Relative Expression and Distribution of nAChRs within Evanescent Field

The pH sensitivity of SEP enables intracellular nAChRs in the endoplasmic reticulum to be distinguished from nAChRs residing on the plasma membrane. By measuring the fluorescence intensity of the same cells at varying pHs, the relative location of SEP-labeled nAChRs within the TIRF field of view can be determined. Since SEP is pH dependent, the fluorescence of SEP-labeled nAChRs on the plasma membrane is determined by the pH of the extracellular solution. When the pH of the extracellular solution is 7.4, receptors within the peripheral endoplasmic reticulum and plasma membrane fluoresce. The extracellular solution can then be exchanged to an otherwise identical solution of pH 5.4, causing nAChRs on the plasma membrane to transition into an off state, meaning all detected fluorescence is from nAChRs within the endoplasmic reticulum [115, 198, 227]. This process is illustrated in Figure 2.2. The relative number

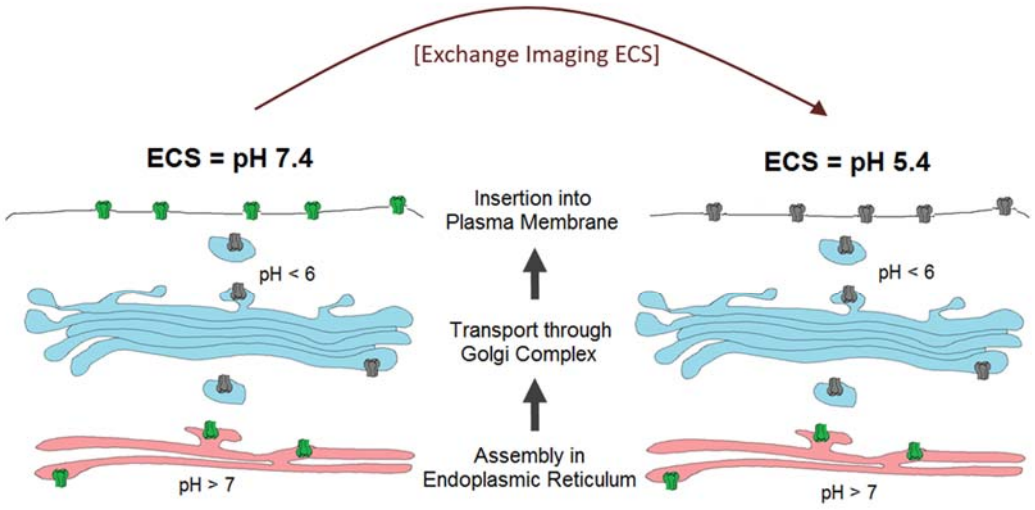

Figure 2.2 Cartoon illustrating changes in SEP detection with pH. When the extracellular solution (ECS) is at pH 7.4, SEP-labeled nAChRs in the endoplasmic reticulum and on the plasma membrane fluoresce. When the ECS is exchanged to an identical solution at pH 5.4, SEP-labeled nAChRs on the plasma membrane transition into an off state and are no longer detected.

of nAChRs on the plasma membrane, known as plasma membrane integrated density (PMID), is mathematically calculated by subtracting the integrated density of fluorescence intensity at pH 5.4, corresponding to ER resident nAChRs, from the integrated density at pH 7.4, corresponding to the total number of detected nAChRs. The difference between these values corresponds to the PMID, or relative measure of nAChRs localized to the plasma membrane, as shown in Equation 2.1.

$$PMID = Total\ ID\ (pH\ 7.4) - ER\ ID\ (pH\ 5.4) \qquad \text{(Eq. 2.1)}$$

Images of a representative cell exposed to pH 7.4 and pH 5.4 is shown in Figure 2.3. In Figure 2.3A, cells at pH 7.4 appear the most intense, with a combination of the reticulated pattern of the ER and a smoother pattern of nAChRs dispersed across the PM both visible. In Figure 2.3B, only the reticulated pattern is detected, as nAChRs located on the PM in an off state at pH 5.4. The difference, shown in Figure 2.3C, corresponds to the smoother fluorescence pattern of those nAChRs localized to the PM. The PMID of cells exposed to cotinine is measured in comparison to control cells. Upregulation of nAChRs corresponds to an increase in PMID, or relative number of receptors on the plasma membrane. Once the relative number of nAChRs on the plasma membrane is calculated, this value can be compared to the total number of nAChRs within the field of view to quantify changes in distribution as a result of cotinine exposure. PMID is divided by the total integrated density at pH 7.4, and converted to a percentage, as shown in Equation 2.2.

$$\%\ PM = \frac{PMID}{Total\ ID\ (pH\ 7.4)}\ x\ 100 \qquad \text{(Eq. 2.2)}$$

The percentage of detected nAChRs located on the plasma membrane is a measure of nAChR trafficking. Changes in % PM as a result of cotinine exposure are measured.

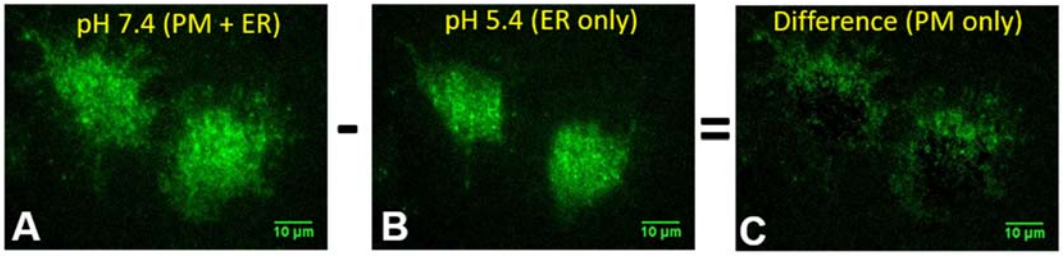

Figure 2.3 Example of an N2a cell expressing SEP-nAChRs. (A) All SEP-labeled nAChRs within the TIRF field of view fluoresce when ECS is pH 7.4. (B) SEP-labeled nAChRs on the plasma membrane fail to fluoresce when ECS is pH 5.4, meaning all detected fluorescence is from ER resident nAChRs. (C) Visual representation of the differences between cell at pH 7.4 and pH 5.4, corresponding to SEP-labeled nAChRs located on the plasma membrane.

Increases in % PM corresponds to increased trafficking of nAChRs towards the plasma membrane.

2.2.2.2 Detection of Single Vesicle nAChR Insertion Events

Since trafficking vesicles inherently have a pH less than 6, SEP-labeled nAChRs within these vesicles do not fluoresce [217]. Upon insertion into the plasma membrane, these fluorophores of the low pH trafficking vesicle are then exposed to a higher physiological extracellular pH of 7.4 at the plasma membrane, causing them to transition into an on state. This appears as a burst of fluorescence at the plasma membrane as SEP-nAChRs transition to a fluorescent state. Figure 2.4 illustrates an increase in fluorescence intensity and spreading across the membrane as nAChRs are inserted and diffuse across the plasma membrane amongst previously inserted nAChRs. The number of insertion events per cell are counted, allowing the number of trafficking vesicle arrival events to be quantified. Changes in frequency of insertion events upon exposure to cotinine are compared to control cells. An increase in the number of insertion events corresponds to an increase in the number of transport vesicles carrying nAChRs to the plasma membrane.

2.2.3 Green Fluorescent Protein (GFP) to Measure Stoichiometry

Labeling individual subunits with GFP provides a means to measure stoichiometry of assembled nAChRs. Our lab has developed a novel method that isolates individual nAChRs in nanoscale containers derived from the native cell membrane [228]. Once single nAChRs are isolated, single molecule photobleaching of GFP molecules is used to deduce stoichiometry. In these studies, the alpha subunits of the nAChR are genetically encoded

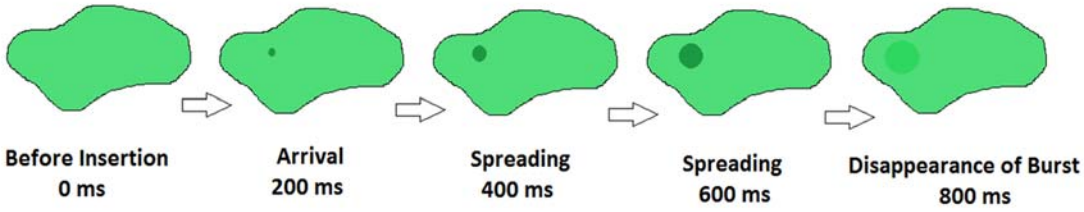

Figure 2.4 Cartoon of a single vesicle insertion event. SEP-labeled nAChRs are trafficked to the plasma membrane in low pH trafficking vesicles. Upon arrival of a trafficking vesicle at the plasma membrane, SEP is exposed to a pH of 7.4, causing these fluorophores to turn on. As the vesicle fuses with the plasma membrane, a burst of fluorescence is seen on the plasma membrane, followed by a spreading of this burst. After insertion, the newly inserted nAChRs blend in with the bulk fluorescence of previously inserted nAChRs on the plasma membrane.

with a GFP fluorophore. HEK-293T cells transiently expressing α4-GFP / β2 nAChRs underwent nitrogen cavitation to trap a single α4β2 nAChR in a nanovesicle derived from the native cell membrane. Once vesicles containing α4β2 nAChRs are formed, they are spatially isolated on a glass substrate by a conventional pull-down mechanism using an anti-GFP antibody to capture GFP-labeled nAChRs within nanovesicles. This process is illustrated in comparison to live cell SEP based experiments in Figure 2.5. Isolated nAChRs are imaged with TIRF to detect single GFP molecules. In Figure 2.6, α4-GFP/β2 nAChRs isolated on a glass coverslip (Figure 2.6B) are shown in contrast to a live cell expressing α4-GFP/β2 in TIRF (Figure 2.6A). Each field of view of isolated nAChRs undergo continuous 488 nm excitation. Changes in fluorescence intensity over time is measured for vesicles in each region. Since GFP inherently stochastically undergoes photobleaching when excited, the number of bleaching steps, or transitions into off states, can be measured. A bleaching step is measured as a stepwise decrease in fluorescence intensity, corresponding to a single fluorophore losing fluorescence. Since only one nAChR is present at each isolated location, detection of two bleaching steps corresponds to the presence of two alpha subunits, or $(\alpha4)_2(\beta2)_3$ stoichiometry (Figure. 2.7A). In contrast, detection of three bleaching steps signifies three alpha subunits are present, and thus $(\alpha4)_3(\beta2)_2$ stoichiometry. The number of bleaching steps detected in vesicles derived from cells exposed to cotinine are compared to control vesicles. Counted bleaching steps are fit to a binomial distribution, accounting for a 90% probability that GFP will be folded correctly and fluorescent during experimentation. The fitted distribution provides a ratio of α4β2 isoforms present at each condition. An increase in the number of vesicle showing

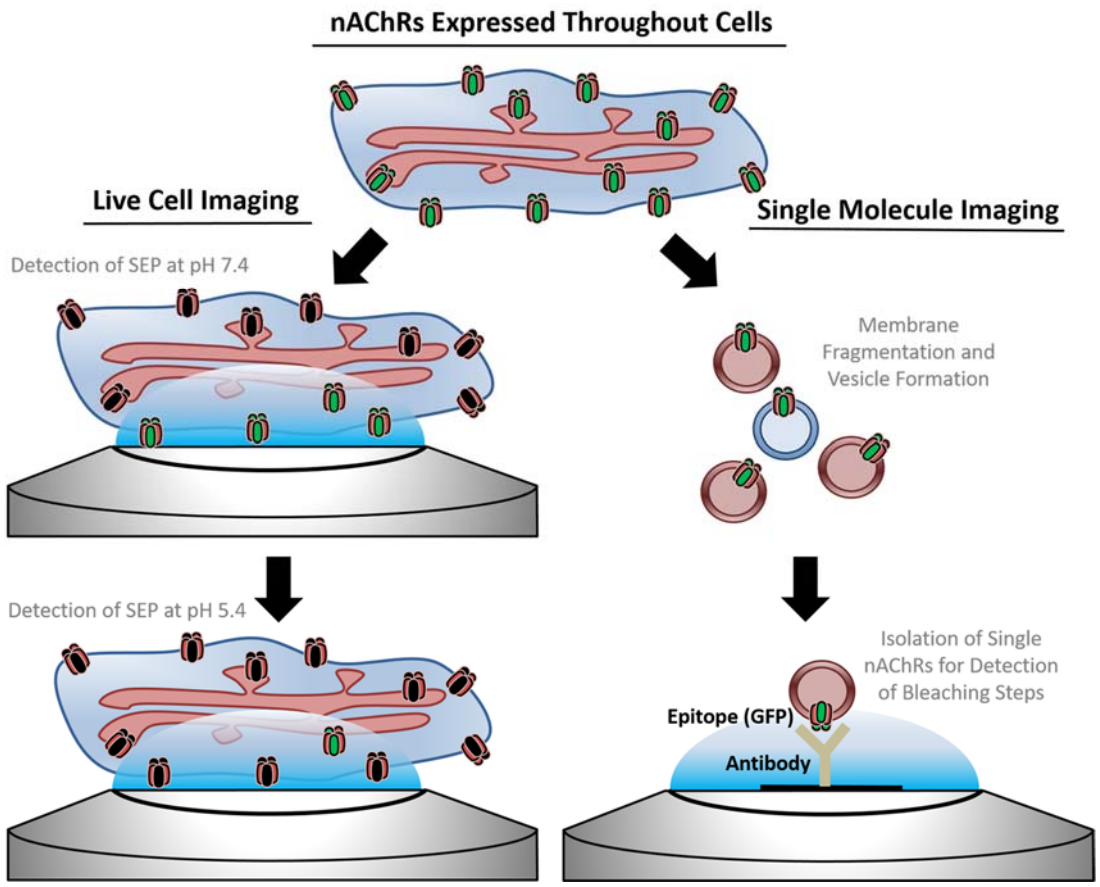

Figure 2.5 Cartoon illustrating isolation of nAChRs for single molecule imaging. In the SEP studies, live cells are imaged at pH 7.4 and pH 5.4 to determine localization to the plasma membrane. In the single molecule studies, live cells undergo nitrogen cavitation, encapsulating single nAChRs in their native membranes at that time. Nanovesicles are then isolated on a glass surface and imaged to detect single GFP bleaching steps.

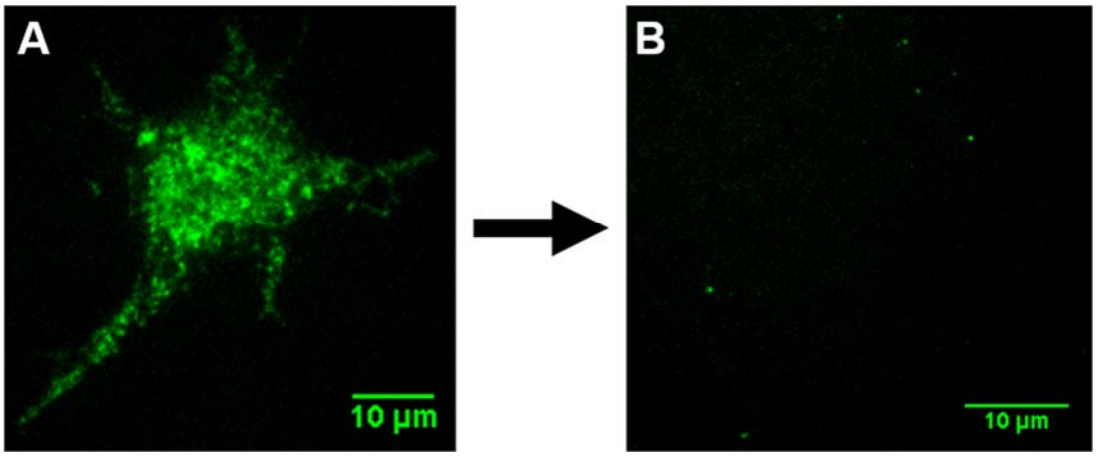

Figure 2.6 Formation of nanovesicles from cells expressing α4-GFP/β2. (A) TIRF image showing a cell expressing nAChRs. (B) Isolated nanovesicles each contain a single α4β2 nAChR.

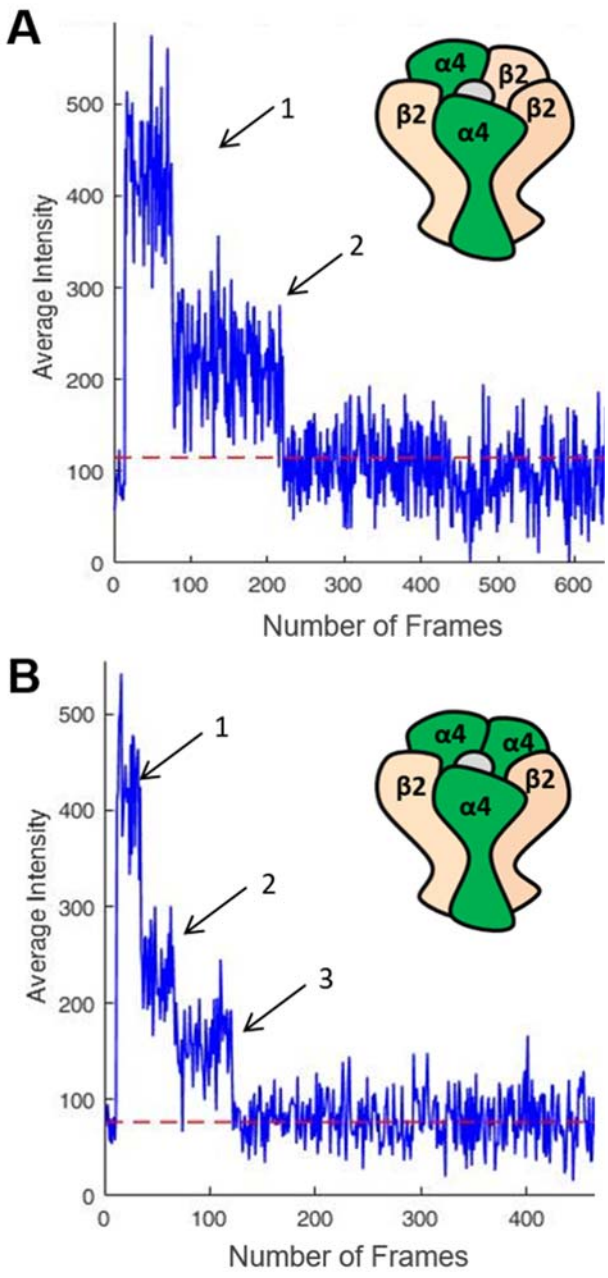

Figure 2.7 Representative time traces showing stepwise decreases in fluorescence intensity. Time traces of α4-GFP/β2 showing two (A) or three (B) bleaching steps are used to determine the stoichiometry of that nAChR.

two bleaching steps, or two GFP-labeled alpha subunits, corresponds to a shift in assembly to preferentially form the $(\alpha4)_2(\beta2)_3$ isoform.

2.3 nAChR Ligands Alter Expression, Trafficking, and Assembly of α4β2

Changes in nAChRs as a response to nicotine exposure have been the most widely characterized. Nicotine upregulates α4β2 and increases expression of the high sensitivity, $(\alpha4)_2(\beta2)_3$ isoform [85, 154]. Many smoking cessation agents target the α4β2* subtype of nAChRs. Some of these drugs, including mecamylamine and varenicline, have been shown to upregulate the α4β2* nAChRs [150, 176, 178]. Another cessation agent, cytisine, has been shown to increase expression of the low sensitivity, $(\alpha4)_3(\beta2)_2$, isoform at the plasma membrane [85]. These therapeutics have varying pharmacological properties and binding sites, but all seem to interact with specific nAChR stoichiometries or induce upregulation of these nAChRs. Understanding the effects of existing drugs on expression and assembly of α4β2 would provide insight into the mechanism of successful smoking cessation with these agents. We hypothesized that current smoking cessation agents may also alter the distribution between intracellular and plasma membrane resident nAChRs. In order to test this hypothesis, N2a cells were transiently transfected with α4β2 and exposed to cytisine, varenicline, or bupropion for 48 hours. Alpha 4 subunits were genetically labeled with the pH sensitive fluorophore, SEP. TIRF microscopy was used to measure expression and distribution of SEP-labeled nAChRs within the field of view, as shown above in Figure 2.2. Increases in PMID and % PM correspond to upregulation in number of α4β2 nAChRs and distribution towards the plasma membrane, respectively. We further hypothesized that cytisine, varenicline, and bupropion may alter stoichiometry of α4β2 throughout the whole

cell. To test this hypothesis, alpha subunits were encoded with a GFP molecule to undergo single molecule photobleaching. Transiently transfected HEK-293T cells expressing α4-GFP/β2 underwent nitrogen cavitation to form cell-derived nanoscale vesicles, as shown in Figure 2.5. Bleaching steps were detected for vesicles formed from cells exposed to cytisine, varenicline, or bupropion. The number of bleaching steps corresponds to the number of alpha subunits present, and thus the stoichiometry. Bleaching steps are counted and fit to a binomial distribution to obtain a distribution of each α4β2 isoform present. Changes in the number of bleaching steps detected indicates a shift in predominate stoichiometry when exposed to that drug.

2.4 Nicotine Intracellularly Alters α4β2 Stoichiometry

Despite correlations between nAChR upregulation and nicotine addiction, the mechanism of nicotine induced upregulation has not been fully resolved. Recent evidence supports the theory that nicotine acts intracellularly to induce upregulation, known as "inside-out" neuropharmacology [160]. In such a way, nicotine would act intracellularly to increase maturation enhancement of subunits and pharmacologically chaperone nascent nAChRs [55, 97, 115, 153]. This requires nicotine to permeate cell membranes, interact with intracellular receptors, and alter the expression of nAChRs internally to favor a high sensitivity $(\alpha4)_2(\beta2)_3$ stoichiometry. FRET, Förster resonance energy transfer, based studies show an increase in the number of α4 and β2 subunits in close proximity within the whole-cell region measured, which includes the endoplasmic reticulum [115, 196, 197]. However, no structural changes solely within the endoplasmic reticulum have been measured. This is primarily due to a lack of existing techniques that can directly measure

complex structural assembly of membrane proteins intracellularly. We hypothesized that nicotine alters the assembly of α4β2 nAChRs within the endoplasmic reticulum, and this could be detected using a single molecule analysis of nAChRs embedded in cell-derived nanovesicles. To test this hypothesis, we developed a technique to separate nAChRs localized to the endoplasmic reticulum or plasma membrane. HEK-293T cells transiently expressing α4-GFP/β2 nAChRs underwent nitrogen cavitation to trap a single α4β2 nAChR in a nanovesicle derived from the native cell membrane, as discussed above in Figure 2.5. During nitrogen cavitation, the pressure is increased to promote fragmentation of the plasma membrane. Once vesicles containing α4β2 nAChRs are formed, density gradient centrifugation is used to separate nanovesicles derived from the membranes of the endoplasmic reticulum and plasma membrane, as illustrated in Figure 2.8. After separation of ER and PM derived nanovesicles containing a single nAChR, they are spatially isolated on a glass substrate using the same pull-down mechanism mentioned earlier (Figure 2.6). The stoichiometry of α4β2 is determined by counting single molecule bleaching steps of the GFP-labeled alpha subunits. Two bleaching steps corresponds to $(\alpha4)_2(\beta2)_3$, whereas three bleaching steps corresponds to $(\alpha4)_3(\beta2)_2$ stoichiometry of the nAChR in that location. By separating nAChRs based on the membrane of origin, structural differences and preferential trafficking between receptors located within the ER can be differentiated from those on the PM. Changes in stoichiometry of α4β2 within the ER and PM upon exposure to nicotine are compared to control cell by fitting the counted number of bleaching steps in each condition to a binomial distribution. In addition, preferential trafficking of an assembly with or without nicotine is measured.

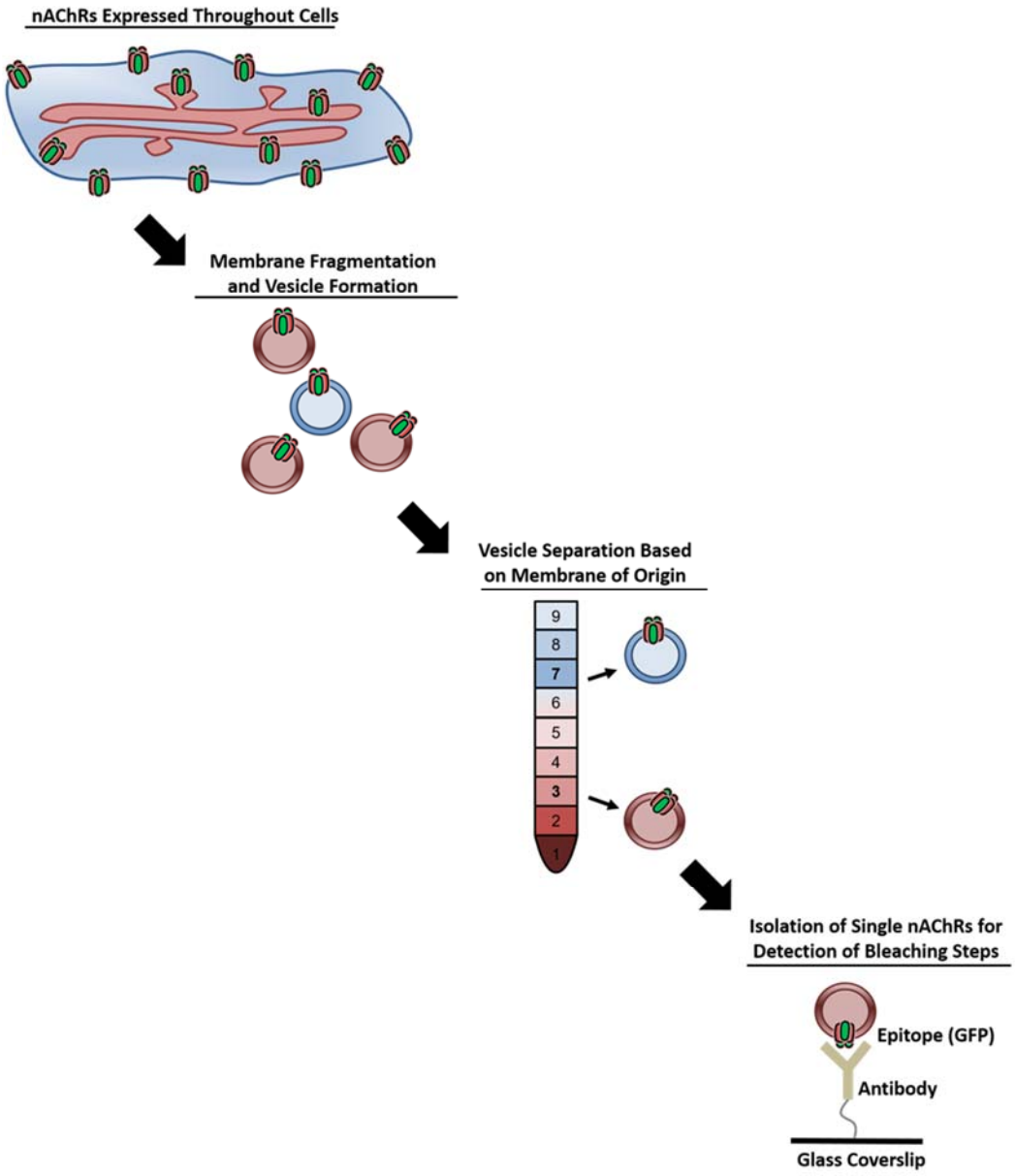

Figure 2.8 Cartoon illustrating separation of ER and PM derived nanovesicles. Cells undergo nitrogen cavitation, encapsulating single nAChRs in their native membranes at that time. nAChRs originating from the ER and PM are separated on a density gradient. Nanovesicles are then isolated on a glass surface and imaged to detect single GFP bleaching steps.

CHAPTER 3: MATERIALS AND METHODS

3.1 Materials

3.1.1 Pharmacological Agents

(-)-Nicotine hydrogen tartrate salt (≥ 98%), (-)-cotinine (≥ 98%), cytisine (≥ 99%), varenicline (≥ 98%), and bupropion hydrochloride (≥ 98%), were purchased from Sigma-Aldrich.

3.1.2 Reagents

Poly-D-lysine was purchased from VWR. Lipofectamine 2000 transfection reagent was purchased from Fisher Scientific. 35 mm glass bottom petri dishes were obtained from Cell E&G. Biotin-PEG-silane was purchased from Laysan Bio., Inc. NeutrAvidin was obtained from Thermo Scientific.

3.1.3 Antibodies

Biotinylated polyclonal (GOAT) anti-GFP antibody was purchased from Rockland Immunochemicals, Inc. Polyclonal rabbit anti-calnexin and polyclonal mouse anti-plasma membrane calcium ATPase were obtained from Santa Cruz Biotechnology. Secondary rabbit and mouse antibodies were obtained from Jackson ImmunoResearch.

3.1.4 Nicotinic Receptor Plasmid Constructs

All nAChR subunit plasmids are of mouse origin. Super ecliptic pHluorin (SEP) fluorophores were incorporated on the C-terminus of α4, α6, and α3 subunits in a pCI-neo

vector. The α4-SEP was previously constructed using PCR amplification with a forward primer sequence of 5'-CATGGTTGGCTGGTATGATCAGTAAAGGAGAAGAACTT-3' and a reverse primer sequence of 5'-ATGGATGAACTATACAAATAGGGAATAGC GGCACCT-3' using Pfu-Turbo polymerase [198]. Plasmids containing nAChRs labeled on the C-terminus with SEP have previously been shown to be functional based on whole cell patch clamp studies [85, 115, 198]. A green fluorescent protein (GFP) fluorophore was previously incorporated into the TM3-TM4 loop of the α4 subunit. All plasmids assemble normally and have been used in previous reports [196, 198]. The QuikChange II XK site-directed mutagenesis kit was used to create the α5-D398N mutation commonly associated with an increase in risk of smoking and lung cancer. The D398N corresponds to an aspartic acid to asparagine change in position 397 in the mouse plasmid [126].

3.2 Methods to Determine nAChR Expression and Trafficking

3.2.1 Cell Culture

Undifferentiated mouse neuroblastoma 2a (N2a) cells were cultured using standard tissue culture techniques at 37 ^{o}C and 5% CO_2. N2a cells were maintained in growth media consisting of Dulbecco's Modified Eagle Medium (DMEM) and Opti-MEM Reduced Serum Media, supplemented with 10% fetal bovine serum, penicillin, and streptomycin [151, 198].

3.2.2 Transfection

N2a cells were plated by adding 90,000 cells to poly-D-lysine coated 35-mm glass bottom dishes. The following day, growth medium was replaced with Opti-MEM for cell

transfection. Cells were transfected with 500 ng of each nAChR subunit plasmid mixed in 250 µL Opti-MEM. The plasmids for alpha subunits contained a sequence for super-ecliptic pHluorin (SEP). A separate aliquot of 2 µL Lipofectamine-2000 and 250 µL Opti-MEM were incubated at room temperature for 5 minutes then combined with the plasmid solution for an additional 25 minutes before being added to pre-plated N2a cells. After 24 hours at 37°C, transfection mixture was replaced with growth media and incubated for an additional 24 hours at 37°C before imaging.

3.2.3 Exposure to Pharmacological Agents

For drug exposed cells, the indicated concentration of the appropriate drug was added at the time of the transfection and replenished in the growth medium replacement for a total of 48 hours of exposure before imaging. Nicotine and its metabolite, cotinine, were added at varying concentrations. Cytisine, varenicline, and buproprion were added at a concentration of 500 nM. Transfection efficiency was approximately 80% and was not influenced by the presence of a drug.

3.2.4 TIRF Imaging of Super-Ecliptic pHluorin

Samples were imaged with objective style total internal reflection fluorescence microscopy with an inverted fluorescence microscope (Olympus ix83). TIRF imaging reduces background fluorescence by focusing on a single optical plane. Excitation of fluorophores is limited to within approximately 100-200 nm from the cell-glass bottom dish interface, visualizing receptors localized to the plasma membrane or peripheral endoplasmic reticulum [211]. Within this region, resolution is greatly increased,

particularly at the plasma membrane. SEP were excited with a 488 nm DPSS laser (~1.00 W/cm^2) fiber coupled stepper motor to adjust the critical angle of the excitation beam. The excitation beam travels through the objective (Olympus, 1.49NA, 60x oil immersion) and is detected by an electron multiplying charge coupled device (EMCCD) (Andor iXon Ultra 897). To obtain total internal reflection (TIR), the laser was focused on the back aperture of the objective lens and the angle was adjusted using a stepper motor to translate the beam laterally across the objective lens. Due to low excitation intensity, photobleaching is not an issue on the timescale of these measurements.

3.2.5 Measuring Receptor Expression and Distribution

The pH sensitivity of SEP was utilized to determine subcellular location within the TIRF field. SEP undergoes 488 nm excitation at neutral pH but is dark under acidic conditions of pH < 6 [217], enabling differentiation between intracellular and inserted nAChRs. The SEP tag is fused with the C terminus of the nAChR subunit so that it is exposed to the pH on the luminal side of the organelles within the secretory pathway. Before imaging, growth medium was exchanged for extracellular solution (150 mM NaCl, 4 mM KCl, 2 mM $MgCl_2$, 2 mM $CaCl_2$, 10 mM HEPES and 10 mM glucose) adjusted to pH 7.4 using NaOH. Receptors in the ER (pH > 7), and on the PM (pH of ECS, 7.4) are visible, while those in the lower pH environments of the Golgi and secretory vesicles are not fluorescent [198, 229]. After images were collected at pH 7.4, the solution was exchanged with an otherwise identical solution adjusted to pH 5.4 using HCl. When the pH of the ECS is < 6, nAChRs located on the PM transition into the off state, so the observed fluorescence is solely from nAChRs in the peripheral ER [115, 211, 230]. The

integrated density of cells imaged in TIRF, showing relative number of fluorescent receptors, are collected at both pH 7.4 and pH 5.4. The integrated density at pH 5.4 is subtracted from the total integrated density of fluorophores in the ER and on the PM shown at pH 7.4 to determine the integrated density of receptors on the plasma membrane (PMID). The ratio of receptors on the plasma membrane (% PM) is the PMID divided by the total integrated density at pH 7.4, multiplied by 100, to provide a percentage of receptors within the TIRF view that reside on the membrane. Increased PMID reflects an upregulation in the number of receptors found on the PM. An increase in the percentage of receptors found on the plasma membrane (% PM) corresponds to a change in the distribution of receptors between the ER and PM.

3.2.6 Receptor Expression Data Analysis

Quantification of fluorescence intensity was determined using ImageJ by manually selecting an intensity-based threshold and region of interest. Background was subtracted using the sliding paraboloid method. Plasma membrane integrated density (PMID) was calculated by subtracting the integrated density of a cell at pH 5.4 from the integrated density of the same cell at pH 7.4. The percentage on the plasma membrane within the TIRF field of view (% PM) was calculated by dividing the PMID by the total integrated density at pH 7.4, multiplied by 100. All figures show results from a single imaging session that are representative of data collected on at least three separate occasions. All graphs show the mean with error bars representing S.E.M. P-values were determined using a two-tailed t-test with equal variance not assumed.

3.2.7 Measuring Receptor Trafficking

Real time images were acquired at a frame rate of 200 ms for 1500 frames to capture fusion of nAChR containing transport vesicles with the plasma membrane. These studies allow us to identify changes in the number of vesicles that contain SEP-labeled nAChRs but not in total number of vesicles. Insertion events were manually counted per cell during a randomly chosen 50 frames (10 seconds) using ImageJ. Insertion events were defined as a burst of fluorescence at the PM lasting at least 2 frames (400 ms) and including lateral spreading of fluorophores to ensure transient full fusion of the vesicle and delivery of nAChRs to the membrane. Persistent, continuously repeating bursts of fluorescence were not counted since a discrete exocytic event could not be guaranteed. Statistical differences in the number of insertion events in the presence of cotinine were determined using a two-tailed t-test with equal variance not assumed.

3.3 Methods to Determine nAChR Assembly

3.3.1 Cell Culture

Undifferentiated human embryonic kidney 293T (HEK-293T) cells were cultured using standard tissue culture techniques at 37 ^{o}C and 5% CO_2. HEK-293T cells were maintained in growth media consisting of DMEM, supplemented with 10% fetal bovine serum, penicillin, and streptomycin. Flasks were coated with matrigel matrix (VWR), a solubilized basement membrane preparation, to encourage cell adherence and differentiation in culture.

3.3.2 Transfection

HEK-293T cells were plated by adding 3 million cells to matrigel coated T75 cell culture flasks. The following day, growth medium was replaced with Opti-MEM for cell transfection. Cells were transfected with 3500 ng of each nAChR subunit plasmid mixed in 250 μL Opti-MEM. The alpha subunits contained the genetic sequence for green fluorescent protein (GFP). A separate aliquot of 14 μL Lipofectamine-2000 and 250 μL Opti-MEM were incubated at room temperature for 5 minutes then combined with the plasmid solution for an additional 25 minutes before being added to pre-plated HEK-293T cells. After 24 hours at 37°C, transfection mixture was removed prior to vesicle formation.

Biased transfections were performed by adding unequal amounts of α4-GFP and β2-wt plasmid during the transfection of HEK-293T cells. These control studies were completed using 10:1, 4:1, and 1:4 ratios of α4-GFP to β2-wt plasmid. Equal amounts of plasmid were used for all other studies.

3.3.3 Exposure to Pharmacological Agents

nAChR ligands were added at the time of transfection. Nicotine, cytisine, varenicline, and bupropion were all added at a concentration of 500 nM. Cotinine was added at a concentration of 1 μM. Transfection efficiency was approximately 80% and was not influenced by the presence of a drug.

3.3.4 Preparation of Nanovesicles for Whole Cell Stoichiometry

Vesicles were prepared from HEK-293T cells expressing α4-GFP/ β2-wt using nitrogen cavitation [228]. Briefly, transfection mix is removed from previously transfected

cells. Cells were then washed with 1X PBS, and detached from the flask by incubation with 5 mL 1X versene (Invitrogen) at 37 ºC for 5 minutes. The cells were pelleted from the collected cell slurry by centrifugation at 200 x g for 5 minutes. The cell pellet was resuspended in 5 mL sucrose-HEPES buffer supplemented with a protease inhibitor (250 mM sucrose, 10 mM HEPES, 1 Pierce protease inhibitor mini tablet per 10 mL buffer (ThermoScientific), pH 7.5). Once resuspended, cells were added to a commercially available nitrogen decompressor (Parr Instrument Company, Illinois, USA), attached to a nitrogen tank. Nitrogen cavitation at a pressure of 250 psi for 20 minutes was used to lyse cells. In this method, cells are saturated with pressurized gas, causing the cells to expand. Rapid decompression of the gas causes the cell membranes to rupture. Cell lysate containing nanovesicles is collected once the pressure valve on the nitrogen decompressor is released. Cell lysate was then centrifuged at 4000 x g for 10 minutes. Supernatant was collected and centrifuged at 10,000 x g for 20 minutes. Supernatant was again collected and centrifuged at 100,000 x g for 1 hour. The pellet was resuspended in 800 µL sucrose HEPEs buffer (250 mM sucrose, 10 mM HEPES, pH 7.5). Nanovesicles were stored at -80 ºC until use.

3.3.5 Cleaning Glass Bottom Dishes for Single Molecule Imaging

Fluorescence impurity on the glass imaging substrates were removed before the functionalization and addition of vesicles. Glass coverslips (22 mm x 22 mm, #1.5, ThermoScientific) were cleaned by sonication in 5 M NaOH for 60 minutes at 50 ºC, followed by thorough rinsing with deionized H_2O (18 MΩ) and denatured ethanol three times. Glass coverslips were then sonicated in 0.1 M HCl for an additional 60 minutes at

50 ºC, and rinsed with deionized H_2O (18 MΩ) and denatured ethanol three times. After the final rinsing, glass coverslips were dried with nitrogen gas and glued to a 35 mm petri dish with a 13 mm opening in the center (Cell E&G). Assembled dishes were then treated in an oxygen plasma cleaner (21% O_2) (Harrick PDC-32G) on high for at least 5 minutes to ensure fluorescent organic impurities were completely removed.

3.3.6 Immobilization on Glass

Vesicles were immobilized on clean glass bottom dishes functionalized with 1 mg/mL Biotin-PEG-Silane (Laysan Bio, Inc.), 0.1 mg/mL NeutrAvidin (Thermo Scientific), and 1 µg/mL biotinylated anti-GFP antibody. On a cleaned, assembled, glass bottom dish, 200 µl of 1 mg/mL Biotin-PEG Silane dissolved in 95% ethanol was added. The dish was incubated for 35 minutes and rinsed three times with 95% ethanol and once with 1X PBS. After rinsing, 200 µL of 0.1 mg/mL NeutrAvidin in 1X PBS was incubated on the dish for 30 minutes, then rinsed three times with 1X PBS. A biotinylated anti-GFP antibody was then added at 1 µg/mL in 1X PBS and incubated for 30 minutes. Excess antibody was removed by rinsing three times with 1X PBS. Prepared vesicles were unthawed and diluted approximately 1:100 to ensure single vesicle level binding to the antibody. Vesicles were incubated on the dish for 45 minutes, then rinsed three times with 1X PBS. Vesicles were maintained in 1 mL 1X PBS. All incubations were done at room temperature.

Single vesicles were spatially isolated and immobilized using the GFP in the receptor binding to a substrate immobilized anti-GFP antibody. Generating small enough vesicles, based on the pressure used during nitrogen cavitation, limits the probability of

capturing more than one receptor in a single vesicle. Control experiments using monomeric receptors showed that there was a low probability of having more than one receptor per isolated vesicle. Of the vesicles generated via nitrogen cavitation approximately 15% contain a receptor [228].

3.3.7 TIRF Imaging of GFP Photobleaching

Single molecule isolation and immobilization of these vesicles within the TIRF illumination enables single receptor measurements. Samples were imaged with objective style total internal reflection fluorescence microscopy with an inverted fluorescence microscope (Olympus ix83). Green fluorescent protein (GFP) were excited with a 488 nm DPSS laser (~60 W/cm^2), fiber coupled to a stepper motor to adjust the critical angle of the excitation beam. The excitation beam travels through the objective (Olympus, 1.49NA, 100x oil immersion) and is detected by an electron multiplying charge coupled device (EMCCD) (Andor iXon Ultra 897). Each field of view was imaged continuously for 1000 frames with an exposure time of 100 ms while undergoing continuous 488 nm excitation with an intensity of 60 W/cm^2. Auto focus (Olympus ZDC2) was used to minimize focal drift.

3.3.8 Time Trace Analysis

A customized Matlab program was written in our lab to accumulate time traces for each immobilized vesicle in the field of view. Briefly, a 3-pixel x 3-pixel region of interest (ROI) was selected around each vesicle based on the mean intensity of this region, determined by a manually defined threshold. Background was subtracted from each ROI

by calculating the mean value of pixels located along a 5-pixel x 5-pixel concentric ring around the selected ROI. The calculated background intensity was subtracted from the ROI mean value. Time traces that showed a decrease in fluorescence intensity over time were identified by measuring the difference in mean intensities between the first 20 and last 20 frames in the time trace. If this difference was greater than twice the standard deviation of the last 20 frames, the time trace was collected and analyzed. A second customized Matlab program was written in our lab to display time traces for manual determination of bleaching steps.

3.3.9 Photobleaching Step Analysis

Photobleaching steps are identified as stepwise decreases in fluorescence decay, corresponding to a single molecule transitioning into a dark state. Photobleaching steps were determined manually as previously described [224, 228, 231]. Previously, a discrete bleaching step was confirmed to correspond to one subunit [228, 231]. A single molecule was considered present in a time trace if at least one clear bleaching step was distinguishable. Time traces showing a continuous decrease in fluorescence intensity or indistinct number of bleaching steps were rejected. To qualify as a bleaching step, the GFP molecule fluorescence had to last at least 1 second (10 frames). The mean intensity also needed to be three times higher than the standard deviation of the mean of the background intensity. Each data set was independently analyzed three times. Upon comparison of results from each round of independent analysis, time traces that were assigned the same number of bleaching steps were accepted. Data reported is an accumulation of counted bleaching steps over the course of all imaging sessions and sample preparations.

3.3.10 Fitting Data to a Binomial Distribution

GFP fails to mature a small percentage of the time leading to some subunits not exhibiting typical fluorescence, which would result in the occasional undercounting of bleaching events [224, 228]. To account for this, the probability of observing one, two, or three photobleaching steps in the time traces for each stoichiometry were calculated using a custom Matlab script by fitting data to a binomial distribution, using the probability of GFP fluorescing equal to 0.90 [224]. The agreement of theoretical and experimental data was determined using a chi squared goodness of fit analysis. The probability of observing a specific number of photobleaching steps, for a receptor with fixed number of subunits is calculated using:

$$F(k, n, p) = \frac{n!}{k!(n-k)!}\, p^k (1-p)^{n-k} \quad \text{(Eq. 3.1)}$$

Where, n is the total number of labeled subunits, k is the number of observed units, p is the probability of GFP being in an observable state, and F is the probability of observing k number of photobleaching steps from n number of labeled subunits. Modeling the probability of observing a specific number of photobleaching steps for α4β2 requires two binomial distributions (Equation 3.2) for k = 1, 2, and 3 for both F_1 and F_2.

$$F_{tot} = a_1 \cdot F_1(k, n_1, p) + a_2 \cdot F_2(k, n_2, p) \quad \text{(Eq. 3.2)}$$

Where F_1 corresponds to the case when n_1 GFP labeled subunits are in a receptor and F_2 when there are n_2. Observed results are plotted beside the expected fit based on the binomial probability. Error bars on the observed data are calculated as the square root of the number of counted events, corresponding to a Poisson distribution of counting events. Once the data was fit to a binomial distribution, percentage distributions are summarized in a single graph to highlight differences in the fraction of each isoform present. Error bars

on these percentage based graphs correspond to confidence intervals based on the number of vesicles analyzed. Confidence intervals are calculated based on the equation:

$$p \pm z_{1-a/2}\sqrt{\frac{p(1-p)}{n}} \qquad \text{(Eq. 3.3)}$$

Where z is 1.96 for a 95% confidence internal, and n is the number of vesicles analyzed.

3.4 Methods to Separate ER and PM Derived Vesicles

3.4.1 Cell Culture and Transfection

As described in detail above, HEK-293T cells were maintained in matrigel matrix coated T75 flasks in a growth media of DMEM supplemented with 10% fetal bovine serum, penicillin, and streptomycin. The day before transfection, 3 million cells were plated. Cells were transfected with 3500 ng of each nAChR subunit plasmid mixed in 250 µL Opti-MEM. The alpha subunits contained the sequence for green fluorescent protein (GFP). A separate aliquot of 14 µL Lipofectamine-2000 and 250 µL optiMEM were incubated at room temperature for 5 minutes then combined with the plasmid solution for an additional 25 minutes before being added to pre-plated HEK-293T cells. After 24 hours at 37°C, transfection mixture removed was prior to vesicle formation.

3.4.2 Preparation of Organelle Specific Vesicles

Plasma membrane and endoplasmic reticulum derived vesicles were prepared from transfected HEK-293T cells using nitrogen cavitation [228]. The day after transfection, half of the HEK-293T cell flasks were rinsed one time with 1X PBS and incubated for 20 minutes in hypotonic solution (10 mM NaCl, 10 mM Tris-HCl, 1.5 mM $MgCl_2$, 0.2 mM $CaCl_2$, pH 7.4) at 0 ºC. This hypotonic solution swells cells, to increase fragmentation of

the plasma membrane for the formation of PM derived nanovesicles containing a single nAChR. After the 20 minute incubation for plasma membrane vesicle destined flasks, all cells were treated with 5 mL of 1X versene and incubated 37 ºC for 5 minutes to detach cells from the flask. Cells were then pelleted by centrifugation at 200 x g for 5 minutes and resuspended in 3 mL sucrose buffer plus protease inhibitors (250 mM sucrose, 10 mM HEPES, 1 Pierce protease inhibitor mini tablet per 10 mL buffer (ThermoScientific), pH 7.5) before undergoing nitrogen cavitation in a nitrogen decompressor (Parr Instrument Company, IL, USA). The flasks that were previously swollen in hypotonic solution, to prepare plasma membrane nanovesicles, were pressurized to approximately 600 psi for 20 minutes. This higher pressure increases the fragmentation of the plasma membrane. The other flasks, to prepare endoplasmic reticulum nanovesicles, were pressurized to approximately 250 psi for 20 minutes. At this pressure, plasma membrane rupturing is minimal and therefore nanoscale vesicle formation from this organelle is negligible. In each case, cell lysate was collected and dispensed onto an OptiPrep gradient.

3.4.3 Separation of Organelle Specific Vesicles

After vesicle formation by nitrogen cavitation, a three step OptiPrep (60% (w/v) iodixanol in H_2O, Accurate Chemical & Scientific Corp., NY, USA) gradient was used to isolate plasma membrane and endoplasmic reticulum nanovesicles. The 60% (w/v) iodixanol stock solution was diluted to 30%, 20%, and 10% in sucrose buffer (250 mM sucrose, 10 mM HEPES, pH 7.5) to prepare OptiPrep gradient solutions. OptiPrep solutions were stored at 4 ºC until use. The gradient was prepared in an Ultra-Clear centrifuge tube (Beckman Coulter), with the densest, 30%, fraction added first. Each

concentration used was dispensed in a 3 mL volume. Cell lysate was added to the top of the 10% fraction. Endoplasmic reticulum and plasma membrane nanovesicle containing cell lysates were added to individual columns. The lysate gradient was then centrifuged at 112,000 x g for 1.5 hours. After centrifugation, fractions were collected using a peristalic pump. Tubing connected to the pump was vertically inserted into the centrifuge tube so that the highest density fraction is collected first. The volume of each collected fraction was 1.5 mL, with nanovesicles localizing to fraction interfaces. After fractions were collected, nanovesicles were centrifuged at 10,000 x g for 1 hour to remove OptiPrep and resuspended in 500 μL sucrose HEPES buffer (250 mM sucrose, 10 mM HEPES, pH 7.5). Purified vesicles were stored at -80 ºC until used.

3.4.4 Western Blot Analysis

Western blots were used to determine which fractions from the OptiPrep gradient contain plasma membrane or endoplasmic reticulum vesicles. Gradient fractions, from lysate formed at 250 psi or 600 psi, were loaded on prepackaged NuPAGE 4-12% Bis-Tris gels (Life Technologies). Fractions from lysate at each pressure were loaded onto separate gels, for detection of both endoplasmic reticulum and plasma membrane markers individually in each condition. Following electrophoresis, bands were transfered to a nitrocellulose membrane. Prior to antibody binding, the membrane was blocked with a PBST solution (5% non-fat milk, 0.1% Tween in 1X Phosphate Buffered Saline) for one hour at room temperature. Primary antibodies specific for endogenous membrane proteins were used to detect fractions with ER and PM vesicles. Endoplasmic reticulum vesicles were detected with calnexin (Santa Cruz, calnexin antibody (H-70): sc-11397), while

plasma membrane vesicles were identified with plasma membrane calcium ATPase (PMCA) (Santa Cruz, PMCA antibody (D-1): sc-271193). Endogenous calnexin is solely found in the membrane of the endoplasmic reticulum, while PMCA is expressed on the plasma membrane, therefore enabling the identification fractions that consist of exclusively endoplasmic reticulum or plasma membranes. Primary antibodies were added to the membrane in a 1:1000 dilution, and incubated overnight at 4 ^{o}C. The following morning, excess primary antibodies were rinsed off with four repeated five minute washes with PBST. Secondary rabbit or mouse antibody were added in a 1:5000 dilution, to bind calnexin or PMCA antibodies, respectively. Secondary antibodies were incubated for one hour at room temperature, followed by a series of four five minute rinses with PBST. Western blotting substrate for chemiliminescence (Clarity, Bio-Rad) was reacted with the bands to enable visualization. Blots were imaged on a Chemi-Doc system (Bio-Rad).

3.4.5 Vesicle Immobilization and TIRF Imaging

Vesicles were spatially isolated on clean glass coverslips, as discussed above. Briefly, background fluorescence was removed from glass by 1 hour incubations in 5 M NaOH and 0.1 M HCl, followed by plasma cleaning. Vesicles were immobilized on coverslips functionalized with 1 mg/mL Biotin-PEG-Silane (Laysan Bio, Inc.), 0.1 mg/mL NeutrAvidin (Thermo Scientific), and 1 µg/mL biotinylated anti-GFP antibody. Samples were imaged in TIRF with excitation from a 488 nm DPSS laser traveling through the objective (Olympus, 1.49NA, 100x oil immersion). Each field of view was imaged continuously at an intensity of about 60 W/cm^2 for 1000 frames at a frame rate of 100 ms.

Auto focus (Olympus ZDC2) was used to minimize focal drift. Emission was detected by an electron multiplying charge coupled device (EMCCD) (Andor iXon Ultra 897).

3.4.6 GFP Photobleaching Analysis

Stepwise decreases in fluorescence intensity were identified manually as described above [224, 228, 231]. Time traces showing at least one distinct bleaching steps were counted, while time traces showing an indistinct number or a continuous decrease in fluorescence intensity were discarded. Each data set was independently analyzed three times, and consistent results from each round were assigned bleaching steps. Since GFP occasionally fails to fluorescence, counted bleaching steps were fit to a binomial distribution based on the probability of observing one, two, or three photobleaching steps for each isoform, as discussed in detail above. The agreement of theoretical and experimental data was determined using a chi squared goodness of fit analysis. Data reported is an accumulation of counted bleaching steps over the course of all imaging sessions and sample preparations.

CHAPTER 4: RESULTS

4.1 Cotinine Alters Expression and Trafficking of α4β2

4.1.1 Nicotine Upregulates α4β2

Super-ecliptic pHluorin (SEP), a pH sensitive variant of green fluorescent protein (GFP) [198, 217, 232], was used to quantify the upregulation of α4β2 nAChRs in the presence of nicotine and cotinine. SEP undergoes 488 nm excitation and exhibits green fluorescence at neutral pH but is not fluorescent under acidic conditions of pH < 6 [217]. N2a cells expressing α4-SEP and β2-wt subunits were exposed to nicotine or cotinine for 48 hours. Nicotine induced upregulation has been measured in a variety of systems over the last few decades. In this study, we successfully detected nicotine induced upregulation using our TIRF microscopy setup. SEP-labeled nAChRs within the TIRF field of view were analyzed. The extent of upregulation was quantified by calculating the PM integrated density (PMID) of α4β2 nAChRs with and without nicotine or cotinine. PMID was calculated by subtracting the integrated density of cells at pH 5.4 from the total integrated density of the same cell at pH 7.4 (Equation 2.1). Distribution of α4β2 receptors within the cell are compared using percent plasma membrane (% PM), calculated by dividing the PMID by the total integrated density of receptors fluorescing on the PM and ER at pH 7.4, multiplied by 100 (Equation 2.2).

N2a cells were exposed to 200 nM or 500 nM nicotine for 48 hours, and compared to control cells with no drug exposure. The PMID of control cells was $4.8 \times 10^5 \pm 3.3 \times 10^4$. Upon nicotine exposure, the PMID of cells expressing α4β2 was increased nearly two-fold for cells exposed to 200 nM nicotine ($8.5 \times 10^5 \pm 8.9 \times 10^4$) or three-fold for those exposed to 500 nM nicotine ($1.4 \times 10^6 \pm 2.0 \times 10^5$) (Figure 4.1A). An increase in distribution of α4β2 towards the plasma membrane was also observed, shown by a shift in % PM from 20.4 ± 0.8% for control cells compared to 26.1 ± 1.2% for 200 nM and 28.8 ± 1.5% for 500 nM nicotine exposure (Figure 4.1B). The α4β2 PMID and % PM values upon exposure to 200 nM or 500 nM nicotine were significantly higher than control values, based on a two-tailed t-test. This shows nicotine increases the expression of α4β2 on the plasma membrane, as well as alters the distribution of this subtype to favor trafficking towards the plasma membrane (Figure 4.1; $P < 0.001$).

4.1.2 Cotinine Upregulates α4β2

To measure cotinine induced changes in α4β2 expression levels, N2a cells were exposed to physiologically relevant concentrations of cotinine ranging from 50 nm to 10 μM. Increased expression of α4β2 on the plasma membrane was observed when cells were treated with as little as 100 nM cotinine, showing a 25% increase in number of receptors on the membrane, (Figure 4.2A; $P < 0.05$), with a PMID of $1.4 \times 10^6 \pm 1.8 \times 10^5$ compared to a control PMID of $9.0 \times 10^5 \pm 1.3 \times 10^5$. The highest levels of upregulation were reached in the presence of 1 μM cotinine, resulting in more than a two-fold increase in PMID at $2.3 \times 10^6 \pm 3.2 \times 10^5$, compared to control (Figure 4.2A; $P < 0.001$). Exposure to 500 nM and 5 μM cotinine also showed an increase in α4β2 over no drug, with PMIDs of $1.9 \times 10^6 \pm$

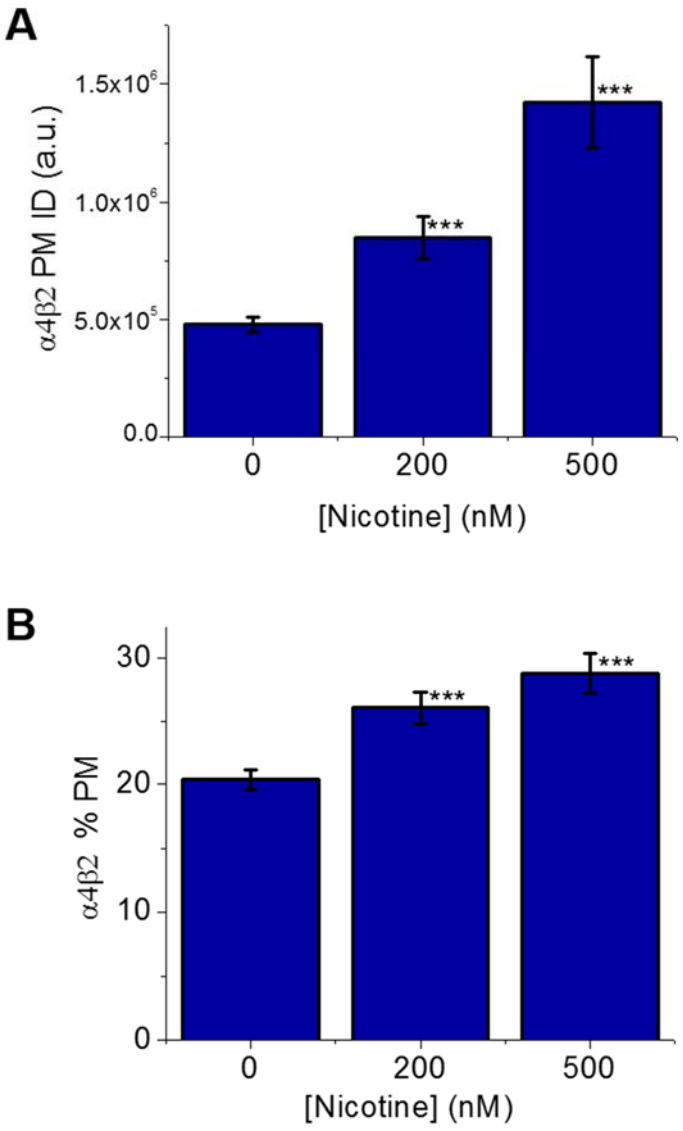

Figure 4.1 Nicotine induced upregulation of α4β2. (A) Quantification of α4β2 PMID shows an upregulation of α4β2 nAChRs with exposure to nicotine. (B) Nicotine also alters the distribution of α4β2 nAChRs within the field of view, as shown by an increase in % PM. (n = 40, 29, 22) Data are mean values ± SEM (***, $P < 0.001$), *a.u.,* arbitrary units.

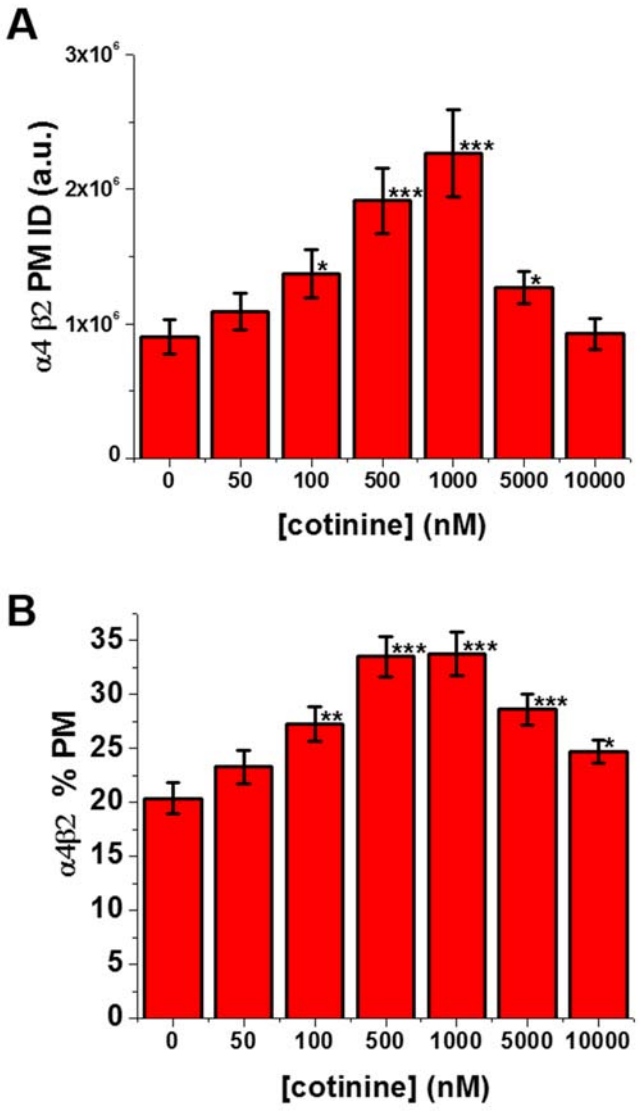

Figure 4.2 Cotinine induced upregulation of α4β2. (A) Quantification of α4β2 PMID shows an upregulation of α4β2 nAChRs with exposure to as little as 100 nM cotinine. (B) Cotinine also alters the distribution of α4β2 nAChRs within the field of view, as shown by an increase in % PM. (n = 40, 21, 21, 23, 13) Data are mean values ± SEM (*, $P < 0.05$; **, $P < 0.01$; ***, $P < 0.001$), *a.u.,* arbitrary units.

2.4 x 10^5 and 1.3 x 10^6 ± 1.2 x 10^5, respectively, but the effect was much less than observed with 1 μM cotinine (Figure 4.2A; $P < 0.05$). Similar results were observed at low and high concentrations where exposure to 50 nM or 10 μM cotinine did not result in a significant increase in number of receptors on the PM (Figure 4.2A), with PMIDs of 1.1 x 10^6 ± 1.4 x 10^5 and 9.2 x 10^5 ± 1.2 x 10^5, respectively.

These SEP based studies also show cotinine alters the distribution of α4β2 to favor the plasma membrane. Upon exposure to 1 μM cotinine, there is almost a 50% shift in distribution toward the plasma membrane (Figure 4.2B; $P < 0.001$), with an increase in % PM to 33.8 ± 2.0% from a control of 20.4 ± 1.5%. Increases in % PM were also seen at lower concentrations of 100 nM (27.3 ± 1.6%) and 500 nM (33.5 ± 1.8%), but not at 50 nM cotinine (23.2 ± 1.5%). A concentration of 5 μM cotinine increased % PM to 28.6 ± 1.4%. Although 10 μM cotinine did not increase the relative number of α4β2 on the PM, since PMID was unaltered, the distribution of receptors at 10 μM slightly favors the PM with a % PM of 24.8 ± 1.1% (Figure 4.2B; $P < 0.05$). These values suggest that some pharmacologically relevant concentrations of cotinine increase the trafficking of α4β2 towards the plasma membrane.

Figure 4.3 shows representative TIRF images of N2a cells expressing α4-SEP/β2-wt treated with no drug (Figure 4.3A), 500 nM nicotine (Figure 4.3B) or 1 μM cotinine (Figure 4.3C). For all rows, the *first column* shows a cell imaged in TIRF with an extracellular pH of 7.4 (ER and PM fluorescing), the *second column* shows an image of the same cell at pH 5.4 (fluorescence from ER only), and the *third column* shows a subtracted image representing just the PM component. Brighter images in the *third column* in the presence of nicotine or cotinine corresponds to a higher number of α4-SEP/β2

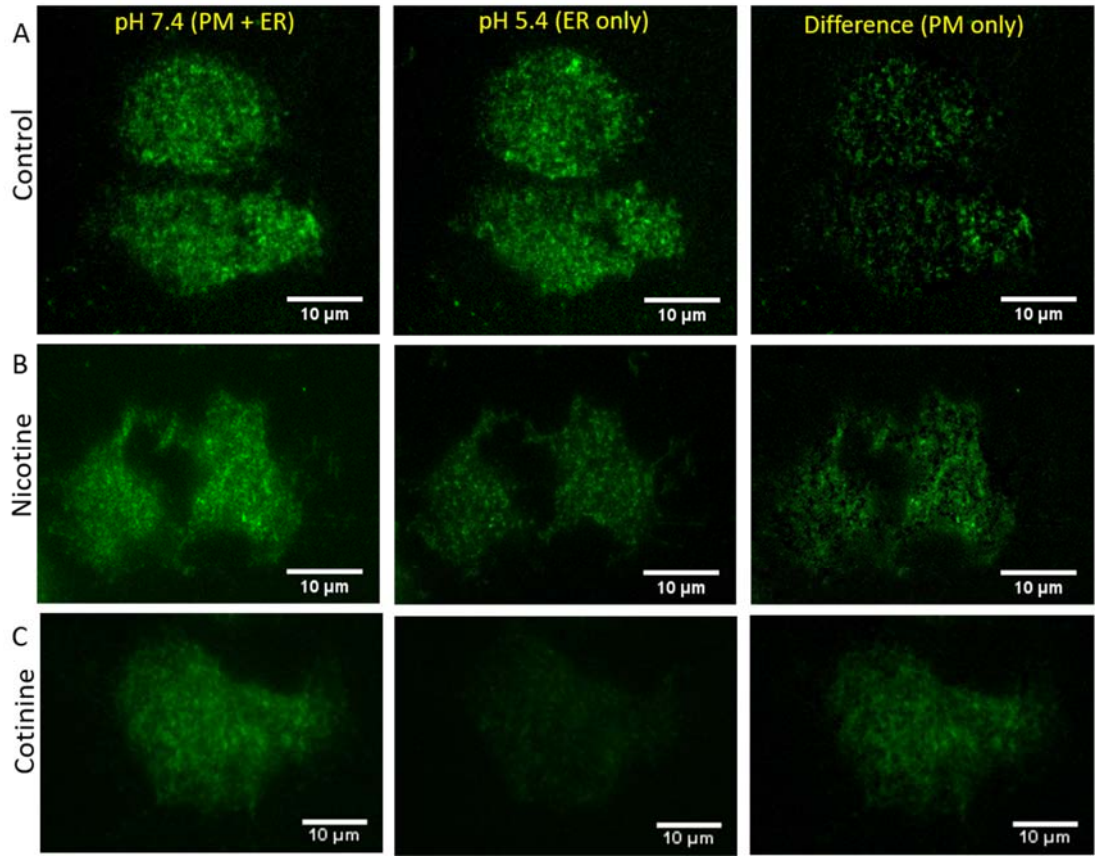

Figure 4.3 TIRFM images illustrating increased α4β2 PMID with nicotine or cotinine exposure. Representative TIRFM images of α4-SEP/β2 exposed to no drug (A), 500 nM nicotine (B), or 1 µM cotinine (C). The *first column* shows respective cells at pH 7.4, with nAChRs on the plasma membrane and endoplasmic reticulum fluorescing, whereas the *second column* shows the same cells at pH 5.4 with all fluorescence from nAChRs in the endoplasmic reticulum. The *third column* shows images constructed by subtracting the pH 5.4 image from the pH 7.4 image, resulting in receptors located on the plasma membrane (PMID).

nAChRs residing on the plasma membrane. While the subtracted TIRF footprint shown in the *third column* qualitatively shows PM expression for the given cells, the extent of upregulation was quantified by calculating the PM integrated density (PMID) of α4β2 receptors with and without addition of cotinine.

4.1.3 Co-administration of Nicotine and Cotinine

No additive effects were detected when cells were simultaneously exposed to both nicotine and cotinine at physiological concentrations for 48 hours. An array of concentrations of nicotine and cotinine were used. Cells were exposed to nicotine at 50 nM or 500 nM, and compared to cells also exposed to cotinine at 300 nM, 1 μM, or 5 μM, as shown in Figure 4.4. Control cells exposed to no drug had a PMID of $2.1 \times 10^6 \pm 2.1 \times 10^5$ (Figure 4.4A). When nicotine was added, the PMIDs of cells were measured to be $2.7 \times 10^6 \pm 2.8 \times 10^5$ for 50 nM, and $3.1 \times 10^6 \pm 3.0 \times 10^5$ for 500 nM. Cells exposed to cotinine had PMIDs of $2.8 \times 10^6 \pm 3.1 \times 10^5$ for 300 nM, $3.3 \times 10^6 \pm 2.4 \times 10^5$ for 1 μM, and $2.7 \times 10^6 \pm 3.6 \times 10^5$ for 5 μM. Co-administration of nicotine and cotinine at these concentrations still showed an increase in PMID over the control cells, but were not significantly different than exposure to these concentrations of nicotine or cotinine alone. Cells co-exposed to 300 nM cotinine and 50 nM nicotine had a PMID of $2.6 \times 10^6 \pm 1.9, \times 10^5$, compared to those co-exposed to 300 nM cotinine and 500 nM nicotine with a PMID of $3.2 \times 10^6 \pm 3.7 \times 10^5$. The PMID of cells co-exposed to 1 μM cotinine and 50 nM nicotine was $3.2 \times 10^6 \pm 3.6 \times 10^5$, while those exposed to 1 μM cotinine and 500 nM nicotine showed a PMID of $2.9 \times 10^6 \pm 3.2 \times 10^5$. PMIDs of cell co-exposed to 5 μM cotinine and 50 nM or 500 nM nicotine were $2.7 \times 10^6 \pm 3.0 \times 10^5$ and $3.0 \times 10^6 \pm 3.6 \times 10^5$, respectively. Although all

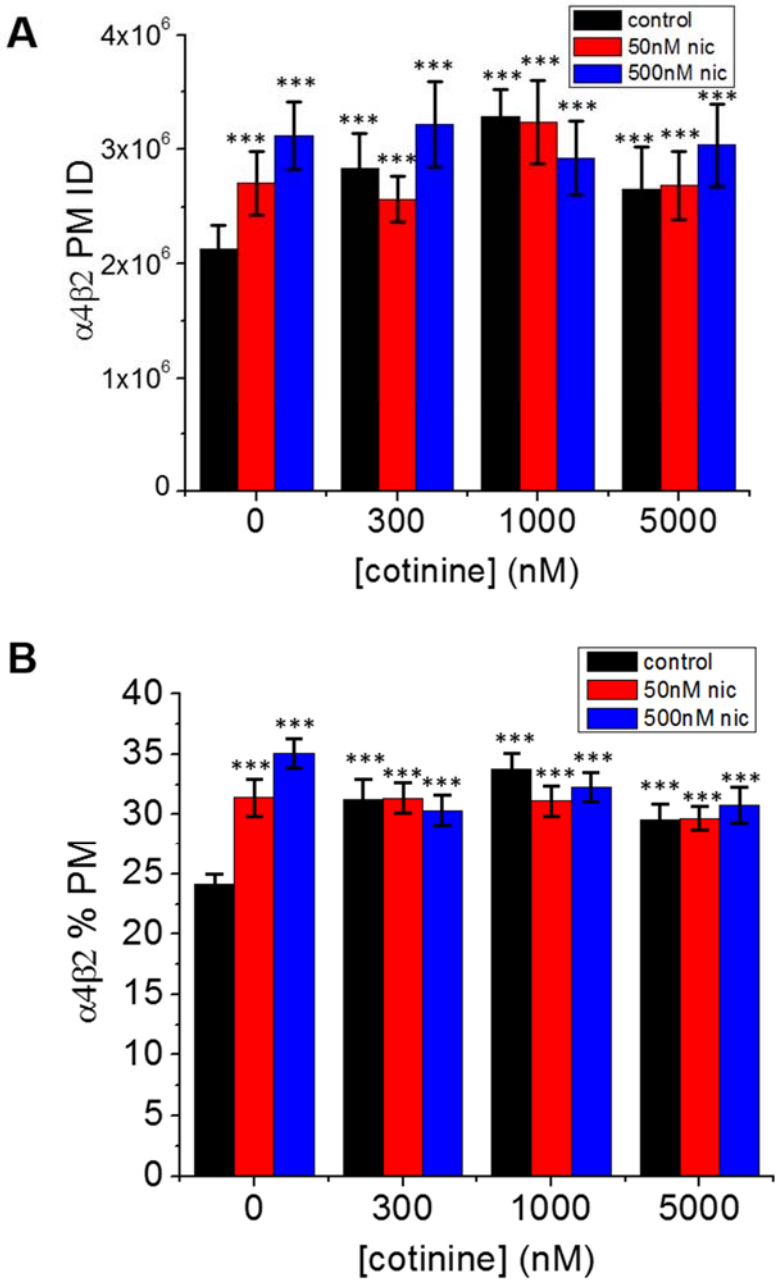

Figure 4.4 Co-administration of nicotine and cotinine. Quantification of α4β2 PMID (A) and % PM (B) upon simultaneous exposure to both nicotine and cotinine did not show any additive effects. Nicotine and cotinine both increased PMID and % PM compared to control cells exposed to no drug. (n = 28, 17, 19, 20, 26, 14, 25, 20, 18, 17, 24, 17) Data are mean values ± SEM (***, $P < 0.001$ compared to no drug controls), *a.u.,* arbitrary units.

values were significantly different than control cells (Figure 4.4A; $P < 0.001$), there were no significant differences in expression on the plasma membrane between samples of different concentrations.

Likewise, differences in distribution towards the plasma membrane were detected in comparison to control cells, but not between samples of varying concentrations of cotinine and nicotine, as shown in Figure 4.4B. Control cells showed 24.1 ± 0.8% of α4β2 nAChRs within the TIRF field of view were located on the plasma membrane. Cells exposed to 50 nM or 500 nM nicotine showed a significant increase in this number to 31.4 ± 1.5% and 35.1 ± 1.2%, respectively. Exposure to cotinine also increased the % PM to 31.2 ± 1.7% for 300 nM cotinine, 33.8 ± 1.3% for 1 μM cotinine, and 29.6 ± 1.3% for 5 μM cotinine. Co-exposure of 300 nM cotinine with 50 nM or 500 nM nicotine lead to increases in % PM to 31.3 ± 1.2% and 30.3 ± 1.3%, respectively. Cells exposed to 1 μM cotinine in addition to 50 nM nicotine had a % PM of 31.1 ± 1.3%, while cells co-exposed to 500 nM nicotine had a % PM of 32.3 ± 1.2%. Exposure to 5 μM cotinine and 50 nM or 500 nM nicotine had % PM values of 29.7± 1% and 30.8 ± 1.5%, respectively. Although all values were significantly different than control cells (Figure 4.4B; $P < 0.001$), there were no significant differences in distribution towards the plasma membrane between samples of different concentrations.

4.1.4 Cotinine Increases Number of α4β2 Insertion Events

SEP-labeled nAChRs were used to quantify α4β2 nAChR containing vesicle trafficking by measuring the number of single vesicle insertion events at the plasma membrane. The SEP tag is oriented on the luminal side of secretory vesicles so they are

maintained at a low pH prior to delivery to the PM. As a result, receptors are not fluorescent as they are trafficked to the PM but turn on as the vesicle fuses with the PM, when the SEP tag is exposed to the extracellular solution of pH 7.4 [217, 232]. In this study, an insertion event is defined as a burst of fluorescence appearing at the plasma membrane and lasting for more than two frames, or 400 ms, which corresponds to the insertion of an SEP-tagged nAChR into the plasma membrane. After the initial insertion of a trafficking vesicle, a lateral spread of fluorescence was observed corresponding to full fusion of the vesicle and subsequent diffusion of the SEP-labeled nAChRs. Figure 4.5 shows a representative series of TIRF images of an insertion event in an N2a cell, illustrating a whole cell (Figure 4.5A) and a close up of frames prior to insertion (Figure. 4.5 B1), during arrival of the vesicle shown as a burst of fluorescence (Figure 4.5 B2), followed by a lateral spread (Figure 4.5 B3-B6) and diffusion across the membrane (Figure 4.5 B7-B9).

Insertion events were manually counted in cells expressing α4β2, α4β2α5, or α4β2α5-D398N, comparing those exposed to no drug or 1 μM cotinine, as shown in Figure 4.6. Cells treated with 1 μM cotinine exhibited approximately a 30% increase in the number of trafficking vesicles that contained α4β2 compared to untreated cells (Figure 4.6; $P < 0.001$), with the detected number of insertion events increasing from 15.4 ± 0.4 to 19.4 ± 0.7 within the measured ten seconds per cell. When the α5D or α5N auxiliary subunit was co-expressed with α4 and β2 subunits, there were no differences in the trafficking rate of nAChRs in the presence of cotinine. Cells expressing α4β2α5 showed 15.8 ± 0.4 insertion events in the absence of a drug, but 15.4 ± 0.5 when 1 μM cotinine is present. Similarly, cells expressing α4β2α5-D398N showed 16.0 ± 0.5 insertion events in the ten second span

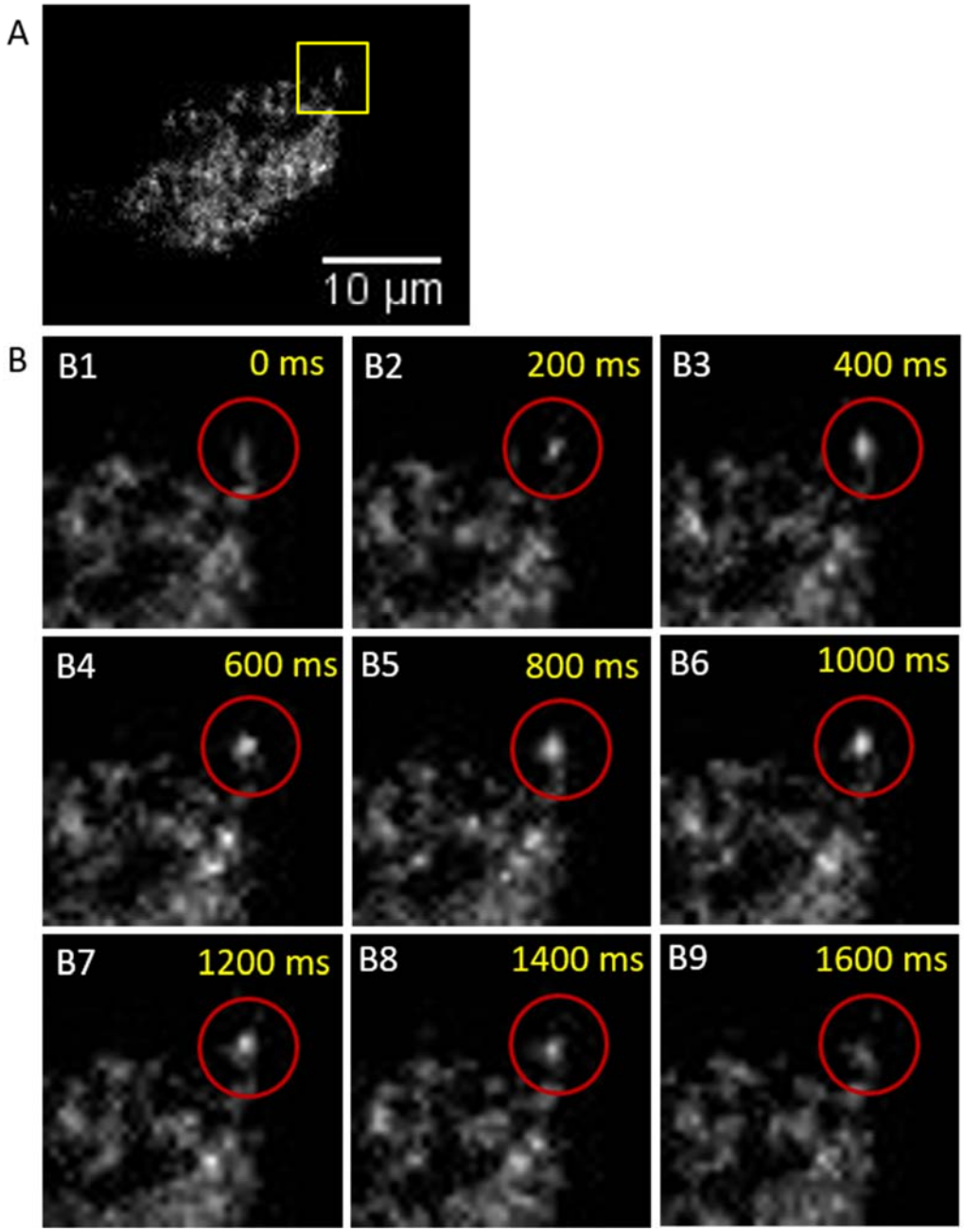

Figure 4.5 Representative TIRFM images during an insertion event. (A) A representative N2a cell expressing α4-SEP and a close up of frames (B) during series of images illustrating an insertion event prior to insertion (B1), during arrival of the vesicle shown as a burst of fluorescence (B2), followed by a lateral spread (B3-B6) and diffusion across the membrane (B7-B9).

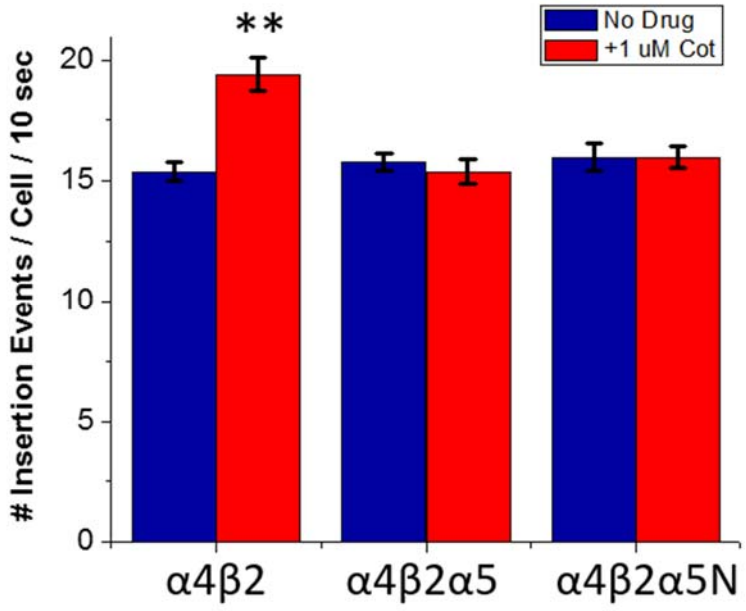

Figure 4.6 Cotinine increases the number of α4β2 insertion events. Insertion events were counted for α4-SEP/β2, α4-SEP/β2/α5, and α4-SEP/β2/α5-D398N after exposure to 1 μM cotinine for 48 hours. Data are mean values ± SEM (**, $P < 0.01$) (n = 5).

when no drug was present, and 16.0 ± 0.4 when 1 μM cotinine is present (Figure 4.6). Overall, an increase in α4β2 trafficking events was seen in the presence of cotinine. Cotinine did not alter the number of insertion events in α4β2α5 or α4β2α5-D398N under these conditions.

4.2 Upregulation of α4β2 is Lost Upon Incorporation of α5

4.2.1 Nicotine does not Upregulate α4β2α5D or α4β2α5N

When α4β2 is exposed to 500 nM nicotine, an increase in PMID is detected as previously described. However, when the α5 subunit is incorporated into this pentamer, this nicotine induced upregulation effect is not detected in these SEP based studies. In the absence of nicotine, the PMID of α4β2 is $7.6 \times 10^5 \pm 9.3 \times 10^4$ (Figure 4.7A). When α5 in incorporated, the PMID is $7.2 \times 10^5 \pm 1.1 \times 10^5$ and $6.9 \times 10^5 \pm 9.3 \times 10^4$ upon addition of 500 nM nicotine. When the α5-D398N subunit is present in the α4β2 pentamer, a statistically significant increase in PMID was not detected upon addition of nicotine. Measured PMID values for the α4β2α5-D398N pentamer are $6.8 \times 10^5 \pm 1.1 \times 10^5$ in the absence of nicotine and $1.1 \times 10^6 \pm 2.1 \times 10^5$ after nicotine is added (Figure 4.7A). Nicotine increased the expression of α4β2, but not α4β2α5 or α4β2α5-D398N (Figure 4.7; $P < 0.001$).

No statistical differences in the distribution towards the plasma membrane as a result of nicotine exposure are detected in these studies for either α5 containing subtypes (Figure 4.7B). Upon addition of nicotine, the % PM of α4β2 is increased to 32.3 ± 2.9% from a control of 19.1 ± 1.4% (Figure 4.7B; $P < 0.001$). In α4β2α5, % PM is measured as 21.8 ± 1.9% and 23.6 ± 2.7% for cells in the absence or presence of nicotine, respectively.

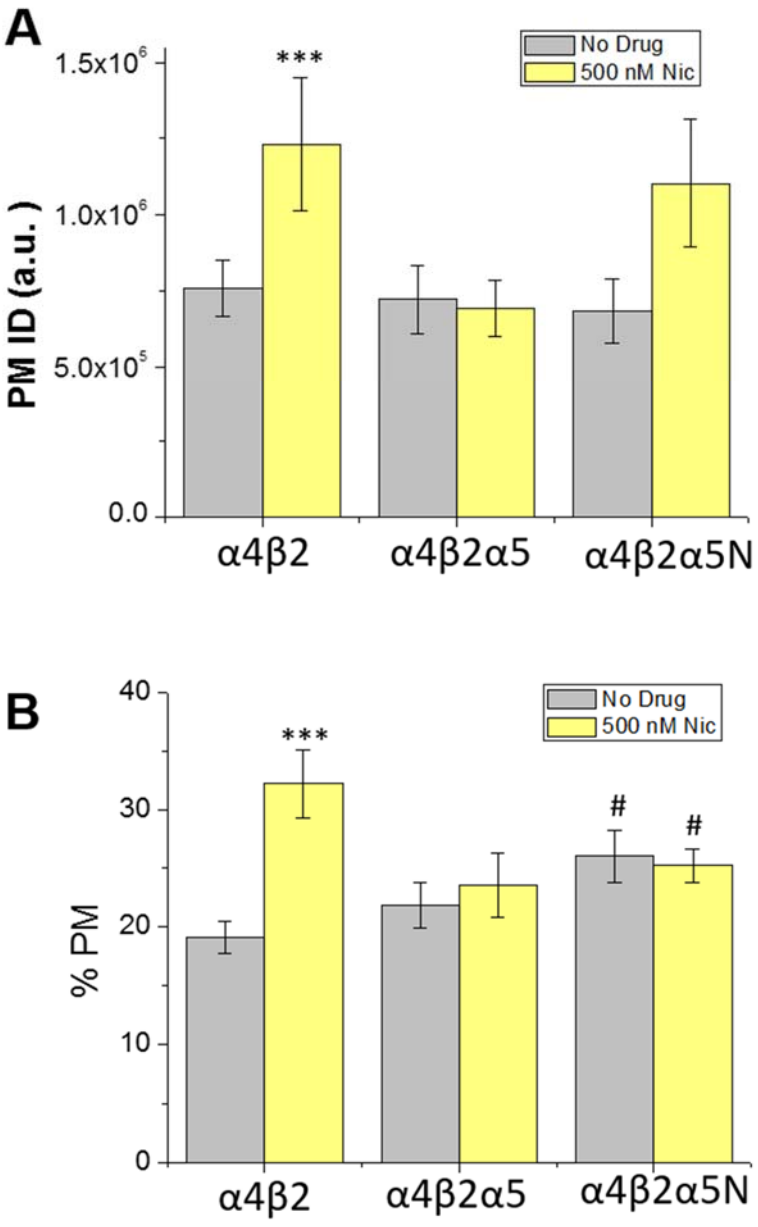

Figure 4.7 Nicotine upregulates α4β2 but not α4β2α5D or α4β2α5N. Nicotine causes an increase in PMID (A) and % PM (B) of α4β2, but not α4β2α5D or α4β2α5N. α4β2α5N has a higher % PM than α4β2α5D, independent of nicotine exposure. (n = 14, 15, 13, 11, 16, 10) Data are mean values ± SEM (#, $P < 0.05$ compared to α4β2α5D; ***, $P < 0.001$ compared to α4β2 without nicotine), *a.u.,* arbitrary units.

For cells expressing α4β2α5-D398N, the % PM is 26.0 ± 2.2% with no drug exposure and 25.2 ± 1.4% after the addition of nicotine. Both of these values are higher than the % PM of α4β2 or α4β2α5D, although this increase in distribution appears to be independent of the presence of nicotine (Figure 4.7B; $P < 0.001$). Nicotine increases the distribution of α4β2 towards the plasma membrane, but does not alter trafficking of α4β2α5 or α4β2α5-D398N.

4.2.2 Cotinine does not Upregulate α4β2α5D

No significant changes in the expression levels or distribution towards the plasma membrane were measured in these SEP based studies in α4β2α5D upon exposure to cotinine, as shown in Figure 4.8. PMID was detected for α4β2α5D exposed to varying concentrations of cotinine from 100 nM to 5 μM. Control α4β2α5D cells with no exposure to cotinine had a PMID of $4.2 \times 10^5 \pm 5.2 \times 10^4$ (Figure 4.8A). Cells exposed to 100 nM, 500 nM, 1 μM or 5 μM cotinine had PMIDs of $4.4 \times 10^5 \pm 6.1 \times 10^4$, $4.5 \times 10^5 \pm 4.1 \times 10^4$, $4.5 \times 10^5 \pm 7.7 \times 10^4$, and $4.3 \times 10^5 \pm 4.4 \times 10^4$, respectively. No significant differences in α4β2α5D PMID were detected between control cells and those exposed to cotinine at any concentration evaluated.

There were also no significant differences detected in the distribution of α4β2α5D upon exposure to cotinine. The % PM of α4β2α5D in the absence of cotinine is 24.8 ± 1.9% (Figure 4.8B). Upon addition of cotinine, the % PM is measured as 25.1 ± 1.4%, 23.8 ± 1.7%, 26.2 ± 1.7%, and 24.1 ± 1.3% for cells exposed to 100 nM, 500 nM, 1 μM or 5 μM cotinine, accordingly. Cotinine did not alter the % PM of α4β2α5D at any concentration used in this study. Representative images of cells transiently transfected

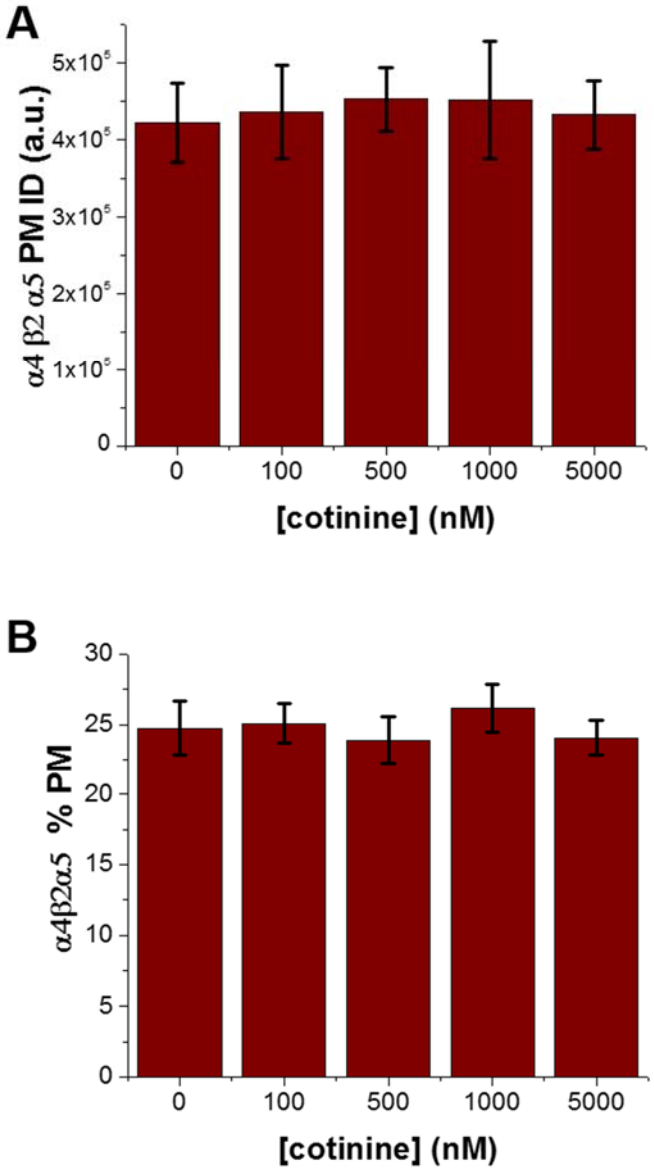

Figure 4.8 Cotinine does not alter expression of α4β2α5D. Quantification of (A) PMID or (B) % PM show no significant differences when α4β2α5D is exposed to 100 nM to 5 μM cotinine. (n = 19, 21, 20, 10, 37) Data are mean values ± SEM, *a.u.,* arbitrary units.

with α4β2α5D are shown in Figure 4.9. Cells expressing α4β2α5D in the absence of drug (Figure 4.9A), or in the presence of nicotine (Figure 4.9B), or cotinine (Figure 4.9C), appear similar in distribution of α4-SEP/β2/α5D towards the plasma membrane and relative expression of these nAChRs on the plasma membrane.

4.2.3 Incorporation of α5-D398N into α4β2 Increases Distribution to the PM

Similar to α4β2 pentamers containing α5D, incorporation of α5-D398N resulted in a loss of upregulation in expression or trafficking of α4β2 when exposed to cotinine. The PMID of cells transfected with α4β2α5-D398N in the absence of any drug was $7.4 \times 10^5 \pm 1.1 \times 10^5$ (Figure 4.10A). Upon the addition of 100 nM, 500 nM, 1 μM, or 5 μM cotinine, the PMIDs were $7.6 \times 10^5 \pm 1.1 \times 10^5$, $8.0 \times 10^5 \pm 9.8 \times 10^4$, $7.3 \times 10^5 \pm 7.0 \times 10^4$, and $7.7 \times 10^5 \pm 6.7 \times 10^4$, respectively. Addition of cotinine did not significantly change PMID of α4β2α5-D398N at the concentrations measured in this study. There were also no statistical differences between the PMID of cells expressing α4β2α5-D398N compared to those expressing α4β2α5D, with a PMID of $5.8 \times 10^5 \pm 1.0 \times 10^5$ (Figure 4.10A).

Likewise, no cotinine dependent differences in distribution towards the plasma membrane were detected in cells expressing α4β2α5-D398N (Figure. 4.10B). In the absence of cotinine, the % PM for α4β2α5-D398N cells was 30.8 ± 2.2%. This value was measured to be 32.2 ± 3.3%, 30.1 ± 2.3%, 35.3 ± 2.8%, and 37.5 ± 2.8% for cells exposed to 100 nM, 500 nM, 1 μM, and 5 μM cotinine, respectively (Figure 4.10B). Interestingly, the % PM for all cells expressing the α5-D398N version of the accessory subunit was significantly higher than the % PM of cells expressing the α5D version. The % PM for α4β2α5D was lower than α4β2α5-D398N, with a % PM of 19.4 ± 2.6% (Figure 4.10B; P

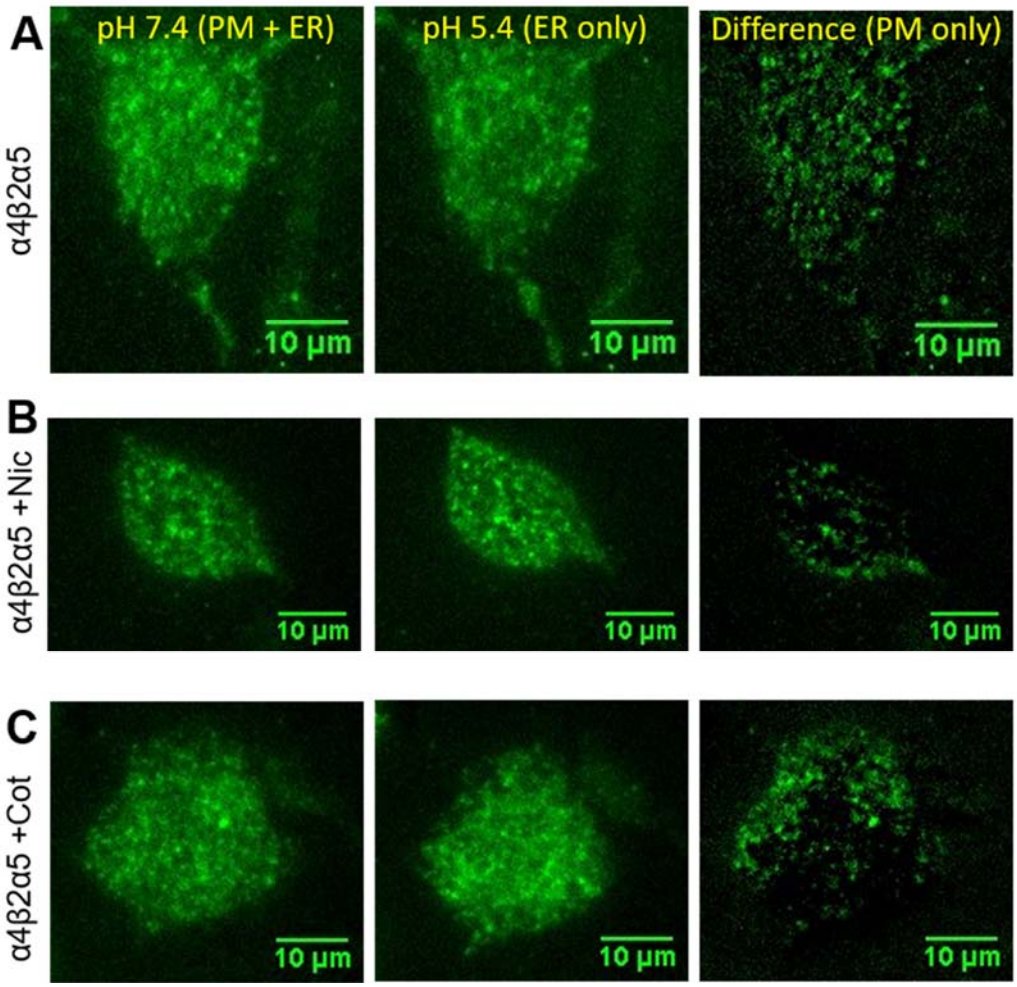

Figure 4.9 Representative TIRF images of cells expressing α4β2α5D. N2a cells expressing α4-SEP/β2/α5D exposed to (A) no drug, (B) 500 nM nicotine, or (C) 1 µM cotinine at pH 7.4, and pH 5.4. Similar PMID footprints are detected in each condition.

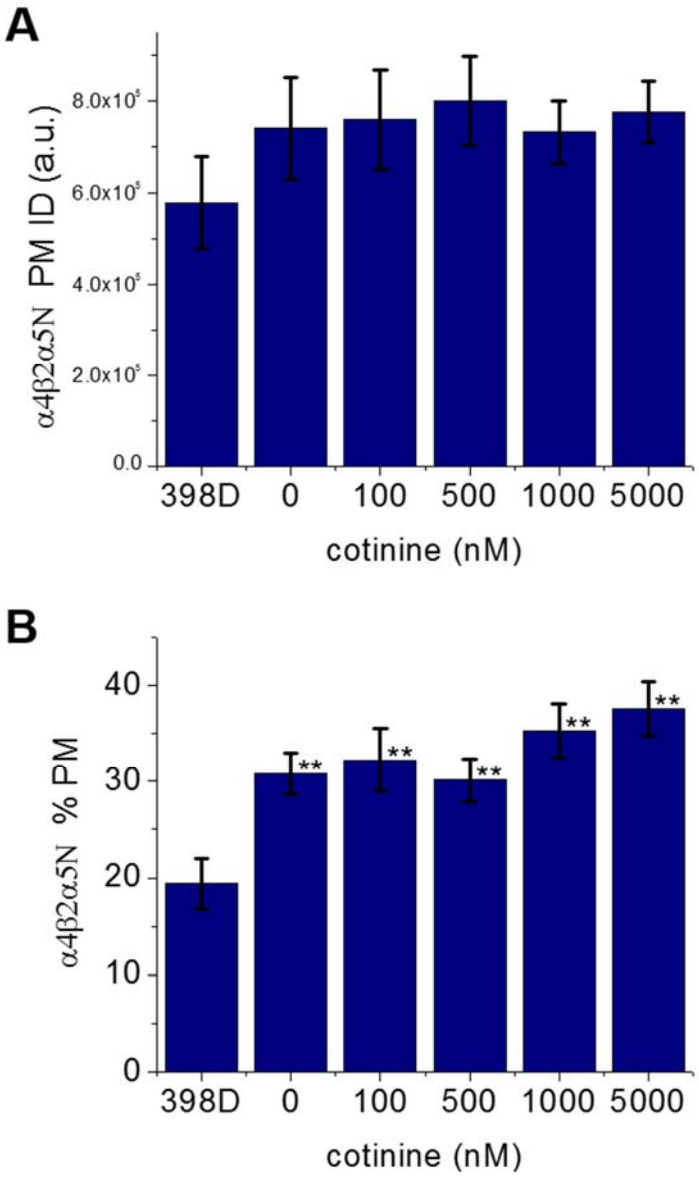

Figure 4.10 Incorporation of α5-D398N increases distribution towards the PM. No significant changes in PMID (A) are seen between α4β2α5D and α4β2α5-D398N, or α4β2α5-D398N exposed to cotinine, but α4β2α5-D398N has a higher % PM than α4β2α5D (B) independent of cotinine concentration. (n = 14, 23, 26, 33, 24, 30) Data are mean values ± SEM (**, $P < 0.01$ compared to 398D), *a.u.,* arbitrary units.

< 0.01). This increase in distribution towards the plasma membrane appears to be independent of the presence of cotinine, since all % PM values of α4β2α5-D398N expressing cells are not significantly different from each other. Representative images of cells transiently transfected with α4β2α5-D398N compared to α4β2α5D, with or without nicotine or cotinine are shown in Figure 4.11. Cells in the absence of drug expressing α4β2α5D (Figure 4.11A), or α4β2α5-D398N (Figure 4.11B) show higher distribution towards the plasma membrane when α5-D398N is present. There are no apparent differences in relative expression or distribution towards the plasma membrane in cell expressing α4β2α5-D398N upon exposure to nicotine (Figure 4.11C), or cotinine (Figure 4.11D).

4.3 Low Concentrations of Cotinine Decreases α6β2β3 nAChR Density on the PM

4.3.1 Cotinine does not Upregulate α6β2

Labeling the α6 subunit with SEP for pH sensitive studies showed that the density of α6β2 nAChRs on the plasma membrane does not depend on the presence of cotinine. There were no detected changes in the PMID of α6β2 nAChRs when cells were exposed physiologically relevant concentrations of cotinine. The PMID of cells expressing α6β2 in the absence of drug was $8.9 \times 10^5 \pm 1.2 \times 10^5$ (Figure 4.12A). The relative levels of expression of these cells upon addition of cotinine are $8.7 \times 10^5 \pm 7.5 \times 10^4$, $8.5 \times 10^5 \pm 1.0 \times 10^5$, $8.9 \times 10^5 \pm 9.1 \times 10^4$, and $9.5 \times 10^5 \pm 1.7 \times 10^5$ at concentrations of 100 nM, 500 nM, 1 μM or 5 μM cotinine, respectively. No significant differences in α6β2 PMID were detected between control cells and those exposed to any concentrations of cotinine evaluated in this study (Figure 4.12A).

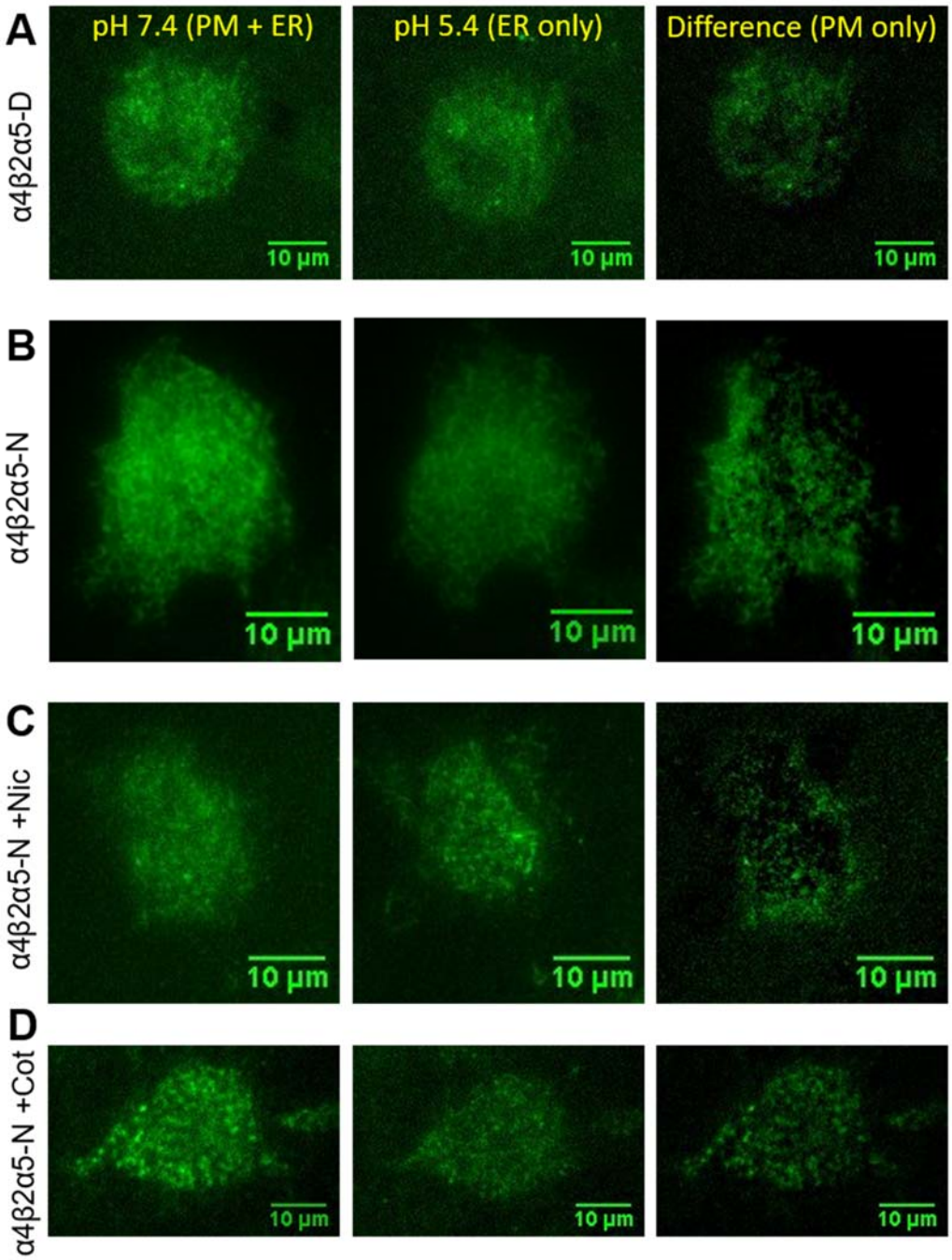

Figure 4.11 Representative TIRF images of cells expressing α4β2α5-D398N. N2a cells expressing α4-SEP/β2/α5-D398N exposed to (B) no drug, (C) 500 nM nicotine, or (D) 1 µM cotinine show a higher % PM than α4β2α5D (A) but no difference in PMID.

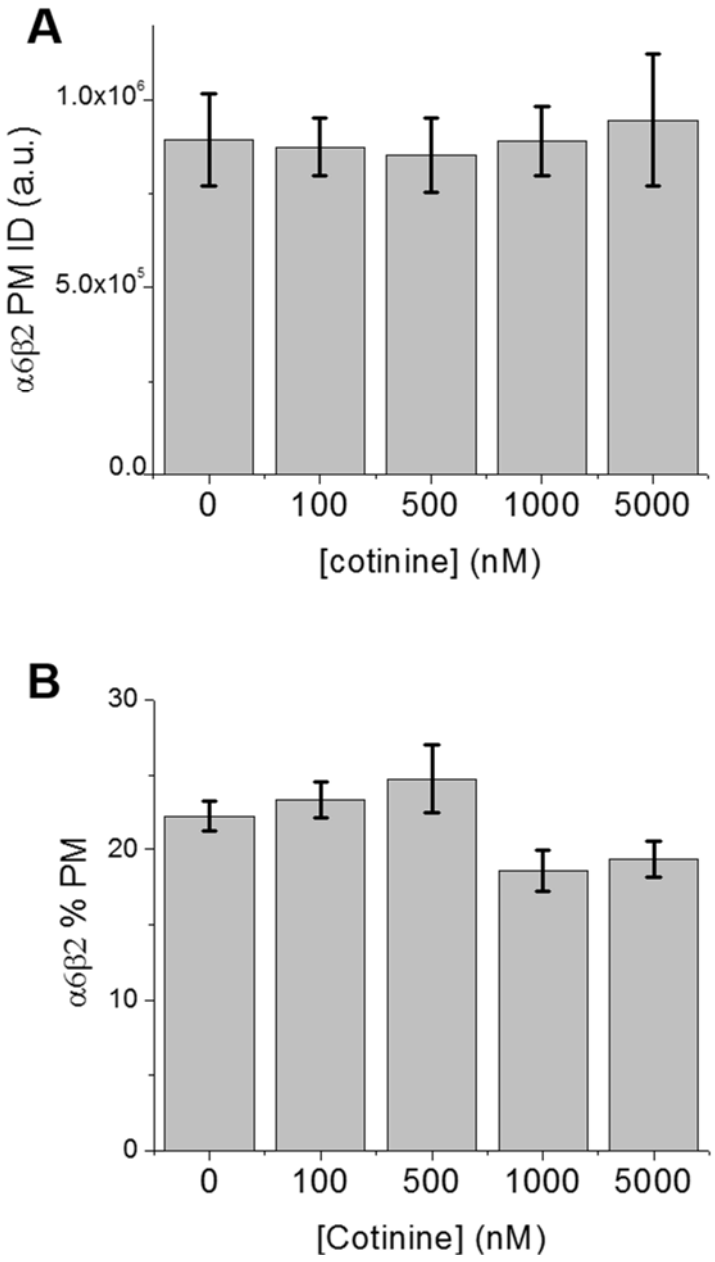

Figure 4.12 Cotinine does not alter expression of α6β2. Quantification of (A) PMID or (B) % PM show no significant differences when α6β2 is exposed to 100 nM to 5 μM cotinine. (n = 18, 11, 9, 18, 8) Data are mean values ± SEM, *a.u.,* arbitrary units.

The distribution of α6β2 towards the plasma membrane was also not affected by the addition of cotinine. Control cells expressing α6β2 showed a % PM of 22.2 ± 1.0% (Figure 4.12B). The % PM upon exposure to 100 nM, 500 nM, 1 μM or 5 μM cotinine were 23.4 ± 1.2%, 24.7 ± 2.2%, 18.6 ± 1.3%, and 19.4 ± 1.1%, respectively. This SEP based method did not show any significant differences in the distribution of α6β2 between the plasma membrane and peripheral endoplasmic reticulum at any concentrations of cotinine measured (Figure 4.12).

4.3.2 Low Concentrations of Cotinine Decreases α6β2β3 nAChR Density on the PM

The effect of cotinine on the expression of α6β2β3 nAChRs was also evaluated. Matching previous reports, these SEP based studies with the α6 subunit labeled show that incorporation of the β3 subunit into an α6β2 pentamer increases expression levels on the plasma membrane [115] (Figure 4.13A; $P < 0.05$), with the PMID of α6β2β3 being 1.2 x $10^6 \pm 1.5$ x 10^5 compared to that of α6β2 at 8.3 x $10^5 \pm 6.5$ x 10^4. Once β3 is included in the pentamer, there appears to be a cotinine concentration dependent response resulting in lower levels of α6β2β3 nAChR on the plasma membrane. At low levels of cotinine (100 nM), there is a trend towards a decreased number of α6β2β3 nAChRs, with a PMID of 7.8 x $10^5 \pm 1.7$ x 10^5. This decrease reaches a level of significance with 500 nM cotinine (Figure 4.13A; $P < 0.05$), with a PMID corresponding to 8.1 x $10^5 \pm 5.9$ x 10^4. The downregulated level of expression of α6β2β3 with 500 nM cotinine is comparable to that of α6β2 when the β3 subunit is absent. Downregulation is less pronounced, although not significant, when cotinine treatment was increased to 1 μM cotinine, with a PMID of 9.2 x $10^5 \pm 1.1$ x 10^5. At 5 μM cotinine, downregulation is completely lost, as the PMID of 1.2

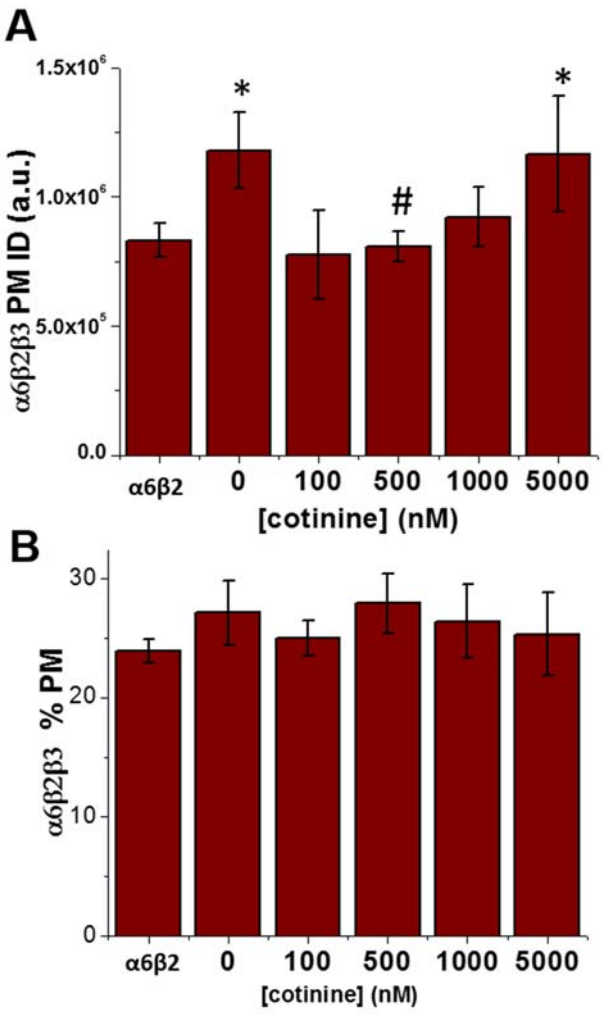

Figure 4.13 Cotinine induced downregulation of α6β2β3. (A) Quantification of PMID for α6β2β3 compared to α6β2 shows a significant increase in number of receptors on the PM when β3 is incorporated. When β3 is present, 500 nM cotinine significantly decreases the PMID. (B) No changes in % PM in the presence of cotinine or compared to α6β2 were detected. (n = 18, 19, 27, 16, 11, 11) Data are mean values ± SEM (*, $P < 0.05$ compared to α6β2; #, $P < 0.05$ compared to α6β2β3 with no drug), *a.u.,* arbitrary units.

x $10^6 \pm 2.2 \times 10^5$ is comparable to α6β2β3 with no drug (Figure 4.13A). This shows α6β2β3 nAChRs are downregulated at low concentrations of cotinine (500 nM) in this study.

The percentage of α6β2β3 within the TIRF field of view was not altered by the addition of cotinine (Figure 4.13B). Also, the % PM value for α6β2β3 nAChRs were not significantly different than the % PM of α6β2. The % PM of α6β2β3 was 27.1 ± 2.7%, compared to 23.9 ± 1.0% for α6β2. Exposing α6β2β3 nAChRs to 100 nM, 500 nM, 1 μM or 5 μM cotinine lead to % PM values of 25.0 ± 1.5%, 27.9 ± 2.5%, 26.4 ± 3.1% and 25.3 ± 3.5%, respectively. No significant differences were measured when comparing the % PM of α6β2 to α6β2β3, or between α6β2β3 nAChRs upon addition of any concentration of cotinine (Figure 4.13B). Representative cell images expressing α6β2 and α6β2β3 in the presence or absence of cotinine are shown in Figure 4.14. Exposing α6β2 expressing cells to cotinine does not alter the relative number of nAChRs located on the plasma membrane. Incorporating the accessory β3 subunit increases the PMID, evident by a higher intensity on the plasma membrane. Upon addition of 500 nM cotinine, the α6β2β3 are downregulated to a level comparable to α6β2 alone, as seen in cells with a similar PMID footprint.

4.4 Nicotine and Cotinine do not Alter Expression or Distribution of α3β4 nAChRs

4.4.1 Nicotine does not Increase Expression of α3β4 nAChRs

Cells were transiently transfected with α3-SEP/β4, with or without the accessory α5 or α5-D398N subunit. These cells were exposed to a physiologically relevant concentration of 500 nM nicotine for 48 hours. Detection of SEP-labeled nAChRs showed no differences in relative expression of α3β4 on the plasma membrane upon addition of

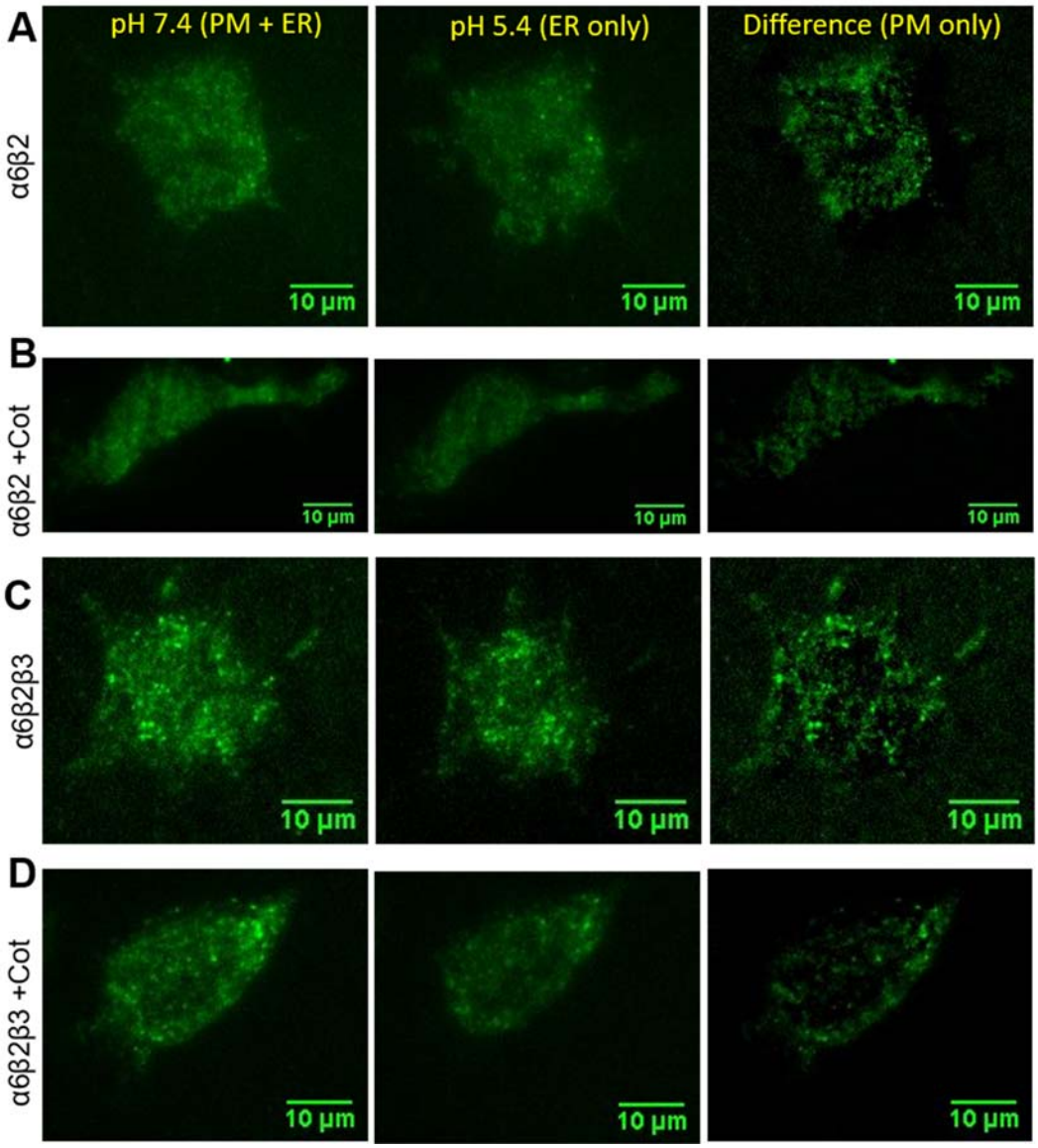

Figure 4.14 Representative TIRF images of cells expressing α6β2 or α6β2β3. N2a cells expressing α6-SEP/β2 exposed to no drug (A), or 500 nM cotinine (B), show no significant changes. However, α6β2β3 is significantly downregulated upon exposure to 500 nM cotinine (D), compared to no drug (C).

nicotine, as measured by PMID (Figure 4.15A). The PMID of α3β4 with no drug exposure was 3.3 x 10^6 ± 7.5 x 10^5, compared to 2.9 x 10^6 ± 3.7 x 10^5 after exposure to 500 nM nicotine. After α5 is incorporated into the pentamer, the PMID of α3β4α5 is 3.2 x 10^6 ± 6.8 x 10^5 versus 3.6 x 10^6 ± 5.1 x 10^5 after addition of nicotine. Including α5-D398N in α3β4 also does not change the PMID, with values of 3.8 x 10^6 ± 6.9 x 10^5 and 2.8 x 10^6 ± 7.1 x 10^5 before and after the addition of nicotine, respectively. There were no statistical differences in the PMID of cells expressing α3β4, α3β4α5, or α3β4α5-D398N regardless of exposure to 500 nM nicotine (Figure 4.15A).

4.4.2 Nicotine does not Alter Distribution of α3β4 nAChRs

Cells expressing α3β4, with or without an accessory α5 or α5-D398N subunit, were also evaluated for changes in distribution of nAChRs within the plasma membrane and peripheral endoplasmic reticulum when exposed to nicotine (Figure 4.15B). The % PM of α3β4 was 48.1 ± 3.5%, compared to 49.9 ± 2.6% after exposure to nicotine. Cells expressing α3β4α5 had a % PM of 50.9 ± 2.5% without exposure to a drug and 45.7 ± 4.1% after addition of nicotine. Cells with incorporation of the α5-D398N subunit into the α3β4 pentamer had a % PM of 40.1 ± 3.9%, and 46.5 ± 2.7% with nicotine exposure. In each case, there were no significant changes in the distribution of these nAChR subtypes towards the plasma membrane when 500 nM nicotine is present (Figure 4.15B).

4.4.3 Cotinine does not Increase Expression of α3β4 nAChRs

Cells transfected with α3β4, α3β4α5, or α3β4α5-D398N were exposed to 1 μM cotinine to evaluate changes in expression levels. No signficant differences in relative

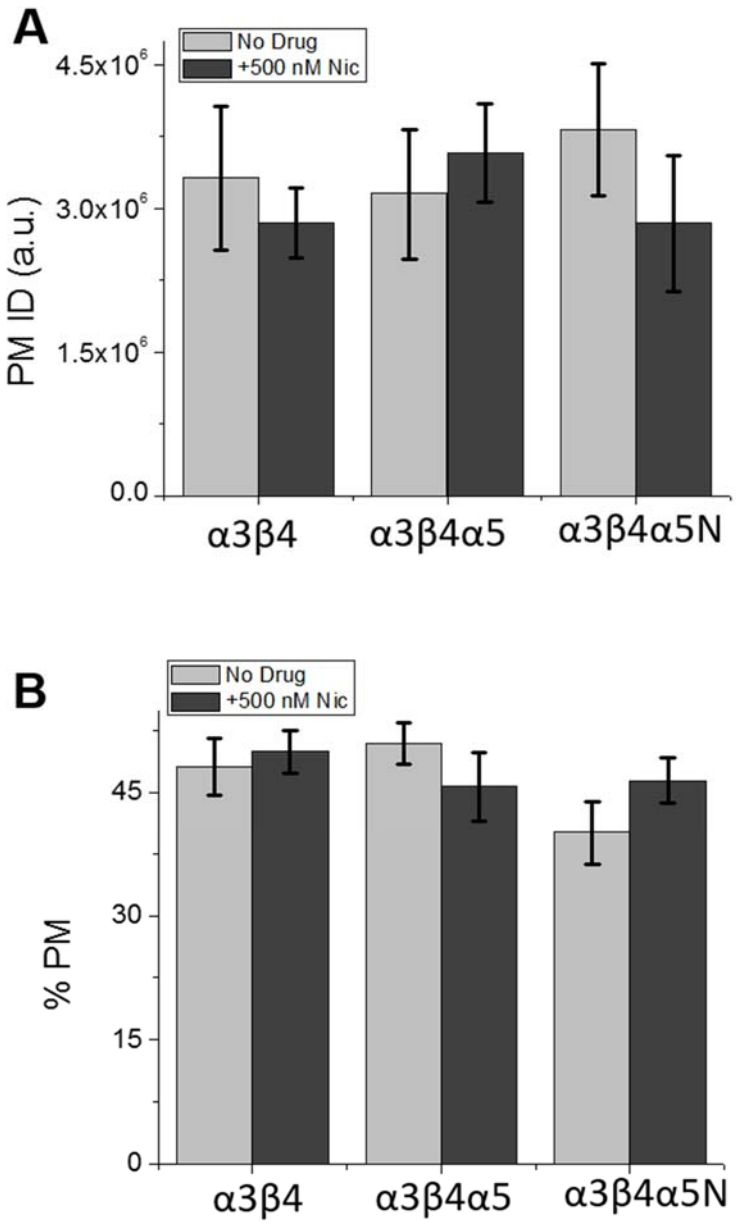

Figure 4.15 Nicotine does not alter expression of α3β4. Quantification of (A) PMID or (B) % PM show no significant differences in nAChR number or distribution when α3β4, α3β4α5, or α3β4α5-D398N is exposed to 500 nM nicotine. (n = 13, 14, 11, 11, 4, 8) Data are mean values ± SEM, *a.u.,* arbitrary units.

expression on the plasma membrane were detected upon addition of nicotine, as measured by the PMID of SEP-labeled nAChRs (Figure 4.16A). The PMID of control α3β4 was 3.3 x $10^6 \pm 7.5$ x 10^5, and 2.7 x $10^6 \pm 4.5$ x 10^5 after exposure to cotinine. When α5 is combined with the α3β4 pentamer, the PMID is 3.2 x $10^6 \pm 6.8$ x 10^5 with no drug exposure, compared to 3.0 x $10^6 \pm 6.2$ x 10^5 in the presence of cotinine. Cells expressing α3β4α5-D398N showed a PMID of 3.8 x $10^6 \pm 6.9$ x 10^5 without drug, and 3.0 x $10^6 \pm 4.3$ x 10^5 upon addition of cotinine. No statistical differences in the PMID of cells expressing α3β4, α3β4α5, or α3β4α5-D398N were measured in the absence or presence of 1 μM cotinine (Figure 4.15A).

4.4.4 Cotinine does not Alter Distribution of α3β4 nAChRs

Changes in distribution of nAChRs within the TIRF field of view was also assessed for cells expressing α3β4, with or without an accessory α5 or α5-D398N subunit after exposure to cotinine. No differences in % PM were measured using the SEP based technique (Figure 4.16B). The % PM of cells expressing α3β4 was 48.1 ± 3.5% and 46.4 ± 2.9% with and without the addition of cotinine, respectively. The % PM of control α3β4α5 cells was 50.9 ± 2.5% compared to 44.1 ± 3.3% upon the addition of cotinine. Cells expressing α3β4α5-D398N showed a % PM of 40.1 ± 3.9% without exposure to drug or 45.7 ± 3.5% after cotinine is added. No statistically different changes in trafficking were detected with α3β4, α3β4α5, or α3β4α5-D398N expressing cells were exposed to 1 μM cotinine for 48 hours (Figure 4.16B).

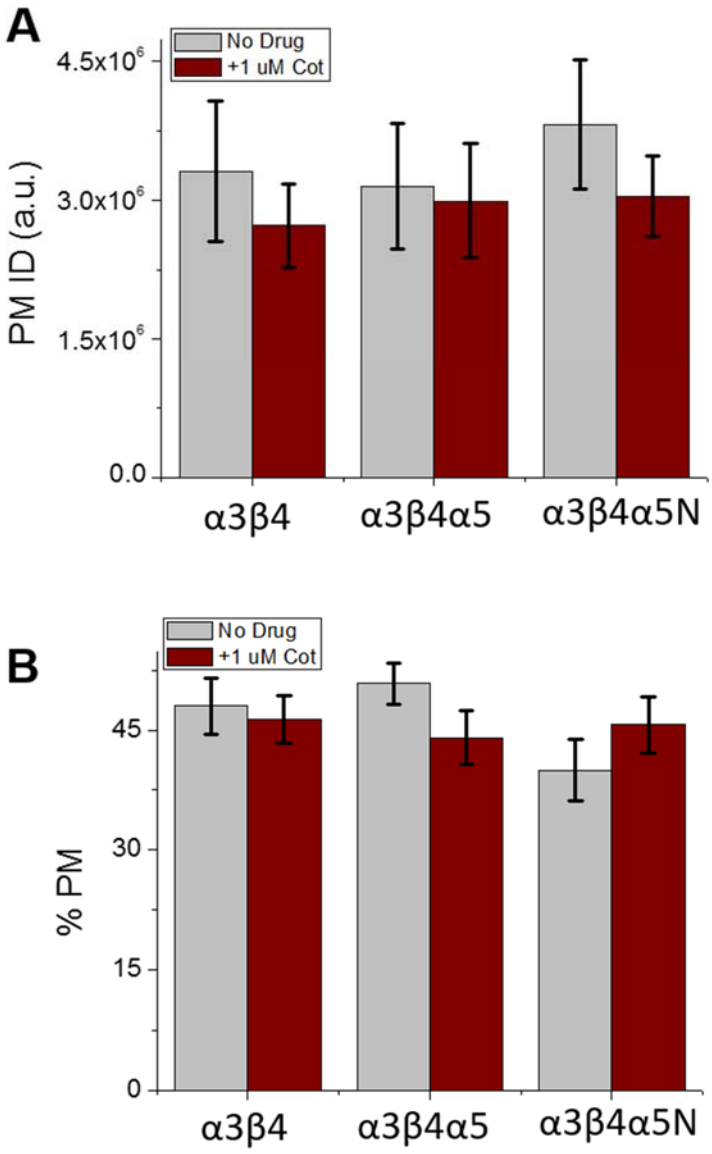

Figure 4.16 Cotinine does not alter expression of α3β4. Quantification of (A) PMID or (B) % PM show no significant differences in nAChR number or distribution when α3β4, α3β4α5, or α3β4α5-D398N are exposed to 1 μM cotinine (n = 13, 14, 11, 7, 4, 18) Data are mean values ± SEM, *a.u.,* arbitrary units.

Representative TIRF images of N2a cells expressing α3β4, α3β4α5, or α3β4α5-D398N with and without exposure to 500 nM nicotine or 1 μM cotinine are shown in Figure 4.17, Figure 4.18, and Figure 4.19, respectively. In each case, the PMID footprint of control cells compared to those exposed to nicotine or cotinine appear similar in intensity, corresponding to no changes in the expression levels of these nAChRs on the plasma membrane. Also, no changes in trafficking were measured, meaning the relative intensity differences between cells at pH 7.4 and pH 5.4 are similar. However, the distribution of α3β4, α3β4α5, and α3β4α5-D398N favors expression on the plasma membrane to a higher degree than β2-containing nAChRs, such as α4β2* or α6β2*. This is evident by a more pronounced PMID footprint in the *third column* of these figures.

4.5 Cotinine Exposure Results in Preferential Assembly of $(\alpha4)_2(\beta2)_3$

Since nAChRs are pentameric, α4β2 can assemble with either $(\alpha4)_3(\beta2)_2$ or $(\alpha4)_2(\beta2)_3$ stoichiometry. To determine assembly, a technique that our lab recently developed was used to perform single molecule analysis of subunit stoichiometry by spatially isolating nAChRs embedded in cell-membrane derived vesicles [228]. Vesicles were generated from cells expressing α4-GFP and β2-wt subunits. These vesicles were isolated on glass substrates, and TIRF microscopy was used to visualize the GFP fluorescence signal. Single step photobleaching of GFP was used to identify the number of α4-GFP subunits in each receptor. The number of bleaching steps corresponds to the number of GFP-tagged subunits present and, therefore, indicates the stoichiometry of the receptor [85, 224]. The number of individual vesicles showing one, two, or three bleaching steps was fit to a binomial distribution to account for the 90% probability that GFP will be

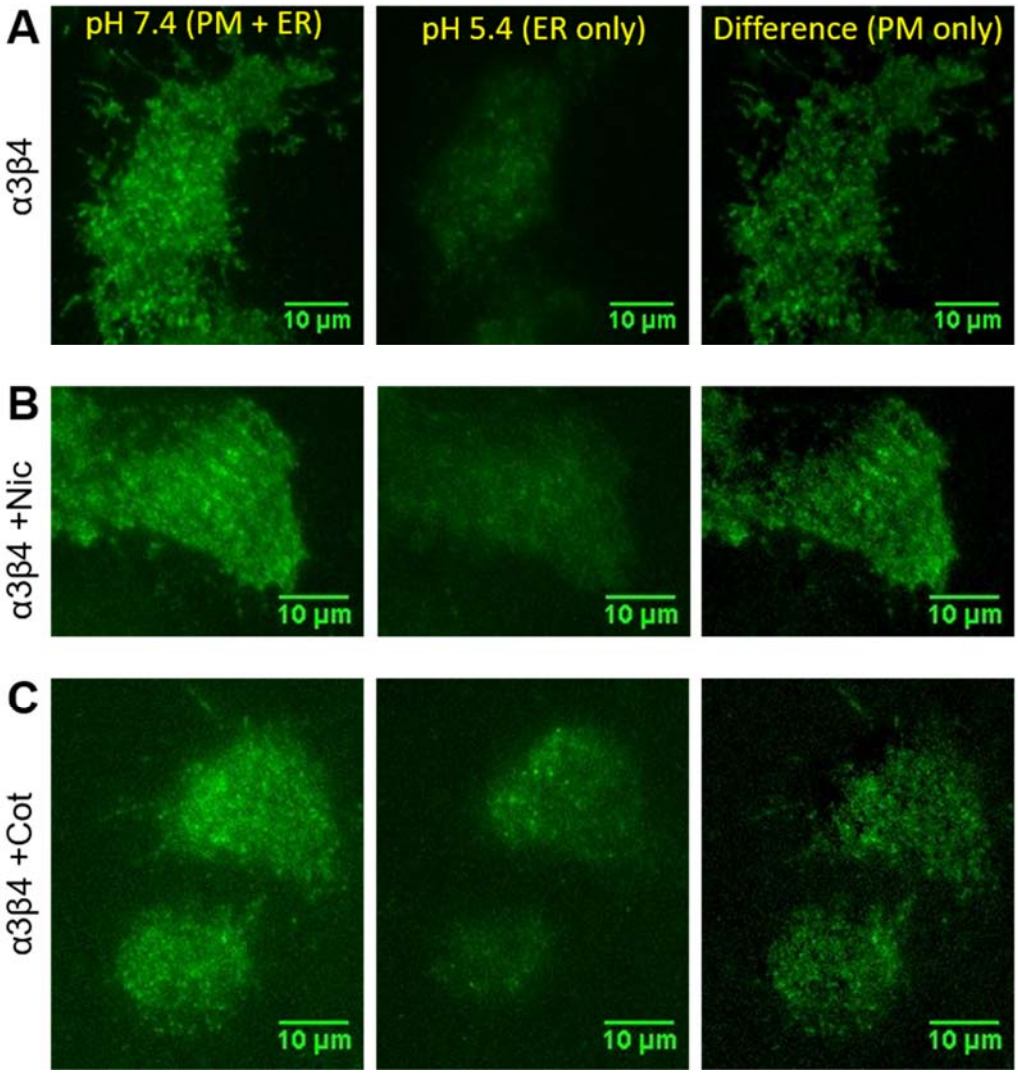

Figure 4.17 Representative TIRF images of cells expressing α3β4. N2a cells expressing α3-GFP/β4 exposed to (A) no drug, (B) 500 nM nicotine, or (C) 1 μM cotinine show no significant differences in the PMID footprint.

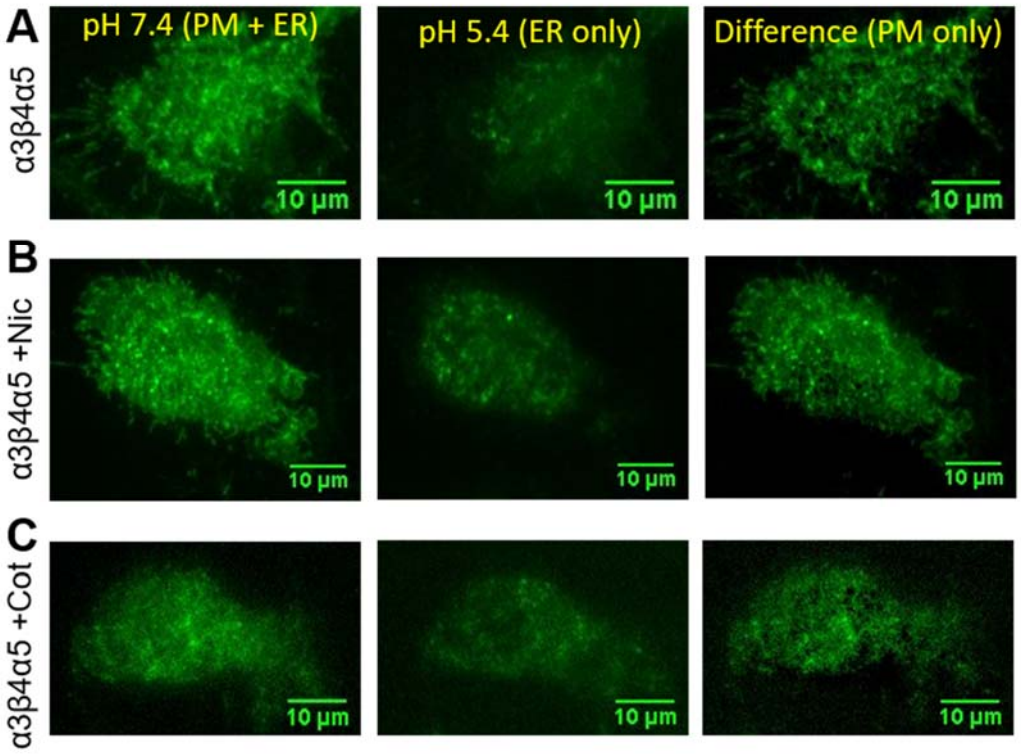

Figure 4.18 Representative TIRF images of cells expressing α3β4α5D. N2a cells expressing α3-GFP/β4/α5 exposed to (A) no drug, (B) 500 nM nicotine, or (C) 1 μM cotinine show no significant differences in the PMID footprint.

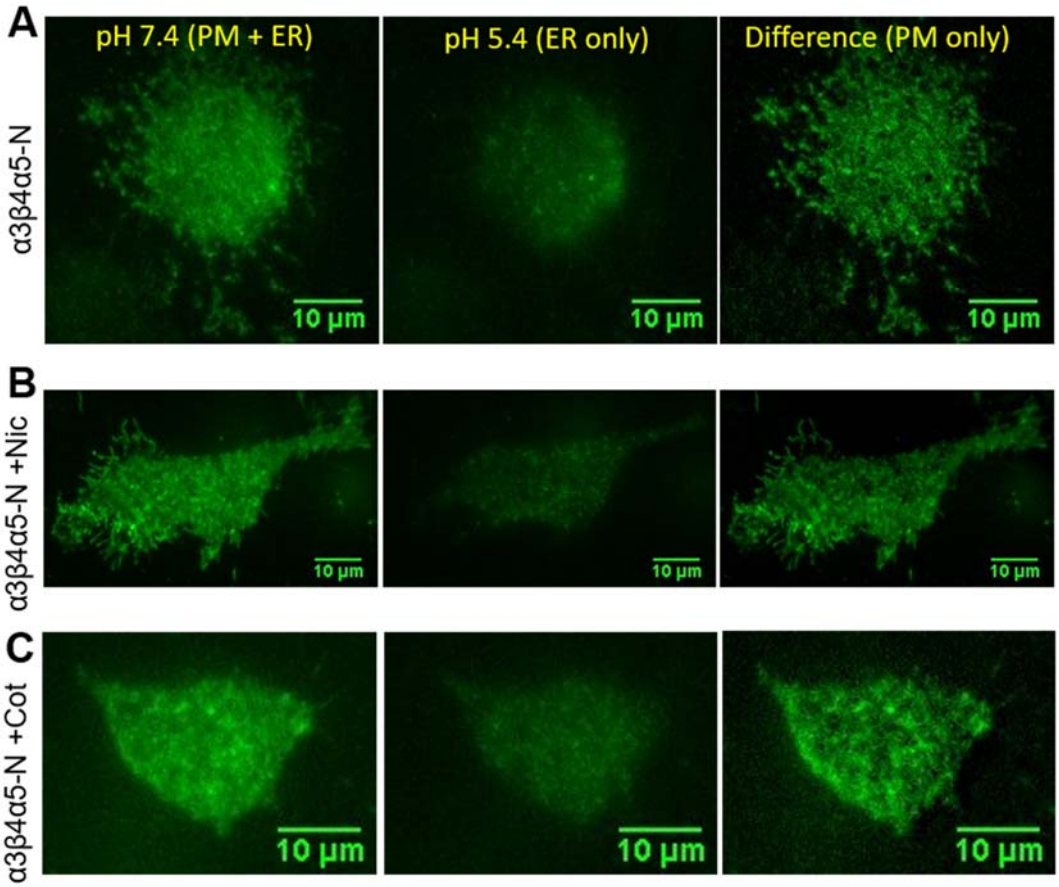

Figure 4.19 Representative TIRF images of cells expressing α3β4α5-D398N. N2a cells expressing α3-GFP/β4/α5-D398N exposed to (A) no drug, (B) 500 nM nicotine, or (C) 1 μM cotinine show no significant differences in the PMID footprint.

in a fluorescent state. The total number of observed one, two, or three bleaching steps in the presence of no drug, nicotine, or cotinine, is included in Table 4.1.

For cells not exposed to any compound, binomial distributions weighted for 40% $(\alpha4)_2(\beta2)_3$ and 60% $(\alpha4)_3(\beta2)_2$ fit the observed distribution. This distribution is verified using a chi-squared goodness of fit analysis. In the control sample, 8 ± 1% of vesicles showed one bleaching step, 48 ± 4% showed two bleaching steps, and 45 ± 4% showed three bleaching steps. These percentages correspond to observed fractions of 0.08 ± 0.01, 0.48 ± 0.04, and 0.45 ± 0.04, respectively, as shown in blue in Figure 4.20A. Error bars represent the square root of the number of counted events, given a Poisson distribution. These ratios are compared to expected fractions based on a 40:60 binomial distribution. Since α4β2 can assemble with either a $(\alpha4)_3(\beta2)_2$ or $(\alpha4)_2(\beta2)_3$, only two or three GFP molecules will be present. For two GFP molecules seen in $(\alpha4)_2(\beta2)_3$, with a 90% probability of GFP being in a fluorescent state, the contributions of 0.07 from one steps and 0.33 from two steps should be expected, shown in black in Figure 4.20A. For three GFP-labeled subunits, as in $(\alpha4)_3(\beta2)_2$, again fluorescing 90% of the time, the contributions of 0.02 from one steps, 0.15 from two steps, and 0.44 from three steps is expected, shown in red in Figure 4.20A. Taken together, the total number of one steps detected is expected to be 0.07 (from two GFPs) plus 0.02 (from three GFPs), or 0.09 as an expected value. This expected fraction of one steps, 0.09, is compared to the observed fraction of 0.08 ± 0.01 to get a chi-squared goodness of fit for detecting one bleaching step. For two steps, 0.33 (from two GFPs) and 0.15 (from three GFPs) are added for an expected value of 0.48, compared to the observed 0.48 ± 0.04 fraction of two counted bleaching steps. For three steps, the 0.44 (from three GFPs) is compared to the observed 0.45 ± 0.04. These expected

Table 4.1: Total Distribution of Observed α4-GFP/β2 Bleaching Steps with Nicotine or Cotinine Exposure

	# Vesicles Counted	1 Step	2 Steps	3 Steps	4 Steps
No Drug	359	28	171	160	12
Nicotine	325	40	202	83	11
Cotinine	305	47	194	64	10

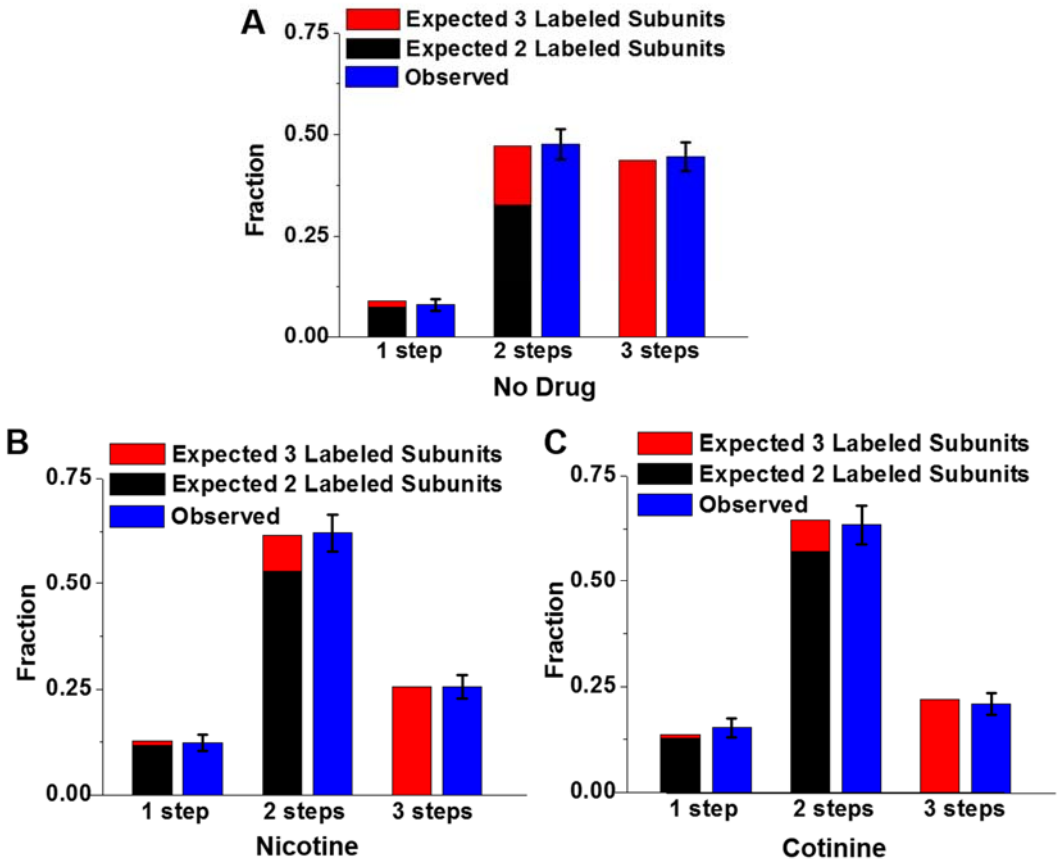

Figure 4.20 Binomial distributions showing a shift in stoichiometry when nicotine or cotinine are present. Observed (blue bars) and fitted (black/red bars) distributions of one, two, or three bleaching steps when α4-GFP/β2 is exposed to no drug (A), 500 nM nicotine (B) or 1 μM cotinine (C). Error bars are the square root of the number of vesicles counted.

versus observed distributions fit a binomial of 40% $(\alpha4)_2(\beta2)_3$ and 60% $(\alpha4)_3(\beta2)_2$ for control cells, verified by a chi-squared goodness of fit.

Treatment with 500 nM nicotine altered the stoichiometric distribution with a shift toward a higher percentage of receptors with the high sensitivity $(\alpha4)_2(\beta2)_3$ stoichiometry. The distribution of nicotine exposed cells was best fit for binomial distributions weighted with 65% $(\alpha4)_2(\beta2)_3$ and 35% $(\alpha4)_3(\beta2)_2$ (Figure 4.20B). This was derived from observed fractions of 0.12 ± 0.02 for one step, 0.62 ± 0.04 for two bleaching steps, and 0.26 ± 0.03 for three bleaching steps. The observed fractions were compared to expected values for a 35:65 distribution. The expected fraction of one steps is 0.13, or 0.12 from two α4-GFPs and 0.01 from three α4-GFPs. The expected fraction of two steps is 0.62, or 0.53 from two GFP molecules and 0.09 from three GFP molecules. The expected fraction of three steps is 0.26 with all three α4-GFPs in a pentamer fluorescing, with no contribution from two GFPs. A chi-squared test verified that the observed fractions fit a binomial distribution of 65% $(\alpha4)_2(\beta2)_3$ and 35% $(\alpha4)_3(\beta2)_2$.

The presence of 1 μM cotinine also resulted in a shift in the stoichiometric distribution toward the high sensitivity $(\alpha4)_2(\beta2)_3$ version. The observed distribution fit to binomials weighted 70% $(\alpha4)_2(\beta2)_3$ and 30% $(\alpha4)_3(\beta2)_2$ (Fiure. 4.20C). This corresponds to observed fractions of 0.15 ± 0.02 one steps, 0.64 ± 0.05 two steps, and 0.21 ± 0.03 three steps. This fits expected values for the 30:70 $(\alpha4)_2(\beta2)_3$ to $(\alpha4)_3(\beta2)_2$ distribution. The expected fraction of one steps for this distribution is 0.14, with 0.13 from two GFP-labeled subunits, and 0.01 from three GFP-labeled subunits. The expected fraction of two steps is 0.65, or 0.57 from two GFPs and 0.07 from three α4-GFPs. The expected fraction of three steps is 0.22 when three GFPs are present, with no contribution from two α4-GFPs. The

fit to a 70% $(\alpha4)_2(\beta2)_3$ and 30% $(\alpha4)_3(\beta2)_2$ binomial was verified with a chi-squared goodness of fit test.

Figure 4.21 compares the stoichiometries derived from the weighted fits of α4β2 with no drug, nicotine, and cotinine. Error bars are 95% confidence intervals. In the absence of a pharmacological agent, the inherent distribution fits a binomial of 40 ± 5% $(\alpha4)_2(\beta2)_3$ and 60 ± 4% $(\alpha4)_3(\beta2)_2$. Once nicotine is added, this distribution is shifted to fit a binomial of 65 ± 4% $(\alpha4)_2(\beta2)_3$ and 35 ± 6% $(\alpha4)_3(\beta2)_2$. Cotinine also alters the distribution towards the high sensitivity version, fitting a binomial of 70 ± 4% $(\alpha4)_2(\beta2)_3$ and 30 ± 6% $(\alpha4)_3(\beta2)_2$. Based on the 95% confidence intervals, both nicotine and cotinine distributions are different from the control distribution, although they are not different from each other ($P < 0.05$). This shows exposure to either nicotine or cotinine results in the preferential assembly of the high sensitivity $(\alpha4)_2(\beta2)_3$ receptor.

4.6 Biased Transfection of α4:β2 to Verify Changes in Stoichiometry

Previous studies have altered the primary stoichiometry of α4β2 expressed using biased transfections. During transfection, unequal amounts of plasmid encoding a nAChR subunit are added, leading to one subunit expressed at higher levels than the other within the cell [151, 154, 191, 233, 234]. These types of studies have primarily used Xenopus oocyte expression systems with changes in stoichiometry determined from changes in the biphasic dose response based on whole cell current measurements. To verify our observations of nicotine and cotinine induced changes in α4β2 stoichiometry, a control experiment was performed with biased transfection ratios of 10:1, 4:1, 1:1, and 1:4 (α4:β2).

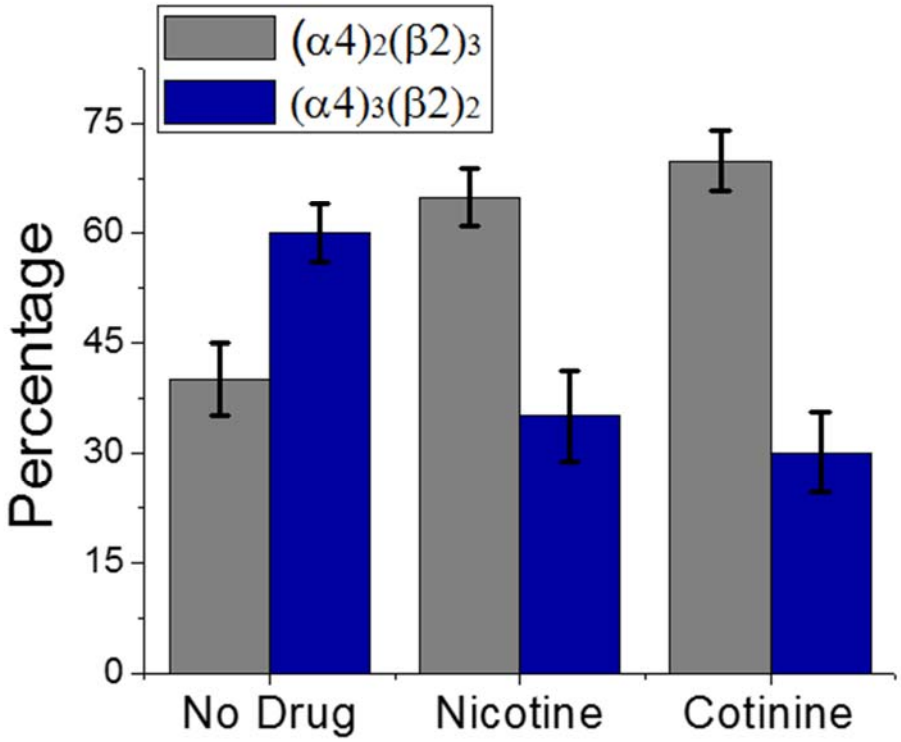

Figure 4.21 Nicotine and cotinine increase $(\alpha4)_2(\beta2)_3$ expression. When no drug is present, the counted bleaching steps fit a distribution of 40 ± 5% $(\alpha4)_2(\beta2)_3$ and 60 ± 4% $(\alpha4)_3(\beta2)_2$. The nicotine distribution fits a binomial of 65 ± 4% $(\alpha4)_2(\beta2)_3$ and 35 ± 6% $(\alpha4)_3(\beta2)_2$. The cotinine distribution fits a binomial of 70 ± 4% $(\alpha4)_2(\beta2)_3$ and 30 ± 6% $(\alpha4)_3(\beta2)_2$. Error bars are 95% confidence intervals.

The total number of counted vesicles for each ratio of plasmid, including those showing one, two, or three bleaching steps, is shown in Table 4.2. Binomial distributions for each biased transfection are shown in Figure 4.22, with error bars corresponding to the square root of the number of counted events.

The 10:1 (α4:β2) biased transfection fit a 30:70 $(\alpha4)_2(\beta2)_3$ to $(\alpha4)_3(\beta2)_2$ binomial distribution (Figure 4.22A). Fractions of observed one, two, and three bleaching steps were 0.08 ± 0.02, 0.40 ± 0.05, and 0.52 ± 0.06, respectively. The observed fractions of each number of bleaching steps were compared to expected fractions based on GFP fluorescing 90% of the time. The expected fraction of one steps for this fit is 0.07, with 0.05 from two GFP labeled subunits and 0.02 from three GFP labeled subunits. The expected fraction for two bleaching steps is 0.42, or 0.25 from two α4-GFPs and 0.17 from three α4-GFPs. The expected fraction for three bleaching steps is 0.51, corresponding to all three present GFP molecules fluorescing. Overall, the 10:1 biased transfection fit a 30% $(\alpha4)_2(\beta2)_3$ to 70% $(\alpha4)_3(\beta2)_2$ distribution.

Both 4:1 (Figure 4.22B) and 1:1 (Figure 4.22C) α4:β2 transfections fit a 40:60 $(\alpha4)_2(\beta2)_3$ to $(\alpha4)_3(\beta2)_2$ binomial distribution. The expected fraction of one steps for this distribution are 0.09, or 0.07 from two GFP molecules and 0.02 from three GFP molecules. The expected fraction of two steps is 0.47, with 0.33 from two GFP-labeled subunits and 0.15 from three GFP-labeled subunits. The expected fraction of three steps is 0.44 if all three GFP-labeled subunits fluoresce, with no contribution from two GFP-labeled subunits. The observed fractions in the 4:1 transfection were 0.08 ± 0.02, 0.49 ± 0.06, and 0.43 ± 0.05 for one, two, and three bleaching steps, respectively. The 1:1 transfection had observed fractions of 0.08 ± 0.02 for one step, 0.48 ± 0.04 for two steps, and 0.47 ±

Table 4.2: Total Distribution of Observed α4-GFP/β2 Bleaching Steps for Biased Transfections

	# Vesicles Counted	1 Step	2 Steps	3 Steps	4 Steps
10:1 α4GFP: β2wt	159	13	64	82	2
4:1 α4GFP: β2wt	146	12	71	63	5
1:1 α4GFP: β2wt	359	28	171	160	12
1:4 α4GFP: β2wt	187	24	116	47	0

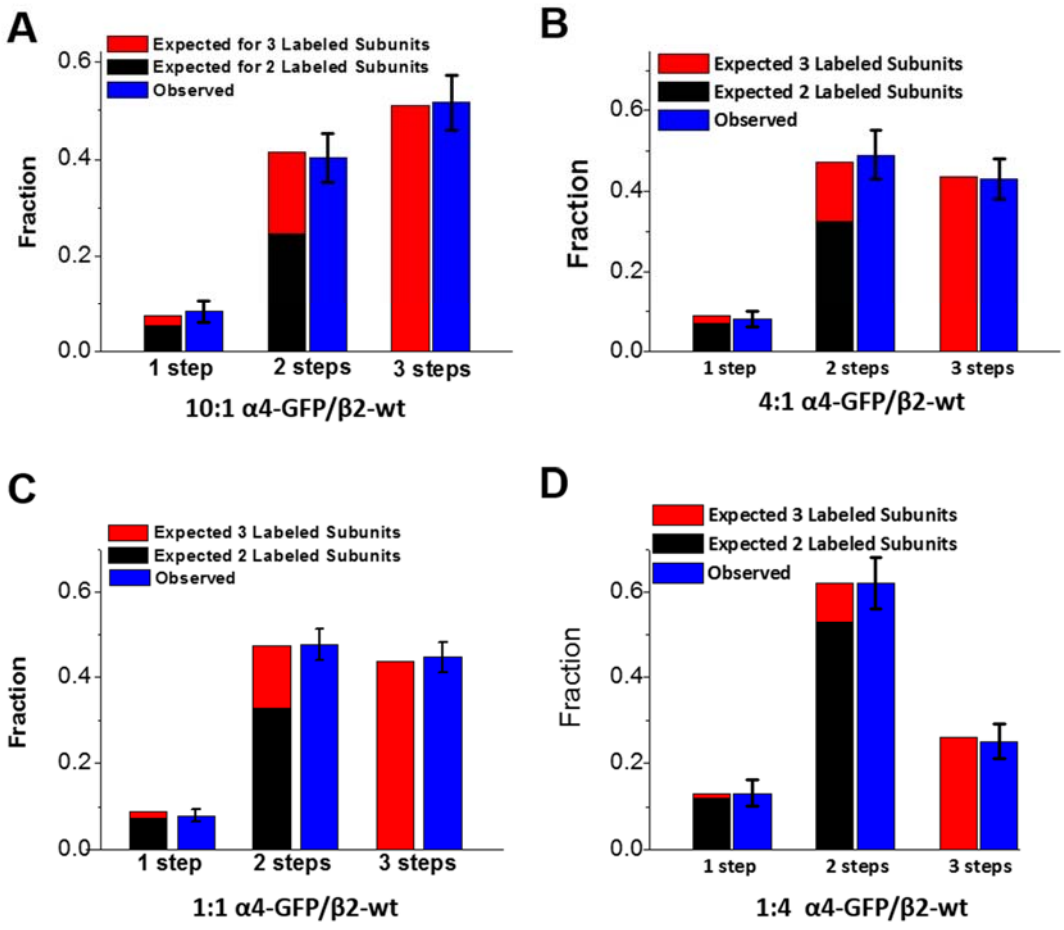

Figure 4.22 Binomial distributions for biased transfections. Observed and expected distributions of one, two, or three bleaching steps when α4-GFP/β2 is transfected in varying ratios of 10:1 (A), 4:1 (B), 1:1 (C), or 1:4 (D). Error bars are the square root of the number of vesicles counted.

0.04 for three steps. Both 4:1 and 1:1 α4:β2 transfections fit a binomial distribution of 40% $(\alpha4)_2(\beta2)_3$ to 60% $(\alpha4)_3(\beta2)_2$, verified to match expected values with a chi squared test, as defined earlier.

The 1:4 (α4:β2) biased transfection fit a 65:35 $(\alpha4)_2(\beta2)_3$ to $(\alpha4)_3(\beta2)_2$ binomial distribution (Figure 4.22D). The expected fraction of one step is 0.13, with 0.12 from two GFP-labeled subunits and 0.01 from three GFP-labeled subunits. The expected fraction of two steps is 0.62, with 0.53 from two GFP molecules and 0.09 from three GFP molecules. The expected fraction of three steps is 0.26, all from three GFP-labeled subunits. This distribution fit the observed data with fractions of 0.13 ± 0.03, 0.62 ± 0.06, and 0.25 ± 0.04 corresponding to one, two, and three bleaching steps, accordingly. A chi-squared goodness of fit test verified the observed number of bleaching steps fit a binomial weighted to 65% $(\alpha4)_2(\beta2)_3$ and 35% $(\alpha4)_3(\beta2)_2$.

Figure 4.23 compares the changes in α4β2 stoichiometry for all biased transfection ratios (α4:β2). Error bars are 95% confidence intervals. The 10:1 biased transfection fits a distribution of 30 ± 7 % $(\alpha4)_2(\beta2)_3$ and 70 ± 7% $(\alpha4)_3(\beta2)_2$. The 4:1 biased transfection fits a distribution of 40 ± 7% $(\alpha4)_2(\beta2)_3$ and 60 ± 4% $(\alpha4)_3(\beta2)_2$. The 1:1 transfection, as shown above, fits a 40 ± 4% $(\alpha4)_2(\beta2)_3$ and 60 ± 5% $(\alpha4)_3(\beta2)_2$. Finally, the 1:4 biased transfection fits a distribution of 65 ± 6% $(\alpha4)_2(\beta2)_3$ and 35 ± 9% $(\alpha4)_3(\beta2)_2$. Based on the 95% confidence intervals, the fraction of $(\alpha4)_3(\beta2)_2$ was reduced and the fraction of $(\alpha4)_2(\beta2)_3$ increased when higher levels of β2 were transfected (1:4 (α4:β2)) (Figure 4.23).

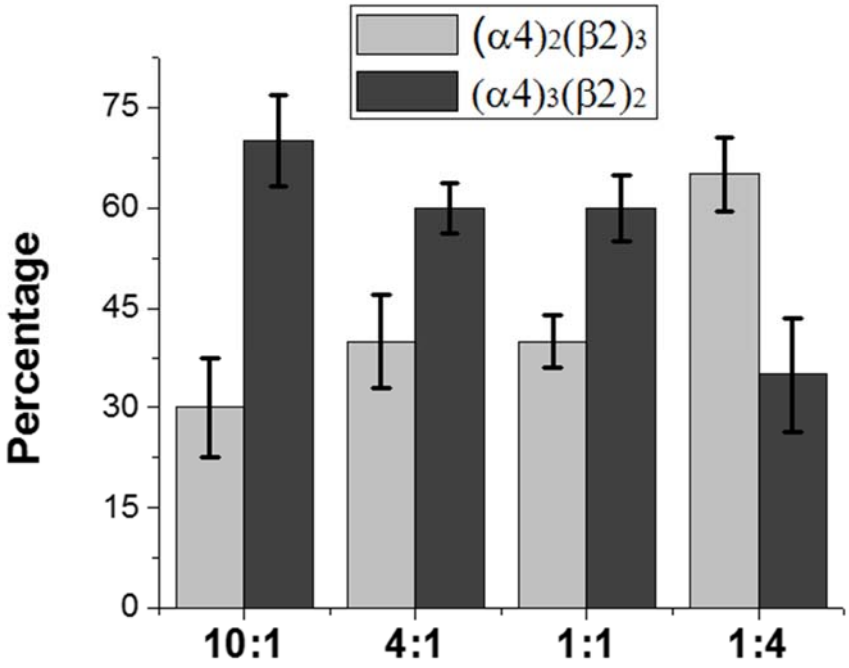

Figure 4.23 Biased transfections shift the distribution of $(\alpha4)_2(\beta2)_3$. The 10:1 bias transfection fits a distribution of 30 ± 7% $(\alpha4)_2(\beta2)_3$ and 70 ± 7% $(\alpha4)_3(\beta2)_2$. The 4:1 bias transfection fits a distribution of 40 ± 7% $(\alpha4)_2(\beta2)_3$ and 60 ± 4% $(\alpha4)_3(\beta2)_2$. The 1:1 transfection fits a 40 ± 4% $(\alpha4)_2(\beta2)_3$ and 60 ± 5% $(\alpha4)_3(\beta2)_2$. Finally, the 4:1 bias transfection fits a distribution of 65 ± 5% $(\alpha4)_2(\beta2)_3$ and 35 ± 9% $(\alpha4)_3(\beta2)_2$. Error bars are 95% confidence intervals.

4.7 Other nAChR Ligands Alter Expression, Trafficking, and Assembly of α4β2

4.7.1 Cytisine Upregulates α4β2

Cells transiently expressing α4-SEP/β2 were exposed to 500 nM of the partial agonist cytisine to evaluate changes in α4β2 expression and trafficking due to the presence of this ligand. The SEP based studies showed an upregulation of α4β2 upon exposure to cytisine (Figure 4.24). An increase in expression of α4β2 was measured as an increase in PMID, corresponding to $2.8 \times 10^6 \pm 2.1 \times 10^5$ for control cells and $7.3 \times 10^6 \pm 6.4 \times 10^5$ after exposure to 500 nM cytisine (Figure 4.24C; $P < 0.001$). Trafficking of α4β2 is also altered by the presence of cytisine. The distribution of α4β2 between the plasma membrane and peripheral endoplasmic reticulum is increased when cells are exposed to cytisine. This is shown by an increase in the % PM, being 21.5 ± 0.8% without drug and 36.9 ± 1.5% upon addition of cytisine (Figure 4.24D; $P < 0.001$). Representative TIRF images of cells expressing α4β2 with and without exposure to cytisine are shown in Figure 4.24. A PMID footprint with a relatively higher intensity corresponds to an increase in the number of α4-SEP/β2 nAChRs localized to the plasma membrane.

4.7.2 Varenicline Upregulates α4β2

Differences in expression and trafficking were also measured in cells expressing α4β2 after exposure to 500 nM varenicline, a partial agonist. A higher number of α4β2 nAChRs are found on the plasma membrane when varenicline is present, evinced by an increase in PMID from $2.8 \times 10^6 \pm 2.1 \times 10^5$ in the absence of drug to $5.6 \times 10^6 \pm 5.5 \times 10^5$ upon addition of varenicline (Figure 4.25C; $P < 0.001$). Trafficking of nAChRs towards the plasma membrane is also increased upon addition of varenicline, evident by an increase

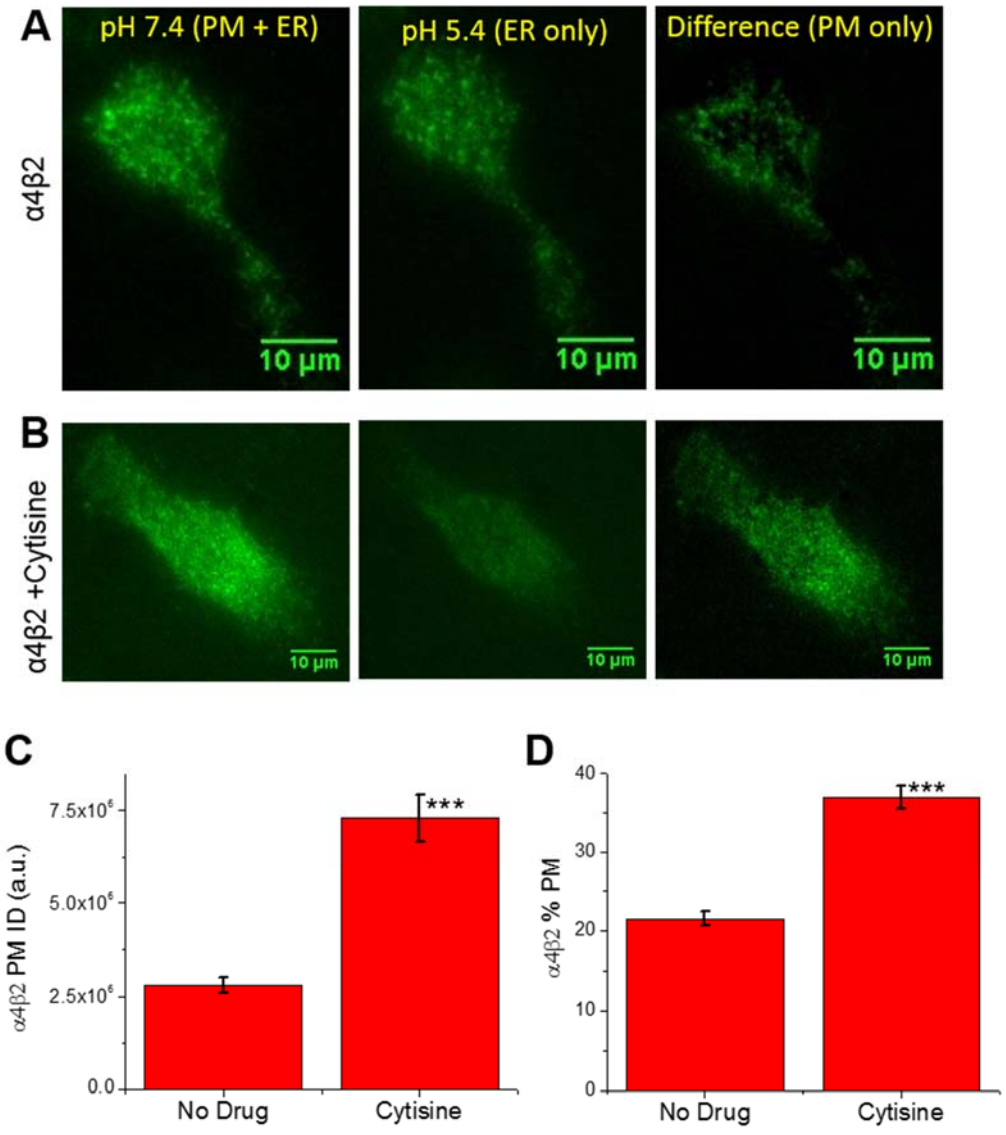

Figure 4.24 Cytisine upregulates α4β2. Representative cell images expressing α4-GFP/β2 exposed to no drug (A) or 500 nM cytisine (B). Cytisine increases the expression of α4β2 on the plasma membrane (C) and the distribution towards the plasma membrane (D). (n = 61, 42) Data are mean values ± SEM (***, $P < 0.001$), *a.u.,* arbitrary units.

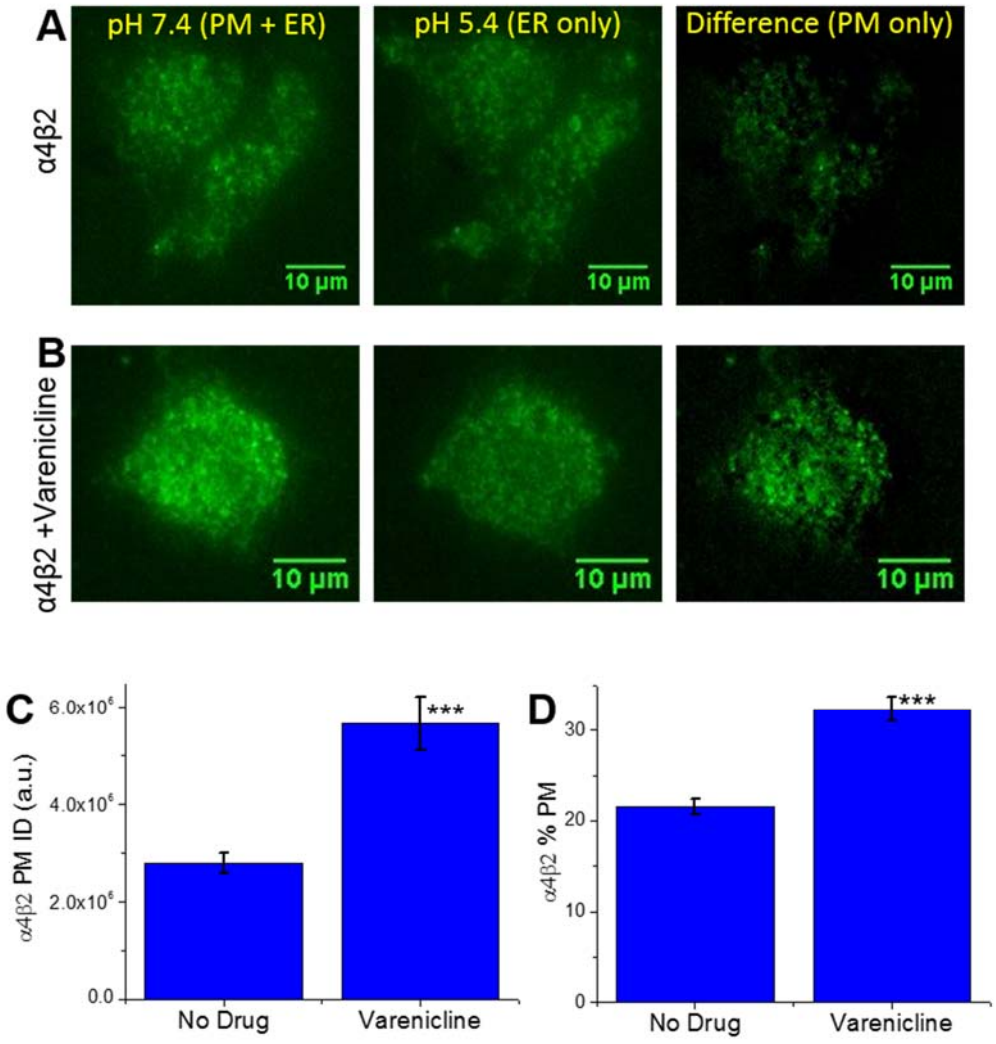

Figure 4.25 Varenicline upregulates α4β2. Representative cell images expressing α4-GFP/β2 exposed to no drug (A) or 500 nM varenicline (B). An increased PMID (C) and % PM (D) is measured when varenicline is present. (n = 61, 38) Data are mean values ± SEM (***, P < 0.001), *a.u.,* arbitrary units.

in % PM from 21.5 ± 0.8% to 32.3 ± 1.3% (Figure 4.25D; $P < 0.001$). This is qualitatively shown in representative cell images exposed to varenicline, as seen in Figure 4.25. Addition of varenicline to cells increases the PMID and % PM, evident by a brighter PMID footprint.

4.7.3 Bupropion Upregulates α4β2

Bupropion, a noncompetitive antagonist, was also administered to cells expressing α4β2 at a concentration of 500 nM. At this concentration, bupropion upregulates expression and trafficking of α4β2, as shown in Figure 4.26. Cells exposed to bupropion show an increase in PMID, from $2.8 \times 10^6 \pm 2.1 \times 10^5$ with no drug to $4.6 \times 10^6 \pm 3.6 \times 10^5$ upon bupropion exposure (Figure 4.26C; $P < 0.001$). The distribution of α4β2 nAChRs towards the plasma membrane from the endoplasmic reticulum is also increased. The % PM of control cells, 21.5 ± 0.8%, is increased to 31.4 ± 1.3% after exposure to bupropion (Figure 4.26D; $P < 0.001$). This upregulation is seen in representative cell images exposed to no drug (Figure 4.26A) or bupropion (Figure 4.26B). The increase in the PMID footprint reflects the increase in number of SEP-labeled α4β2 nAChRs located on the plasma membrane.

4.7.4 Ligands Alter Assembly of α4β2

In collaboration with another member of the Richards' group, Faruk H. Moonschi, single molecule photobleaching was also used to detect changes in the stoichiometry of α4β2 when cytisine, varenicline, or bupropion are present. Vesicles, generated from cells expressing α4-GFP/β2, were immobilized and imaged with TIRF microscopy. Table 4.3

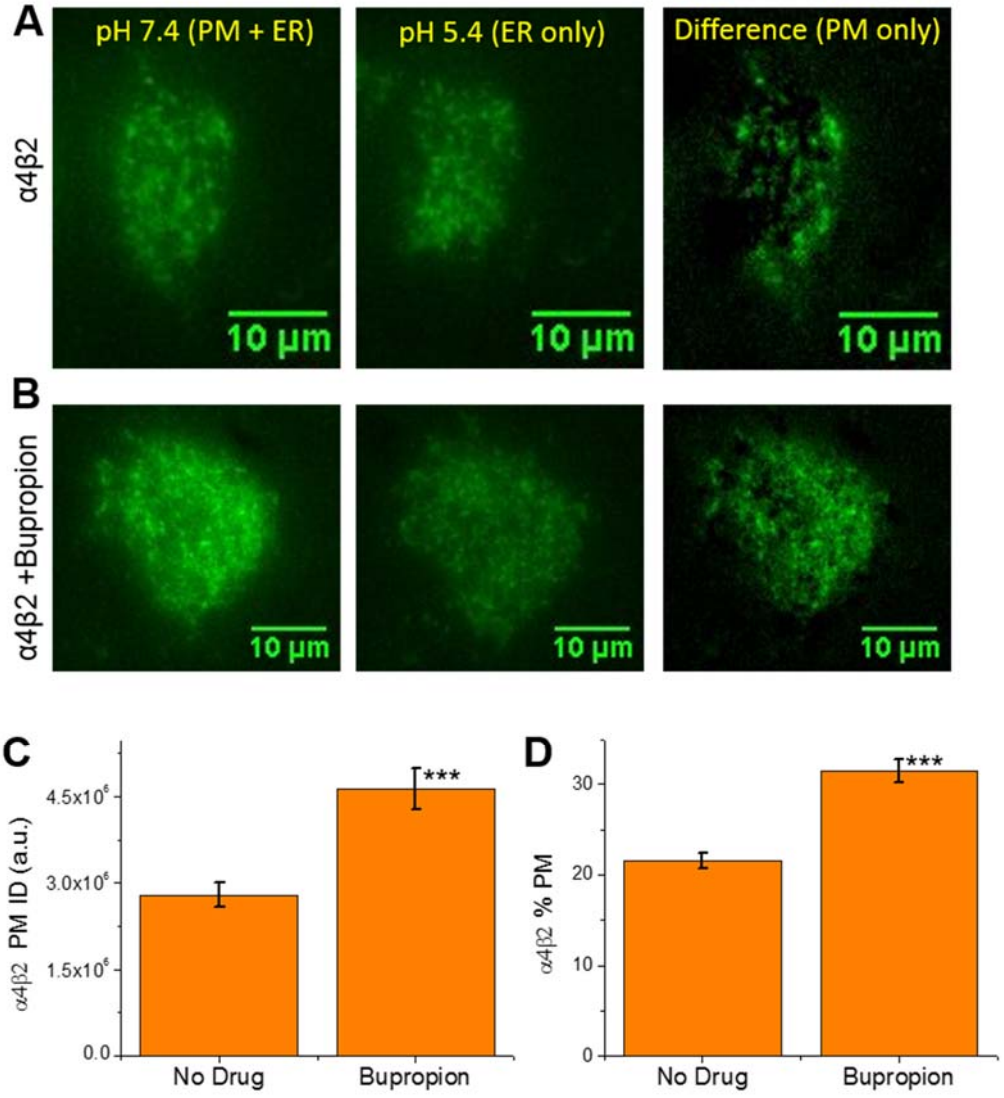

Figure 4.26 Bupropion upregulates α4β2. Representative cell images expressing α4-GFP/β2 exposed to no drug (A) or 500 nM bupropion (B). Bupropion increases the expression levels of α4β2 on the plasma membrane (C) and trafficking of α4β2 towards the plasma membrane (D). (n = 61, 51) Data are mean values ± SEM (***, $P < 0.001$), *a.u.,* arbitrary units.

Table 4.3: Total Distribution of Observed Bleaching Steps for α4-GFP/β2 Upon Exposure to Cytisine, Varenicline, or Bupropion

	# Vesicles Counted	1 Step	2 Steps	3 Steps	4 Steps
Cytisine	357	41	187	130	17
Varenicline	833	94	459	280	30
Bupropion	1089	102	598	389	43

shows the total number of counted vesicles showing one, two, or three bleaching steps for each condition. These values were fit to a binomial distribution to account for the 90% probability that GFP will be in a fluorescent state. When α4β2 is not exposed to a pharmacological agent, a distribution of 40% $(\alpha4)_2(\beta2)_3$ and 60% $(\alpha4)_3(\beta2)_2$ was verified using a chi squared goodness of fit analysis, as discussed in detail above.

Upon addition of 500 nM cytisine, this distribution is shifted to 50% $(\alpha4)_2(\beta2)_3$ and 50% $(\alpha4)_3(\beta2)_2$, as shown in Figure 4.27B. The observed fraction of one steps was 0.12 ± 0.02, compared to an expected fraction of 0.10, with 0.09 from two-GFP labeled subunits and 0.01 from three-GFP labeled subunits. The observed fraction of two steps was 0.52 ± 0.04, compared to an expected fraction of 0.53, with 0.41 from two GFP molecules and 0.12 from three GFP molecules in the pentamer. The observed fraction of three steps was 0.36 ± 0.03, corresponding to an expected ratio of 0.37 when three GFP-labeled subunits fluoresce.

The presence of 500 nM varenicline also shifts the α4β2 distribution to 54% $(\alpha4)_2(\beta2)_3$ and 46% $(\alpha4)_3(\beta2)_2$, seen in Figure 4.27C. The observed fraction of one steps was 0.11 ± 0.01, compared to an expected fraction of 0.11, with 0.10 from two GFP labeled subunits and 0.01 from three-GFP labeled subunits. The observed fraction of two steps was 0.55 ± 0.03, compared to an expected fraction of 0.55, with 0.44 from two GFP molecules and 0.11 from three GFP molecules in the pentamer. The observed fraction of three steps was 0.34 ± 0.02, corresponding to an expected ratio of 0.34 when three GFP-labeled subunits fluoresce.

Treatment with 500 nM bupropion alters the α4β2 distribution to 55% $(\alpha4)_2(\beta2)_3$ and 45% $(\alpha4)_3(\beta2)_2$, as shown in Figure 4.27D. The observed fraction of one steps was

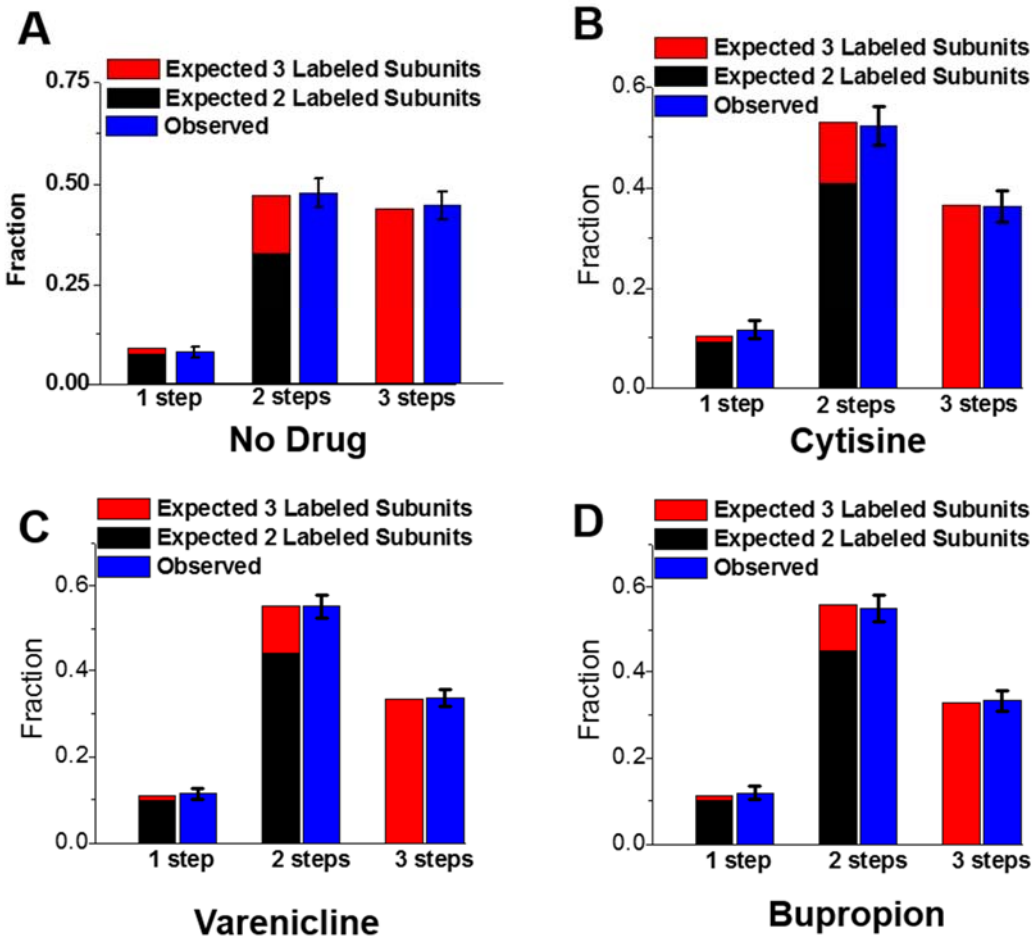

Figure 4.27 Binomial distributions showing a shift in α4β2 stoichiometry when cytisine, varenicline, or bupropion are present. Observed and expected distributions for one, two, and three bleaching steps when α4-GFP/β2 is exposed to no drug (A), cytisine (B), varenicline (C), or bupropion (D). Error bars are the square root of the number of vesicles counted.

0.12 ± 0.02, compared to an expected fraction of 0.11, with 0.10 from two GFP-labeled subunits and 0.01 from three GFP-labeled subunits. The observed fraction of two steps was 0.55 ± 0.03, compared to an expected fraction of 0.56, with 0.45 from two GFP molecules and 0.11 from three GFP molecules in the pentamer. The observed fraction of three steps was 0.33 ± 0.02, corresponding to an expected ratio of 0.33 when three GFP-labeled subunits are present.

Changes in the stoichiometric distribution of α4β2 upon addition of each ligand is shown in Figure 4.28. Error bars are 95% confidence intervals. As mentioned above, the control fits a distribution of 40 ± 4% $(\alpha4)_2(\beta2)_3$ and 60 ± 5% $(\alpha4)_3(\beta2)_2$. Cytisine slightly alters the assembly towards the high sensitivity version, shifting the distribution to 50 ± 4% $(\alpha4)_2(\beta2)_3$ and 50 ± 5% $(\alpha4)_3(\beta2)_2$. Varenicline exposure also alters the preferential assembly of the high sensitivity stoichiometry, evinced by a distribution of 54 ± 3% $(\alpha4)_2(\beta2)_3$ and 46 ± 4% $(\alpha4)_3(\beta2)_2$. Similarly, addition of bupropion alters the distribution to fit 55 ± 2% $(\alpha4)_2(\beta2)_3$ and 45 ± 3% $(\alpha4)_3(\beta2)_2$. In each case, the nAChR ligand shifts the overall stoichiometric distribution of α4β2 towards the high sensitivity $(\alpha4)_2(\beta2)_3$ isoform.

4.8 PM and ER Derived Nanovesicles can be Separated Based on Density

A single nAChR can be spatially isolated in a nanovescicle derived from native cell membranes [228]. Since nAChRs are pentameric, α4β2 can assemble with either a $(\alpha4)_3(\beta2)_2$ or $(\alpha4)_2(\beta2)_3$ stoichiometry. These pentamers are assembled in the endoplasmic reticulum, then trafficked to the plasma membrane to function as ion channels. Changes in assembly upon exposure to nicotine, cotinine, cytisine, varenicline, and bupropion,

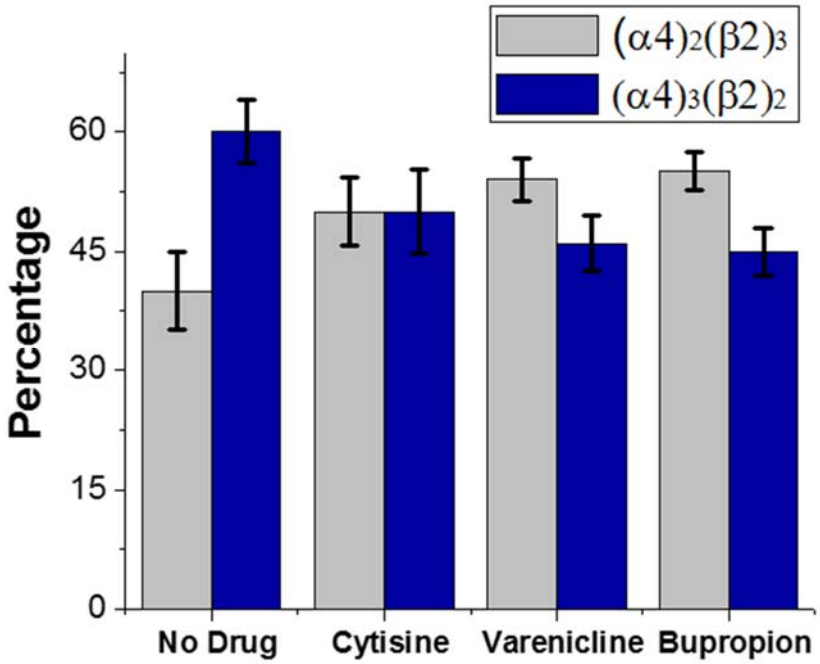

Figure 4.28 Cytisine, varenicline, and bupropion increase $(\alpha4)_2(\beta2)_3$ expression. Control cells expressing α4-GFP/β2 fits a distribution of 40 ± 4% $(\alpha4)_2(\beta2)_3$ and 60 ± 5% $(\alpha4)_3(\beta2)_2$. Cytisine slightly alters the assembly, shifting the distribution to 50 ± 4% $(\alpha4)_2(\beta2)_3$ and 50 ± 5% $(\alpha4)_3(\beta2)_2$. Varenicline exposure results in distribution of 54 ± 3% $(\alpha4)_2(\beta2)_3$ and 46 ± 4% $(\alpha4)_3(\beta2)_2$. Similarly, addition of bupropion alters the distribution to fit 55 ± 2% $(\alpha4)_2(\beta2)_3$ and 45 ± 3% $(\alpha4)_3(\beta2)_2$. Error bars are 95% confidence intervals.

discussed in sections 4.5 and 4.7.4 above, were measured for nAChRs isolated from membranes throughout the whole cell. Recent evidence suggests nicotine acts intracellularly to induce upregulation [55, 97, 115, 153]. This suggests nicotine permeates cell membranes and internally alters the assembly of nAChRs to favor a high sensitivity $(\alpha4)_2(\beta2)_3$ stoichiometry. The single molecule analysis studies discussed above were expanded to detect organelle specific changes in nAChR stoichiometry. Nanovesicles were generated from cells expressing α4-GFP and β2-wt subunits using nitrogen cavitation pressures of 250 psi or 600 psi for 20 minutes. Membranes were fragmented upon rapid decompression of nitrogen gas. Cell lysate containing nanovesicles was added to a three step OptiPrep gradient at concentrations of 30%, 20%, and 10% in sucrose-HEPES buffer. After centrifugation, 1.0 mL fractions were collected, purified, ran on prepackaged NuPAGE 4-12% Bis-Tris gel, and transferred to a nitrocellulose membrane. Primary antibodies specific for endogenous localized membrane proteins were used to detect fractions with ER and PM vesicles. Endoplasmic reticulum derived vesicles were detected with calnexin. Plasma membrane derived vesicles were identified with plasma membrane calcium ATPase (PMCA). Imaged blots are shown in Figure 4.29. Calnexin and PMCA were detected in whole cell lysate at 250 psi or 600 psi. Calnexin is primarily detected upon formation at 250 psi, while PMCA is more prominent at 600 psi. Figure 4.29A shows calnexin containing nanovesicles localize to fractions 1, 2, and 3 upon cavitation of 250 psi. Fraction 2 is collected for endoplasmic reticulum specific studies. Although fraction 1 has a higher relative number of nanovesicles, fraction 2 is chosen to avoid contamination from dense species at the bottom of the column. Figure 4.29D shows PMCA containing nanovesicles localize most densely to fractions 5, 7, and 9. Fraction 7 is collected for

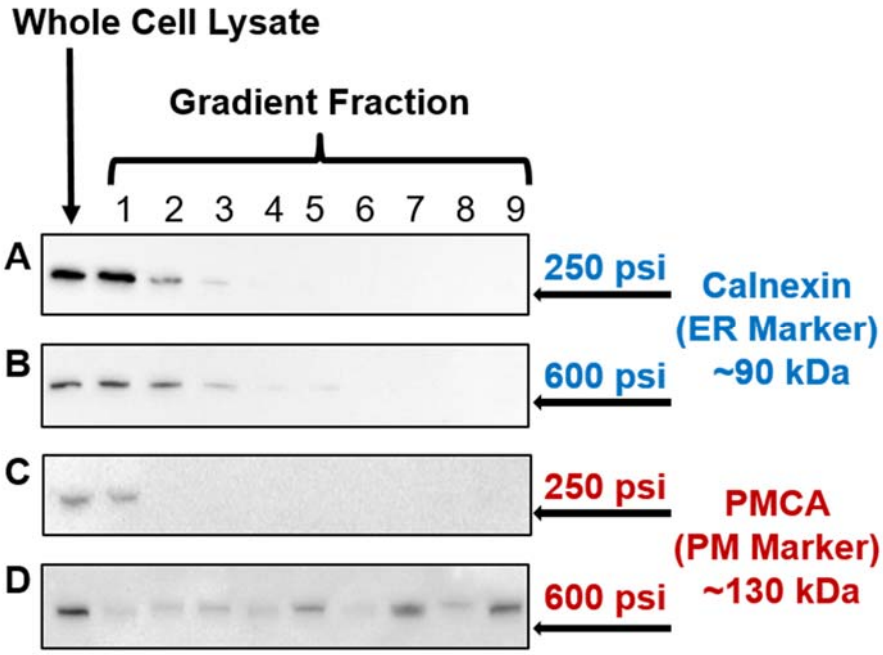

Figure 4.29 Western blots showing separation of ER and PM derived vesicles. Calnexin is detected in higher density fractions when vesicles are formed at 250 psi (A) and at 600 psi (B). A higher amount of PMCA is detected after swelling with a hypotonic solution and higher cavitation pressure of 600 psi (D), than at 250 psi (C). Fraction 2 at 250 psi is collected for ER vesicles. Fraction 7 at 600 psi is collected for PM vesicles.

plasma membrane specific studies, to avoid contamination from endoplasmic reticulum derived vesicles in denser fractions (Figure 4.29B).

4.9 Nicotine Increases Preferential Assembly of $(\alpha4)_2(\beta2)_3$ in the ER

Endoplasmic reticulum specific vesicles were collected from fraction 2 of the OptiPrep gradient. Purified fractions contained single nAChRs that were resident in the endoplasmic reticulum at the time of nitrogen cavitation, now encapsulated in nanovesicles. These vesicles were isolated on glass substrates, and TIRF microscopy was used to visualize the GFP fluorescence signal. Single step photobleaching of GFP was used to identify the number of α4-GFP subunits in each receptor, since the number of bleaching steps corresponds to the number of GFP-tagged subunits present [85, 224]. Representative time traces showing two (Figure 4.30A) or three (Figure 4.30B) bleaching steps from α4-GFP/β2 nAChRs encapsulated in endoplasmic reticulum derived nanovesicles are shown. Table 4.4 shows the total number of counted endoplasmic reticulum vesicles expressing α4-GFP/β2 showing one, two, or three bleaching steps. These values were fit to a binomial distribution to account for the 90% probability that GFP will be in a fluorescent state.

For cells not exposed to any compound, the α4β2 nAChRs expressed in the endoplasmic reticulum primarily assemble in the low sensitivity version, fitting a binomial distribution weighted for 30% $(\alpha4)_2(\beta2)_3$ and 70% $(\alpha4)_3(\beta2)_2$. This distribution is shown in Figure 4.31A, with error bars being the square root of the number of counted vesicles. The fit to a 30:70 distribution is verified using a chi-squared goodness of fit test. The observed fraction of one steps was 0.06 ± 0.01, compared to an expected fraction of

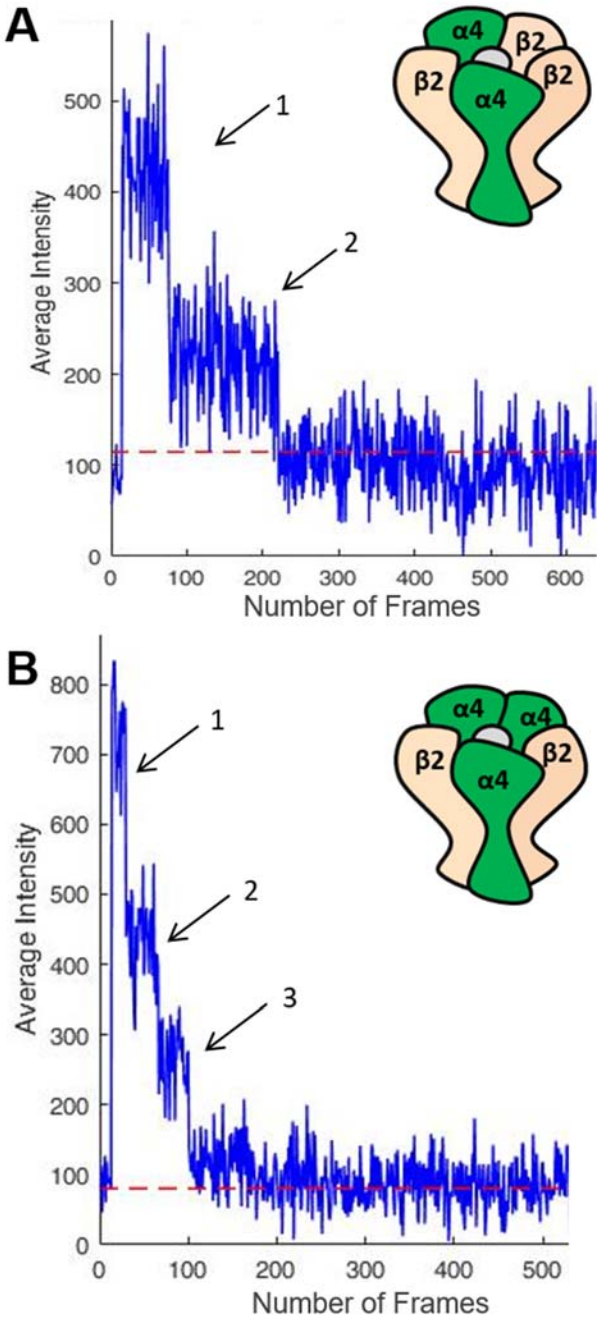

Figure 4.30 Representative bleaching steps from ER derived vesicles. Isolation $(\alpha4)_2(\beta2)_3$ or $(\alpha4)_3(\beta2)_2$ is determined by the detection of two (A) or three (B) GFP bleaching steps.

Table 4.4: Total Distribution of Observed Bleaching Steps for ER-Derived Vesicles Expressing α4-GFP/β2

	# Vesicles Counted	1 Step	2 Steps	3 Steps	4 Steps
ER No Drug	458	26	199	233	14
ER +500 nM Nic	465	40	273	152	27

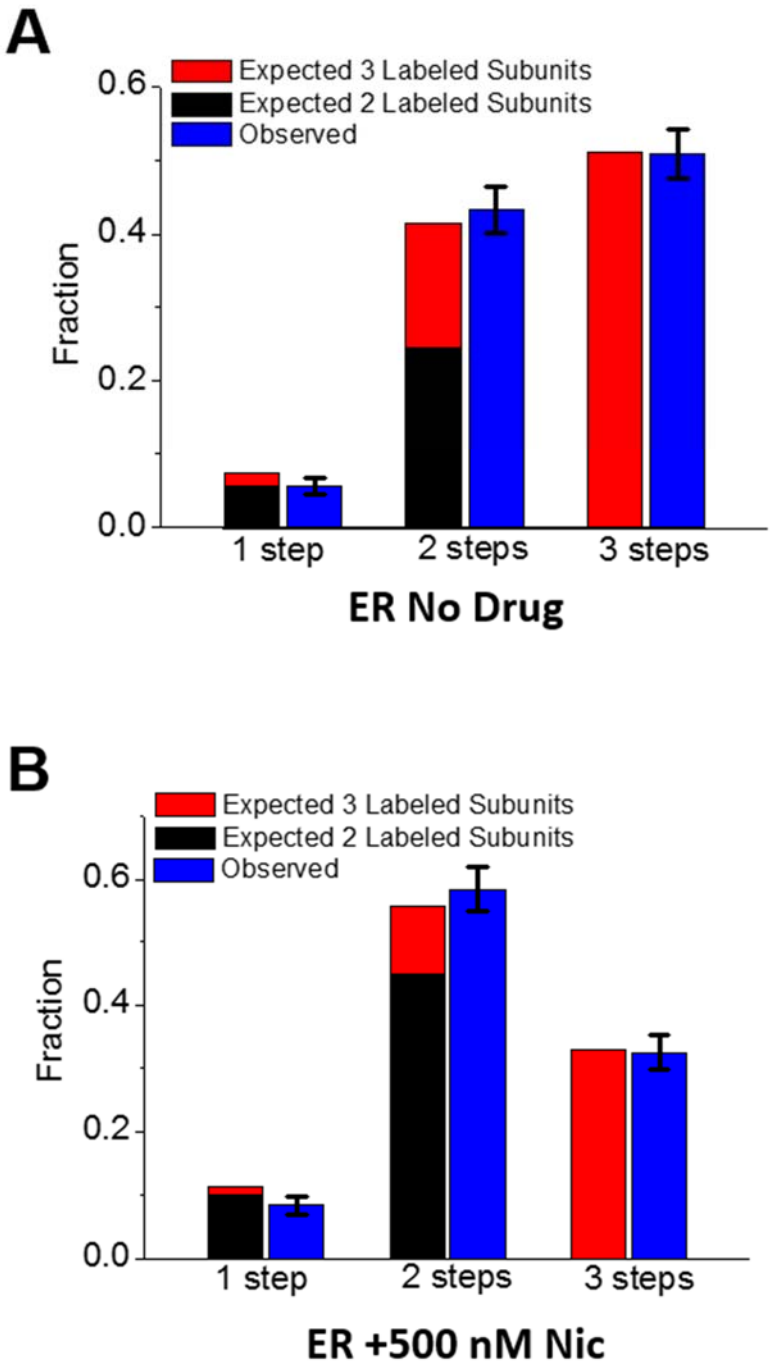

Figure 4.31 Binomial distributions showing nicotine increases $(\alpha 4)_2(\beta 2)_3$ within the ER. Observed and expected fractions of one, two, and three steps within the endoplasmic reticulum with (A) or without nicotine (B). Error bars are the square root of the number of vesicles counted.

0.07 with 0.05 from two-GFP labeled subunits and 0.02 from three-GFP labeled subunits. The observed fraction of two steps was 0.43 ± 0.03, compared to an expected fraction of 0.42, with 0.25 from two GFP molecules and 0.17 from three GFP molecules in the pentamer. The observed fraction of three steps was 0.51 ± 0.03, corresponding to an expected ratio of 0.51. In the absence of a pharmacological agent, α4β2 is predominately present as $(\alpha4)_3(\beta2)_2$ in the endoplasmic reticulum.

Upon exposure to 500 nM nicotine, there is a shift in the distribution of α4β2 present in the endoplasmic reticulum. When nicotine is present, single molecule bleaching step analysis shows the majority of endoplasmic α4β2 is the high sensitivity isoform, fitting a 55% $(\alpha4)_2(\beta2)_3$ and 45% $(\alpha4)_3(\beta2)_2$ distribution, as shown in Figure 4.31B. The observed fraction of one steps was 0.09 ± 0.01, compared to an expected value of 0.11, with 0.1 from two GFP labeled subunits and 0.01 from three GFP labeled subunits. The observed fraction of two steps was 0.59 ± 0.04, compared to an expected fraction of 0.56, with 0.45 from two GFP molecules and 0.12 from three GFP molecules. The observed fraction of three steps was 0.33 ± 0.03, compared to the expected 0.33 value when three subunits are labeled with GFP. When nicotine is present in the endoplasmic reticulum, there is a shift in the distribution of α4β2 to favor the high sensitivity $(\alpha4)_2(\beta2)_3$ isoform.

Figure 4.32 shows the change in α4β2 stoichiometry within the endoplasmic reticulum when nicotine is present. Error bars are 95% confidence intervals. When no nicotine is present, the α4β2 stoichiometry within the endoplasmic reticulum inherently favors the low sensitivity version, evinced by a distribution of 30 ± 4% $(\alpha4)_2(\beta2)_3$ and 70 ± 4% $(\alpha4)_3(\beta2)_2$. Once cells are exposed to nicotine, this distribution is shifted to 55 ± 4% $(\alpha4)_2(\beta2)_3$ and 45 ± 5 % $(\alpha4)_3(\beta2)_2$ favoring assembly of the high sensitivity stoichiometry

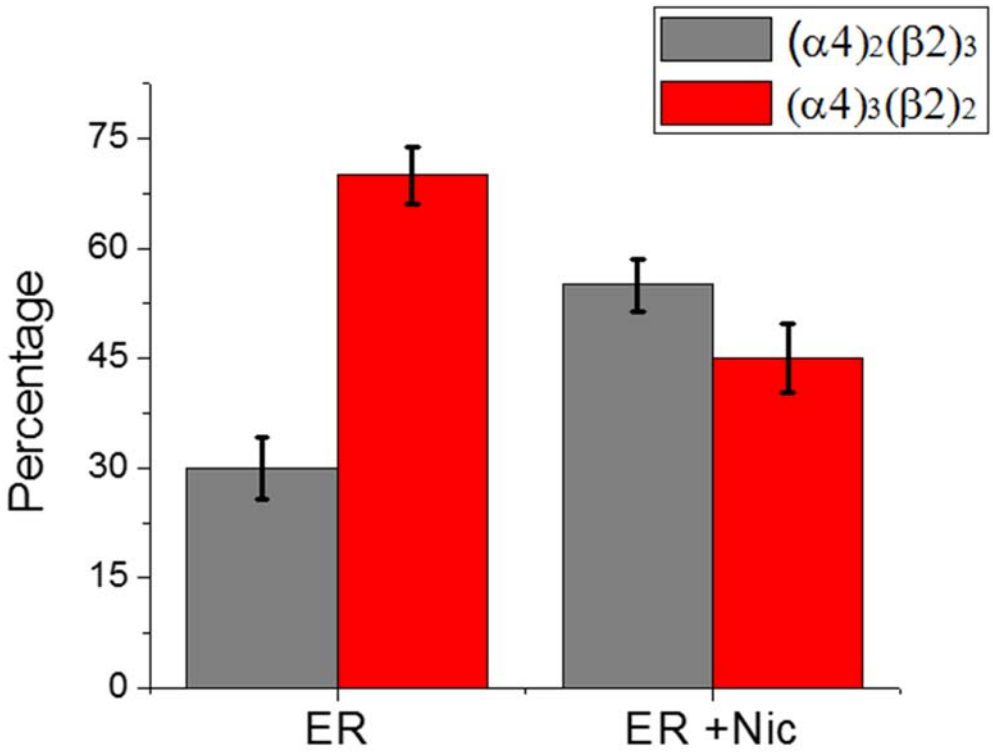

Figure 4.32 Nicotine increases the assembly of $(\alpha4)_2(\beta2)_3$ within the ER. When no nicotine is present, the α4β2 stoichiometry fits a distribution of 30 ± 4% $(\alpha4)_2(\beta2)_3$ and 70 ± 4% $(\alpha4)_3(\beta2)_2$. Once cells are exposed to nicotine, this distribution is shifted to 55 ± 4% $(\alpha4)_2(\beta2)_3$ and 45 ± 5 % $(\alpha4)_3(\beta2)_2$. Error bars are 95% confidence intervals.

within the endoplasmic reticulum. Based on the 95% confidence intervals, the fraction of α4β2 present in the high sensitivity $(\alpha4)_2(\beta2)_3$ stoichiometry is increased within the ER when nicotine is present.

4.10 Higher Expression of $(\alpha4)_2(\beta2)_3$ on the PM

When nanovesicles were formed at a pressure of 250 psi during nitrogen cavitation, fragmentation of the plasma membrane was minimal. To encourage nanovesicle formation from the plasma membrane, cells were first swollen in a hypotonic solution, then pressurized to 600 psi during nitrogen cavitation for increased fragmentation before separation on an OptiPrep gradient. Plasma membrane specific nanovesicles formed from cells expressing α4-GFP/β2 were collected from fraction 7 of the OptiPrep gradient. The purified fraction contains single nAChRs encapsulated in nanovesicles formed from the plasma membrane at the time of nitrogen cavitation. The plasma membrane specific α4β2 vesicles were isolated on glass substrates. TIRF microscopy was used to visualize single step photobleaching of GFP. The number of detected bleaching steps corresponds to the number of α4-GFP subunits in each receptor [85, 224]. Representative time traces of α4-GFP/β2 isolated in plasma membrane derived nanovesicles showing two (Figure 4.33A) or three (Figure 4.33B) bleaching steps are shown. Table 4.5 shows the total number of counted plasma membrane vesicles showing one, two, or three bleaching steps. These values were fit to a binomial distribution to account for the 90% probability that GFP will be in a fluorescent state.

In control cells not exposed drug, the inherent distribution of α4β2 stoichiometries localized to the plasma membrane slightly favored the high sensitivity stoichiometry. PM

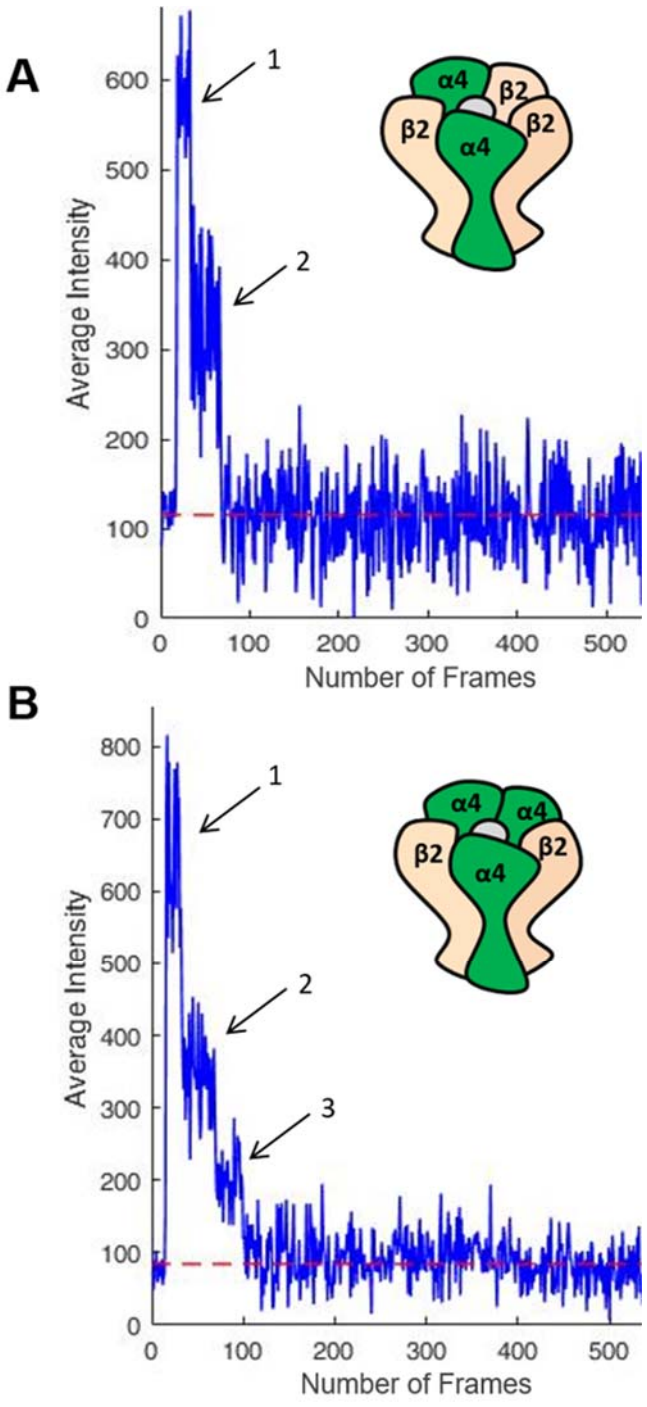

Figure 4.33 Representative bleaching steps from PM derived vesicles. Detecting two (A) or three (B) GFP bleaching steps corresponds to $(\alpha4)_2(\beta2)_3$ or $(\alpha4)_3(\beta2)_2$ stoichiometry.

Table 4.5: Total Distribution of Observed Bleaching Steps for PM-Derived Vesicles Expressing α4-GFP/β2

	# Vesicles Counted	1 Step	2 Steps	3 Steps	4 Steps
PM No Drug	545	26	199	233	1
PM + 500 nM Nic	883	100	592	191	18

α4β2 fit binomial distributions weighted for 56% $(\alpha4)_2(\beta2)_3$ and 44% $(\alpha4)_3(\beta2)_2$, shown in Figure 4.34A. The observed fraction of one steps was 0.12 ± 0.02, compared to an expected ratio of 0.11, with 0.10 from two GFP-labeled subunits and 0.01 from three GFP-labeled subunits. The observed fraction of two steps was 0.56 ± 0.03, compared to an expected ratio of 0.57, with 0.46 from two GFP molecules and 0.11 from three GFP molecules. The observed fraction of three steps was 0.32 ± 0.02, corresponding with the 0.32 expected value when three subunits are labeled with GFP. In the absence of a pharmacological agent, α4β2 on the plasma membrane slightly favors $(\alpha4)_2(\beta2)_3$ stoichiometry.

Upon exposure to nicotine, the distribution of α4β2 on the plasma membrane is shifted more towards the high sensitivity version. When nicotine is present, plasma membrane resident α4β2 fits a 70% $(\alpha4)_2(\beta2)_3$ and 30% $(\alpha4)_3(\beta2)_2$ distribution, shown in Figure 4.34B. The observed fraction of one steps was 0.11 ± 0.01, compared to an expected ratio of 0.14 with 0.13 from two GFP-labeled subunits and 0.01 from three GFP-labeled subunits. The observed fraction of two steps was 0.67 ± 0.03, compared to an expected ratio of 0.65, with 0.57 from two GFP molecules and 0.07 from three GFP molecules in the nAChR pentamer. The observed fraction of three steps was 0.22 ± 0.02, corresponding with the 0.22 expected value when three α4-GFP subunits are present. When nicotine is present, a higher percentage of α4β2 on the plasma membrane has $(\alpha4)_2(\beta2)_3$ stoichiometry.

Figure 4.35 shows the increase in $(\alpha4)_2(\beta2)_3$ stoichiometry on the plasma membrane when nicotine is present. Error bars are 95% confidence intervals. When no nicotine is present, the α4β2 stoichiometry on the plasma membrane fits a distribution of 56 ± 3%

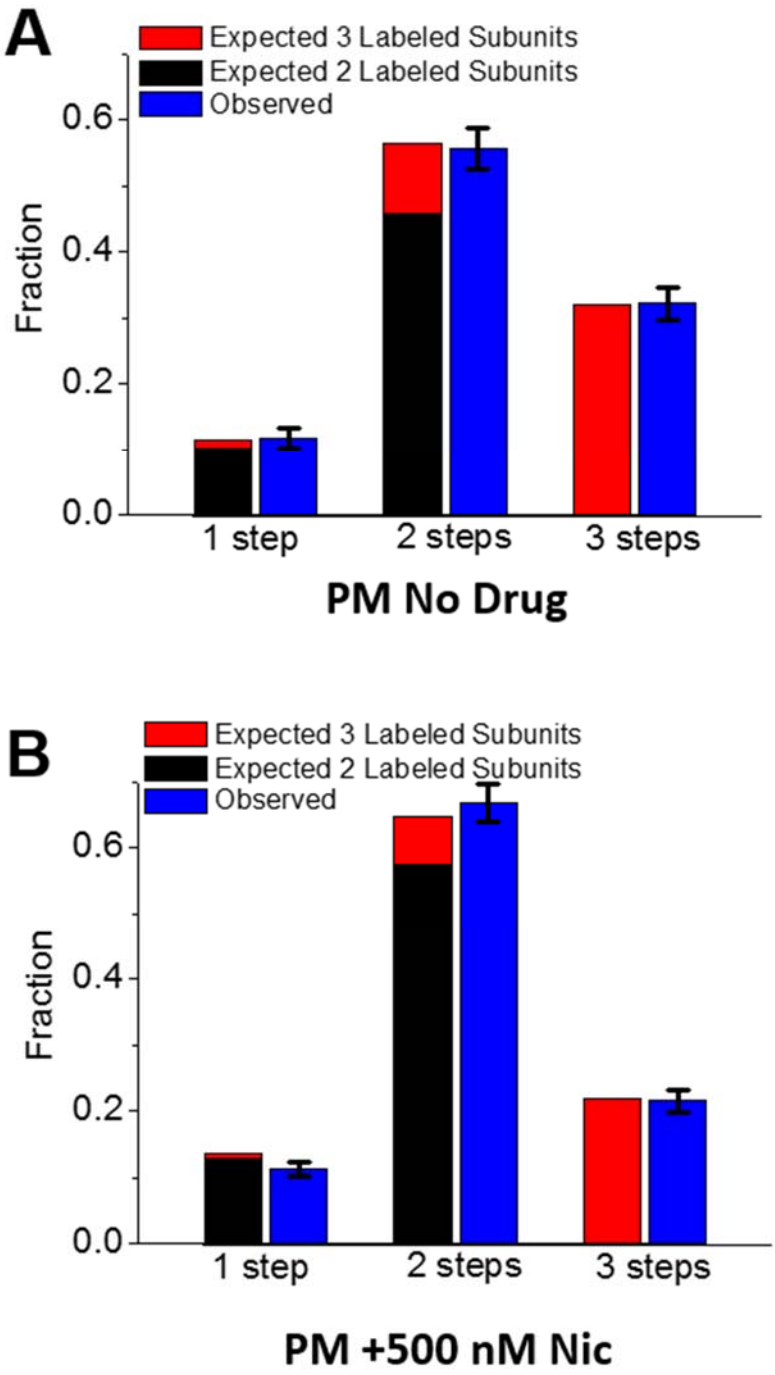

Figure 4.34 Binomial distributions showing $(\alpha4)_2(\beta2)_3$ is the predominate stoichiometry on the PM. Observed and expected fractions of one, two, and three steps from vesicles expressing α4-GFP/β2 on the plasma membrane with (A) or without nicotine (B). Error bars are the square root of the number of vesicles counted.

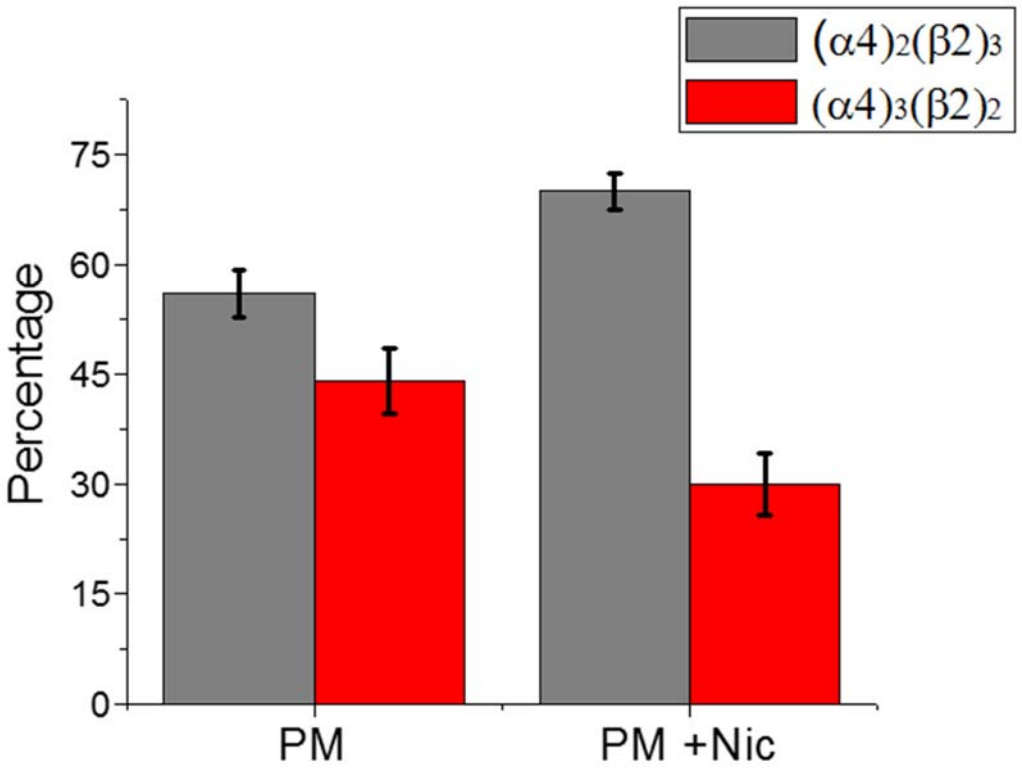

Figure 4.35 Nicotine increases the fraction of $(\alpha4)_2(\beta2)_3$ on the PM. When no nicotine is present, the α4β2 stoichiometry on the plasma membrane fits a distribution of 56 ± 3% $(\alpha4)_2(\beta2)_3$ and 44 ± 4% $(\alpha4)_3(\beta2)_2$. Upon the addition of nicotine, this distribution is increased to 70 ± 2% $(\alpha4)_2(\beta2)_3$ and 30 ± 4% $(\alpha4)_3(\beta2)_2$. Error bars are 95% confidence intervals.

$(\alpha4)_2(\beta2)_3$ and 44 ± 4% $(\alpha4)_3(\beta2)_2$. Upon the addition of nicotine, this distribution is increased further towards the high sensitivity version, fitting a binomial of 70 ± 2% $(\alpha4)_2(\beta2)_3$ and 30 ± 4% $(\alpha4)_3(\beta2)_2$. Based on the 95% confidence intervals, nicotine increases the percentage of the $(\alpha4)_2(\beta2)_3$ isoform found on the plasma membrane.

CHAPTER 5: DISCUSSION

Tobacco consumption is the world's leading preventable cause of death, affecting approximately one billion people world-wide today [1, 2]. The majority of users admit they would like to quit, but the addictive nature of tobacco prevents them from doing so [8]. Current smoking cessation therapeutics have not been tremendously successful is helping users overcome the barriers of nicotine addiction. In order to develop more efficient therapeutics, the mechanism of nicotine addiction needs to be further resolved and specific nAChR subtypes and assemblies need to be identified as therapeutic targets. Nicotine is known to interact with nAChRs, resulting in changes to reward systems in the brain upon chronic exposure. On a molecular scale, upregulation of nAChRs as a result of chronic nicotine exposure, potentially altering nAChR-dependent signaling, has been given significant interest [6, 45, 55, 64, 66, 76, 160]. Upregulation is considered an increase in nAChR number, changes in trafficking, and altered stoichiometric assembly [55, 97, 152-155]. Upregulation seems to be brain region, cell type, and subtype specific. As a result of this complexity, the underlying mechanism of upregulation, and its connection to nicotine addiction, is not fully understood. Resolving the mechanisms of upregulation on a molecular scale advances the understanding of nicotine addiction, and therefore paves the way towards the development of new therapeutic targets aimed at facilitating smoking cessation. This dissertation utilizes novel techniques to elucidate the mechanism of nicotine induced changes in expression, trafficking, and stoichiometry to identify target nAChR structures for the development of smoking cessation therapeutics.

5.1 Cotinine Induces Upregulation of a Subset of nAChRs

It is well established that chronic nicotine exposure upregulates and alters the assembly of α4β2 nAChRs [51, 97, 161, 235], but the effects of nicotine metabolites on nAChR assembly and trafficking are not well studied. In this work, drug induced changes in trafficking and expression of SEP-labeled nAChRs were measured using TIRF microscopy. This technique is complementary to traditional methods of nAChR detection, offering particular advantages for analysis of receptors located near the plasma membrane. Autoradiographic studies have been monumental in providing detailed maps of distribution of nAChRs throughout mouse and rat brains [10, 159, 236, 237]. These studies typically measure the amount of radio-labeled ligand binding, such as [^{3}H]-nicotine, [^{3}H]-acetylcholine, [^{125}I]-epibatidine or [^{125}I]-bungarotoxin, either on the plasma membrane or throughout the whole cell. Detection is limited to the radioactivity of the bound ligand, instead of detecting the nAChR itself. Distribution can be roughly measured by quantifying the proportion of radioligand binding sites on the cell surface, but this requires a comparison between multiple fixed samples. Immunoblotting is also used to measure expression levels [238]. Antibodies are designed to be specific for one nAChR subunit, meaning assembled pentamers and unassembled subunits are indistinguishable in whole cell samples. However, specificity to one single type of nAChR subunit is hard to achieve due to homology between subunit sequences. These measurements are also complicated by the possibility that the specificity of an antibody can be conformation specific for one type of subunit [190, 191, 239]. Cell surface biotinylation assays are often used to quantify the ratio of nAChRs on the plasma membrane compared to the whole cell as well. This process involves incubating cell lysates overnight with streptavidin agarose beads to

recover plasma membrane resident nAChRs [136, 191]. Again, this technique involves a comparison between samples once cells are lysed. In contrast, the SEP-based technique used in this dissertation measures a genetically encoded reporter molecule, super-ecliptic pHluorin, which eliminates nonspecific binding or subunit conformation dependent detection. Fluorescence intensity is directly related to the number of SEP-labeled nAChRs present. Coupled with TIRF microscopy, superior resolution at the plasma membrane is achieved within the 150 nm field of TIRF excitation. This allows surface nAChRs and those in the peripheral endoplasmic reticulum to be measured simultaneously in the same sample for an accurate depiction of nAChR distribution within this region. Changes in distribution within this narrow region upon addition of a pharmacological agent correspond to differences in nAChR trafficking, since only plasma membrane resident or nearby nAChRs are detected. These studies also measure nAChR expression in living cells. Due to the pH sensitivity of SEP, single vesicle insertion events can be captured and resolved in real time. Increases in α4β2 expression on the plasma membrane upon exposure to nicotine have been measured in this system and parallel the degree of upregulation seen in other systems.

Due to structural similarities between nicotine and cotinine, we hypothesized that cotinine could also induce changes in expression levels or trafficking of nAChRs. Cotinine has been shown bind to nAChRs and evoke dopamine release [41, 42, 240], meaning it could also alter expression of nAChRs. To test this hypothesis, N2a cells were exposed to physiologically relevant levels of cotinine, ranging from 50 nM to 500 nM. These values are centered around those matching the average reported values of cotinine in a smoker's blood, urine, or brain [29, 241, 242]. Measuring SEP-labeled α4β2 nAChRs with TIRF

microscopy shows that cotinine upregulates the expression and distribution of α4β2 towards the plasma membrane, as shown by an increase in PMID and % PM (Figure 4.2; $P < 0.001$). The highest level of upregulation of α4β2 nAChRs is seen at a concentration of 1 μM cotinine, which corresponds to the average concentration of cotinine in the blood of a typical smoker [241]. Cotinine induces significant increases in both α4β2 PMID and % PM at as little as 100 nM. This suggests that cotinine could potentially contribute to α4β2 upregulation in smokers since brain concentrations of cotinine are estimated to be approximately 300 nM [26]. However, at higher concentrations of cotinine, this upregulation effect is lost. This could be a result of overwhelming stress on the endoplasmic reticulum, given a significant increase in assembly and trafficking involving this organelle. A recent functional study exposing α4β2 in oocytes to 10 μM cotinine for 48 hours did not detect any differences in acetylcholine-evoked response at this concentration compared to control [243]. Since 10 μM cotinine did not alter the functional response of α4β2, it is likely that expression of α4β2 is unaltered as well at the higher concentration of cotinine used in that study.

Recent studies to elucidate the mechanism of nicotine induced upregulation suggest nicotine acts intracellularly to increase maturational enhancement of subunits and pharmacologically chaperone nascent subunits, stabilizing subunit-subunit interactions in their lowest energy state [55, 97, 115, 123, 153]. This idea is supported by the fact upregulation occurs at low concentrations of nicotine, 100-200 nM, that remain in the brain of smokers at a steady state. At these concentrations, few $(\alpha4)_2(\beta2)_3$ are activated, while no low sensitivity $(\alpha4)_3(\beta2)_2$ are activated [55], corresponding to the EC_{50} value for nicotine being 0.1 to 4.0 μM based on stoichiometry [80, 97-99]. Similarly, upregulation

of α4β2 occurs in the presence of as little as 100 nM cotinine. This is well below the concentration of cotinine required to evoke dopamine release from rat striatal slices, with an EC_{50} value of 30 μM or higher reported [42, 240]. Since both nicotine and cotinine induce upregulation at concentrations below those required to induce a response, it is possible that both drugs are acting by a similar mechanism. Both nicotine and cotinine are able to cross the blood-brain barrier [40, 244], and bind to nAChRs [41, 42]. Cotinine is also able to penetrate the cell membrane, given a log *P* value of -0.3 [245]. Nicotine and cotinine, as well as other upregulating ligands, likely permeate cell membranes, interact with intracellular receptors, and alter the expression of nAChRs internally.

Nicotine also increases trafficking of α4β2 and insertion into the plasma membrane [198]. Since cotinine exposure increases the number of α4β2 receptors located on the plasma membrane, we hypothesized that the number of insertion events of α4β2 nAChR carrying vesicles could also be increased. Using SEP-labeled α4β2, the number of nAChR carrying single vesicle insertion events were quantified in the presence of 1 μM cotinine. When cotinine is present, the number of α4-SEP/β2 single vesicle insertion events is increased. This suggests that cotinine, similar to nicotine, increases the trafficking of α4β2 from the endoplasmic reticulum to the plasma membrane. Therefore, the higher PMID and % PM resulting from cotinine exposure are at least partially the result of an increased frequency of insertion of vesicles containing α4β2 receptors. It is likely that the increase in trafficking is a result of increased assembly within the endoplasmic reticulum. A higher number of assembled α4β2 nAChRs need to be trafficked out of the endoplasmic reticulum, leading to an increase in the number of trafficking vesicles to accommodate this increase. A higher number of trafficking vesicles are then inserted into the plasma membrane,

leading to an increase in expression on the PM. Similar molecular consequences of physiologically relevant concentrations of nicotine and cotinine exposure, in terms of increased trafficking and expression of α4β2 on the plasma membrane, suggest cotinine could be partially responsible for physiological effects in nAChRs previously attributed to nicotine alone.

In the case of nicotine, upregulation is subtype specific. Incorporation of the α5 subunit into the α4β2 pentamer results in a loss of both nicotine induced and cotinine induced upregulation. Some studies suggest that the presence of this accessory α5 subunit alters the ability of the pentameric nAChR to be pharmacologically chaperoned by nicotine. Although α4β2 are believed to be chaperoned by nicotine, α4β2α5 may fail to undergo the same pharmacological chaperoning and therefore do not increase expression on the plasma membrane when a pharmacological chaperone is present [246, 247]. This is possibly due to subtle changes in ligand binding affinity between the two subtypes, which alters the ability to interact with nicotine as a chaperone [248, 249]. Since α4β2α5 also does not result in upregulation when exposed to cotinine, there is a potential that cotinine interacts with this subtype in the same way that nicotine does.

The single nucleotide polymorphism in α5, resulting in a single amino acid change from aspartic acid to asparagine at position 398 (α5-D398N), has been connected to an increased risk of tobacco dependence in individuals with this allele [139-141]. When this accessory subunit is incorporated into the α4β2 pentamer, the resulting subtype α4β2α5-D398N also fails to upregulate in the presence of nicotine or cotinine. This is presumably due to the continued absence of a pharmacological chaperoning effect of nicotine, or cotinine, in this version of α5. However, the SEP-based studied reveal that a higher ratio

of α4β2α5-D398N is located on the plasma membrane than in the peripheral endoplasmic reticulum, compared to the α4β2α5D version. This redistribution of α4β2α5-D398N is independent of the presence of either nicotine or cotinine. It is unclear if this increase in percentage of α4β2α5-D398N on the plasma membrane is due to an increase in trafficking towards the PM or a decrease in turnover once on the plasma membrane. However, this difference in distribution between α4β2α5D and α4β2α5-D398N could lead to downstream consequences that result in an increased rate of smoking, particularly if the α4β2α5-D398N on the plasma membrane are functional.

It appears that subtypes with a higher basal plasma membrane density are not subjected to nicotine induced upregulation at physiological concentrations, possibly because receptor transport is already efficient. For instance, basal levels of α3β4 nAChRs are three times higher than β2* containing nAChRs. Studies show that β4* nAChRs are exported from the endoplasmic reticulum to the plasma membrane more efficiently than β2* nAChRs [196, 198]. This increase in export efficiency can be attributed to the presence of trafficking motifs within the variable loop between TM3 and TM4 transmembrane regions. The trafficking motifs are believed to control export of assembled pentameric receptors out of the endoplasmic reticulum [75, 76]. To date, it is known that export LXM motifs (where X is any amino acid), located in the TM3-TM4 loop of α4, α3, and β4 subunits, govern trafficking out of the endoplasmic reticulum. Also, a retention RXRR motif in the β2 subunit is associated with retention in the endoplasmic reticulum [76]. Combinations of these subunits into pentamers result in combinations of trafficking motifs, potentially accounting for differences in subcellular location of subtypes of receptors. The β2* nAChRs are inefficiently exported, while β4* are exported very efficiently. When

both types of subunits in the pentamer contain the same export trafficking motif, such as in α3β4, it is believed that export is already at a maximum rate and therefore trafficking is not influenced by the presence of pharmacological chaperones [66, 76, 139]. This theory is supported by a lack of upregulation of α3β4 when exposed to physiologically relevant concentrations of nicotine [210, 250]. However, upregulation of α3β4 has been shown at much higher concentrations of nicotine (≥ 10 μM) [136]. Recent studies suggest nicotine increases the formation of additional exit sites within the endoplasmic reticulum (ERES) [196, 198]. It is possible that such high concentrations of nicotine increase the number of ERES in the endoplasmic reticulum to such an extent that α3β4 is able to upregulate. In our SEP-based study, α3β4 was not upregulated at the physiologically relevant nicotine or cotinine concentrations used. If cotinine affects nAChRs in a similar pharmacological chaperoning mechanism, α3β4 may not be upregulated by cotinine because of the already high levels of plasma membrane expression. Likewise, incorporation of α5 or α5-D398N into α3β4 did not alter expression levels in the presence or absence of nicotine or cotinine. This suggests that addition of the accessory α5 subunit does not alter the interaction, or lack thereof, between α3β4 and nicotine or cotinine. Unlike incorporation of α5-D398N into α4β2, addition of this accessory subunit did not increase the distribution of α3β4α5-D398N towards the plasma membrane. Presumably, this is due to the inherently higher levels of α3β4α5-D398N already on the plasma membrane.

The idea of reaching a maximal level of expression on the plasma membrane may also explain why no additive effects are measured when cells expressing α4β2 are simultaneously exposed to both nicotine and cotinine. No significant differences were detected in the α4β2 PMID or % PM of cells exposed to 300 nM, 1 μM, or 5 μM cotinine

in addition to 50 nM or 500 nM nicotine, although all values were significantly higher than those exposed to no drug (Figure 4.4; $P < 0.001$). It is possible that an approximately 50% increase in PMID over the control is the maximum increase in α4β2 expression that can be achieved by pharmacological chaperoning at these physiologically relevant concentrations of nicotine and cotinine in this cell system, potentially because the two drugs are acting in the same way.

Although α4β2 shows clear upregulation when exposed to nicotine, contradictory results have been reported for α6β2*, with claims of upregulation, downregulation, or no change when chronically exposed to nicotine [114, 251, 252]. Likewise, contradictory results have been reported for the ability of α6β2* to be chaperoned by nicotine. Many reports suggest that nicotine fails to chaperone α6β2* [247, 253-255], while others suggest this subtype can be chaperoned when the accessory β3 subunit is present [115, 251]. These discrepancies may be due to the presence or absence of the accessory β3 subunit within different expression systems or concentrations of chaperoning ligand used. In partial resolution of this inconsistency, a dose dependent response of α6β2β3 to nicotine has been measured [115]. Low concentrations of 50 nM nicotine are shown to upregulate α6β2β3, while higher concentrations of 500 nM nicotine downregulate α6β2β3. In addition, α6β2β3 expresses at higher levels on the plasma membrane than α6β2 alone [115]. Our data also show that the incorporation of a β3 accessory subunit resulted in higher levels of expression on the PM as compared to α6β2 alone, as well as a dose dependent downregulation of α6β2β3 in the presence of cotinine (Figure 4.13A; $P < 0.05$). The concentrations of cotinine used here did not alter the distribution of α6β2 or α6β2β3 nAChRs between the plasma membrane and peripheral endoplasmic reticulum, evident by no significant changes in %

PM. Recent evidence suggests a KKK motif within the TM3-TM4 loop of the β3 subunit plays a regulatory role in α6β2* expression when nicotine is present [115]. This motif is essential for nicotine induced upregulation of α6β2β3, possibly acting as a recognition site for COPI binding [115]. Cotinine potentially differs in its interaction with the KKK motif as compared to nicotine. This suggests that nicotine is able to chaperone α6β2β3, at least at low concentrations, while cotinine is not. Cotinine may also alter the likelihood of β3 incorporation into the α6β2 pentamer. It is feasible that at low concentrations of cotinine, 500 nM, $(\alpha6)_2(\beta2)_3$ or $(\alpha6)_3(\beta2)_2$ is favored over α6β2β3, resulting in an apparent decrease in PMID levels that correspond to α6β2 alone. Interestingly, another study has shown that cotinine only interacts with a subset of α6β2* nAChRs while the entire population is sensitive to nicotine [42]. The lack of cotinine-induced upregulation of α6β2β3 is potentially related to its action on only a portion of this receptor population. This effect could also contribute to discrepancies between groups that detect upregulation [115, 251, 252] or downregulation [253] in varying brain regions based on concentrations of nicotine, or cotinine, present.

5.2 Cotinine Exposure Results in Preferential Assembly of $(\alpha4)_2(\beta2)_3$

As a heteropentamer composed of two types of subunits, α4β2 can assemble with either $(\alpha4)_3(\beta2)_2$ or $(\alpha4)_2(\beta2)_3$ stoichiometry. These isoforms of the same α4β2 subtype vary in sensitivity to agonists, calcium flux, and rates of desensitization [56, 80, 81]. It is well established that nicotine increases the expression of the high sensitivity $(\alpha4)_2(\beta2)_3$ isoform [85, 151, 154, 233, 256, 257], but the reason for this change has not been determined. This observation is heavily based on bulk measurements and

electrophysiology studies. Bulk studies use western blots to measure levels of protein based on binding of a subunit specific antibody or metabolic labeling of subunits. Typically, a ratio of expression of the α subunit versus the β subunit is calculated. Changes in this ratio upon ligand exposure is attributed to changes in stoichiometry [136, 153, 154, 258, 259]. The increase in $(\alpha4)_2(\beta2)_3$ stoichiometry in the presence of nicotine is determined by an increase in amount of the β2 subunit compared to the α4 subunit detected. These measurements provide estimates of changes in levels of each subunit, but do not fully resolve any structural information about the present stoichiometry of each nAChR. Functional studies showing a biphasic response to nicotine, corresponding to $(\alpha4)_3(\beta2)_2$ or $(\alpha4)_2(\beta2)_3$ stoichiometry, were used to determine an increase in the high sensitivity version of α4β2 when nicotine is present [154, 167, 233, 234]. The EC_{50} values for the high sensitivity $(\alpha4)_2(\beta2)_3$ and low sensitivity $(\alpha4)_3(\beta2)_2$ are estimated to be 116 nM and 2700 nM, respectively. Since nicotine induces upregulation at concentrations lower than those required for activation, functional studies do not provide insight into the mechanism of an increase in the $(\alpha4)_2(\beta2)_3$ isoform.

Most studies agree that the increase in the high sensitivity $(\alpha4)_2(\beta2)_3$ stoichiometry is the result of altered assembly of α4β2, rather than an altered binding affinity or functional state of an assembled nAChR. However, direct structural studies of assembled nAChRs have primarily been limited to bulk fluorescence techniques [210, 260, 261]. One such technique is Förster resonance energy transfer (FRET), in which α4 and β2 subunits are labeled with donor and acceptor fluorescent proteins such as GFP and derivatives. The efficiency of energy transfer from the donor to acceptor molecule is inversely proportional to the sixth power of the distance between the two fluorophores [151, 262]. A theoretical

FRET efficiency for $(\alpha4)_3(\beta2)_2$ or $(\alpha4)_2(\beta2)_3$ stoichiometry is calculated based on estimated differences between each isoform and compared to observed values to make conclusions about the predominate stoichiometry in the presence of a ligand [210]. This technique can detect general shifts in nAChRs assembly, but requires a range of assumptions about the geometry and distance between fluorophores in the structure.

Single molecule fluorescence studies are ideally suited to reveal structural changes in nAChRs that cannot be resolved by ensemble techniques [263-266]. However, single molecule measurements are often obstructed by high background fluorescence or rely on purification of the protein outside of the cellular environment. Measuring membrane proteins on a single molecule level is particularly challenging due to constant diffusion of proteins within a membrane and natural accumulation of membrane receptors on the plasma membrane [225, 267]. One of the few single molecule fluorescence studies capable of resolving structural assembly of nAChRs in a live cell use nanoscale plasmonic devices known as zero-mode waveguides [85]. Zero-mode waveguides are nanostructures with subwavelength wells constructed on a thin layer of aluminum. The narrow width of the wells prevents the penetration of the beam of excitation, resulting in an attenuating evanescent field and reduction of background fluorescence from the whole cell. The plasma membrane of N2a cells grown on top of the zero-mode waveguides are able to penetrate the wells, meaning only nAChRs within the wells are detected. This prevents the lateral diffusion and aggregation of nAChRs, allowing isolated nAChRs to be evaluated on a single molecule level. However, measurements are limited to nAChRs residing on the plasma membrane. Also, the expression and trafficking of nAChRs isolated within this subwavelength size well may not reflect the population of the whole cell, or even typical

nAChR trafficking to the plasma membrane. Even so, these experiments show single molecule fluorescence is capable of quantitatively determining the stoichiometry of individual α4β2 nAChRs isolated in a cellular environment.

Our lab recently developed a novel technique to spatially isolate nAChRs embedded in vesicles formed from endogenous cell membranes [228]. Upon fragmentation of membranes using nitrogen cavitation, single nAChRs become trapped in their membrane of origin. This allows single nAChRs to be isolated in their endogenous cellular environment, without the use of artificial bilayers or detergents. Once single nAChRs are isolated in cell membrane derived nanovesicles, single molecule photobleaching is used to determine subunit stoichiometry. Vesicles were generated from cells expressing α4-GFP and β2-wt subunits. These vesicles containing α4-GFP/β2 were isolated on glass substrates, and visualized by TIRF microscopy. Single step photobleaching of GFP molecules within α4 subunits was used to identify the number of α4-GFP subunits in each nAChR. The number of bleaching steps corresponds to the number of GFP-tagged subunits present and, therefore, indicates the stoichiometry of the receptor [85, 224]. Since the probability of GFP being in a fluorescent state is 90%, the number of counted one, two, or three bleaching steps was fit to a binomial distribution to quantify changes in assembly.

Since cotinine alters the trafficking and expression of α4β2 in a similar way as nicotine, we hypothesized that cotinine could also alter the assembly of α4β2. In the absence of a pharmacological agent, the fifth position of the α4β2 pentamer slightly favors occupation by an α4 subunit fitting a binomial distribution of 40 ± 5% $(\alpha4)_2(\beta2)_3$ and 60 ± 4% $(\alpha4)_3(\beta2)_2$ (Figure 4.21). A higher ratio of α4β2 with $(\alpha4)_3(\beta2)_2$ throughout the cell is

also measured with whole-cell electrophysiology [154, 167]. In the presence of cotinine or nicotine, α4β2 preferentially assembles in the high sensitivity, $(\alpha4)_2(\beta2)_3$, stoichiometry. The distribution of α4β2 in the presence of nicotine fits a binomial of 65 ± 4% $(\alpha4)_2(\beta2)_3$ and 35 ± 6% $(\alpha4)_3(\beta2)_2$, providing structural evidence to support results from other studies showing that nicotine exposure increases preferential assembly of high sensitivity α4β2 nAChRs. This alteration does not require surface receptor activating concentrations of nicotine, but is thought to be linked to the mechanism of nicotine addiction. This study shows that the presence of cotinine also shifts the assembly of α4β2 to favor the high sensitivity version, fitting a binomial of 70 ± 4% $(\alpha4)_2(\beta2)_3$ and 30 ± 6% $(\alpha4)_3(\beta2)_2$. Based on the 95% confidence intervals, both nicotine and cotinine distributions are different from the control distribution, although they are not different from each other (Figure 4.21; $P < 0.05$). This suggests that cotinine may be at least partially responsible for the increase in α4β2 sensitivity measured in other studies.

As a control to verify our observations of nicotine and cotinine induced changes in α4β2 stoichiometry, biased transfections were performed with varying ratios of α4-GFP and β2 plasmid. Previous studies have altered the primary stoichiometry of α4β2 expressed using biased transfections, with one subunit expressed at higher levels than the other [151, 154, 191, 233, 234]. These types of studies have primarily used Xenopus oocyte expression systems with changes in stoichiometry determined from changes in the biphasic dose response based on whole cell current measurements. Here biased transfection ratios of 10:1, 4:1, 1:1, and 1:4 (α4:β2) were used to determine the stoichiometry of α4β2 nAChR in each condition. A 1:10 transfection bias towards the β2 subunit was not viable in the HEK-293T clonal cell line used for these studies. When an excess amount of the α4 subunit

is transfected, there is only a slight shift in assembly towards the $(\alpha4)_3(\beta2)_2$ isoform. As mentioned, equal amounts of α4 and β2 plasmid result in a distribution of 40 ± 4% $(\alpha4)_2(\beta2)_3$ and 60 ± 5% $(\alpha4)_3(\beta2)_2$. A 10:1 (α4:β2) biased transfection shifts this distribution to 30 ± 7% $(\alpha4)_2(\beta2)_3$ and 70 ± 7% $(\alpha4)_3(\beta2)_2$, while the 4:1 transfection fit a binomial of 40 ± 7% $(\alpha4)_2(\beta2)_3$ and 60 ± 4% $(\alpha4)_3(\beta2)_2$, respectively. On the converse, a 1:4 biased transfection with an excess amount of the β2 subunit fits a distribution of 65 ± 5% $(\alpha4)_2(\beta2)_3$ and 35 ± 9% $(\alpha4)_3(\beta2)_2$. Based on the 95% confidence intervals, the fraction of $(\alpha4)_3(\beta2)_2$ reduced and the fraction of $(\alpha4)_2(\beta2)_3$ increased when higher levels of β2 were transfected (1:4 (α4:β2)) (Figure 4.23). However, over expression of the α4 subunit did not seem to significantly alter the assembly from the approximately 40:60 distribution seen in a 1:1 transfection. This observation suggests there could be a natural bias, or higher amounts of α4 subunits, typically found in the endoplasmic reticulum. This effect has also been observed in biased transfections for functional studies, showing higher levels of the $(\alpha4)_3(\beta2)_2$ isoform [154]. One possibility for this effect is that unassembled β2 subunits are degraded more rapidly than α4 subunits within the endoplasmic reticulum [154, 191].

These studies show that nicotine's primary metabolite, cotinine, has a similar effect on the trafficking and assembly of nAChRs as seen with nicotine. Cotinine has a longer half-life and higher sustained concentration than nicotine in the human body. This means that cotinine may be at least partially responsible for physiological changes in nAChRs previously attributed to nicotine alone. It is also possible that variations in the concentration of cotinine resulting from gene variation and clearance rates in different ethnicities could account for some differences in rates of nicotine addiction seen in these individuals.

5.3 nAChR Ligands Alter Expression, Trafficking, and Assembly of α4β2

Most smoking cessation agents have targeted the α4β2* nAChR subtype. Cytisine and varenicline, both partial agonists of α4β2, have previously been shown to increase the number of α4β2 nAChRs on the plasma membrane [176, 178, 210, 238, 258]. We hypothesized that cytisine and varenicline could also alter the distribution of α4β2 towards the plasma membrane, or alter the assembly of α4β2. Using SEP-labeled α4β2, we show both of these drugs also increase the distribution of α4β2 towards the plasma membrane, as well as increase the integrated density on the plasma membrane. This shows trafficking of α4β2 is increased in addition to expression on the plasma membrane. These increases occur upon exposure to 500 nM of either drug. This concentration is lower than the EC_{50} values for cytisine and varenicline, which are both in the low micromolar range [177, 268]. At a concentration of 500 nM, cytisine and varenicline both alter the assembly of α4β2. Previous studies have suggested cytisine exposure results in a preference for the low sensitivity, $(\alpha4)_3(\beta2)_2$ isoform [85, 151]. This increase in $(\alpha4)_3(\beta2)_2$ in the presence of cytisine has been primarily detected at the plasma membrane. In contrast, the single molecule bleaching analysis of nAChRs isolated in cell-derived nanovesicles, developed in our lab, evaluates primarily intracellular nAChRs. Using this method, we show a slight shift in the assembly to favor the $(\alpha4)_2(\beta2)_3$ isoform in the presence of cytisine. This difference is potentially the result of measuring stoichiometry of α4β2 in different subcellular regions. Since SEP studies show cytisine increases the fraction of α4β2 nAChRs that reside on the plasma membrane, $(\alpha4)_3(\beta2)_2$ could be preferentially trafficked towards the plasma membrane when cytisine is present. Varenicline exposure causes a pronounced shift towards the $(\alpha4)_2(\beta2)_3$ isoform. The partial agonists cytisine and

varenicline induce changes in trafficking, expression, and assembly of α4β2 at concentrations lower than those required for activation of these nAChRs.

Bupropion, originally marketed as an antidepressant in 1989, has also been approved as a smoking cessation agent [180, 181]. As an antidepressant, bupropion acts as a norepinephrine and dopamine reuptake inhibitor, with no effect on serotonergic activity [180, 269, 270]. Recently, bupropion was also determined to act as a noncompetitive antagonist of α4β2, α3β4 and α7 nAChRs, with IC_{50} values ranging from 0.4 to 60 μM [271, 272]. Photoaffinity labeling studies show bupropion has two distinct binding sites in the *Torpedo* nAChR transmembrane domain, one in each the resting state and desensitized state. One high affinity site is found in the middle of the ion channel, within TM2. Bupropion binds this site when the nAChR is in a resting state, or closed channel state. Bupropion binds a second site near the extracellular end of TM1 within α subunits with three-fold higher affinity. This binding occurs when the nAChR is in an agonist-induced desensitized state [181]. SEP-labeling of α4β2 nAChRs shows 500 nM bupropion upregulates the number of α4β2 nAChRs on the plasma membrane, and alters the distribution of these nAChRs towards the plasma membrane (Figure 4.26; $P < 0.001$). Although bupropion is not specific for nAChRs, it is able to upregulate the number of α4β2 on the plasma membrane and affect the subcellular distribution. Bupropion also alters the stoichiometric distribution of α4β2 nAChRs, as shown by single molecule analysis of GFP-labeled α4 subunits in α4β2. In the presence of 500 nM bupropion, the assembly is shifted towards the high sensitivity version of α4β2, fitting a binomial of 55 ± 2% $(\alpha4)_2(\beta2)_3$ and 45 ± 3% $(\alpha4)_3(\beta2)_2$. Based on the 95% confidence intervals, bupropion significantly shifts the assembly of α4β2 towards the high sensitivity version, from the 40 ± 4% $(\alpha4)_2(\beta2)_3$ and

60 ± 5% $(\alpha4)_3(\beta2)_2$ distribution when no drug is present (Figure 4.26; $P < 0.05$). The increase in $(\alpha4)_2(\beta2)_3$ in the presence of bupropion is likely the result of an altered assembly of α4β2, given that the majority of measured nAChRs originate from intracellular organelles in this study. This gives rise to the potential that bupropion, a noncompetitive antagonist, also penetrates the cell membrane and interacts with nascent nAChRs as a pharmacological chaperone. Unlike cytisine and varenicline, which are both partial agonists of α4β2, bupropion does not bind in the orthosteric ligand binding site of α4β2. However, bupropion still upregulates α4β2, in terms of increased expression on the plasma membrane, a change in distribution towards the plasma membrane, and preferential assembly of $(\alpha4)_2(\beta2)_3$. Other antagonists have also been shown to upregulate α4β2. Mecamylamine, a noncompetitive open channel blocker, increases [^{3}H]-nicotine binding [150, 188, 273] and [^{125}I]-epibatidine binding [274]. Dihydro-β-erythroidine (DhβE), a competitive antagonist, functionally upregulates α4β2 and increase the fraction of high affinity receptors [167], as well as increases [^{125}I]-epibatidine binding [274]. This further supports the idea that upregulation does not require surface activation. It has been suggested that pharmacological chaperones stabilize an assembled pentameric nAChR, rather than unassembled subunits, in its most stable state within the endoplasmic reticulum. It is possible that intracellular binding and stabilization of nAChRs promotes upregulation. Overall, a variety of pharmacological agents with various binding properties induce upregulation or promote specific stoichiometries of nAChRs. If these changes occur intracellularly, future therapeutically relevant pharmacological agents may be able to target intracellular processes.

5.4 Subcellular Differences in the Distribution of $(\alpha4)_2(\beta2)_3$ versus $(\alpha4)_3(\beta2)_2$

Although upregulation of α4β2 has been implicated in the addictive nature of nicotine, the actual mechanism of this upregulation remains elusive [6, 45, 46, 55, 64, 66, 76, 151]. New evidence continues to converge on the idea that an intracellular mechanism is responsible for this effect. Upregulation is currently considered an increase in nAChR number, as well as changes in trafficking and stoichiometric assembly. As mentioned, nicotine increases the expression of the high sensitivity $(\alpha4)_2(\beta2)_3$ isoform [85, 151, 154, 233, 256, 257]. This suggests nicotine permeates cell membranes, interacts with intracellular subunits, and alters the expression of nAChRs internally to favor a high sensitivity $(\alpha4)_2(\beta2)_3$ stoichiometry. Despite the connection between α4β2 assembly and its role in nicotine addiction, evidence of changes in assembly distinctively within the endoplasmic reticulum had not been detected prior to this study. This is primarily due to a lack of existing techniques that are capable of directly quantifying subcellular specific structural assembly of complex proteins in a cellular environment. Prior to this research, direct structural studies had been limited to bulk fluorescence methods. FRET, Förster resonance energy transfer, based studies show an increase in the number of α4 and β2 subunits in close proximity within the whole-cell region measured, which includes the endoplasmic reticulum [115, 196, 197]. However, quantitatively determining the stoichiometry of individual α4β2 nAChRs isolated in native subcellular membranes can show exclusive localized changes in preferential assembly within the endoplasmic reticulum or plasma membrane. We hypothesized that nicotine alters the assembly of α4β2 nAChRs within the endoplasmic reticulum, and this could be detected using single molecule analysis of GFP-labeled nAChRs embedded in cell-derived nanovesicles isolated

from specific subcellular regions. To test this hypothesis, we developed a technique to separate nAChRs localized to the endoplasmic reticulum or plasma membrane using an system of gradient centrifugation.

Previously discussed changes in assembly upon exposure to nicotine, cotinine, cytisine, varenicline, and bupropion were measured for nAChRs isolated from membranes throughout the whole cell. These single molecule analysis studies with GFP-labeled subunits, discussed above, were expanded to detect organelle specific changes in nAChR stoichiometry. Once vesicles containing α4β2 nAChRs are formed, an OptiPrep gradient is used to separate nanovesicles derived from the membranes of the endoplasmic reticulum and plasma membrane. Density gradients have previously been used to separate these subcellular regions, but in much larger vesicles that are incompatible with single molecule studies [275-278]. Nanovesicles from the endoplasmic reticulum or plasma membrane were generated from cells expressing α4-GFP and β2-wt subunits at nitrogen cavitation pressures of 250 psi or 600 psi, respectively. A cavitation pressure of 250 psi has been shown to form vesicles encapsulating a single nAChR [228]. At this pressure, a negligible number of nanovesicles were formed from the plasma membrane. Large fragments of plasma membrane could be visualized by fluorescence microscopy in the whole cell lysate at 250 psi, and mostly localized to the bottom fraction of the column (Figure 4.27C). Although fraction 1 has a higher relative number of ER-derived nanovesicles, fraction 2 at 250 psi is chosen to avoid contamination from dense species at the bottom of the column. To encourage the fragmentation of the plasma membrane, cells were swollen in a hypotonic solution [279] prior to nitrogen cavitation at a higher pressure of 600 psi. At 600 psi, ER-derived nanovesicles also localized to higher density fractions (Figure 4.29B). At this

pressure, PMCA containing nanovesicles localize to lower density fractions of 5, 7, and 9. Fraction 7 is collected for plasma membrane specific studies, to avoid contamination from endoplasmic reticulum derived vesicles in denser fractions. This method effectively allows the isolation of organelle specific vesicles originating from the endoplasmic reticulum or plasma membrane.

Endoplasmic reticulum and plasma membrane derived nanovesicles provide a snapshot of nAChR assembly in each location at the time of nitrogen cavitation. Vesicles from each organelle are independently spatially isolated on a glass substrate. The stoichiometry of α4β2 is determined by counting single molecule bleaching steps of the GFP-labeled alpha subunits. By separating nAChRs based on the membrane of origin, structural differences between receptors located within the endoplasmic reticulum can be differentiated from those on the plasma membrane. This also provides a measure of preferential trafficking of one stoichiometry over the other. In addition, organelle specific changes in structural assembly in the presence of nicotine can be determined. Understanding nicotine induced structural changes on a subcellular level is crucial to resolving the mechanism of nicotine addiction. Detecting a shift towards the high sensitivity $(\alpha4)_2(\beta2)_3$ isoform within the endoplasmic reticulum suggests nicotine acts internally.

Endoplasmic reticulum specific vesicles expressing α4-GFP/β2 nAChRs were collected from fraction 2 of the OptiPrep gradient. Purified fractions contained single nAChRs that were resident in the endoplasmic reticulum at the time of nitrogen cavitation, now encapsulated in nanovesicles. In the absence of a pharmacological agent, α4β2 is predominately assembled as $(\alpha4)_3(\beta2)_2$ in the endoplasmic reticulum. The inherent α4β2

stoichiometry within the endoplasmic reticulum fits a distribution of 30 ± 4% $(\alpha4)_2(\beta2)_3$ and 70 ± 4% $(\alpha4)_3(\beta2)_2$. This roughly matches estimates based on whole cell functional measurements [154, 167, 233]. This is not surprising, since ligand binding studies have indicated 85% of [^{3}H]-epibatidine binding sites are intracellular [195]. The higher ratio of α4β2 nAChRs with $(\alpha4)_3(\beta2)_2$ within the endoplasmic reticulum could be related to a higher stability of α4 subunits compared to β2 subunits. It has been proposed that unassembled β2 subunits are degraded more rapidly than α4 subunits within the endoplasmic reticulum [154].

Once cells are exposed to nicotine, single molecule bleaching step analysis shows this distribution is shifted to 55 ± 4% $(\alpha4)_2(\beta2)_3$ and 45 ± 5% $(\alpha4)_3(\beta2)_2$ within the endoplasmic reticulum. Based on the 95% confidence intervals, the fraction of α4β2 present in the high sensitivity $(\alpha4)_2(\beta2)_3$ stoichiometry is significantly increased when nicotine is present. This is the first structural evidence showing a distinct change in α4β2 assembly to favor the $(\alpha4)_2(\beta2)_3$ isoform directly within the endoplasmic reticulum. This finding strongly supports the theory that nicotine acts as a pharmacological chaperone to stabilize the $(\alpha4)_2(\beta2)_3$ version, as nicotine clearly causes an intracellular change in the assembly of α4β2. Previous structural investigations have been limited to measuring α4 and β2 subunits in close proximity by FRET [151]. This finding also correlates with bulk measurements detecting an increase in the amount of β2 subunit compared to α4 subunit [153, 154, 258, 259]. These single molecule bleaching step analysis studies directly measure a change in the assembly of pentameric nAChRs in the presence of nicotine for explicit structural determination of α4β2 within the endoplasmic reticulum for the first time.

Plasma membrane specific nanovesicles formed from cells expressing α4-GFP/β2 were collected from fraction 7 of the OptiPrep gradient. The purified fraction contains single α4β2 nAChRs encapsulated in nanovesicles formed from the plasma membrane at the time of nitrogen cavitation. In the absence of a pharmacological agent, α4β2 on the plasma membrane slightly favors $(\alpha4)_2(\beta2)_3$ stoichiometry. The intrinsic α4β2 stoichiometry on the plasma membrane fits a distribution of 56 ± 3% $(\alpha4)_2(\beta2)_3$ and 44 ± 4% $(\alpha4)_3(\beta2)_2$. This is the first study to show a distribution of α4β2 stoichiometry exclusively on the plasma membrane. Based on 95% confidence intervals, this is a significantly different assembly than the inherent α4β2 distribution of 30 ± 4% $(\alpha4)_2(\beta2)_3$ and 70 ± 4% $(\alpha4)_3(\beta2)_2$ within the endoplasmic reticulum. This suggests that $(\alpha4)_2(\beta2)_3$ is preferentially located on the plasma membrane. Preferential trafficking of this isoform to the plasma membrane could account for this difference in subcellular localization. Another possibility is an increased stability, or decreased internalization, of $(\alpha4)_2(\beta2)_3$ on the plasma membrane.

Upon exposure to nicotine, the distribution of α4β2 on the plasma membrane is shifted further towards the high sensitivity version. When nicotine is present, plasma membrane resident α4β2 fits a 70 ± 2% $(\alpha4)_2(\beta2)_3$ and 30 ± 4% $(\alpha4)_3(\beta2)_2$ distribution. This is a significant increase in $(\alpha4)_2(\beta2)_3$ on the plasma membrane in the presence of nicotine compared to 56 ± 3% $(\alpha4)_2(\beta2)_3$ and 44 ± 4% $(\alpha4)_3(\beta2)_2$ in the absence of a pharmacological agent, based on the 95% confidence intervals. This is the first structural study showing a distribution of α4β2 assembly favoring the $(\alpha4)_2(\beta2)_3$ isoform exclusively on the plasma membrane upon exposure to nicotine. The increase in $(\alpha4)_2(\beta2)_3$ on the PM when nicotine is present is likely the result of an increase in this isoform within the ER,

combined with the increase in trafficking towards the PM. However, this is significant because it shows a higher fraction of α4β2 on the plasma membrane will functionally respond to lower levels of nicotine, thus increasing α4β2 sensitivity. A shift towards the high sensitivity $(\alpha4)_2(\beta2)_3$ isoform on the plasma membrane may account for signaling changes measured in tobacco users.

The increase in assembly of $(\alpha4)_2(\beta2)_3$ within the endoplasmic reticulum provides a molecular basis for upregulation measured at the plasma membrane. In the absence of a pharmacological agent, the majority of α4β2 nAChRs within the endoplasmic reticulum are assembled in the low sensitivity $(\alpha4)_3(\beta2)_2$ version. However, the high sensitivity $(\alpha4)_2(\beta2)_3$ isoform is inherently preferentially trafficked to the plasma membrane. Upon the addition of nicotine, the structural assembly of α4β2 is altered intracellularly within the endoplasmic reticulum to favor the high sensitivity $(\alpha4)_2(\beta2)_3$ isoform. Since this stoichiometry is intrinsically preferentially trafficked to the plasma membrane, the increase in $(\alpha4)_2(\beta2)_3$ within the endoplasmic reticulum results in an increase in trafficking towards the plasma membrane. The net result is an upregulation of $(\alpha4)_2(\beta2)_3$, both within the endoplasmic reticulum and on the plasma membrane. These shifts in stoichiometry within each subcellular location upon the addition of nicotine are summarized in Figure 5.1. This is the first study to show subcellular differences in stoichiometry of α4β2, as well as a shift towards the high sensitivity version within the ER when nicotine is present.

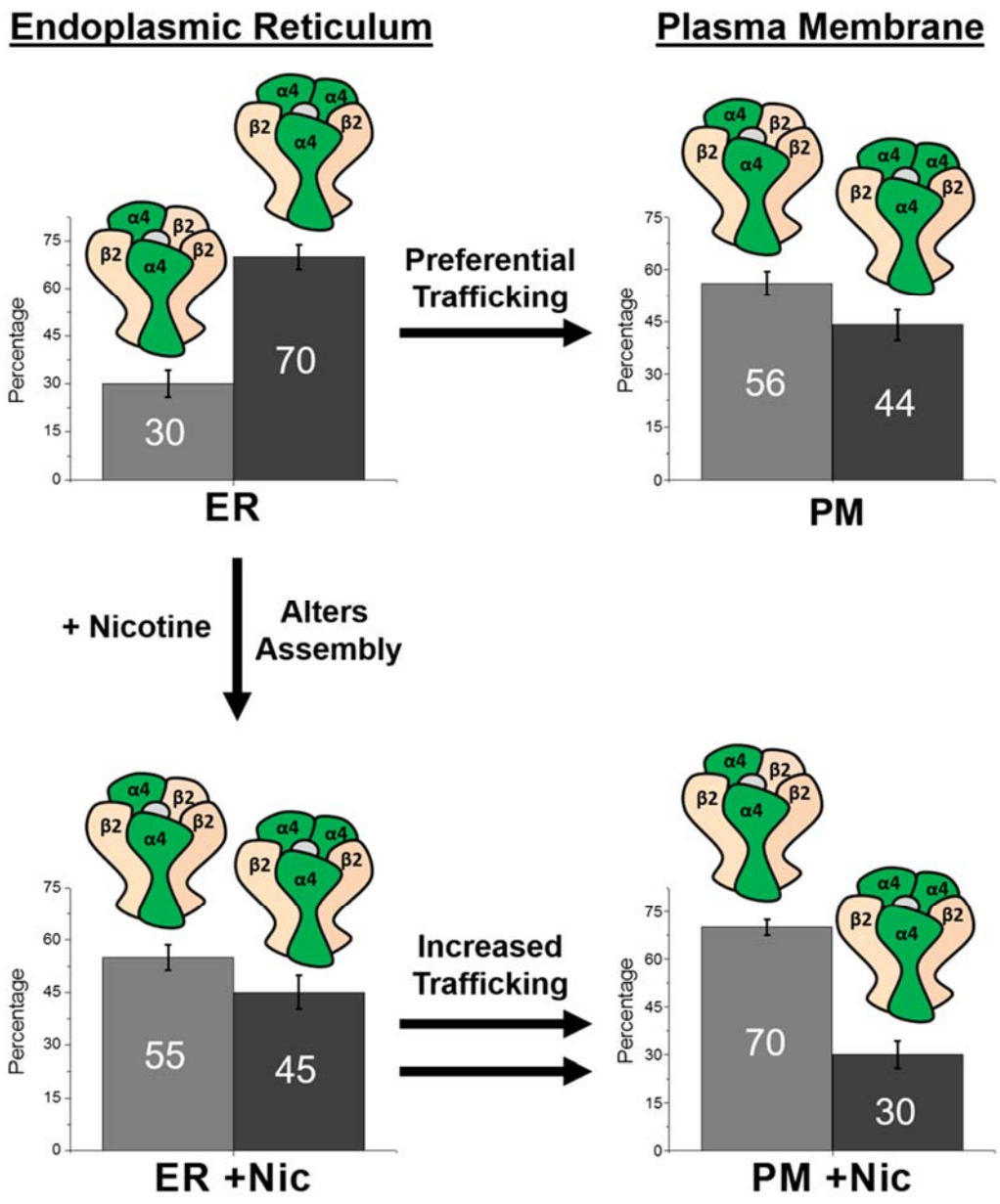

Figure 5.1 Nicotine alters assembly within the ER and increases trafficking to the PM. When no nicotine is present, the α4β2 favors the $(\alpha4)_3(\beta2)_2$ stoichiometry in the ER. However, the $(\alpha4)_2(\beta2)_3$ version is preferentially trafficked to the PM. Upon exposure to nicotine, assembly is shifted within the ER towards $(\alpha4)_2(\beta2)_3$ isoform. Increased trafficking when nicotine is present increases the fraction of $(\alpha4)_2(\beta2)_3$ on the PM. Error bars are 95% confidence intervals.

CHAPTER 6: CONCLUSION

This dissertation exploits and expands novel fluorescence microscopy techniques to progress the understanding of the mechanism of nicotine induced upregulation in order to identify target nAChR structures for the development of smoking cessation therapeutics. Changes in nAChR number, stoichiometry, and trafficking are well-established consequences of exposure to nicotine [51, 55, 97, 161, 198], yet a full mechanism for this upregulation has not been determined. An intracellular process is believed to be responsible for these changes in expression, but definitive evidence of a shift in assembly within the endoplasmic reticulum had not been detected prior to this study.

In this work, cutting edge methodologies are developed and employed to pinpoint distinct changes in localization, assembly, export, vesicle trafficking and stoichiometry in order to further understand the physiology of these receptors. In this work, drug induced changes in trafficking and expression of SEP-labeled nAChRs were measured using TIRF microscopy. This technique is complementary to traditional methods of nAChR detection, offering particular advantages for analysis of receptors located near the plasma membrane. The majority of nAChR are thought to be intracellular [195], yet functional consequences of nAChR upregulation occur upon insertion into the plasma membrane. Quantification of trafficking and distribution effects upon exposure to a ligand are made possible with this imaging technique. A combination of pH sensitive fluorophores and TIRF microscopy enables the differentiation of nAChRs inserted into the plasma membrane, compared to those resident in the peripheral endoplasmic reticulum. For this reason, relative numbers of nAChR located on the plasma membrane (PMID), as well as trafficking features such

as percentage of nAChRs on the plasma membrane (% PM) and single vesicle insertion events can be resolved.

Although chronic nicotine exposure upregulates and alters the assembly of α4β2 nAChRs [51, 97, 161, 235], the effects of nicotine metabolites on nAChR assembly and trafficking are not well studied. In this work, N2a cells were exposed to physiologically relevant concentrations of cotinine, centered around the average reported concentrations of cotinine in the blood and brain of an average smoker [29, 241, 242]. Measuring α4-SEP/β2 nAChRs with TIRF microscopy shows that cotinine upregulates the expression and distribution of α4β2 towards the plasma membrane. This suggests that cotinine could potentially contribute to α4β2 upregulation measured in smokers, since this effect is seen at concentrations of cotinine even lower than estimated to be found in the brain [26]. Cotinine also increases the number of insertion events of single vesicles carrying α4β2 nAChRs. The increase in insertion events, in addition to an increase in % PM, suggests that cotinine influences trafficking of α4β2. Similar to nicotine, incorporation of α5 into the α4β2 pentamer results in a loss of cotinine induced upregulation. However, the SEP-based studies reveal that when α5 has a single nucleotide polymorphism, D398N, a higher percentage of α4β2α5-D398N are found on the plasma membrane compared to α4β2α5D. This increase is independent of either nicotine or cotinine exposure. Neither drug appears to affect expression or trafficking of α3β4 upon exposure to physiologically relevant concentrations. Interestingly, α6β2β3 shows a concentration dependent downregulation in the presence of 500 nM cotinine [227]. This is an opposite effect as seen with nicotine, which has been shown to upregulate α6β2β3 at low physiological concentrations (50 nM), while downregulating at higher concentrations (500 nM) [115].

Our lab recently developed a novel technique to spatially isolate membrane proteins by encapsulation in vesicles formed from endogenous cell membranes [228]. This nitrogen cavitation based fragmentation method isolates single nAChRs in their endogenous cellular environment. Individual nAChRs embedded in nanovesicles can then be spatially isolated on a glass surface and imaged with TIRF microscopy. Single step photobleaching of GFP molecules within α4 subunits is used to identify the number of α4-GFP subunits in each nAChR, and thus the stoichiometry. This novel method is used to determine that cotinine, the primary metabolite of nicotine, also shifts the assembly of α4β2. Upon exposure to 1 μM cotinine, the stoichiometry of α4β2 is shifted to favor the high sensitivity $(\alpha4)_2(\beta2)_3$ isoform. Exposure to nicotine also favors this stoichiometry, causing an overall shift from the preferentially expressed low sensitivity version in the absence of a pharmacological agent. This method primarily detects intracellular nAChRs, meaning these changes are likely to be internal.

Parallel effects in the presence of cotinine and nicotine suggest it is possible that cotinine-induced upregulation of α4β2 results from a similar mechanism as nicotine, potentially acting inside the cell by binding immature subunits to enhance the maturation and stabilization of nAChRs [76, 160]. Cotinine increases expression and trafficking of α4β2, as well as alters the assembly to favor the high sensitivity $(\alpha4)_2(\beta2)_3$ version. Cotinine has a longer half-life and higher sustained concentration than nicotine in the human body. It is possible that variations in the concentration of cotinine resulting from gene variation and clearance rates in different ethnicities could account for some differences in rates of nicotine addiction.

Many current smoking cessation agents are typically ligands of the α4β2* nAChR subtype. Cytisine and varenicline, both partial agonists of α4β2, have previously been shown to increase the number of α4β2 nAChRs on the plasma membrane [176, 178, 210, 238, 258]. SEP-labeled α4β2 is used to show both of these drugs also increase the distribution of α4β2 towards the plasma membrane, as well as increase the integrated density on the plasma membrane. This suggests trafficking of α4β2 is increased in addition to expression on the plasma membrane. By encapsulating a single α4-GFP/β2 nAChR in a nanovesicle derived from a cell exposed to cytisine or varenticline, single molecule photobleaching is used to show both drugs alter the assembly of α4β2. The effect of bupropion, a noncompetitive antagonist of α4β2, on expression is evaluated for the first time in this SEP-based study. Bupropion is shown to upregulate the number of α4β2 nAChRs on the plasma membrane, and alters the distribution of these nAChRs towards the plasma membrane. Bupropion also alters the stoichiometric distribution of α4β2 nAChRs to favor the high sensitivity $(\alpha4)_2(\beta2)_3$ version, as shown by single molecule analysis of GFP-labeled α4 subunits in α4β2. Although bupropion is not specific for nAChRs, it is able to upregulate the number of α4β2 on the plasma membrane and affect the subcellular distribution. Overall, a variety of pharmacological agents with various binding properties induce upregulation of nAChRs. The shift in α4β2 assembly suggests these ligands penetrate the cell membrane and interact with nascent nAChRs, potentially as a pharmacological chaperone. It is possible that intracellular binding and stabilization of nAChRs promotes upregulation. On a broader scale, smoking cessation agents causing upregulation of α4β2, similar to nicotine, could explain why these agents have not been tremendously successful in aiding smoking cessation. It is possible that current drugs only

maintain a steady upregulated expression of α4β2 as seen in tobacco users. Understanding how existing therapeutics alter trafficking and structural assembly of α4β2 provides the framework required to develop more effective cessation therapeutics. If these changes occur intracellularly, future therapeutically relevant pharmacological agents may be able to target intracellular processes.

Nicotine and other ligands are thought to induce upregulation by permeating cell membranes and interacting with intracellular receptors. However, a lack of existing techniques that are capable of directly quantifying subcellular specific structural assembly of nAChRs has prohibited the detection of these changes specifically within the endoplasmic reticulum. In this work, a technique was developed to separate nAChRs localized to the endoplasmic reticulum from those localized to the plasma membrane. Individual nAChRs embedded in a nanoscale vesicle formed from the original ER or PM membranes are separated on a density gradient. Endoplasmic reticulum and plasma membrane derived nanovesicles provide a snapshot of nAChR assembly in each location at the time of nitrogen cavitation. In addition, organelle specific changes in structural assembly in the presence of nicotine can be determined. Understanding nicotine induced structural changes on a subcellular level is crucial to resolving the mechanism of nicotine addiction.

ER-derived nanovesicles expressing α4-GFP/β2 are used to show that in the absence of a pharmacological agent, α4β2 is predominately assembled as $(\alpha4)_3(\beta2)_2$ in the endoplasmic reticulum. The higher ratio of α4β2 nAChRs with $(\alpha4)_3(\beta2)_2$ within the ER could be related to a higher stability of α4 subunits compared to β2 subunits. Once cells are exposed to nicotine, this distribution is shifted to favor the high sensitivity $(\alpha4)_2(\beta2)_3$

isoform within the endoplasmic reticulum. This is the first structural evidence showing a distinct change in α4β2 assembly to favor the $(\alpha4)_2(\beta2)_3$ isoform directly within the endoplasmic reticulum. This finding strongly supports the theory that nicotine acts as a pharmacological chaperone, as nicotine clearly causes an intracellular change in the assembly of α4β2.

PM-derived vesicles reveal α4β2 slightly favors $(\alpha4)_2(\beta2)_3$ stoichiometry on the plasma membrane, even in the absence of a pharmacological agent. This is the first study to show a distribution of α4β2 stoichiometry exclusively on the plasma membrane. This suggests that $(\alpha4)_2(\beta2)_3$ is preferentially trafficked to the plasma membrane. Upon addition of nicotine, the distribution of α4β2 on the plasma membrane is shifted further towards the high sensitivity isoform. This is the first structural study showing a distribution of α4β2 assembly favoring the $(\alpha4)_2(\beta2)_3$ isoform on the plasma membrane in the presence of nicotine. The significance of this finding lies in the possible functional consequences of an increase in α4β2 sensitivity on the plasma membrane when nicotine is present. The increase in the high sensitivity $(\alpha4)_2(\beta2)_3$ isoform on the plasma membrane could account for differences in nAChR activation measured in tobacco users.

The work in this dissertation provides strong evidence that nicotine, and other upregulating ligands, induce intracellular changes in nAChRs. Nicotine, and its primary metabolite cotinine, increase the distribution of α4β2 towards the plasma membrane and increase the number of vesicles carrying α4β2 being inserted into the plasma membrane. Both also increase the assembly of the $(\alpha4)_2(\beta2)_3$ isoform throughout the cell. Current smoking cessation agents acting as partial agonists or noncompetitive antagonists induce changes in expression, trafficking, and assembly of α4β2. Organelle specific studies show

the shift in $(\alpha4)_2(\beta2)_3$ assembly in the presence of nicotine occurs within the endoplasmic reticulum. An increase in the ratio of α4β2 with $(\alpha4)_2(\beta2)_3$ is also found on the plasma membrane when nicotine is present.

These studies provide structural evidence for the pharmacological chaperoning theory of upregulation, suggesting a ligand permeates cell membranes and interacts with nAChRs within the endoplasmic reticulum to increase the stability and therefore assembly of nAChR pentamers. An intracellular mechanism of upregulation has important implications in the discovery of therapeutics targeting nAChRs, since intracellular regions and processes can also be targeted instead of focusing solely on the plasma membrane. This is directly related to the development of more effective smoking cessation therapeutics. An internal mechanism of upregulation could also explain an inverse correlation between the history of smoking and developing Parkinson's disease [155, 196, 280-282]. Understanding an intracellular mechanism for nicotine addiction level is important to the development of nAChRs as drug targets for a variety of neurological disorders including Alzheimer's disease, Parkinson's disease, ADHD, epilepsy, and schizophrenia, as well as tobacco addiction [59-65].

The technique developed in this dissertation to isolate endoplasmic reticulum and plasma membrane derived nanovesicles can be expanded to study assembly and trafficking in a variety of classes of membrane proteins. For example, this technique is currently being employed in our lab to investigate changes in the trafficking of the cystic fibrosis transmembrane conductance regulator (CFTR) channel in the presence of current therapeutics. Ideally, this technique will impact and advance research related to any

membrane protein that varies in expression between the endoplasmic reticulum and plasma membrane.

APPENDIX: LIST OF ABBREVIATIONS

% PM – Percent Plasma Membrane

ACh – Acetylcholine

Bup – Bupropion

Cot – Cotinine

Cyt – Cytisine

DPSS- Diode-Pumped Solid State

EC_{50} – Half Maximal Effective Concentration

ECS – Extracellular Solution

EMCCD – Electron Multiplying Charge Transfer Device

ER – Endoplasmic Reticulum

ERES – Endoplasmic Reticulum Exit Site

fMRI – Functional Magnetic Resonance Imaging

FRET – Förster Resonance Energy Transfer

GABA – γ-Aminobutryic Acid

GFP – Green Fluorescent Protein

HEK-293T – Human Embryonic Kidney-293T

ID – Integrated Density

N2a – Neuroblastoma

nAChR – Nicotinic Acetylcholine Receptor

Nic – Nicotine

PBS – Phosphate Buffered Saline

PET – Positron Emission Tomography

PM – Plasma Membrane

PMCA – Plasma Membrane Calcium ATPase

PMID – Plasma Membrane Integrated Density

SNc – Substantia Nigra Pars Compacta

SNr – Substantia Nigra Pars Reticulata

SEM – Standard Error of the Mean

SEP – Super-Ecliptic Phluorin

TIRF – Total Internal Reflection Fluorescence

TIRFM – Total Internal Reflection Fluorescence Microscopy

TM – Transmembrane

Var – Varenicline

VTA – Ventral Tegmental Area

Wt – wild type

5-HT_3 – 5-hydroxytryptamine

REFERENCES

1. Center for Disease Control and Prevention CDC (2016) Smoking and Tobacco Use Fast Facts *http://www.cdc.gov/tobacco/data_statistics/fact_sheets/fast_facts/index.htm*.
2. World Health Organization WHO (2016) Tobacco Media Centre Fact Sheet. . (http://www.who.int/mediacentre/factsheets/fs339/en/).
3. Moran VE (2012) Cotinine: Beyond that Expected, More than a Biomarker of Tobacco Consumption. *Front. Pharmacol.* 3:173.
4. Baker F, S Ainsworth, J Dye, C Crammer, M Thun, D Hoffmann, J Repace, J Henningfield, J Slade, J Pinney, T Shanks, D Burns, G Connolly, & D Shopland (2000) Health risks associated with cigar smoking. *JAMA* 284(6):735-740.
5. Anonymous (*2014 Surgeon General's Report: The Health Consequences of Smoking - 50 Years of Progress* (U.S. Department of Health and Human Services, Centers for Disease Control and Prevention, National Center for Chronic Disease Prevention and Health Promotion, Office on Smoking and Health, Atlanta).
6. Stolerman IP & MJ Jarvis (1995) The scientific case that nicotine is addictive. *Psychopharmacology* 117(1):2-10.
7. Anonymous (2012) *Is nicotine addictive?* (https://www.drugabuse.gov/publications/research-reports/tobacco/nicotine-addictive), (National Institute on Drug Abuse).
8. Balfour DJ (1994) Neural mechanisms underlying nicotine dependence. *Addiction* 89(11):1419-1423.
9. Dani JA & S Heinemann (1996) Molecular and cellular aspects of nicotine abuse. *Neuron* 16(5):905-908.
10. Clarke PB, RD Schwartz, SM Paul, CB Pert, & A Pert (1985) Nicotinic binding in rat brain: autoradiographic comparison of [3H]acetylcholine, [3H]nicotine, and [125I]-α-bungarotoxin. *J. Neurosci.* 5(5):1307-1315.
11. Hossain AM & SM Salehuddin (2013) Analytical determination of nicotine in tobacco leaves by gas chromatography–mass spectrometry. *Abrab. J. Chem.* 6(3):275-278.
12. Rodu B (2012) Nicotine levels in American smokeless tobacco products. in *Tobacco Truth* (http://rodutobaccotruth.blogspot.com/2012/11/nicotine-levels-in-american-smokeless.html).
13. Benowitz NL (1999) Biomarkers of Environmental Tobacco Smoke Exposure. *Environ. Health Perspect.* 107(2):349-355.
14. Benowitz NL, J Hukkanen, & P Jacob, 3rd (2009) Nicotine chemistry, metabolism, kinetics and biomarkers. *Handb. Exp. Pharmacol.* 192:29-60.
15. Jiloha RC (2010) Biological basis of tobacco addiction: Implications for smoking-cessation treatment. *Indian J. Psy.* 52(4):301-307.
16. Levin ED (2002) Nicotinic receptor subtypes and cognitive function. *J. Neurobiol.* 53(4):633-640.
17. Newhouse PA, A Potter, & A Singh (2004) Effects of nicotinic stimulation on cognitive performance. *Curr. Opin. Pharmacol.* 4(1):36-46.
18. Pons S, L Fattore, G Cossu, S Tolu, E Porcu, JM McIntosh, JP Changeux, U Maskos, & W Fratta (2008) Crucial role of α4 and α6 nicotinic acetylcholine

receptor subunits from ventral tegmental area in systemic nicotine self-administration. *J. Neurosci.* 28(47):12318-12327.
19. Rezvani AH & ED Levin (2001) Cognitive effects of nicotine. *Biol. Psychiatry* 49(3):258-267.
20. Gutkin BS, S Dehaene, & JP Changeux (2006) A neurocomputational hypothesis for nicotine addiction. *Proc. Natl. Acad. Sci. U. S. A.* 103(4):1106-1111.
21. Visoni S, N Meireles, L Monteiro, A Rossini, & LF Pinto (2008) Different modes of inhibition of mouse Cyp2a5 and rat CYP2A3 by the food-derived 8-methoxypsoralen. *Food Chem. Toxicol.* 46(3):1190-1195.
22. Nakajima M, T Yamamoto, K-i Nunoya, T Yokoi, K Nagashima, K Inoue, Y Funae, N Shimada, T Kamataki, & Y Kuroiwa (1996) Characterization of CYP2A6 in 3'-hydroxylation of cotinine in human liver microsomes. *J. Pharmacol. Exp. Ther.* 277:1010-1015.
23. Grizzell JA & V Echeverria (2015) New Insights into the Mechanisms of Action of Cotinine and its Distinctive Effects from Nicotine. *Neurochem. Res.* 40(10):2032-2046.
24. Lewis DFV, M Dickins, BG Lake, PJ Eddershaw, MH Tarbit, & PS Goldfarb (1999) Molecular modelling of the human cytochrome P450 isoform CYP2A6 and investigations of CYP2A substrate selectivity. *Toxicology* 133:1-33.
25. Echeverria V & R Zeitlin (2012) Cotinine: a potential new therapeutic agent against Alzheimer's disease. *CNS Neurosci. Ther.* 18(7):517-523.
26. Buccafusco JJ & AV Terry (2003) The potential role of cotinine in the cognitive and neuroprotective actions of nicotine. *Life Sci.* 72(26):2931-2942.
27. Yamanaka H, M Nakajima, K Nishimura, R Yoshida, T Fukami, M Katoh, & T Yokoi (2004) Metabolic profile of nicotine in subjects whose CYP2A6 gene is deleted. *Eur. J. Pharm. Sci.* 22(5):419-425.
28. Zhu AZ, CC Renner, DK Hatsukami, GE Swan, C Lerman, NL Benowitz, & RF Tyndale (2013) The ability of plasma cotinine to predict nicotine and carcinogen exposure is altered by differences in CYP2A6: the influence of genetics, race, and sex. *Cancer Epidemiol. Biomarkers Prev.* 22(4):708-718.
29. Caraballo RS, GA Giovino, TF Pechacek, PD Mowery, PA Richter, WJ Strauss, DJ Sharp, MP Eriksen, JL Pirkle, & KR Maurer (1998) Racial and Ethnic Differences in Serum Cotinine Levels of Cigarette Smokers. *JAMA* 280(2):135-139.
30. Wagenknecht LE, GR Cutter, NJ Haley, S Sidney, TA Manolio, GH Hughes, & DR Jacobs (1990) Racial differences in serum cotinine levels among smokers in the coronary artery risk development in (young) adults study. *Am. J. Public Health* 80(9):1053-1056.
31. Bramer SL & BA Kallungal (2003) Clinical considerations in study designs that use cotinine as a biomarker. *Biomarkers* 8(3-4):187-203.
32. Clark PI, S Gautam, & LW Gerson (1996) Effect of menthol cigarettes on biochemical markers of smoke exposure among black and white smokers. *Chest* 110:1194-1198.
33. Benowitz N, B Herrera, & PJ 3rd (2004) Mentholated cigarette smoking inhibits nicotine metabolism. *J. Pharmacol. Exp. Ther.* 282:7-13.

34. Alsharari S, J King, J Nordman, P Muldoon, A Jackson, A Zhu, R Tyndale, N Kabbani, & M Damaj (2015) Effects of menthol on nicotine pharmacokinetic, pharmacology and dependence in mice. *PLoS One* 10(9):e0137070.
35. Henderson BJ, TR Wall, BM Henley, CH Kim, WA Nichols, R Moaddel, C Xiao, & HA Lester (2016) Menthol Alone Upregulates Midbrain nAChRs, Alters nAChR Subtype Stoichiometry, Alters Dopamine Neuron Firing Frequency, and Prevents Nicotine Reward. *J. Neurosci.* 36(10):2957-2974.
36. Brody A, A Mukhin, JL Charite, K Ta, J Farahi, C Sugar, M Mamoun, E Vellios, M Archie, M Kozman, J Phuong, F Arlorio, & M Mandelkern (2013) Up-regulation of nicotinic acetylcholine receptors in menthol cigarette smokers. *Int. J. Neuropsychopharmacol.* 16:957-966.
37. Grizzell JA, A Iarkov, R Holmes, T Mori, & V Echeverria (2014) Cotinine reduces depressive-like behavior, working memory deficits, and synaptic loss associated with chronic stress in mice. *Behav. Brain Res.* 268:55-65.
38. Terry JAV, CM Hernandez, EJ Hohnadel, KP Bouchard, & JJ Buccafusco (2005) Cotinine, a neuroactive metabolite of nicotine: potential for treating disorders of impaired cognition. *CNS Drug Rev.* 11(3):229-252.
39. Karaeonji B (2005) Facts about nicotine toxicity. *Arh. Hig. Rada. Toksiko.* 56:363-371.
40. Riah O, P Courriere, J-C Dousset, N Todeschi, & C Labat (1998) Nicotine is more efficient than cotinine at passing the blood-brain barrier in rats. *Cell. Mol. Neurobiol.* 18(3):311-318.
41. Vainio PJ & RK Tuominen (2001) Cotinine binding to nicotinic acetylcholine receptors in bovine chromaffin cell and rat brain membranes. *Nic. & Tob. Res.* 3(2):177-182.
42. O'Leary K, N Parameswaran, JM McIntosh, & M Quik (2008) Cotinine selectively activates a subpopulation of alpha3/alpha6beta2 nicotinic receptors in monkey striatum. *J. Pharmacol. Exp. Ther.* 325(2):646-654.
43. Abood L, D Reynolds, H Booth, & J Bidlack (1981) Sites and mechanisms for nicotine's action in the brain. *Neurosci. Biobehav. Rev.* 5(4):479-486.
44. Sloan J, G Todd, & W Martin (1984) Nature of nicotine binding to rat brain P2 fraction. *Pharmacol. Biochem. Behav.* 20(6):899-909.
45. Taly A, PJ Corringer, D Guedin, P Lestage, & JP Changeux (2009) Nicotinic receptors: allosteric transitions and therapeutic targets in the nervous system. *Nat Rev Drug Discov* 8(9):733-750.
46. Albuquerque EX, EF Pereira, M Alkondon, & SW Rogers (2009) Mammalian nicotinic acetylcholine receptors: from structure to function. *Physiol. Rev.* 89(1):73-120.
47. Dani JA & D Bertrand (2007) Nicotinic acetylcholine receptors and nicotinic cholinergic mechanisms of the central nervous system. *Annu Rev Pharmacol Toxicol* 47:699-729.
48. De Biasi M (2002) Nicotinic mechanisms in the autonomic control of organ systems. *J Neurobiol*:568-579.
49. Connolly C & K Wafford (2004) The Cys-loop superfamily of ligand-gated ion channels: the impact of receptor structure on function. *Biochem. Soc. Trans.* 32(3):529-534.

50. Karlin A (2002) Emerging structure of the nicotinic acetylcholine receptors. *Nat. Rev. Neurosci.* 3(2):102-114.
51. Colombo SF, F Mazzo, F Pistillo, & C Gotti (2013) Biogenesis, trafficking and up-regulation of nicotinic ACh receptors. *Biochem. Pharmacol.* 86(8):1063-1073.
52. Millar NS & PC Harkness (2008) Assembly and trafficking of nicotinic acetylcholine receptors. *Mol. Membr. Biol.* 25(4):279-292.
53. Nemecz A, MS Prevost, A Menny, & PJ Corringer (2016) Emerging Molecular Mechanisms of Signal Transduction in Pentameric Ligand-Gated Ion Channels. *Neuron* 90(3):452-470.
54. Morales-Perez CL, CM Noviello, & RE Hibbs (2016) X-ray structure of the human alpha4beta2 nicotinic receptor. *Nature* 538:411-415.
55. Lester HA, C Xiao, R Srinivasan, CD Son, J Miwa, R Pantoja, MR Banghart, DA Dougherty, AM Goate, & JC Wang (2009) Nicotine is a selective pharmacological chaperone of acetylcholine receptor number and stoichiometry. Implications for drug discovery. *AAPS J* 11(1):167-177.
56. Lester RA & JA Dani (1995) Acetylcholine receptor desensitization induced by nicotine in rat medial habenula neurons. *J. Neurophysiol.* 74(1):195-206.
57. Benwell ME, DJ Balfour, & CE Birrell (1995) Desensitization of the nicotine-induced mesolimbic dopamine responses during constant infusion with nicotine. *Br. J. Pharmacol.* 114(2):454-460.
58. Pidoplichko VI, M DeBiasi, JT Williams, & JA Dani (1997) Nicotine activates and desensitizes midbrain dopamine neurons. *Nature* 390(6658):401-404.
59. Dineley KT, AA Pandya, & JL Yakel (2015) Nicotinic ACh receptors as therapeutic targets in CNS disorders. *Trends Pharmacol. Sci.* 36(2):96-108.
60. Buckingham SD, AK Jones, LA Brown, & DB Sattelle (2009) Nicotinic Acetylcholine Receptor Signalling: Roles in Alzheimer's Disease and Amyloid Neuroprotection. *Pharmacol. Rev.* 61(1):39-61.
61. Perry E, C Martin-Ruiz, M Lee, M Griffiths, M Johnson, M Piggott, V Haroutunian, JD Buxbaum, J Nasland, K Davis, C Gotti, F Clementi, S Tzartos, O Cohen, H Soreq, E Jaros, R Perry, C Ballard, I McKeith, & J Court (2000) Nicotinic receptor subtypes in human brain ageing, Alzheimer and Lewy body diseases. *Eur. J. Pharmacol.* 393(1-3):215-222.
62. Woodruff-Pak DS & TJ Gould (2002) Neuronal nicotinic acetylcholine receptors: involvement in Alzheimer's disease and schizophrenia. *Behav Cogn Neurosci Rev* 1(1):5-20.
63. Xie A, J Gao, L Xu, & D Meng (2014) Shared mechanisms of neurodegeneration in Alzheimer's disease and Parkinson's disease. *Biomed. Res. Int.* 2014:648740.
64. Changeux JP (2010) Nicotine addiction and nicotinic receptors: lessons from genetically modified mice. *Nat. Rev: Neurosci.* 11(6):389-401.
65. Court JA, MA Piggott, S Lloyd, N Cookson, CG Ballard, IG McKeith, RH Perry, & EK Perry (2000) Nicotine binding in human striatum: elevation in schizophrenia and reductions in dementia with Lewy bodies, Parkinson's disease and Alzheimer's disease and in relation to neuroleptic medication. *Neuroscience* 98(1):79-87.

66. Govind AP, P Vezina, & WN Green (2009) Nicotine-induced upregulation of nicotinic receptors: underlying mechanisms and relevance to nicotine addiction. *Biochem. Pharmacol.* 78(7):756-765.
67. Sargent PB (1993) The diversity of neuronal nicotinic acetylcholine receptors. *Ann. Rev. Neurosci.* 16:403-443.
68. Flores CM, SW Rogers, LA Pabreza, BB Wolfe, & KJ Kellar (1992) A subtype of nicotinic cholinergic receptor in rat-brain is composed of a4 subunit and b2-subunit and is up-regulated by chronic nicotine treatment. *Mol. Pharmacol.* 41:31-37.
69. Gotti C, M Zoli, & F Clementi (2006) Brain nicotinic acetylcholine receptors: native subtypes and their relevance. *Trends in Pharmacol. Sci.* 27(9):482-491.
70. McIntosh JM, PV Plazas, M Watkins, ME Gomez-Casati, BM Olivera, & AB Elgoyhen (2005) A novel α-conotoxin, PeIA, cloned from Conus pergrandis, discriminates between Rat α9α10 and α7 nicotinic cholinergic receptors. *J. Biol. Chem.* 28(34):30107-30112.
71. Wada E, K Wada, J Boulter, E Deneris, S Heinemann, J Patrick, & LW Swanson (1989) Distribution of alpha2, alpha3, alpha4, and beta2 neuronal nicotinic receptor subunit mRNAs in the central nervous system: A hybridization histochemical study in the rat. *J. Comp. Neurology* 284(2):314-335.
72. Karlin A & MH Akabas (1995) Toward a structural basis for the function of nicotinic acetylcholine receptors and their cousins. *Neuron* 15:1231-1244.
73. Pascual JM & A Karlin (1998) State-dependent accessibility and electrostatic potential in the channel of the acetylcholine receptor. Inferences from rates of reaction of thiosulfonates with substituted cysteines in the M2 segment of the a subunit. *J. Gen. Physiol.* 111:717-739.
74. Leonard S & D Bertrand (2001) Neuronal nicotinic receptors: from structure to function. *Nicotine Tob Res* 3(3):203-223.
75. St. John PA (2009) Cellular trafficking of nicotinic acetylcholine receptors. *Acta Pharmacol Sin* 30(6):656-662.
76. Srinivasan R, BJ Henderson, HA Lester, & CI Richards (2014) Pharmacological chaperoning of nAChRs: A therapeutic target for Parkinson's disease. *Pharmacol. Res.* 83:20-29.
77. Dougherty DA (1996) Cation-p interactions in chemistry and biology: A new view of benzene, Phe, Tyr, and Trp. *Science* 271(5246):163-168.
78. Xiu X, NL Puskar, JA Shanata, HA Lester, & DA Dougherty (2009) Nicotine binding to brain receptors requires a strong cation-pi interaction. *Nature* 458(7237):534-537.
79. Beene DL, GS Brandt, W Zhong, NM Zacharias, HA Lester, & DA Dougherty (2002) Cation-p interactions in ligand recognition by serotonergic (5-$HT3_A$) and nicotinic acetylcholine receptors: the anomalous binding properties of nicotine. *Biochemistry* 41(32):10262-10269.
80. Carbone AL, M Moroni, PJ Groot-Kormelink, & I Bermudez (2009) Pentameric concatenated (alpha4)(2)(beta2)(3) and (alpha4)(3)(beta2)(2) nicotinic acetylcholine receptors: subunit arrangement determines functional expression. *Br. J. Pharmacol.* 156(6):970-981.

81. Tapia L, A Kuryatov, & J Lindstrom (2007) Ca^{2+} permeability of the $(\alpha4)_3(\beta2)_2$ stoichiometry greatly exceeds that of $(\alpha4)_2(\beta2)_3$ human acetylcholine receptors. *Mol. Pharmacol.* 71(3):769-776.
82. Mazzaferro S, N Benallegue, A Carbone, F Gasparri, R Vijayan, PC Biggin, M Moroni, & I Bermudez (2011) Additional Acetylcholine (ACh) Binding Site at α4/α4 Interface of (α4β2)2α4 Nicotinic Receptor Influences Agonist Sensitivity. *J. Biol. Chem.* 286(35):31043-31054.
83. Mazzaferro S, F Gasparri, K New, C Alcaino, M Faundez, PI Vasquez, R Vijayan, PC Biggin, & I Bermudez (2014) Non-equivalent Ligand Selectivity of Agonist Sites in (alpha4beta2)2alpha4 Nicotinic Acetylcholine Receptors: A Key Determinant of Agonist Efficacy. *J. Biol. Chem.*
84. Wang J, A Kuryatov, A Sriram, Z Jin, TM Kamenecka, PJ Kenny, & J Lindstrom (2015) An Accessory Agonist Binding Site Promotes Activation of alpha4beta2* Nicotinic Acetylcholine Receptors. *J. Biol. Chem.* 290(22):13907-13918.
85. Richards CI, K Luong, R Srinivasan, SW Turner, DA Dougherty, J Korlach, & HA Lester (2012) Live-Cell Imaging of Single Receptor Composition Using Zero-Mode Waveguide Nanostructures. *Nano Lett.* 12(7):3690-3694.
86. Brown RW, AC Collins, JM Lindstrom, & P Whiteaker (2007) Nicotinic alpha5 subunit deletion locally reduces high-affinity agonist activation without altering nicotinic receptor numbers. *J. Neurochem.* 103(1):204-215.
87. Kuryatov A, W Berrettini, & J Lindstrom (2011) Acetylcholine receptor (AChR) alpha5 subunit variant associated with risk for nicotine dependence and lung cancer reduces (alpha4beta2)(2)alpha5 AChR function. *Mol. Pharmacol.* 79(1):119-125.
88. Cui C, TK Booker, RS Allen, SR Grady, P Whiteaker, MJ Marks, O Salminen, T Tritto, CM Butt, WR Allen, JA Stitzel, JM McIntosh, J Boulter, AC Collins, & SF Heinemann (2003) The b3 nicotinic receptor subunit: a component of a-conotoxin MII-binding nicotinic acetylcholine receptors that modulate dopamine release and related behaviors. *J. Neurosci.* 23(35):11045-11053.
89. Wonnacott S & J Barik (2007) Nicotinic ACh Receptors. *Tocris Reviews* 28.
90. Lukas RJ, JP Changeux, N Le Novere, EX Albuquerque, DJ Balfour, DK Berg, D Bertrand, VA Chiappinelli, PB Clarke, AC Collins, JA Dani, SR Grady, KJ Kellar, JM Lindstrom, MJ Marks, M Quik, PW Taylor, & S Wonnacott (1999) Current status of the nomenclature for nicotinic acetylcholine receptors and their subunits. *Pharmacol. Rev.* 51(2):397-401.
91. Exley R & SJ Cragg (2008) Presynaptic nicotinic receptors: a dynamic and diverse cholinergic filter of striatal dopamine neurotransmission. *Br. J. Pharmacol.* 153(Suppl 1):283-297.
92. Whiting PJ & JM Lindstrom (1987) Purification and characterization of a nicotinic acetylcholine receptor from rat-brain. *Proc. Natl. Acad. Sci. U.S.A.* 84:595-599.
93. Goldman D, E Deneris, W Luyten, A Kochhar, J Patrick, & S Heinemann (1987) Members of a nicotinic acetylcholine receptor gene family are expressed in different regions of the mammalian central nervous system. *Cell* 48:965-973.

94. Picciotto MR, M Zoli, V Zachariou, & JP Changeux (1997) Contribution of nicotinic acetylcholine receptors containing the β2-subunit to the behavioural effects of nicotine. *Biochem. Soc. Trans.* 25(3):824-829.
95. Marubio LM & J Changeux (2000) Nicotinic acetylcholine receptor knockout mice as animal models for studying receptor function. *Eur. J. Pharmacol.* 393(1-3):113-121.
96. Anonymous (Nicotine. in *The Binding Database* (http://www.bindingdb.org/MonoNames?name=Nicotine_50004108).
97. Kuryatov A, J Luo, J Cooper, & J Lindstrom (2005) Nicotine acts as a pharmacological chaperone to up-regulate human a4b2 acetylcholine receptors. *Mol. Pharmacol.* 68(6):1839-1851.
98. Grady SR, MJ Marks, & AC Collins (1994) Desensitization of nicotine-stimulated [3H]dopamine release from mouse striatal synaptosomes. *J. Neurochem.* 62(4):1390-1398.
99. Rao TS, LD Correa, P Adams, EM Santori, & AI Sacaan (2003) Pharmacological characterization of dopamine, norepinephrine and serotonin release in the rat prefrontal cortex by neuronal nicotinic acetylcholine receptor agonists. *Brain Res.* 990(1-2):203-208.
100. Tapper AR, SL McKinney, R Nashmi, J Schwarz, P Deshpande, C Labarca, P Whiteaker, MJ Marks, AC Collins, & HA Lester (2004) Nicotine activation of α4* receptors: sufficient for reward, tolerance and sensitization. *Science* 306(5698):1029-1032.
101. Picciotto MR, M Zoli, R Rimondini, C Lena, LM Marubio, EM Pich, K Fuxe, & JP Changeux (1998) Acetylcholine receptors containing the b2 subunit are involved in the reinforcing properties of nicotine. *Nature* 391(6663):173-177.
102. Davis JA, JW Kenney, & TJ Gould (2007) Hippocampal α4β2 nicotinic acetylcholine receptor involvement in the enhancing effect of acute nicotine on contextual fear conditioning. *J. Neurosci.* 27(40):10870-10877.
103. Brunzell DH, JR Chang, B Schneider, P Olausson, JR Taylor, & MR Picciotto (2006) b2-Subunit-containing nicotinic acetylcholine receptors are involved in nicotine-induced increases in conditioned reinforcement but not progressive ratio responding for food in C57BL/6 mice. *Psychopharmacology* 184(3-4):328-338.
104. Madsen HB, HS Koghar, T Pooters, JS Massalas, J Drago, & AJ Lawrence (2014) Role of alpha4- and alpha6-containing nicotinic receptors in the acquisition and maintenance of nicotine self-administration. *Addict. Biol.* 20(3):500-512.
105. McCallum SE, AC Collins, R Paylor, & MJ Marks (2006) Deletion of the β2 nicotinic acetylcholine receptor subunit alters development of tolerance to nicotine and eliminates receptor upregulation. *Psychopharmacology* 184(3-4):314-327.
106. Besson M, S Suarez, A Cormier, JP Changeux, & S Granon (2008) Chronic nicotine exposure has dissociable behavioural effects on control and β2-/- mice. *Behav. Genet.* 38(5):503-514.
107. Walters CL, S Brown, JP Changeux, B Martin, & MI Damaj (2006) The beta 2 but not alpha 7 subunit of the nicotinic acetylcholine receptor is required for nicotine-conditioned place preference in mice. *Psychopharmacology* 184(3-4):339-344.

108. Salminen O, P Whiteaker, SR Grady, AC Collins, JM McIntosh, & MJ Marks (2005) The subunit composition and pharmacology of a-Conotoxin MII-binding nicotinic acetylcholine receptors studied by a novel membrane-binding assay. *Neuropharmacology* 48(5):696-705.
109. Klink R, A de Kerchove d'Exaerde, M Zoli, & JP Changeux (2001) Molecular and physiological diversity of nicotinic acetylcholine receptors in the midbrain dopaminergic nuclei. *J. Neurosci.* 21(5):1452-1463.
110. Le Novere N, M Zoli, & JP Changeux (1996) Neuronal nicotinic receptor a6 subunit mRNA is selectively concentrated in catecholaminergic nuclei of the rat brain. *Eur. J. Neurosci.* 8(11):2428-2439.
111. Le Novere N, M Zoli, C Lena, R Ferrari, MR Picciotto, E Merlo-Pich, & JP Changeux (1999) Involvement of a6 nicotinic receptor subunit in nicotine-elicited locomotion, demonstrated by in vivo antisense oligonucleotide infusion. *Neuroreport* 10(12):2497-2501.
112. Drenan RM, SR Grady, P Whiteaker, T McClure-Begley, SR McKinney, J Miwa, S Bupp, N Heintz, JM McIntosh, M Bencherif, MA Marks, & HA Lester (2008) *In Vivo* Activation of Midbrain Dopamine Neurons via Sensitized, High-Affinity α6* Nicotinic Acetylcholine Receptors. *Neuron* 60:123-136.
113. Wen L, Z Yang, W Cui, & MD Li (2016) Crucial roles of the CHRNB3-CHRNA6 gene cluster on chromosome 8 in nicotine dependence: update and subjects for future research. *Transl Psychiatry* 6(6):e843.
114. Tumkosit P, A Kuryatov, J Luo, & J Lindstrom (2006) b3 subunits promote expression and nicotine-induced up-regulation of human nicotinic a6* nicotinic acetylcholine receptors expressed in transfected cell lines. *Mol. Pharmacol.* 70(4):1358-1368.
115. Henderson BJ, R Srinivasan, WA Nichols, CN Dilworth, DF Gutierrez, EDW Mackey, S McKinney, RM Drenan, CI Richards, & HA Lester (2014) Nicotine exploits a COPI-mediated process for chaperone-mediated up-regulation of its receptors. *J. Gen. Physiol.* 143(1):51-66.
116. Jackson KJ, JM McIntosh, DH Brunzell, SS Sanjakdar, & MI Damaj (2009) The role of alpha6-containing nicotinic acetylcholine receptors in nicotine reward and withdrawal. *J. Pharmacol. Exp. Ther.* 331(2):547-554.
117. Murray TA, D Bertrand, RL Papke, AA George, R Pantoja, R Srinivasan, Q Liu, J Wu, P Whiteaker, HA Lester, & RJ Lukas (2012) alpha7beta2 nicotinic acetylcholine receptors assemble, function, and are activated primarily via their alpha7-alpha7 interfaces. *Mol. Pharmacol.* 81(2):175-188.
118. Moretti M, M Zoli, AA George, RJ Lukas, F Pistillo, U Maskos, P Whiteaker, & C Gotti (2014) The novel alpha7beta2-nicotinic acetylcholine receptor subtype is expressed in mouse and human basal forebrain: biochemical and pharmacological characterization. *Mol. Pharmacol.* 86(3):306-317.
119. Khiroug SS, PC Harkness, PW Lamb, SN Sudweeks, L Khiroug, NS Millar, & JL Yakel (2002) Rat nicotinic ACh receptor α7 and β2 subunits co-assemble to form functional heteromeric nicotinic receptor channels. *J. Physiol.* 540(2):425-434.
120. Barrantes GE, AT Rogers, J Lindstrom, & S Wonnacott (1995) a-Bungarotoxin binding sites in rat hippocampal and cortical cultures: initial characterisation,

colocalisation with a7 subunits and up-regulation by chronic nicotine treatment. *Brain Res.* 672(1-2):228-236.
121. Delbono O, M Gopalakrishnan, M Renganathan, L Monteggia, M Messi, & J Sullivan (1997) Activation of the recombinant alpha7 nicotinic acetylcholine receptor significantly raises intracellular free calcium. *J. Pharmacol. Exp. Ther.* 280:428 - 438.
122. Morley B & H Happe (2000) Cholinergic receptors: dual roles in transduction and plasticity. *Heart Research* 147(1-2):104-112.
123. Corringer P, J Sallette, & J Changeux (2006) Nicotine enhances intracellular nicotinic receptor maturation: a novel mechanism of neural plasticity? *J. Physiol. Paris* 99(2-3):162-171.
124. Grady SR, NM Meinerz, J Cao, AM Reynolds, MR Picciotto, JP Changeux, JM McIntosh, MJ Marks, & AC Collins (2001) Nicotinic agonists stimulate acetylcholine release from mouse interpeduncular nucleus: a function mediated by a different nAChR than dopamine release from striatum. *J. Neurochem.* 76(1):258-268.
125. Salas R, F Pieri, B Fung, JA Dani, & M De Biasi (2003) Altered anxiety-related responses in mutant mice lacking the β4 subunit of the nicotinic receptor. *J. Neurosci.* 23(15):6255-6263.
126. Frahm S, MA Slimak, L Ferrarese, J Santos-Torres, B Antolin-Fontes, S Auer, S Filkin, S Pons, JF Fontaine, V Tsetlin, U Maskos, & I Ibanez-Tallon (2011) Aversion to Nicotine Is Regulated by the Balanced Activity of beta 4 and alpha 5 Nicotinic Receptor Subunits in the Medial Habenula. *Neuron* 70(3):522-535.
127. Salas R, F Pieri, & M De Biasi (2004) Decreased signs of nicotine withdrawal in mice null for the b4 nicotinic acetylcholine receptor subunit. *J. Neurosci.* 24(45):10035-10039.
128. Salas R, KD Cook, L Bassetto, & M De Biasi (2004) The a3 and b4 nicotinic acetylcholine receptor subunits are necessary for nicotine-induced seizures and hypolocomotion in mice. *Neuropharmacology* 47(3):401-407.
129. Boulter J, A O'Shea-Greenfield, RM Duvoisin, JG Connolly, E Wada, A Jensen, PD Gardner, M Ballivet, ES Deneris, D McKinnon, S Heinemann, & J Patrick (1990) a3, a5, and b4: Three members of the rat neuronal nicotinic acetylcholine receptor-related gene family form a gene cluster. *J. Biol. Chem.* 265(8):4472-4482.
130. Erlich PM, SN Hoffman, M Rukstalis, JJ Han, X Chu, WH Linda Kao, GS Gerhard, WF Stewart, & JA Boscarino (2010) Nicotinic acetylcholine receptor genes on chromosome 15q25.1 are associated with nicotine and opioid dependence severity. *Hum. Genet.* 128(5):491-499.
131. Grucza RA, JC Wang, JA Stitzel, AL Hinrichs, SF Saccone, NL Saccone, KK Bucholz, CR Cloninger, RJ Neuman, JP Budde, L Fox, S Bertelsen, J Kramer, V Hesselbrock, J Tischfield, JI Nurnberger, Jr., L Almasy, B Porjesz, S Kuperman, MA Schuckit, HJ Edenberg, JP Rice, AM Goate, & LJ Bierut (2008) A risk allele for nicotine dependence in CHRNA5 is a protective allele for cocaine dependence. *Biol. Psychiatry* 64(11):922-929.

132. Gerzanich V, F Wang, A Kuryatov, & J Lindstrom (1998) Alpha 5 Subunit Alters Desensitization, Pharmacology, Ca++Permeability and Ca++ Modulation of Human Neuronal Nicotinic Receptors. *J. Pharmacol. Exp. Ther.* 286:311–320.
133. Salas R, A Orr-Urtreger, R Broide, A Beaudet, R Paylor, & MD Biasi (2003) The nicotinic acetylcholine receptor subunit alpha 5 mediates short-term effects of nicotine in vivo. *Mol. Pharmacol.* 63(5):1059-1066.
134. Jackson KJ, MJ Marks, RE Vann, X Chen, TF Gamage, JA Warner, & MI Damaj (2010) Role of alpha5 nicotinic acetylcholine receptors in pharmacological and behavioral effects of nicotine in mice. *J. Pharmacol. Exp. Ther.* 334(1):137-146.
135. Improgo MR, MD Scofield, AR Tapper, & PD Gardner (2010) The nicotinic acetylcholine receptor CHRNA5/A3/B4 gene cluster: Dual role in nicotine addiction and lung cancer. *Prog Neurobiol* 92(2):212-226.
136. Mazzo F, F Pistillo, G Grazioso, F Clementi, N Borgese, C Gotti, & SF Colombo (2013) Nicotine-modulated subunit stoichiometry affects stability and trafficking of alpha3beta4 nicotinic receptor. *J. Neurosci.* 33(30):12316-12328.
137. Baker TB, RB Weiss, D Bolt, A von Niederhausern, MC Fiore, DM Dunn, ME Piper, N Matsunami, SS Smith, H Coon, WM McMahon, MB Scholand, N Singh, JR Hoidal, SY Kim, MF Leppert, & DS Cannon (2009) Human neuronal acetylcholine receptor A5-A3-B4 haplotypes are associated with multiple nicotine dependence phenotypes. *Nic. & Tob. Res.* 11(7):785-796.
138. Bierut LJ, PA Madden, N Breslau, EO Johnson, D Hatsukami, OF Pomerleau, GE Swan, J Rutter, S Bertelsen, L Fox, D Fugman, AM Goate, AL Hinrichs, K Konvicka, NG Martin, GW Montgomery, NL Saccone, SF Saccone, JC Wang, GA Chase, JP Rice, & DG Ballinger (2007) Novel genes identified in a high-density genome wide association study for nicotine dependence. *Hum. Mol. Genet.* 16(1):24-35.
139. Tammimaki A, P Herder, P Li, C Esch, JR Laughlin, G Akk, & JA Stitzel (2012) Impact of human D398N single nucleotide polymorphism on intracellular calcium response mediated by alpha3beta4alpha5 nicotinic acetylcholine receptors. *Neuropharmacology* 63(6):1002-1011.
140. George AA, LM Lucero, MI Damaj, RJ Lukas, X Chen, & P Whiteaker (2012) Function of human alpha3beta4alpha5 nicotinic acetylcholine receptors is reduced by the alpha5(D398N) variant. *J. Biol. Chem.* 287(30):25151-25162.
141. Picciotto MR & PJ Kenny (2013) Molecular mechanisms underlying behaviors related to nicotine addiction. *Cold Spring Harb Perspect Med* 3(1):a012112.
142. Mukhin AG, AS Kimes, SI Chefer, JA Matochik, CS Contoreggi, AG Horti, DB Vaupel, O Pavlova, & EA Stein (2008) Greater nicotinic acetylcholine receptor density in smokers than in nonsmokers: a PET study with 2-18F-FA-85380. *J. Nucl. Med.* 49(10):1628-1635.
143. Brody AL, MA Mandelkern, ED London, RE Olmstead, J Farahi, D Scheibal, J Jou, V Allen, E Tiongson, SI Chefer, AO Koren, & AG Mukhin (2006) Cigarette smoking saturates brain a4b2 nicotinic acetylcholine receptors. *Arch. Gen. Psychiatry* 63(8):907-915.
144. Breese CR, MJ Marks, J Logel, CE Adams, B Sullivan, AC Collins, & S Leonard (1997) Effect of smoking history on [^{3}H]nicotine binding in human postmortem brain. *J. Pharmacol. Exp. Ther.* 282(1):7-13.

145. Liu L, R Zhao-Shea, JM McIntosh, PD Gardner, & AR Tapper (2012) Nicotine Persistently Activates Ventral Tegmental Area Dopaminergic Neurons via Nicotinic Acetylcholine Receptors Containing α4 and α6 Subunits. *Mol. Pharmacol.* 81(4):541-548.
146. DiChiara G & A Imperato (1988) Drugs abused by humans preferentially increase synaptic dopamine concentrations in the mesolimbic system of freely moving rats. *Proc. Natl. Acad. Sci. U. S. A.* 85:5274-5278.
147. Corrigall WA, KM Coen, & KL Adamson (1994) Self-Administered Nicotine Activates the Mesolimbic Dopamine System Through the Ventral Tegmental Area. *Brain Res.* 653(1-2):278-284.
148. Grilli M, M Parodi, M Raiteri, & M Marchi (2005) Chronic nicotine differentially affects the function of nicotinic receptor subtypes regulating neurotransmitter release. *J. Neurochem.* 93(5):1353-1360.
149. Imperato A, A Mulas, & G Di Chiara (1986) Nicotine preferentially stimulates dopamine release in the limbic system of freely moving rats. *Eur. J. Pharmacol.* 132(2-3):337-338.
150. Pauly JR, MJ Marks, SF Robinson, JL van de Kamp, & AC Collins (1996) Chronic nicotine and mecamylamine treatment increase brain nicotinic receptor binding without changing a4 or b2 mRNA levels. *J. Pharmacol. Exp. Ther.* 278(1):361-369.
151. Srinivasan R, CI Richards, C Dilworth, FJ Moss, DA Dougherty, & HA Lester (2012) Forster Resonance Energy Transfer (FRET) Correlates of Altered Subunit Stoichiometry in Cys-Loop Receptors, Exemplified by Nicotinic alpha 4 beta 2. *Int. J. Mol. Sci.* 13(8):10022-10040.
152. Darsow T, TK Booker, JC Pina-Crespo, & SF Heinemann (2005) Exocytic trafficking is required for nicotine-induced up-regulation of a4b2 nicotinic acetylcholine receptors. *J. Biol. Chem.* 280(18):18311-18320.
153. Sallette J, S Pons, A Devillers-Thiery, M Soudant, L Prado de Carvalho, JP Changeux, & PJ Corringer (2005) Nicotine upregulates its own receptors through enhanced intracellular maturation. *Neuron* 46(4):595-607.
154. Nelson ME, A Kuryatov, CH Choi, Y Zhou, & J Lindstrom (2003) Alternate stoichiometries of a4b2 nicotinic acetylcholine receptors. *Mol. Pharmacol.* 63(2):332-341.
155. Miwa JM, R Freedman, & HA Lester (2011) Neural Systems Governed by Nicotinic Acetylcholine Receptors: Emerging Hypotheses. *Neuron* 70(1):20-33.
156. Marks MJ, JR Pauly, SD Gross, ES Deneris, I Hermans-Borgmeyer, SF Heinemann, & AC Collins (1992) Nicotine binding and nicotinic receptor subunit RNA after chronic nicotine treatment. *J. Neurosci.* 12(7):2765-2784.
157. Doura MB, AB Gold, AB Keller, & DC Perry (2008) Adult and periadolescent rats differ in expression of nicotinic cholinergic receptor subtypes and in the response of these subtypes to chronic nicotine exposure. *Brain Res.* 1215:40-52.
158. Nashmi R & H Lester (2007) Cell autonomy, receptor autonomy, and thermodynamics in nicotine receptor up-regulation. *Biochem. Pharmacol.* 74(8):1145-1154.

159. Pauly JR, MJ Marks, SD Gross, & AC Collins (1991) An autoradiographic analysis of cholinergic receptors in mouse brain after chronic nicotine treatment. *J. Pharmacol. Exp. Ther.* 258(3):1127-1136.
160. Henderson BJ & HA Lester (2015) Inside-out neuropharmacology of nicotinic drugs. *Neuropharmacology* 96(Pt B):178-193.
161. Marks MJ, SR Grady, O Salminen, MA Paley, CR Wageman, JM McIntosh, & P Whiteaker (2014) alpha6beta2*-subtype nicotinic acetylcholine receptors are more sensitive than alpha4beta2*-subtype receptors to regulation by chronic nicotine administration. *J. Neurochem.* 130(2):185-198.
162. Xiao C, R Nashmi, S McKinney, H Cai, JM McIntosh, & HA Lester (2009) Chronic nicotine selectively enhances α4β2* nicotinic acetylcholine receptors in the nigrostriatal dopamine pathway. *J. Neurosci.* 29:12428-12439.
163. McClure-Begley TD, NM King, AC Collins, JA Stitzel, JM Wehner, & CM Butt (2009) Acetylcholine-stimulated [^{3}H]GABA release from mouse brain synaptosomes is modulated by α4β2 and α4α5β2 nicotinic receptor subtypes. *Mol. Pharmacol.* 75(4):918-926.
164. Champtiaux N, ZY Han, A Bessis, FM Rossi, M Zoli, L Marubio, JM McIntosh, & JP Changeux (2002) Distribution and pharmacology of a6-containing nicotinic acetylcholine receptors analyzed with mutant mice. *J. Neurosci.* 22(4):1208-1217.
165. Champtiaux N, C Gotti, M Cordero-Erausquin, DJ David, C Przybylski, C Lena, F Clementi, M Moretti, FM Rossi, N Le Novere, JM McIntosh, AM Gardier, & JP Changeux (2003) Subunit composition of functional nicotinic receptors in dopaminergic neurons investigated with knock-out mice. *J. Neurosci.* 23(21):7820-7829.
166. Buisson B & D Bertrand (2002) Nicotine addiction: the possible role of functional upregulation. *Trends Pharmacol. Sci.* 23(3):130-136.
167. Buisson B & D Bertrand (2001) Chronic exposure to nicotine upregulates the human alpha 4 beta 2 nicotinic acetylcholine receptor function. *J. Neurosci.* 21(6):1819-1829.
168. Nashmi R, C Xiao, P Deshpande, S McKinney, SR Grady, P Whiteaker, Q Huang, T McClure-Begley, JM Lindstrom, C Labarca, AC Collins, MJ Marks, & HA Lester (2007) Chronic nicotine cell specifically upregulates functional α4* nicotinic receptors: basis for both tolerance in midbrain and enhanced long-term potentiation in perforant path. *J. Neurosci.* 27(31):8202-8218.
169. Barazangi N & LW Role (2001) Nicotine-induced enhancement of glutamatergic and GABAergic synaptic transmission in the mouse amygdala. *J. Neurophysiol.* 86(1):463-474.
170. Lukas R (2007) *Phamacological effects of nicotine and nicotinic receptor subtype pharmacological profiles* (CRC Press LLC, Boca Raton, FL).
171. Etter JF (2006) Cytisine for smoking cessation: a literature review and a meta-analysis. *Arch Intern Med*:1553-1559.
172. Zatonski W CM, Tutka P, West R (2006) An uncontrolled trial of cytisine (Tabex) for smoking cessation. *Tob Control*:481-484.
173. Hajek P, H McRobbie, & K Myers (2013) Efficacy of cytisine in helping smokers quit: systematic review and meta-analysis. *Thorax* 68(11):1037-1042.

174. Hajek P, LF Stead, R West, M Jarvis, J Hartmann-Boyce, & T Lancaster (2013) Relapse prevention interventions for smoking cessation. *Cochrane Database Syst Rev*.
175. Marotta CB, I Rreza, HA Lester, & DA Dougherty (2014) Selective ligand behaviors provide new insights into agonist activation of nicotinic acetylcholine receptors. *ACS Chem. Biol.* 9(5):1153-1159.
176. Turner JR, LM Castellano, & JA Blendy (2011) Parallel anxiolytic-like effects and upregulation of neuronal nicotinic acetylcholine receptors following chronic nicotine and varenicline. *Nic. & Tob. Res.* 13(1):41-46.
177. Mihalak KB, FI Carroll, & CW Luetje (2006) Varenicline is a partial agonist at α4β2 and a full agonist at α7 neuronal nicotinic receptors. *Mol. Pharmacol.* 70(3):801-805.
178. Marks MJ, HC O'Neill, KM Wynalda-Camozzi, NC Ortiz, EE Simmons, CA Short, CM Butt, JM McIntosh, & SR Grady (2015) Chronic treatment with varenicline changes expression of four nAChR binding sites in mice. *Neuropharmacology* 99:142-155.
179. Rose JE, FM Behm, EC Westman, ED Levin, RM Stein, & GV Ripka (1994) Mecamylamine combined with nicotine skin patch facilitates smoking cessation beyond nicotine patch treatment alone. *Clin. Pharmacol. Ther.* 56(1):86-99.
180. Stahl SM, JF Pradko, BR Haight, JG Modell, CB Rockett, & S Learned-Coughlin (2004) A Review of the Neuropharmacology of Bupropion, a Dual Norepinephrine and Dopamine Reuptake Inhibitor. *Prim Care Companion J Clin Psychiatry* 6:159-166.
181. Pandhare A, AK Hamouda, B Staggs, S Aggarwal, PK Duddempudi, JR Lever, DJ Lapinsky, M Jansen, JB Cohen, & MP Blanton (2012) Bupropion binds to two sites in the *Torpedo* nicotinic acetylcholine receptor transmembrane domain: A photoaffinity labeling study with the bupropion analogue [125I]-SADU-3-72. *Biochemistry* 51:2425-2435.
182. Xiao Y FH, Musachio JL, Wei ZL, Chellappan SK, Kozikowski AP, Kellar KJ (2006) Sazetidine-A, a novel ligand that desensitizes alpha4beta2 nicotinic acetylcholine receptors without activating them. *Mol Pharmacol*:1454-1460.
183. Zwart R CA, Moroni M, Bermudez I, Mogg AJ, Folly EA, Broad LM, Williams AC, Zhang D, Ding C, Heinz BA, Sher E (2008) Sazetidine-A is a potent and selective agonist at native and recombinant alpha 4 beta 2 nicotinic acetylcholine receptors. *Mol Pharmacol*:1838-1843.
184. Fu XW, J Lindstrom, & ER Spindel (2009) Nicotine activates and up-regulates nicotinic acetylcholine receptors in bronchial epithelial cells. *Am. J. Respir. Cell Mol. Biol.* 41(1):93-99.
185. Gentry CL & RJ Lukas (2002) Regulation of nicotinic acetylcholine receptor numbers and function by chronic nicotine exposure. *Curr. Drug Targets CNS Neurol. Disord.* 1(4):359-385.
186. Fenster CP, TL Whitworth, EB Sheffield, MW Quick, & RA Lester (1999) Upregulation of surface a4b2 nicotinic receptors is initiated by receptor desensitization after chronic exposure to nicotine. *J. Neurosci.* 19(12):4804-4814.
187. Kishi M & JH Steinbach (2006) Role of the agonist binding site in up-regulation of neuronal nicotinic α4β2 receptors. *Mol. Pharmacol.* 70(6):2037-2044.

188. Peng X, V Gerzanich, R Anand, PJ Whiting, & J Lindstrom (1994) Nicotine-induced increase in neuronal nicotinic receptors results from a decrease in the rate of receptor turnover. *Mol. Pharmacol.* 46(3):523-530.
189. Picciotto MR, NA Addy, YS Mineur, & DH Brunzell (2008) It is not "either/or": Activation and desensitization of nicotinic acetylcholine receptors both contribute to behaviors related to nicotine addiction and mood. *Prog Neurobiol* 84(4):329-342.
190. Vallejo YF, B Buisson, D Bertrand, & WN Green (2005) Chronic nicotine exposure upregulates nicotinic receptors by a novel mechanism. *J. Neurosci.* 25(23):5563-5572.
191. Govind AP, H Walsh, & WN Green (2012) Nicotine-induced upregulation of native neuronal nicotinic receptors is caused by multiple mechanisms. *J. Neurosci.* 32(6):2227-2238.
192. Hukkanen J, P Jacob, 3rd, & NL Benowitz (2005) Metabolism and disposition kinetics of nicotine. *Pharmacol. Rev.* 57(1):79-115.
193. Matta SG, DJ Balfour, NL Benowitz, RT Boyd, JJ Buccafusco, AR Caggiula, CR Craig, AC Collins, MI Damaj, EC Donny, PS Gardiner, SR Grady, U Heberlein, SS Leonard, ED Levin, RJ Lukas, A Markou, MJ Marks, SE McCallum, N Parameswaran, KA Perkins, MR Picciotto, M Quik, JE Rose, A Rothenfluh, WR Schafer, IP Stolerman, RF Tyndale, JM Wehner, & JM Zirger (2007) Guidelines on nicotine dose selection for *in vivo* research. *Psychopharmacology* 190(3):269-319.
194. Bencherif M, K Fowler, RJ Lukas, & PM Lippiello (1995) Mechanisms of up-regulation of neuronal nicotinic acetylcholine receptors in clonal cell lines and primary cultures of fetal rat brain. *J. Pharmacol. Exp. Ther.* 275(2):987-994.
195. Whiteaker P, CG Sharples, & S Wonnacott (1998) Agonist-induced up-regulation of a4b2 nicotinic acetylcholine receptors in M10 cells: pharmacological and spatial definition. *Mol. Pharmacol.* 53(5):950-962.
196. Srinivasan R, R Pantoja, FJ Moss, EDW Mackey, C Son, J Miwa, & HA Lester (2011) Nicotine upregulates α4β2 nicotinic receptors and ER exit sites via stoichiometry-dependent chaperoning. *J. Gen. Physiol.* 137:59-79.
197. Son CD, FJ Moss, BN Cohen, & HA Lester (2009) Nicotine normalizes intracellular subunit stoichiometry of nicotinic receptors carrying mutations linked to autosomal dominant nocturnal frontal lobe epilepsy. *Mol. Pharmacol.* 75(5):1137-1148.
198. Richards CI, R Srinivasan, C Xiao, EDW Mackey, JM Miwa, & HA Lester (2011) Trafficking of α4* Nicotinic Receptors Revealed by Superecliptic Phluorin. *J. Biol. Chem.* 286(36):31241-31249.
199. Shoji Y, S Akhtar, A Periasamy, B Herman, & RL Juliano (1991) Mechanism of cellular uptake of modified oligodeoxynucleotides containing methylphosphonate linkages. *Nucleic Acids Res.* 19(20):5543-5550.
200. Liang M, X Liu, D Cheng, K Nakamura, Y Wang, S Dou, G Liu, M Rusckowski, & DJ Hnatowich (2009) Optical antisense tumor targeting in vivo with an improved fluorescent DNA duplex probe. *Bioconjug. Chem.* 20(6):1223-1227.

201. Santra S, H Yang, JT Stanley, PH Holloway, BM Moudgil, G Walter, & RA Mericle (2005) Rapid and effective labeling of brain tissue using TAT-conjugated CdS:Mn/ZnS quantum dots. *Chem. Comm.*:3144-3146.
202. Patterson GH, SM Knobel, WD Sharif, SR Kain, & DW Piston (1997) Use of the green fluorescent protein and its mutants in quantitative fluorescence microscopy. *Biophys. J.* 73(5):2782-2790.
203. Tsien RY (1998) The green fluorescent protein. *Annu. Rev. Biochem.* 67:509-544.
204. Morise H, O Shimomura, F Johnson, & J Winant (1974) Intermolecular energy transfer in the bioluminescent system of Aequorea. *Biochemistry* 13(12):2656-2662.
205. Prasher D, V Eckenrode, W Ward, F Prendergast, & M Cormier (1992) Primary structure of the Aequorea victoria green-fluorescent protein. *Gene* 111(2):229-233.
206. Brejc K, TK Sixma, PA Kitts, SR Kain, RY Tsien, M Ormo, & SJ Remington (1997) Structural basis for dual excitation and photoisomerization of the Aequorea victoria green fluorescent protein. *Proc. Natl. Acad. Sci. U.S.A.* 94:2306-2311.
207. Heim R, D Prasher, & R Tsien (1994) Wavelength mutations and posttranslational autoxidation of green fluorescent protein. *Proc. Natl. Acad. Sci. U. S. A.* 91(26):12501-12504.
208. Cubitt A, L Woollenweber, & R Heim (1999) Understanding structure-function relationships in the Aequorea victoria green fluorescent protein. *Methods Cell Biol.* 58:19-30.
209. Shih PY, SE Engle, G Oh, P Deshpande, NL Puskar, HA Lester, & RM Drenan (2014) Differential expression and function of nicotinic acetylcholine receptors in subdivisions of medial habenula. *J. Neurosci.* 34(29):9789-9802.
210. Srinivasan R, CI Richards, C Xiao, D Rhee, R Pantoja, DA Dougherty, JM Miwa, & HA Lester (2012) Pharmacological Chaperoning of Nicotinic Acetylcholine Receptors Reduces the Endoplasmic Reticulum Stress Response. *Mol. Pharmacol.* 81(6):759-769.
211. Mattheyses AL, SM Simon, & JZ Rappoport (2010) Imaging with total internal reflection fluorescence microscopy for the cell biologist. *J. Cell Sci.* 123:3621-3628.
212. Axelrod D (2008) Total Internal Reflection Fluorescence Microscopy. *Methods Cell Biol.* 89:169-221.
213. Merrifield CJ, ME Feldman, L Wan, & W Almers (2002) Imaging actin and dynamin recruitment during invagination of single clathrin-coated pits. *Nat. Cell Biol.* 4:691-698.
214. Rappoport JZ & SM Simon (2003) Real-time analysis of clathrin-mediated endocytosis during cell migration. *J. Cell Sci.* 116:847-855.
215. Jaiswal JK, M Fix, T Takano, M Nedergaard, & SM Simon (2007) Resolving vesicle fusion from lysis to monitor calcium-triggered lysosomal exocytosis in astrocytes. *Proc. Natl. Acad. Sci. U. S. A.* 104:14151-14156.
216. Demuro A & I Parker (2004) Imaging the activity and localization of single voltage-gated Ca2+ channels by total internal reflection fluorescence microscopy. *Biophys J.* 86:3250-3259.

217. Yudowski GA, MA Puthenveedu, D Leonoudakis, S Panicker, KS Thorn, EC Beattie, & M von Zastrow (2007) Real-time imaging of discrete exocytic events mediating surface delivery of AMPA receptors. *J. Neurosci.* 27(41):11112-11121.
218. Miesenbock G, DA De Angelis, & JE Rothman (1998) Visualizing secretion and synaptic transmission with pH-sensitive green fluorescent proteins. *Nature* 394(6689):192-195.
219. Taraska JW & WN Zagotta (2010) Fluorescence applications in molecular neurobiology. *Neuron* 66(2):170-189.
220. Sako Y, S Minoghchi, & T Yanagida (2000) Single-molecule imaging of EGFR signalling on the surface of living cells. *Nat. Cell Bio.* 2(3):168-172.
221. Sakon JJ & KR Weninger (2010) Detecting the conformation of individual proteins in live cells. *Nat. Methods* 7(3):203-205.
222. Dani A, B Huang, J Bergan, C Dulac, & XW Zhuang (2010) Superresolution Imaging of Chemical Synapses in the Brain. *Neuron* 68(5):843-856.
223. Kim SY, EJ Miller, J Frydman, & WE Moerner (2010) Action of the Chaperonin GroEL/ES on a Non-native Substrate Observed with Single-Molecule FRET. *J. Mol. Biol.* 401(4):553-563.
224. Ulbrich MH & EY Isacoff (2007) Subunit counting in membrane-bound proteins. *Nat. Methods* 4(4):319-321.
225. Fernandes CC, DK Berg, & D Gomez-Varela (2010) Lateral mobility of nicotinic acetylcholine receptors on neurons is determined by receptor composition, local domain, and cell type. *J. Neurosci.* 30(26):8841-8851.
226. Lin DT, Y Makino, K Sharma, T Hayashi, R Neve, K Takamiya, & RL Huganir (2009) Regulation of AMPA receptor extrasynaptic insertion by 4.1N, phosphorylation and palmitoylation. *Nat. Neurosci.* 12(7):879-U895.
227. Fox AM, FH Moonschi, & CI Richards (2015) The nicotine metabolite, cotinine, alters the assembly and trafficking of a subset of nicotinic acetylcholine receptors. *J. Biol. Chem.* 290(40):24403-24412.
228. Moonschi FH, AK Effinger, X Zhang, WE Martin, AM Fox, DK Heidary, JE DeRouchey, & CI Richards (2015) Cell-Derived Vesicles for Single-Molecule Imaging of Membrane Proteins. *Angew. Chem. Int. Ed.* 54(2):481-484.
229. Paroutis P, N Touret, & S Grinstein (2004) The pH of the secretory pathway: measurement, determinants, and regulation. *Physiol. (Bethesda)* 19:207-215.
230. Khiroug SS, E Pryazhnikov, SK Coleman, A Jeromin, K Keinanen, & L Khiroug (2009) Dynamic visualization of membrane-inserted fraction of pHluorin-tagged channels using repetitive acidification technique. *BMC Neurosci.* 10(141).
231. Das SK, Y Liu, S Yeom, DY Kim, & CI Richards (2014) Single-Particle Fluorescence Intensity Fluctuations of Carbon Nanodots. *Nano Lett.* 14(2):620-625.
232. Araki Y, DT Lin, & RL Huganir (2010) Plasma membrane insertion of the AMPA receptor GluA2 subunit is regulated by NSF binding and Q/R editing of the ion pore. *Proc. Natl. Acad. Sci. U. S. A.* 107(24):11080-11085.
233. Moroni M, R Zwart, E Sher, BK Cassels, & I Bermudez (2006) α4β2 nicotinic receptors with high and low acetylcholine sensitivity: pharmacology, stoichiometry, and sensitivity to long-term exposure to nicotine. *Mol. Pharmacol.* 70(2):755-768.

234. Zwart R & HP Vijverberg (1998) Four pharmacologically distinct subtypes of a4b2 nicotinic acetylcholine receptor expressed in Xenopus laevis oocytes. *Mol. Pharmacol.* 54(6):1124-1131.
235. Marks MJ, JB Burch, & AC Collins (1983) Effects of chronic nicotine infusion on tolerance development and nicotinic receptors. *J. Pharmacol. Exp. Ther.* 226(3):817-825.
236. Pauly JR, JA Stitzel, MJ Marks, & AC Collins (1989) An autoradiographic analysis of cholinergic receptors in mouse brain. *Brain Res. Bull.* 22:453-459.
237. Clarke PBS (1987) Recent progress in identifying nicotinic cholinoceptors in mammalian brain. *Trends Pharmacol. Sci.* 8:32-35.
238. Riganti L, C Matteoni, SD Angelantonio, A Nistri, A Gaimarri, F Sparatore, C Canu-Boido, F Clementi, & C Gotti (2005) Long-term exposure to the new nicotinic antagonist 1,2-bisN-cytisinylethane upregulates nicotinic receptor subtypes of SH-SY5Y human neuroblastoma cells. *Br. J. Pharmacol.* 146:1096-1109.
239. Harkness PC & NS Millar (2002) Changes in conformation and subcellular distribution of a4b2 nicotinic acetylcholine receptors revealed by chronic nicotine treatment and expression of subunit chimeras. *J. Neurosci.* 22(23):10172-10181.
240. Dwoskin LP, L Teng, ST Buxton, & PA Crooks (1999) (S)-(-)-cotinine, the major brain metabolite of nicotine, stimulates nicotinic receptors to evoke [3H]dopamine release from rat striatal slices in a calcium-dependent manner. *J. Pharmacol. Exp. Ther.* 288:905–911.
241. Vine MF, Barbara S. Hula, BH Magolin, YK Truong, P-c Hu, MM Schramm, JD Gnffith, M McCann, & RB Everson (1993) Cotinine concentrations in semen, urine, and blood of smokers and nonsmokers. *Am. J. Public Health* 83(9):1335-1338.
242. Ghosheh O, LP Dwoskin, W-K Li, & PA Crooks (1999) Residence times and half-lives of nicotine metabolites in rat brain after acute peripheral administration. *Drug Metab. Dispos.* 27:1448-1455.
243. Terry AV, PM Callahan, & D Bertrand (2015) R-(+) - and S-(-) - Isomers of Cotinine Augment Cholinergic Responses in vitro and in vivo. *J. Pharmacol. Exp. Ther.* 352(2):405-418.
244. Reavill C, B Walther, IP Stolerman, & B Testa (1990) Behavioural and pharmacokinetic studies on nicotine, cytisine, and lobeline. *Neuropharmacology* 29(7):619-624.
245. Li P, WD Beck, PM Callahan, AVT Jr, & MG Bartlett (2012) Quantitation of Cotinine and its Metabolites in Rat Plasma and Brain Tissue by Hydrophilic Interaction Chromatography Tandem Mass Spectrometry (HILIC-MS/MS). *J. Chromatogr. B Analyt Technol Biomed Life Sci* 907:117-125.
246. Mao D, DC Perry, RP Yasuda, BB Wolfe, & KJ Kellar (2008) The alpha4beta2alpha5 nicotinic cholinergic receptor in rat brain is resistant to up-regulation by nicotine in vivo. *J. Neurochem.* 104(2):446-456.
247. Moretti M, M Mugnaini, M Tessari, M Zoli, A Gaimarri, & I Manfredi (2010) A comparative study of the effects of the intravenous self-administration or subcutaneous minipump infusion of nicotine on the expression of brain neuronal nicotinic receptor subtypes. *Mol. Pharmacol.* 78:287-296.

248. Wageman CR, MJ Marks, & SR Grady (2013) Effectiveness of Nicotinic Agonists as Desensitizers at Presynaptic α4β2- and α4α5β2-Nicotinic Acetylcholine Receptors. *Nic. & Tob. Res.* 16(3):297-305.
249. Chatterjee S, N Santos, J Holgate, CL Haass-Koffler, FW Hopf, V Kharazia, H Lester, A Bonci, & SE Bartlett (2013) The α5 Subunit Regulates the Expression and Function of α4*-Containing Neuronal Nicotinic Acetylcholine Receptors in the Ventral-Tegmental Area. *PLoS One* 8(7):e68300.
250. Sallette J, S Bohler, P Benoit, M Soudant, S Pons, N Le Novere, JP Changeux, & PJ Corringer (2004) An extracellular protein microdomain controls up-regulation of neuronal nicotinic acetylcholine receptors by nicotine. *J. Biol. Chem.* 279(18):18767-18775.
251. Perez XA, T Bordia, JM McIntosh, SR Grady, & M Quik (2008) Long-term nicotine treatment differentially regulates striatal a6a4b2* and a6(Nona4)b2* nAChR expression and function. *Mol. Pharmacol.* 74(3):844-853.
252. Walsh H, AP Govind, R Mastro, JC Hoda, D Bertrand, Y Vallejo, & WN Green (2008) Upregulation of nicotinic receptors by nicotine varies with receptor subtype. *J. Biol. Chem.* 283:6022-6032.
253. Perry DC, D Mao, AB Gold, JM McIntosh, JC Pezzullo, & KJ Kellar (2007) Chronic nicotine differentially regulates α6- and β3-containing nicotinic cholinergic receptors in rat brain. *J. Pharmacol. Exp. Ther.* 322(1):306-315.
254. McCallum SE, N Parameswaran, T Bordia, H Fan, JM McIntosh, & M Quik (2006) Differential regulation of mesolimbic a3*/a6*b2 and a4*b2 nicotinic acetylcholine receptor sites and function after long-term oral nicotine to monkeys. *J. Pharmacol. Exp. Ther.* 318(1):381-388.
255. Mugnaini M, M Garzotti, I Sartori, M Pilla, P Repeto, CA Heidbreder, & M Tessari (2006) Selective down-regulation of [^{125}I]Y_0-a-conotoxin MII binding in rat mesostriatal dopamine pathway following continuous infusion of nicotine. *Neuroscience* 137(2):565-572.
256. Briggs CA, EJ Gubbins, MJ Marks, CB Putman, R Thimmapaya, MD Meyer, & CS Surowy (2006) Untranslated region-dependent exclusive expression of high-sensitivity subforms of a4b2 and a3b2 nicotinic acetylcholine receptors. *Mol. Pharmacol.* 70(1):227-240.
257. Zhou Y, ME Nelson, A Kuryatov, C Choi, J Cooper, & J Lindstrom (2003) Human a4b2 acetylcholine receptors formed from linked subunits. *J. Neurosci.* 23(27):9004-9015.
258. Lange-Asschenfeldt C, S Schable, T Suvorava, EG Fahimi, M Bisha, T Stermann, U Henning, & G Kojda (2016) Effects of varenicline on alpha4-containing nicotinic acetylcholine receptor expression and cognitive performance in mice. *Neuropharmacology* 107:100-110.
259. Anand R, W Conroy, R Schoepfer, P Whiting, & J Lindstrom (1991) Neuronal nicotinic acetylcholine receptors expressed in *Xenopus* oocytes have a pentameric quaternary structure. *J. Biol. Chem.* 266:11192-11198.
260. Yasuda R, CD Harvey, HN Zhong, A Sobczyk, L van Aelst, & K Svoboda (2006) Supersensitive Ras activation in dendrites and spines revealed by two-photon fluorescence lifetime imaging. *Nat. Neurosci.* 9(2):283-291.

261. Moss FJ, PI Imoukhuede, K Scott, J Hu, JL Jankowsky, MW Quick, & HA Lester (2009) GABA transporter function, oligomerization state, and anchoring: correlates with subcellularly resolved FRET. *J. Gen. Physiol.* 134(6):489-521.
262. Pollok BA & R Heim (1999) Using GFP in FRET-based applications. *Trends Cell Biol.* 9(2):57-60.
263. Ha TJ, AY Ting, J Liang, WB Caldwell, AA Deniz, DS Chemla, PG Schultz, & S Weiss (1999) Single-molecule fluorescence spectroscopy of enzyme conformational dynamics and cleavage mechanism. *Proc. Natl. Acad. Sci. U. S. A.* 96(3):893-898.
264. Chung HS, K McHale, JM Louis, & WA Eaton (2012) Single-Molecule Fluorescence Experiments Determine Protein Folding Transition Path Times. *Science* 335(6071):981-984.
265. Yang LL, MWP Kao, HL Chen, TS Lim, WS Fann, & RPY Chen (2012) Observation of protein folding/unfolding dynamics of ubiquitin trapped in agarose gel by single-molecule FRET. *Eur. Biophys. J. Biophys. Lett.* 41(2):189-198.
266. Chung HS, JM Louis, & WA Eaton (2009) Experimental determination of upper bound for transition path times in protein folding from single-molecule photon-by-photon trajectories. *Proc. Natl. Acad. Sci. U. S. A.* 106(29):11837-11844.
267. Hille B (2001) *Ionic Channels of Excitable Membranes* (Sinauer, Sunderland, MA) 3rd Ed.
268. Carbonnelle E, F Sparatore, C Canu-Boido, C Salvagno, B Baldani-Guerra, G Terstappen, R Zwart, H Vijverberg, F Clementi, & C Gotti (2003) Nitrogen substitution modifies the activity of cytisine on neuronal nicotinic receptor subtypes. *Eur. J. Pharmacol.* 471(2):85-96.
269. Ferris R & B Cooper (1993) Mechanism of antidpressant activity of bupropion. *J Clin Psychiatry Monograph* 11(1):2-14.
270. Nomikos G, G Damsma, D Wenkstern, & H Fibiger (1989) Acute effects of bupropion on extracellular dopamine concentrations in rat striatum and nucleus accumbens studied by in vivo microdialysis. *Neuropsychopharm.* 2:273-279.
271. Carroll F, B Blough, S Mascarella, H Navarro, J Eaton, R Lukas, & M Damaj (2010) Synthesis and biological evaluation of bupropion analogues as potential pharmacotherapies for smoking cessation. *J. Med. Chem.* 53:2204-2214.
272. Arias H (2010) Molecular interaction of bupropion with nicotine acetylcholine receptors. *J. Pediatr. Biochem.* 1:185-197.
273. Collins A, E Romm, & J Wehner (1994) Sensitivity to nicotine and brain nicotinic receptors are altered by chronic nicotine and mecamylamine infusion. *J. Pharmacol. Exp. Ther.* 271:125-133.
274. Zambrano CA, CA Short, RM Salamander, SR Grady, & MJ Marks (2015) Density of alpha4beta2* nAChR on the surface of neurons is modulated by chronic antagonist exposure. *Pharmacol. Res. Perspect.* 3(2):e00111.
275. Graham JM (2002) Fractionation of golgi, endoplasmic reticulum, and plasma membrane from cultured cells in a preformed continuous iodixanol gradient. *ScientificWorldJournal* 2:1435-1439.
276. Blitzer BL & CB Donovan (1984) A new method for the rapid isolation of basolateral plasma membrane vesicles from rat liver. *J. Biol. Chem.* 259(14):9295-9301.

277. Klempner MS, RB Mikkelsen, DH Corfman, & J Andre-Schwartz (1980) High-yield purification of human neutrophil plasma membrane vesicles by nitrogen cavitation and differential centrifugation. *J. Cell Biol.* 86:21-28.
278. Jethwaney D, MR Islam, KG Leidal, DB de Bernabe, KP Campbell, WM Nauseef, & BW Gibson (2007) Proteomic analysis of plasma membrane and secretory vesicles from human neutrophils. *Proteome Sci.* 5:12.
279. Gilmer PJ (1982) Physical separation and biochemical characterization of H-2b-encoded proteins on target cell plasma membranes and endoplasmic reticulum. *J. Biol. Chem.* 257(13):7839-7846.
280. Allam MF, MJ Campbell, A Hofman, AS Del Castillo, & R Fernandez-Crehuet Navajas (2004) Smoking and Parkinson's disease: systematic review of prospective studies. *Mov Disord* 19(6):614-621.
281. Fagerstrom KO, O Pomerleau, B Giordani, & F Stelson (1994) Nicotine may relieve symptoms of Parkinson's disease. *Psychopharmacology* 116(1):117-119.
282. Quik M (2004) Smoking, nicotine and Parkinson's disease. *Trends Neurosci.* 27(9):561-568.

VITA

Educational Institutions

08/2008 – 05/2012 **Muskingum University**
Bachelor of Science in Chemistry; Forensic Science Certification
Minor: Biology
Summa Cum Laude

08/2004 – 05/ 2008 **Waterford High School**
Valedictorian

Professional Positions

10/2012 – Present **Graduate Student**
Department of Chemistry, University of Kentucky
Mentor: Dr. Christopher I. Richards, Assistant Professor of Chemistry

01/2013 – 05/2013 **General Chemistry Laboratory Teaching Assistant**

08/2012 – 12/2012 **General Chemistry Recitation Teaching Assistant**

09/2011 – 05/2012 **Research Assistant**
Department of Chemistry, Muskingum University
Mentor: Dr. Raymond Rataiczak, Science Division Coordinator, Professor of Chemistry

06/2011 – 08/2011 **REU Program Participant**
Department of Chemistry and Biochemistry, Kent State University
Mentor: Dr. Michael Tubergen, Department Chair, Professor of Chemistry

01/2011 – 05/2011 **Research Assistant**
Department of Chemistry, Muskingum University
Mentors: Dr. Raymond Rataiczak and Dr. Eric Schurter

08/2008 – 05/2012 **Chemistry Preparatory Laboratory Assistant**
Department of Chemistry, Muskingum University

Scholastic and Professional Honors

08/2016 Travel Grant

05/2015 – 08/2016	Research Challenge Trust Fund (RCTF) Assistantship
08/2014 – 12/2016	Lyman T. Johnson Academic Year Fellowship
05/2014 – 03/2016	National Institute on Drug Abuse T32 Fellowship DA016176
10/2015	Travel Grant
08/2013 – 08/2015	Max Steckler Fellowship
08/2014	Jeffery Fellowship for Tobacco Research
08/2014	2014 Center of Membrane Sciences Graduate Student Mentoring Fellowship Merit Award
06/2013 – 03/2014	National Institute on Drug Abuse T32 Fellowship DA016176
05/2012	Outstanding Senior in Chemistry Award
05/2012	Analytical Chemistry Student of the Year

Professional Publications

[6] **Fox-Loe, A.M.,** F.H. Moonschi, C.I. Richards. "Separation of ER and PM derived nanovesicles to resolve intracellular changes in stoichiometry of nAChRs." Under Review.

[5] **Fox-Loe, A.M**., B.J. Henderson, C.I. Richards. "Utilizing pHluorin-tagged receptors to monitor subcellular localization and trafficking." *J. Vis. Exp.* In Press.

[4] Heidary, D.K., **A.M. Fox-Loe**, C.I. Richards, E.C. Glazer. "A high-throughput screening assay using a photoconvertable protein for identifying inhibitors of transcription, translation, or proteasomal degradation." *J. Mol. Screening.* In Press.

[3] **Fox-Loe, A.M**., L.P. Dwoskin, C.I. Richards. "Nicotinic Acetylcholine Receptors as Targets for Tobacco Cessation Therapeutics: Cutting-edge Methodologies to Understand Receptor Assembly and Trafficking." *Neuromethods: Nicotinic Acetylcholine Receptor Technologies.* Ed. Ming Li. 1st ed. Vol. 117. Humana Press, 2016. Print.
DOI: 10.1007/978-1-4939-3768-4

[2] **Fox, A.M**., F.H. Moonschi, and C.I. Richards. 2015. The nicotine metabolite, cotinine, alters the assembly and trafficking of a subset of nicotine acetylcholine receptors. *J. Biol. Chem.* 290:24403-24412.
DOI: 10.1074/jbc.M115.661827

[1] Moonschi, F.H., A.K. Effinger, X. Zhang, W.E. Martin, **A.M. Fox**, D.K. Heidary, J.E. DeRouchey, and C.I. Richards. 2015. Cell-Derived Vesicles for Single-Molecule Imaging of Membrane Proteins. *Angew. Chem. Int. Ed*. 54:484-484.
DOI: 10.1002/anie.201408707